CZECH TECHNICAL UNIVERSITY IN PRAGUE

Faculty of Civil Engineering

Departmen of Steel and Timber Structures

Axial compression and bending interaction of SHS and RHS stainless steel members

DOCTORAL THESIS

Ing. Břetislav Židlický

Doctoral study programme: Civil Engineering

Branch of study: Structural and Transportation Engineering

Doctoral thesis tutor: doc. Ing. Michal Jandera, Ph.D.

Prague, 2020

Abstrakt

Pruty namáhané kombinací tlaku a ohybu jsou jedním z nejčastěji používaných konstrukčních prvků. Chování takovýchto prutů vyrobených z uhlíkové oceli bylo již dříve zkoumáno a na základě získaných dat byly odvozeny návrhové postupy. V případě užití korozivzdorné oceli, v důsledku výrazně odlišných materiálových vlastností obou druhů oceli, však tyto návrhové postupy neplatí. V posledních letech byla provedena řada experimentů a numerických studií poskytujících podklady, ze kterých následně byly odvozeny řady vztahů vystihující chování prutů z korozivzdorné oceli namáhaných kombinací tlaku a ohybu. Bohužel každý z nově odvozených vztahů vykazoval určité nepřesnosti, z tohoto důvodu se tato práce zabývá právě problematikou prutů z korozivzdorné oceli zatížených kombinací tlaku a ohybu se zaměřením na uzavřené čtvercové a obdélníkové průřezy, které jsou pravděpodobně nejpoužívanějšími profily pro nosné konstrukce z korozivzdorné oceli.

Zde uvedený výzkum zahrnuje experimentální studii čítající celkem 20 zhotovených experimentů sestávajících se z prutů o čtvercových a obdélníkových průřezech ze dvou tříd austenitické oceli, jmenovitě třídy 1.4301 a 1.4404. Kvůli získání většího množství dat byl vytvořen numerický model v softwaru Abaqus, který byl validován na základě dat získaných ze zhotovených experimentů, na jehož základě byla zhotovena rozsáhlá numerická parametrická studie, poskytující dostatečné množství dat k následné analytické části práce.

Primárním cílem práce bylo stanovit zjednodušený analytický vztah pro návrh prutů z korozivzdorné oceli o čtvercovém a obdélníkovém průřezu zatížených kombinací tlaku a ohybu. K tomu byla využita data získaná z numerické parametrické studie. Závěry této práce mohou pomoci k rozšíření znalostí o zmíněné problematice a přispět k nejnovější normě pro korozivzdornou ocel.

Klíčová slova: korozivzdorná ocel, kombinace tlaku a ohybu, štíhlost prutu, štíhlost průřezu.

Abstract

Members loaded by the combination of compression and bending are very common structural elements. Behaviour of the carbon steel beam-columns was investigated in the past and based on the obtained data design procedures were derived. In the case of stainless steel beam-columns, the design procedures for carbon steel are not suitable due to significant material behaviour differences of both kinds of steel. In the last years many experimental and numerical studies were carried out to provide data from which some new approach describing stainless steel beam-column behaviour were derived. Unfortunately, each of the derived approaches exhibited some inaccuracies or limitations. Therefore, this thesis investigates the issue of stainless steel beam-columns with focus on the square and rectangular hollow cross-sections which are probably the most widely used cross-sections for stainless steel load-bearing structures.

Presented research includes experimental study consisting of 20 conducted experiments of both square and rectangular hollow section members of two austenitic stainless steel grades, namely 1.4301 and 1.4404. In order to obtain greater amount of data, a numerical model was created in software Abaqus and validated on the experiments. It was used for a comprehensive numerical parametric study providing sufficient amount of data for an analytical part of the research.

The aim of the research was to derive analytical approach for the stainless steel square and rectangular hollow section beam-column design. Data obtained from the numerical parametric study were used for this purpose. The conclusions of this research can broaden the knowledge of the investigated issue and contribute to the recent stainless steel design code.

Key words: stainless steel, combined loading, non-dimensional slenderness, cross-section slenderness, beam-column.

CZECH TECHNICAL UNIVERSITY IN PRAGUE
Faculty of Civil Engineering
Thákurova 7, 166 29 Praha 6

DECLARATION

Ph.D. student's name: Břetislav Židlický

Title of the doctoral thesis: Axial compression and bending interaction of SHS and RHS stainless steel members.

I hereby declare that this doctoral thesis is my own work and effort written under the guidance of the tutor Michal Jandera.
All sources and other materials used have been quoted in the list of references.

The doctoral thesis was written in connection with research on the projects:

GAČR 20-24563S - Global analysis methods for slender structures of stainless steels and other steels with non-linear stress-strain diagram

SGS16 / 203 / OHK1 / 3T / 11 - General method for stainless steel structures

In Prague on 28.5.2020

signature

Poděkování

Poděkování patří zejména mému školiteli doc. Ing. Michalu Janderovi, Ph.D., který mi svými velmi cennými radami a připomínkami, stejně tak jako laskavým a přátelským vedením, dopomohl k provedení veškerých prací a výzkumných činností v průběhu doktorského studia.

Dále bych chtěl poděkovat Katedře ocelových a dřevěných konstrukcí za příležitost doktorského studia, přátelství všech členů katedry a ochotu pomoci při řešení různých problémů.

Za přípravu a provedení tahových a experimentálních zkoušek, provedených v laboratořích Fakulty stavební děkuji všem zúčastněným členům experimentálního centra.

Během doktorského studia mi byla umožněna zahraniční stáž na univerzitě UPC v Barceloně, kde jsem pracoval pod vedením profesorky Esther Real, které bych velmi rád poděkoval za její ochotu a přátelský přístup. Poděkování patří také Dr. Itsaso Arrayago za odborné konzultace, a ostatním členům katedry.

Výzkum byl financován primárně z grantu SGS16/203/OHK1/3T/11 bez jehož podpory by provedení výzkumu nebylo možné.

Závěrem bych rád poděkoval své rodině za poskytnutí zázemí a podpory během celého doktorského studia, zejména pak své manželce Veronice, která mi byla oporou a umožnila mi odjezd na zahraniční stáž, ačkoli se nám před mým odletem narodil syn.

Acknowledgements

I am highly grateful to my supervisor doc. Ing. Michal Jandera, Ph.D., due to his valuable advices and comments, as well as due to his kind and friendly guidance, I was able to conduct all the duties and research activities during my Ph.D. study.

Also, I would like to thank the Department of Steel and Timber Structures of CTU in Prague for the opportunity of the Ph.D. study, friendship of all members of the department and their willingness to help me in solving of various problems.

I would like to thank all participating members of the Experimental Centre for the preparation and conduction of both tensile and experimental tests, performed in laboratories of the Faculty of Civil Engineering, CTU in Prague.

I was allowed to study abroad at UPC in Barcelona where I worked under supervision of Professor Esther Real, whom I would like to thank very much for her willingness and friendly guidance. Furthermore, I would like to thank to Dr. Itsaso Arrayago for professional consultations and other members of the department.

The research was funded primarily by the grant SGS16/203/OHK1/3T/11 without whose support it would be impossible to carry out the research.

Finally, I would like to thank my family for the providing of the background and support during my Ph.D. study. Special thanks to my wife Veronika, who significantly supported me and allowed me to go to study abroad, even though our son was born shortly before my departure.

Content

Chapter 1

Introduction

1.1 What is stainless steel?

Stainless steel is a special family of highly alloyed steels containing at least 10.5 % of chromium with great corrosion resistance and resistance at elevated temperatures. There are many stainless steel grades with various levels of yield strength, ultimate strength, corrosion resistance, ductility, weldability and toughness. The mentioned material properties are influenced by content of the alloying elements which leads to many stainless steel grades with different material properties. Therefore, it is very important to choose the appropriate stainless steel grade for the application in corresponding corrosion environment and required strength. The inappropriate choice of stainless steel grade can leads to an unnecessarily expensive structure or worse, to not satisfactory corrosion resistance.

The corrosion resistance of stainless steel members is ensured by a very thin, about 5 x 10^{-6} mm, transparent and adherent passive layer on the surface of stainless steel. Passive layer arises if the material contains above 10.5 % of chromium, has a clean surface and if it is exposed to the air or any other environment containing oxygen. In the case of surface damage, the passive layer is able to recover by the chemical reaction of chromium contained in the material and oxygen contained in the air, see Figure 1.1.

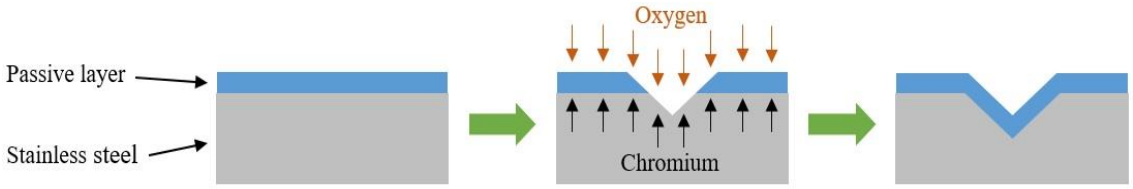

Figure 1.1 *Passive layer recovery.*

1.2 Stainless steel in Constructions

Stainless steel was firstly used as a construction material more than one hundred years ago. It was presented as a corrosion resistant material with great aesthetic properties. However, it was considered as over-expensive in the comparison with the well-known carbon steel. Furthermore, not much information about stainless steel members behaviour existed.

The utilization of stainless steel alloys for structural elements has been significantly increased in the last two decades. Especially in coastal areas where structures are exposed to an aggressive environment stainless steel becoming very popular both for onshore and offshore structures. Architects design this material because of its aesthetic appearance and engineers then for its corrosion resistance, large durability, easy maintenance and appropriate mechanical properties (toughness, ductility, impact resistance, elevated temperature resistance).

Despite the fact that the utilization of stainless steels increased, its use in the comparison with well-known carbon steel is still low. The primary reason for this low use in structural applications is usually the actual cost of stainless steel as a material. High cost of the stainless steel structure may be partially caused by inaccurate, usually conservative, design approaches in standard for stainless steel EN 1993-1-4 [1]. The inaccuracies stems mostly from the fact that EN 1993-1-4 [1] draws from EN 1993-1-1 [2] for carbon steel, because stainless steel data were limited in 2005.

However, the high initial cost of stainless steel structure could be compensated by a lower maintenance cost during the lifecycle of structure in some cases. Carbon steel structures need

coatings to protect the material against corrosion that should be checked and sometimes re-painted in predefined periods. Stainless steel is a corrosive resistant material, therefore, there is a cost save due to corrosion resistant coating elimination.

There are many grades of stainless steel traditionally used in civil engineering. They are divided into several groups regarding to their microstructure, namely austenitic, ferritic, duplex (austenitic-ferritic), martensitic and precipitation hardening, see Figure 1.2. Due to the different microstructure, every stainless steel group has a different material properties. The most commonly used in load-bearing structures are the first three ones. All of mentioned stainless steel groups are described in detail in following chapters.

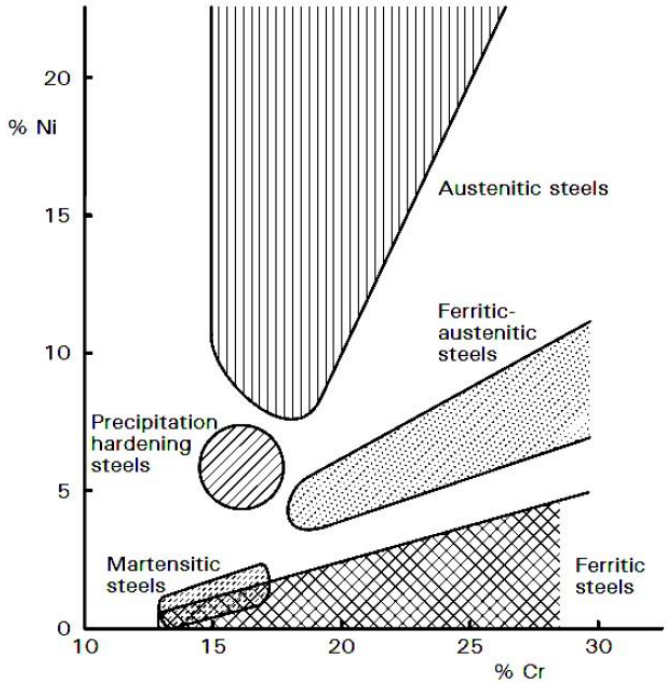

Figure 1.2 *Stainless steel groups according to content of nickel and chromium [3].*

1.2.2 Austenitic stainless steels

Austenitic stainless steel is the most widely used stainless steel group for building applications. Compared to carbon steel, which have body-centred cubic atomic structure, austenitic stainless steel group has a face-centred cubic atomic structure. It is considered that austenitic stainless steels are more corrosion resistant than ferritic stainless steels. To retain austenitic structure at room temperature, some common austenitisers such as nickel, manganese and nitrogen are added. Austenite is formed in carbon steel at 900 °C to 1400 °C as well. Austenitic stainless steel with molybdenum is resistant to a sea water and chloride-bearing solutions; this type of stainless steel is therefore used extensively in aggressive marine and industrial environments. Though austenitic

stainless steels cannot undergo heat treatment, they have tensile strengths up to 1000 MPa and can be also used as reinforcing bars in a concrete. Austenitic grades are non-magnetic in general, however, heavy cold-working can increase magnetic permeability.

1.2.3 Ferritic stainless steels

Ferritic stainless steel group has a body-centred atomic structure. This group of stainless steel is magnetic unless it is heated to above 750 °C. Ferritic stainless steels should contain more than 12 % of chromium and very low content of nickel. Though sometimes small amount of other elements such as aluminium, titanium and molybdenum are added, ferritic steels are considered as binary alloys. Therefore, ferritic stainless steels have a reduced corrosion resistance and its price is usually lower than the price of austenitic stainless steels. The application of ferritic stainless steels in buildings is limited mostly to the interior where corrosion resistance is not so much of a factor. Ferritic steels do not respond to heat treatment and are more difficult to weld and shape than austenitic stainless steels.

1.2.4 Duplex stainless steels

Steels with content of chromium typically from 20 to 26 % and nickel from 1 to 6 % and containing both austenite and ferrite are called duplex stainless steels (or austenitic-ferritic stainless steels). This type of steel has both beneficial and disadvantageous characteristics of the two phases. By adding other austenite and ferrite stabilizers, the composition of the two phases can be varied. A lot of effort has been put into developing the properties of this relatively new stainless steel group which exhibits good ductility and higher strength compared to austenitic one. Duplex stainless steels are normally used when corrosion resistance and strength are equally important. It is a suitable alternative to carbon steel, other types of stainless steel and nickel based alloys.

1.2.5 Martensitic stainless steels

Martensitic stainless steel group contains higher amount of carbon than ferritic steels which leads to a higher strength and hardness but lower ductility. It is usually used in hardened and tempered condition ensuring mentioned material properties enhancement. The utilization of martensitic stainless steel group is tightly connected with its great hardness and abrasion resistance, like bearings for instance. Despite very low ductility, even lower than ferritic steels, martensitic steels can be welded, however, preheating and post-weld heat treatment could be required.

1.2.6 Precipitation hardening stainless steels

These are steels that can dispone by very high strengths due to heat treatment. Material properties of precipitation hardening stainless steels are combination of martensitic and austenitic stainless steel material properties. This stainless steel group is usually not used for welding. It is widely used in aerospace industry, than for bolts, shafts, tension bars and others where combination of high strength and moderate corrosion resistance is required.

Because martensitic and precipitation hardening stainless steels are not widely used as a structural elements only austenitic, ferritic and duplex stainless steel groups are considered and investigated in this thesis.

1.3 Fabrication of stainless steel products

There are many forms of stainless steel members including sheets, plates, coils, strips, bars, square hollow sections (SHS), rectangular hollow sections (RHS), circular hollow sections (CHS), I, H, U and C open sections or angles. Fabrication of the cross-sections is made by cold-forming, hot rolling, extrusion and laser or arc welding.

The most widely used production procedure for hollow cross-sections is a combination of cold rolling and welding, see Figure 1.3.

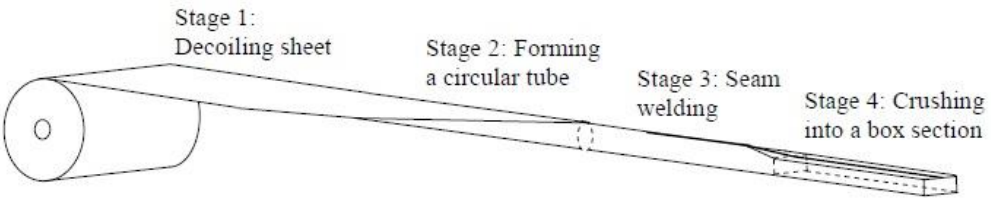

Figure 1.3 *Hollow cross-section forming [4].*

It is necessary to mention that cold-forming changing material properties in the influenced regions. Regarding the cold forming these areas exhibit higher strengths, especially yield strength, but lower ductility.

1.4 Designation and composition of stainless steel grades

European designation system is described in the Eurocode EN 10027-2 [6]. Chemical composition and some basic material properties are given in the Eurocode EN 10088-1 [7]. Technical properties and chemical compositions data for the appropriate materials are provided by EN 10088-4 [8] and EN 10088-5 [9].

European designation of stainless steels is demonstrated in Table 1.1 for the austenitic 1.4307 stainless steel grade. There is a different denotation of stainless steel grades in the American standards AISI, correlation between the European and US denotation is given by Table 1.2.

Table 1.1 *Designation of stainless steels.*

1.	**43**	**07**
Denotes steel	Denotes one group of stainless steels	Individual grade identification

The groups of stainless steel are denoted as:

1.40XX	Stainless steel with Ni < 2.5 % without Mo, Nb and Ti
1.41XX	Stainless steel with Ni < 2.5 % and Mo but without Nb and Ti
1.43XX	Stainless steel with Ni ≥ 2.5 % without Mo, Nb and Ti
1.44XX	Stainless steel with Ni ≥ 2.5 % and Mo but without Nb and Ti
1.45XX	Stainless steels with special additions
1.46XX	Chemical resistant and high temperature Ni grades

The steel name providing some information about chemical steel composition. The name of stainless steel 1.4307 is X2CrNi18-9, which means:

X	**2**	**CrNi**	**18-9**
Denotes high alloy steel	100 x % of carbon	Chemical symbols of main alloying elements	% of main alloying elements

Table 1.2 *The correlation between European and US designation of stainless steels [5].*

Steel grade to EN 10088		**US**	
No.	**Name**	**ASTM Type**	**UNS**
Austenitic			
1.4301	X5CrNi18-10	304	S30400
1.4306	X2CrNi19-11	304L	S30403
1.4307	X2CrNi18-9	304L	S30403
1.4311	X2CrNin18-10	304LN	S30453
1.4318	X2CrNiN18-7	301LN	S30153
1.4401	X5CrNi Mo17-12-2	316	S31600
1.4404	X2CrNiMo17-12-2	316L	S31603
1.4406	X2CrNiMoN17-11-2	316LN	S31653
1.4429	X2CrNiMoN17-13-3	316LN	S31653
1.4432	X2CrNiMo17-12-3	316L	S31603
1.4435	X2CrNiMo18-14-3	316L	-
1.4439	X2CrNiMoN17-13-5	317LMN	S31726
1.4529	X1NiCrMoCuN25-20-7	-	N08926
1.4539	X1NiCrMoCu25-20-5	904 L	N08904
1.4541	X6CrNiTi18-10	321	S32100
1.4547	X1CrNiMoCuN20-18-7	-	S31254
1.4565	X2CrNiMnMoN25-18-6-5	-	S34565
1.4567 *	X3CrNiCu18–9-4		S30430
1.4571	X6CrNiMoTi17-12-2	316Ti	S31635
1.4578 *	X3CrNiCuMo17–11–3-2	-	-
Duplex			
1.4062 *	X2CrNiN22-2--		S32202
1.4162	X2CrMnNiN21-5-1		S32101
1.4362	X2CrNiN23-4	2304#	S32304
1.4410	X2CrNiMoN25-7-4	2507#	S32750
1.4462	X2CrNiMoN22-5-3	2205#	S32205
1.4482 *	X2CrMnNiMoN21–5-3		-
1.4501 *	X2CrNiMoCuWN25–7-4		S32760
1.4507 *	X2CrNiMoCuWN25–7-4		S32520
1.4662 *	X2CrNiMnMoCuN24–4-3–2		S82441
Ferritic			
1.4003	X2CrNi12	-	S41003
1.4016	X6Cr17	430	S43000
1.4509	X2CrTiNb18	441+	S43940
1.4512	X2CrTi12	409	S40900
1.4521	X2CrMoTi18-2	444	S44400
1.4621 *	X2CrNbCu21	-	S44500

All the above steels are in EN 10088-4/5 except for those marked with *, which are currently only in EN 10088-2/3.
Commonly used trade names.
+ 441 is a common trade name for this grade but not an ASTM type.

Chapter 2

Research objectives

Stainless steel square and hollow cross-section members loaded by combination of compressive force and bending moment are one of the most commonly used structural elements. However, the design of these members is still concern. On one hand, there is a significant progress in the stainless steel beam-column investigation during last decades with many design improvements developed. On the other hand, all of them exhibit some drawbacks. Therefore, the objectives of the thesis are to broaden the stainless steel square and rectangular hollow cross-section beam-column behaviour knowledge, to evaluate some existing design procedures and to develop both safe and accurate analytical description of these structural elements.

2.1 Thesis outline

A brief introduction of stainless steel is given in the first chapter, containing utilization of stainless steel in structural engineering, description of stainless steel groups, fabrication of stainless steel and stainless steel chemical content. Then, research objectives and outline of the thesis are given in this chapter as well.

Chapter 3 provides a comprehensive state of the art relevant for the thesis. In the first part, the general information of stainless steel is given, namely mechanical properties, stress-strain diagram, cross-section classification (which is slightly different compared to common carbon steel), imperfections, residual stresses and stainless steel partial factors. Then, design procedures are given. Firstly, flexural buckling and bending load-bearing capacity establishment is described, later, a comprehensive description of stainless steel beam-column procedures follows.

Chapter 4 presents experimental study consisting of both material tensile tests and square and rectangular hollow cross-section members loaded by eccentric compression. Furthermore, measurement of the real dimensions of cross-sections, member lengths and both local and global imperfection amplitude values are given.

Chapter 5 provides numerical part of the research. A numerical model created in software Abaqus is described in detail. Furthermore, its validation based on the experimental data is given. Then, the comprehensive numerical parametric study is presented.

Chapter 6 consists of comparison of the most recent stainless steel beam-column design procedures with numerical results and derivation of a new proposal for the interaction factor calculation. Furthermore, evaluation of the proposed interaction factor for the combination of compressive force and uniform bending moment along the member length is given considering various compressive and bending load-bearing capacity approaches. A brief study of stainless steel beam-columns under moment gradient is given as well, with focus on the evaluation of the mentioned new interaction factor formulae. Complex reliability analysis of the new proposal is given, as well. Additionally, a very brief investigation of the General Method containing current state evaluation and a modification proposal is given.

Chapter 7 provides summary of the conducted work and proposal of topics and aims for future research.

Chapter 8 contains annex with charts for numerical model validation

Chapter 3

Literature review

3.1 Material characteristics

Stainless steel unlike to carbon steel, which displays a linear elastic region and clearly visible yield point followed by a yield plateau and strain hardening, exhibits a rounded stress-strain response without clearly defined yield point but a high degree of strain hardening and ductility. Due to different chemical composition every group of stainless steel (austenitic, ferritic and duplex) exhibits different yield stress level, ductility and curvature of stress-strain diagram curve. Ductility of austenitic stainless steels is around 40 to 60 % which is approximately twice higher than for carbon steels. Ferritic and duplex stainless steels ductility is about 15 to 30 % and 30 to 50 %, respectively. The comparison of representative stress-strain diagrams for all three stainless steel groups together with S355 carbon steel is shown in Figure 3.1 and Figure 3.2, where clear difference in the yield strength and ductility is shown

Cold-worked stainless steel exhibits non-symmetry in strass-strain behaviour which means different material behaviour in tension and compression. Furthermore, there is an anisotropy phenomenon regarding the rolling direction, see Figure 3.3. However, the influence of both phenomena can be neglected if: material model for the appropriate loading direction is considered; material is subsequently annealed; cold-working is not significant.

The yield strength of stainless steel is defined by the proof strength at 0.2 % of plastic strain meaning 0.2 % offset permanent strain. Therefore, the stainless steel proof yield strength is specified as $\sigma_{0.2}$. A definition of 0.2 % proof strength is shown in Figure 3.4.

As was mentioned before, SHS and RHS contain enhanced material properties in corner regions due to cold-forming. It was investigated, both experimentally [10], [11] and numerically [12], [13], that the enhanced corner material properties exceed the pure corner area into the flat parts of the cross-section. The extension was defined as two times the wall thickness. However, a recent study of Mařík and Jandera [14], [15] found that assumption of the enhanced material properties only in the corner is more accurate.

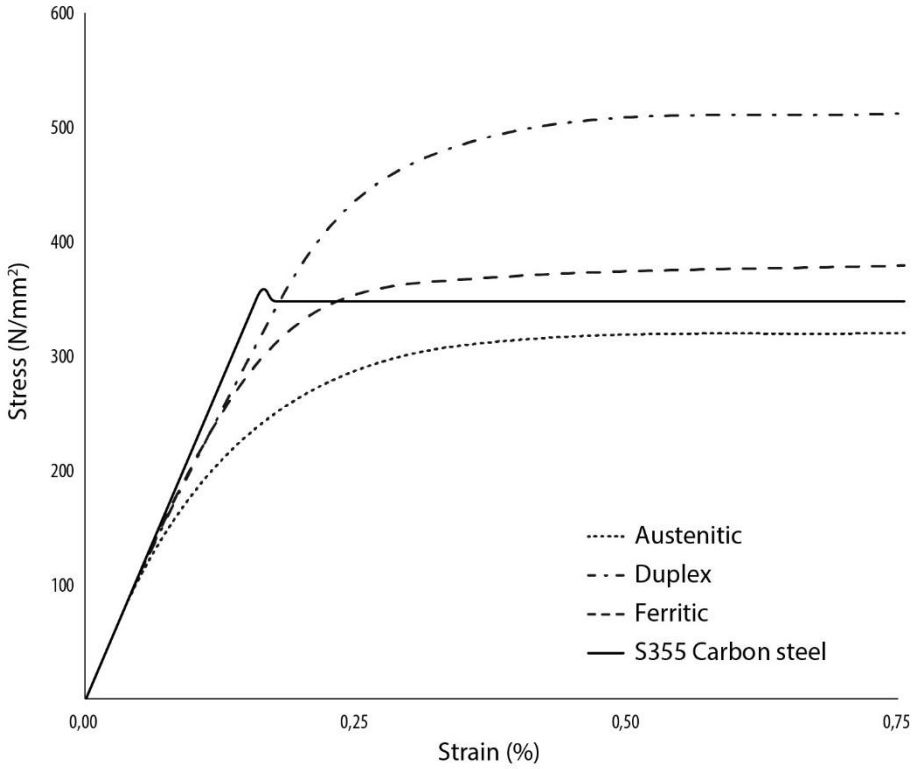

Figure 3.1 *Stress-strain curves for stainless steel and carbon steel from 0 to 0.75 % strain [5].*

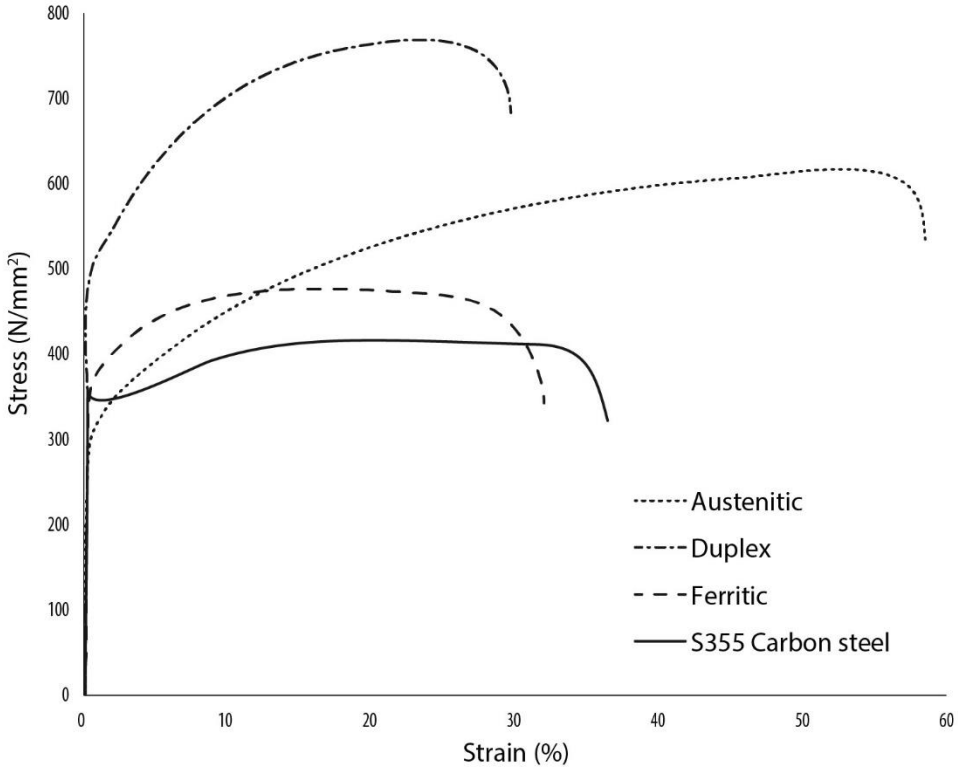

Figure 3.2 *Full range stress-strain curves for stainless steel and carbon steel [5].*

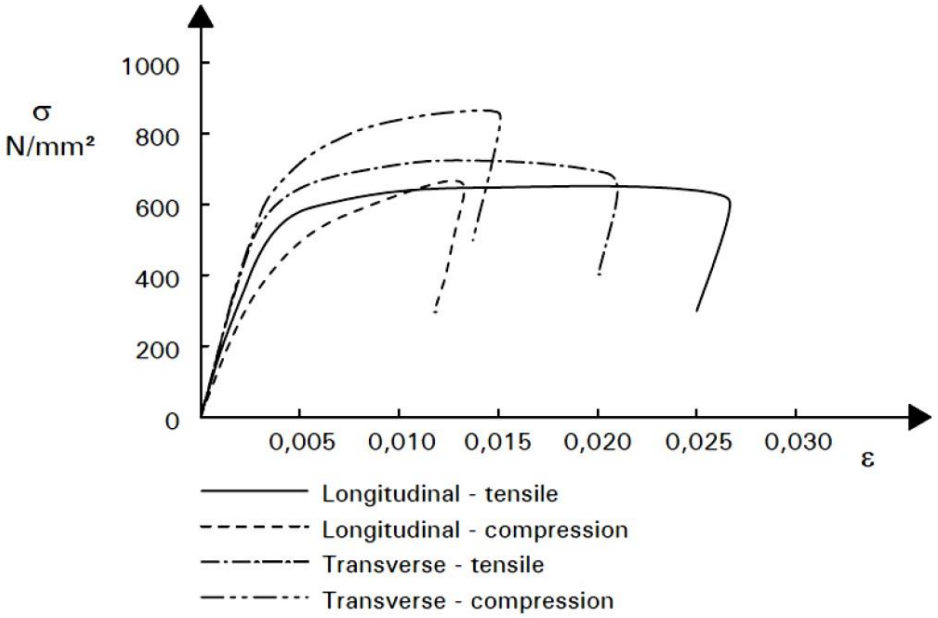

Figure 3.3 *Stress-strain diagram of cold-worked hardened stainless steel 1.4318 grade [16].*

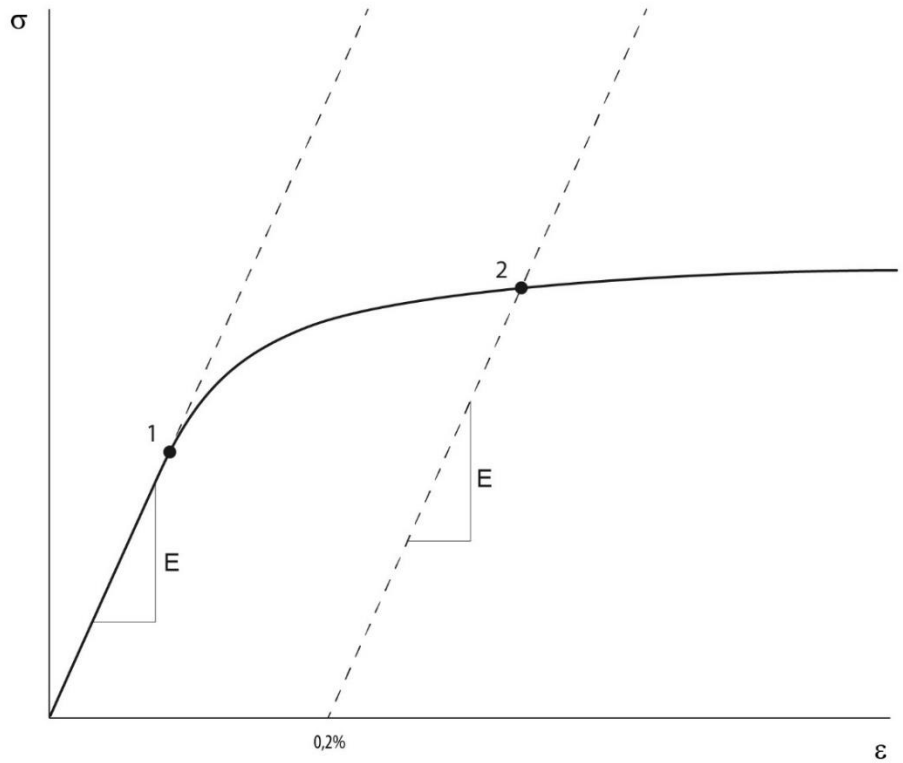

Figure 3.4 *Definition of the 0.2 % proof strength [5].*

3.2 Material response description

In 1943 Ramberg and Osgood [17] developed a very first formula, see Equation (3.1), describing stainless steel material response. It is called Ramberg-Osgood formula.

$$\varepsilon = \frac{\sigma}{E_0} + K\left(\frac{\sigma}{E_0}\right)^n \tag{3.1}$$

where K and n are the model constants, ε is the strain, E_0 is the initial Young's modulus of elasticity and σ is the stress.

The formula represents both elastic and plastic response of stainless steel material which are calculated separately. One year later the Ramberg-Osgood formula was modified by Hill [18], see Equation (3.2). Since in the case of stainless steel the yield strength is defined as a stress corresponding to the 0.2 % of offset plastic strain, Equation (3.2) was slightly changed into the well-known form, Equation (3.3).

$$\varepsilon = \frac{\sigma}{E_0} + c\left(\frac{\sigma}{R_\mathrm{p}}\right)^n \tag{3.2}$$

$$\varepsilon = \frac{\sigma}{E_0} + 0.002\left(\frac{\sigma}{\sigma_{0.2}}\right)^n \tag{3.3}$$

where R_p is a general proof stress, c is the corresponding plastic strain, $\sigma_{0.2}$ is the yield stress corresponding to 0.2 % plastic strain.

The strain hardening exponent n defines degree of roundness of the stress-strain diagram curve and its value can be established according to Equation (3.4). The lower value of the strain hardening exponent the higher the roundness (non-linearity) of the stress-strain diagram curve.

$$n = \frac{\ln\left(\varepsilon_{\mathrm{p}2}/\varepsilon_{\mathrm{p}1}\right)}{\ln(\sigma_2/\sigma_1)} \tag{3.4}$$

where σ_1 and σ_2 are stresses of two stress-strain diagram points (with $\sigma_2 > \sigma_1$), $\varepsilon_{\mathrm{p}1}$ and $\varepsilon_{\mathrm{p}2}$ are the corresponding plastic strains.

According to Ramberg and Osgood [17] and current standards, the $\varepsilon_{\mathrm{p}1}$ value should be considered as 0.01 % plastic strain and σ_1 is equal to corresponding stress level $\sigma_{0.01}$ while σ_2 is the proof yield stress $\sigma_{0.2}$ corresponding to 0.2 % of plastic strain $\varepsilon_{\mathrm{p}2}$. Then, the formula could be simplified to Equation (3.5). Rasmussen and Hancock [19] recommended to consider 0.05 % proof strain instead of 0.01 % which leads to the Equation (3.6). Results are almost the same for both. However, it is expected that in the next revision of stainless steel Eurocode 1993-1-4 [1], this procedure will be implemented.

$$n = \frac{\ln(20)}{\ln(\sigma_{0.2}/\sigma_{0.01})} \tag{3.5}$$

$$n = \frac{\ln(4)}{\ln(\sigma_{0.2}/\sigma_{0.05})} \tag{3.6}$$

Typical n values are about 5 to 15 for stainless steels, 6 to 40 for aluminium alloys and 14 for high strength carbon steels. Recommended values of strain hardening exponent regarding the rolling direction are provided by EN 1993-1-4 [1]. However, Arrayago et al. [20] made a study of strain hardening exponent values depending on stainless steel group and it was shown that values provided by EN 1993-1-4 [1] for duplex stainless steels are developed based on very limited data and are too low. Therefore, it is expected that in the next revision will be replaced by

the values developed by Arrayago et al. [20], involved in Design Manual of Structural Stainless Steel (DMSSS) [5]. The summary of strain hardening exponent values is shown in Table 3.1.

Table 3.1 *Strain hardening parameter values.*

Stainless steel group	Stainless steel grade	EN 1993-1-4		Arrayago et al. [20] DMSSS [5]
		Longitudinal direction	Transverse direction	
Austenitic	1.4301, 1.4306, 1.4307, 1.4318, 1.4541	6	8	7
	1.4401, 1.4401, 1.4432, 1.4435, 1.4539, 1.4571	7	9	
Ferritic	1.4003	7	11	14
	1.4016	6	14	
	1.4512	9	16	
Duplex	1.4462, 1.4362	5	5	8
Note to EN 1993-1-4 values: If the orientation of the member is not known, or cannot be ensured, then it is conservative to use the value for the longitudinal direction.				

The whole model exhibits a good agreement with the real behaviour of stainless steel material in the low stress levels, however, with increasing level of stress it becomes inaccurate. In 2000 Mirambel and Real [21] developed a new two-stage model. The first stage considers stress level up to the 0.2 % proof strength ($\sigma \leq \sigma_{0.2}$) calculated according to Equation (3.3). While the second stage, for stress levels higher than the 0.2 % proof strength ($\sigma > \sigma_{0.2}$) is calculated according to Equation (3.7).

$$\varepsilon = \frac{\sigma - \sigma_{0.2}}{E_{0.2}} + \varepsilon_{\mathrm{pu}} \left(\frac{\sigma - \sigma_{0.2}}{\sigma_{\mathrm{u}} - \sigma_{0.2}} \right)^{n'_{0.2,\mathrm{u}}} + \varepsilon_{0.2} \tag{3.7}$$

with

$$E_{0.2} = \frac{\sigma_{0.2} E_0}{\sigma_{0.2} + 0.002 n E_0} \tag{3.8}$$

$$n'_{0.2,\mathrm{u}} = 1 + 3.5 \frac{\sigma_{0.2}}{\sigma} \tag{3.9}$$

where $E_{0.2}$ is the tangent modulus at the 0.2 % proof stress level, $\varepsilon_{\mathrm{pu}}$ is the ultimate plastic strain component at the ultimate stress, $\varepsilon_{0.2}$ is the plastic strain at the 0.2 % proof stress level, σ_{u} is the ultimate stress and $n'_{0.2,\mathrm{u}}$ is the strain hardening exponent for the second stage of stress-strain curve ($\sigma > \sigma_{0.2}$).

This modification significantly improves stainless steel response description. It is very appropriate for numerical modelling in Finite Element software. However, there is a slight shortcoming. If the stress level is equal to the ultimate stress then the calculated total strain slightly differs from the ε_{pu} ultimate plastic strain. Therefore, Gardner and Nethercot [22] suggested an improvement of this method considering total ultimate strain ε_u instead of the ultimate plastic strain ε_{pu}, see Equation (3.10).

$$\varepsilon = \frac{\sigma - \sigma_{0.2}}{E_{0.2}} + \left(\varepsilon_u - \frac{\sigma_u - \sigma_{0.2}}{E_{0.2}} - \varepsilon_{0.2}\right)\left(\frac{\sigma - \sigma_{0.2}}{\sigma_u - \sigma_{0.2}}\right)^{n'_{0.2,u}} + \varepsilon_{0.2} \tag{3.10}$$

The shortcoming of the different ultimate strains was fixed, nonetheless, the procedure exhibits little inaccuracies beyond the 0.2 % proof stress. Gardner and Nethercot [22] proposed another formula that was recently confirmed by Arrayago et al. [20], see Equation (3.11). It considers stress $\sigma_{1.0}$, corresponding to 1.0 % of plastic strain $\varepsilon_{1.0}$, against ultimate values which leads to a higher accuracy beyond the 0.2 % proof stress at the expense of lower accuracy near the ultimate strength values.

$$\varepsilon = \frac{\sigma - \sigma_{0.2}}{E_{0.2}} + \left(0.008 - \frac{\sigma_{1.0} - \sigma_{0.2}}{E_{0.2}}\right)\left(\frac{\sigma - \sigma_{0.2}}{\sigma_{1.0} - \sigma_{0.2}}\right)^{n'_{0.2,1.0}} + \varepsilon_{0.2} \tag{3.11}$$

Combination of Equation (3.3) with both Equation (3.10) and (3.11) provides very accurate description of stainless steel stress-strain diagram. However, there are still recommendations for the both combinations use. Combination with Equation (3.10) exhibits very good accuracy near the ultimate strain, therefore, it is appropriate to use if large strain values are expected (e.g. connections). On the contrary, combination with Equation (3.11) exhibits great accuracy beyond the 0.2 % strain and lower near the ultimate strain, therefore, it is appropriate to be used if large strains are not expected (up to 10 %), which is the case for the most stainless steel members.

3.3 Geometric imperfections

Imperfections are an inevitable property of each steel member affecting compressive cross-section respectively member stability and resistance. For members in compression, there are two types of geometric imperfections, local imperfections and global imperfections.

3.3.1 Local imperfections

Research in local imperfections of stainless steel square and rectangular hollow cross-section members was made by Gardner and Nethercot [12]. In their research, previous existing procedures were verified firstly. Dawson and Walker [23] developed the initial local imperfection amplitude ω_0 prediction which is given by Equation (3.12).

$$\omega_0 = Kt \tag{3.12}$$

where ω_0 is the initial local imperfection amplitude, K is the constant and t is the thickness of the structural element.

It was shown that determining of initial local imperfection based on the thickness of the structural element and some constant only is quite inappropriate. Therefore, another formula was proposed, see Equation (3.13) [23].

$$\omega_0 = \alpha \left(\frac{\sigma_{0.2}}{\sigma_{\mathrm{cr}}}\right)^{0.5} t \tag{3.13}$$

where σ_{cr} is the structural element critical buckling stress and α is the constant (for stainless steel square and rectangular hollow cross-sections is equal to $7.3 \cdot 10^{-6}$).

However, it was shown that even this formula is not suitable too. Therefore, Dawson and Walker [23] developed the last expression given by Equation (3.14), with the consideration of constant γ value equal to 0.2. However, Gardner and Nethercot [12] found that 0.023 value is much more suitable for stainless steel that was confirmed by Cruise [4] later.

$$\omega_0 = \gamma \left(\frac{\sigma_{0.2}}{\sigma_{\mathrm{cr}}}\right) t \tag{3.14}$$

where γ is the constant (for stainless steels equal to 0.023).

Furthermore, Cruise [4] described an imperfection shape along the member length by Fourier series. The imperfection frequency is defined in reference to a multiple ζ of the cross-section width. Two values of ζ were considered: $\zeta = 1$ represents a half wavelength equal to the cross-section width and $\zeta = 10$ represents a half wavelength of ten times the cross-section width. These two values represent lower and upper boundary values of γ with regard to the manufacturing. Summary of the proposed γ values for the prediction of initial local imperfection amplitudes according to Cruise [4] is given in Table 3.2.

Table 3.2 *Upper and lower limits for γ values according to Cruise [4].*

Cross-section type	γ (ζ = 1)	γ (ζ = 10)
Press-braked equal angles	0.008	0.052
Cold-rolled box sections	0.012	0.111
Hot-rolled equal angles	0.044	0.415

Gardner and Nethercot [12] then verified two more procedures developed by Schafer and Peköz in 1998 [24] but both of these formulae were shown as unsuitable. Both procedures are shown below by Equations (3.15) and (3.16).

$$\omega_0 = 0.006b \tag{3.15}$$

$$\omega_0 = 6te^{-2t} \tag{3.16}$$

where b is the width of the plate and e is the Euler´s constant.

Currently, there are some approaches to calculate initial local imperfection amplitude but most of them are inaccurate or developed on small number of specimens. The prediction formula for the local imperfection amplitude of square and rectangular hollow cross-sections, Equation (3.14), has been confirmed again by Zhao et al. in 2015 [25], [26]. For the circular hollow cross-sections the amplitude could be taken as 0.2t according to Gardner´s and Nethercot´s research [12].

3.3.2 Global imperfections

The effect of initial global imperfection amplitude on the flexural buckling was also investigated by Gardner and Nethercot [12]. Three imperfection amplitudes were considered: L / 1000; L / 2000 and L / 5000, where L is the member length. It was found that the global imperfection amplitude L / 2000 is the most accurate one on average, but generally the amplitude is in the range of L / 1000 to L / 5000. In the parametric studies carried out by Rasmussen and Rondal [27], Rasmussen and Hancock [28], Young [29], Ellobody and Young [30] is the global imperfection for the pin-ended members considered as L / 1500.

Another study of the global imperfection regarding to manufacturing was conducted by Cruise [4], as well in the case of local imperfections. Based on this research, three formulae for determination of global imperfections were established depending on the member length and they are shown in Table 3.3.

Table 3.3 *Global imperfection amplitudes according to Cruise [4].*

Manufacturing	Global imperfection amplitude
Press-braked cross-sections	0.00084*L*
Cold-rolled cross-sections	0.00035*L*
Hot-rolled cross-sections	0.0012*L*

It could be noted, that although value *L* / 1500 was considered in many studies as the initial global imperfection amplitude, value *L* / 1000 would be very appropriate too as was shown in [4]. Furthermore, it is even more conservative due to higher value of the initial global imperfection. Generally, both *L* / 1500 and *L* / 1000 are suitable for stainless steel members. Furthermore, EN 1993-1-5 [31] recommends to consider 80 % of fabrication tolerance that is, according to EN 1090-2 [32], equal to *L* / 750. Again, a very similar value to the previous ones, L / 938.

3.4 Residual stresses

Stresses that exist in the structural cross-sections in the unloaded state are named residual stresses. These stresses in the structural elements are created during production. There are four main methods of producing described: welding; hot rolling; press breaking and cold rolling. Due to different properties of the material, it cannot be simply assumed that the residual stresses in stainless steel cross-sections are of the same magnitude or distribution as those in carbon steel cross-sections.

Welding causes a steep temperature gradient. A temperature peak is situated at the welding site. Cooling of the heat material leads to tension stress in vicinity of the weld that is compensated by compressive stress in farther cross-section parts.

Residual stresses in hot-rolled cross-sections are caused by different cooling rates due to variation of surface to volume ratio. The faster cooling structural elements, such as flanges and webs, are left in residual compression and slower cooling regions, such as plate intersections, are left in residual tension.

Residual stresses in cold-formed cross-sections (press-braked and cold-rolled) are caused due to plastic deformation which occurs during forming of sheet material into a final cross-section.

There are two types of residual stresses in cross-sections: membrane residual stresses (uniform through thickness) and bending residual stresses (variable through thickness). Membrane residual

stresses generally dominate in hot-rolled cross-sections while bending residual stresses are generally dominant in cold-formed (press-braked and cold-rolled) cross-sections.

A comprehensive study of residual stresses influence on the stainless steel member resistance was made by Cruise and Gardner [33] for both hot-rolled and cold-formed cross-sections. For hot-rolled cross-sections the results showed that membrane and bending residual stresses are typically below 10 % and 20 %, respectively, of the material 0.2 % proof stress. For press-braked cross-sections, the membrane and bending residual stresses in the flat regions are generally low, typically below 10 % of the material 0.2 % proof stress, as well. However, higher bending residual stresses are observed in the corner regions, where large plastic deformation occurs that typically reach about 30 % of the material 0.2 % proof stress. In the case of cold-rolled box cross-sections, the results indicate similar membrane residual stresses as those observed in hot-rolled and press-braked cross-sections and considerably greater bending residual stresses which are typically ranged from 30 % to 70 % of the material 0.2 % proof stress.

Further study was made by Jandera et al. [34] for cold-rolled box cross-sections only. Researchers investigated the influence of bending and membrane residual stresses on global and local buckling. Paradoxically, it was found that inclusion of residual stresses to the calculation generally leads to increase of load-bearing capacity. This was attributed mainly to the influence of bending residual stresses on the material stress-strain curve.

Research conducted by Cruise and Gardner [33] indicates that residual stresses caused by hot rolling and press braking are almost negligible and those caused by cold rolling are considerably greater. Jandera et al. [34] proved that these residual stresses may have positive influence on the load-bearing capacity. However, the influence of membrane residual stresses are almost negligible in cold-rolled square and rectangular hollow cross-sections and the bending residual stresses are present in the stress-strain diagram behaviour. Based on these results, it could be concluded, that residual stresses may not be considered in the numerical models for cold-formed box cross-sections because their main effect is inherently present in a stress-strain diagram.

3.5 Partial safety factors

There are different values of partial safety factors for stainless steel provided by stainless steel Eurocode EN 1993-1-4 [1] than for carbon steel according to EN 1993-1-1 [2]. Comparison of these values is shown in Table 3.4.

Table 3.4 *Partial safety factor values.*

γ_i	Carbon steel	Stainless steel
γ_{M0}	1.0	1.1
γ_{M1}	1.0	1.1
γ_{M2}	1.25	1.25

3.6 Cross-section classification

Current codified cross-section classification of hollow cross-sections is based on a bi-linear elastic-perfectly plastic stress-strain material behaviour with not considering of strain hardening phenomenon. That divides the considered stainless steel cross-sections into four classes based on the most slender cross-section element. Due to different loading conditions and maximal stress of the cross-section, there are two kinds of cross-section classification, namely for the compressive resistance and bending resistance. The initial elastic Young's modulus, the yield strength and cross-section dimensions (width to thickness ratio) determines the cross-section Class. Based on the cross-section class, an appropriate cross-section characteristics should be used for calculation of the cross-section resistance. Summary is given in Table 3.5.

Table 3.5 *Cross-section characteristics with respect to the cross-section Class.*

Cross-section Class	Compressive resistance cross-section area	Bending resistance cross-section modulus
Class 1	gross	plastic
Class 2	gross	plastic
Class 3	gross	elastic
Class 4	effective	effective

The effective cross-section characteristics of Class 4 stainless steel cross-sections both for compressive and bending resistance is based on the effective width method developed by Johnson and Winter [35] in 1966. It was modified for stainless steel and implemented to the stainless steel standard. With following Eurocode revision, the slenderness limits for the cross-section classification were slightly changed. The slenderness limits for hollow cross-sections have been revised in the last decade, namely by Gardner and Theofanous in 2008 [36] and Gardner et al. in 2014 [37]. Current reduction factor for local buckling formulae for slender stainless steel cross-

sections have been developed by Gardner and Theofanous [36], however, little modification for square and rectangular hollow cross-sections was suggested by Bock and Real [38].

3.7 Flexural buckling

A very first description of column resistance was developed by Euler in 1744 [39] which provides the critical buckling load of an idealized and perfect-elastic column, see Equation (3.17).

$$N_{\mathrm{cr}} = \frac{\pi^2 EI}{L^2} \tag{3.17}$$

where N_{cr} is the critical buckling load, E is the initial Young's modulus of elasticity, I is the gross cross-section second moment of area and L is the member length.

However, due to material, geometrical and residual stresses is the real column behaviour description more complex. Many investigations of carbon steel columns have been made in order to develop an accurate procedure of column response which led to the development of codified buckling curves considering well-known Ayrton-Perry formula [40]. The same buckling curve formulation was adopted into the EN 1993-1-4 [1] but considering different imperfection factors α and plateau length $\bar{\lambda}_0$ values, see Table 3.6.

Table 3.6 *Current codified values of α and $\bar{\lambda}_0$ according to EN 1993-1-4 [1].*

Buckling mode	Member type	α	$\bar{\lambda}_0$
Flexural	Cold-formed open sections	0.49	0.4
	Hollow sections (welded and seamless)	0.49	0.4
	Welded open sections (major axis)	0.49	0.2
	Welded open sections (minor axis)	0.76	0.2
The values for α and $\bar{\lambda}_0$ do not apply to hollow sections if they are annealed after fabrication (which is rarely the case).			

Current verification condition for stainless steel members is taken from the EN 1993-1-1 [2] for carbon steel and it is given by Equation (3.18). The flexural buckling resistance is given by Equation (3.19).

$$\frac{N_{\mathrm{Ed}}}{N_{\mathrm{b,Rd}}} \leq 1.0 \tag{3.18}$$

$$N_{\mathrm{b,Rd}} = \chi A \frac{f_{\mathrm{y}}}{\gamma_{\mathrm{M1}}} \tag{3.19}$$

where N_{Ed} is the loading compressive force, $N_{\mathrm{b,Rd}}$ is the flexural buckling resistance, χ is the flexural buckling reduction factor, A is the gross cross-section area for Class 1 to Class 3 of the cross-section and for Class 4 of the cross-section it is replaced by effective cross-section area A_{eff}, f_{y} is the yield strength and γ_{M1} is the partial safety factor.

The buckling factor χ takes into account flexural buckling phenomena via non-dimensional slenderness $\bar{\lambda}$, imperfection factor α and plateau length $\bar{\lambda}_0$ and it is given by Equation (3.20).

$$\chi = \frac{1}{\phi + \sqrt{\phi^2 - \bar{\lambda}^2}} \leq 1.0 \tag{3.20}$$

with

$$\phi = 0.5\left[1 + \alpha\left(\bar{\lambda} - \bar{\lambda}_0\right) + \bar{\lambda}^2\right] \tag{3.21}$$

$$\bar{\lambda} = \sqrt{\frac{A f_{\mathrm{y}}}{N_{\mathrm{cr}}}} \tag{3.22}$$

where α is the imperfection factor, $\bar{\lambda}$ is the non-dimensional slenderness, $\bar{\lambda}_0$ is the plateau length and N_{cr} is the critical buckling load.

The adopted buckling curves have been re-evaluated for stainless steel columns by Afshan et al. [41]. It was found that the buckling curves according to EN 1993-1-4 [1] are, especially in the case of cold-formed open cross-sections and cold-formed hollow cross-sections, too optimistic. Furthermore, difference between buckling curves of ferritic stainless steel columns and austenitic and duplex stainless steel columns was found. New imperfection factors α and plateau lengths $\bar{\lambda}_0$ were proposed (see Table 3.7), evaluated and it is expected that these new values will be implemented into the new stainless steel standard revision. Currently, they are published in DMSSS [5].

Table 3.7 *New values of α and $\bar{\lambda}_0$ given by DMSSS [5].*

Member type	Buckling axis	Austenitic and duplex groups		Ferritic group	
		α	$\bar{\lambda}_0$	α	$\bar{\lambda}_0$
Cold-formed angles and U-sections	Any	0.76	0.2	0.76	0.2
Cold-formed C-sections	Any	0.49	0.2	0.49	0.2
Cold-formed SHS and RHS	Any	0.49	0.3	0.49	0.2
Cold-formed CHS and EHS	Any	0.49	0.2	0.49	0.2
Hot-finished SHS and RHS	Any	0.49	0.2	0.34	0.2
Hot-finished CHS and EHS	Any	0.49	0.2	0.34	0.2
Welded open sections	Major	0.49	0.2	0.49	0.2
	Minor	0.76	0.2	0.76	0.2

3.8 Bending

Bending is one of the most common loading case in steel structures. It is typical for horizontal members loaded by vertical loading but it can be a product of eccentric axial loading or end moments. Current codified design approach for stainless steel cross-sections loaded by bending moment provided by Eurocode 1993-1-4 [1] is adopted from EN 1993-1-1 [2] for carbon steel. The verification condition is given by Equation (3.23) for the case of pure bending. Then the cross-section bending moment capacity is calculated by Equation (3.24).

$$\frac{M_{\mathrm{Ed}}}{M_{\mathrm{Rd}}} \leq 1.0 \tag{3.23}$$

$$M_{\mathrm{Rd}} = W \frac{f_{\mathrm{y}}}{\gamma_{\mathrm{M1}}} \tag{3.24}$$

where M_{Ed} is the bending moment, M_{Rd} is the cross-section bending resistance and W is the plastic cross-section modulus (W_{pl}) for Class 1 and 2 of the cross-section, elastic cross-section modulus (W_{el}) for Class 3 of the cross-section and effective cross-section modulus (W_{eff}) for Class 4 of the cross-section for the axis of bending.

As could be seen, the design procedure for pure bending is very simple. For slender members, lateral torsional buckling phenomenon may occur. This phenomenon occurs mainly in the case of

open cross-section (hollow cross-sections are mostly not susceptible to lateral torsional buckling) major axis bending if the compressed cross-section elements are not laterally or torsionally restrained along their length. Therefore, Equation (3.25) includes reduction factor χ_{LT} covering the lateral torsional buckling phenomenon.

$$M_{b,Rd} = \chi_{LT} W \frac{f_y}{\gamma_{M1}} \tag{3.25}$$

where $M_{b,Rd}$ is the beam resistance and χ_{LT} is the reduction factor for lateral torsional buckling calculated according to EN 1993-1-4 [1] by Equation (3.26).

$$\chi_{LT} = \frac{1}{\phi_{LT} + \sqrt{\phi_{LT}^2 - \bar{\lambda}_{LT}^2}} \leq 1.0 \tag{3.26}$$

with

$$\phi_{LT} = 0.5\left[1 + \alpha_{LT}\left(\bar{\lambda}_{LT} - 0.4\right) + \bar{\lambda}_{LT}^2\right] \tag{3.27}$$

$$\bar{\lambda}_{LT} = \sqrt{\frac{W f_y}{M_{cr}}} \tag{3.28}$$

where $\bar{\lambda}_{LT}$ is the lateral non-dimensional slenderness, α_{LT} is the imperfection factor for lateral torsional buckling and M_{cr} is the elastic critical moment for lateral torsional buckling, see [1].

Determination of χ_{LT} is very similar to the procedure for column buckling (χ). The plateau length is always 0.4 for all members and imperfection factor α_{LT} is considered as 0.34 for cold-formed cross-sections and hollow cross-sections and as 0.76 for welded open cross-sections and other cross-sections where no test data are available.

3.9 Cross-section capacity

3.9.1 Continuous Strength Method

The Continuous Strength Method (CSM) is a new approach for calculation of the cross-section axial compressive and bending resistance proposed by Gardner [42] and Gardner and Nethercot [43], later developed by Gardner and Ashraf [44], Ashraf et al. [45], [46], Gardner [47] and Afshan and Gardner [48] and finally by Zhao et al. [49] (furthermore, it was published in the

Design Manual for Structural Stainless Steel [5]). It is a deformation-based procedure which takes into account benefits of strain hardening. CSM consists of two main components:

- material model for the stress-strain response calculation allowing strain hardening;
- base curve defining strain capacity of the cross-section.

The benefits of strain hardening response of stainless steel are introduced by considering an elastic, linear hardening model which is shown in Figure 3.5, where C_i are coefficients given by Table 3.8 and E_{sh} is the strain hardening modulus given by Equation (3.29).

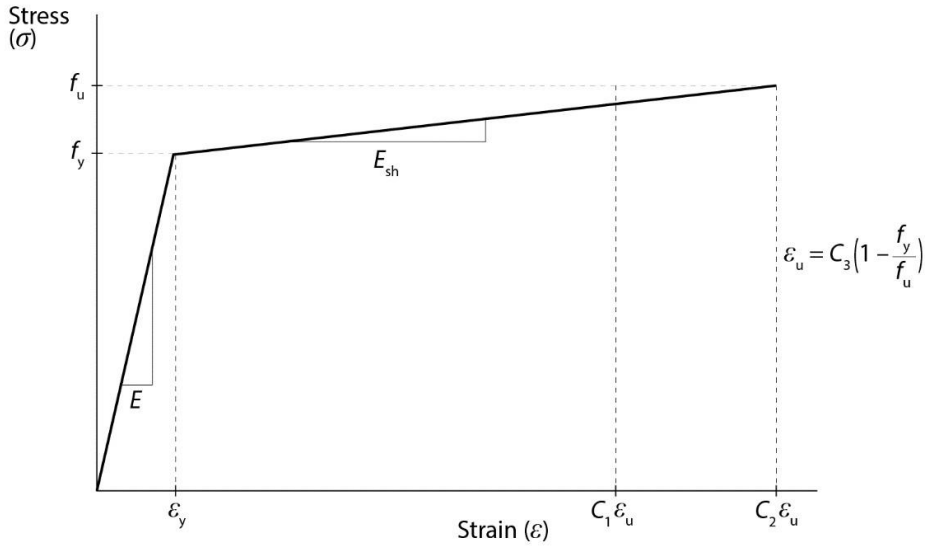

Figure 3.5 *CSM elastic, linear hardening material model [5].*

Table 3.8 *CSM material model coefficients.*

Stainless steel group	C_1	C_2	C_3
Austenitic	0.10	0.16	1.00
Ferritic	0.40	0.45	0.60
Duplex	0.10	0.16	1.00

$$E_{\mathrm{sh}} = \frac{f_{\mathrm{u}} - f_{\mathrm{y}}}{C_2\varepsilon_{\mathrm{u}} - \varepsilon_{\mathrm{y}}} \tag{3.29}$$

The normalised cross-section deformation capacity ε_{csm} / ε_y which is used for the base curve definition for the plated cross-sections is given by Equation (3.30) [49].

$$\frac{\varepsilon_{csm}}{\varepsilon_y} = \begin{cases} \frac{0.25}{\bar{\lambda}_p^{3.6}} \leq \min\left(15; \frac{C_1 \varepsilon_u}{\varepsilon_y}\right) & \text{for } \bar{\lambda}_p \leq 0.68 \\ \left(1 - \frac{0.222}{\bar{\lambda}_p^{1.050}}\right) \frac{1}{\bar{\lambda}_p^{1.050}} & \text{for } \bar{\lambda}_p > 0.68 \end{cases} \tag{3.30}$$

where $\bar{\lambda}_p$ is the full cross-section slenderness taking into account beneficial effect of element interaction if possible.

It should be noted that Equation (3.30) was published very recently, in 2017. Before that, there was no special formula for the cross-sections with $\bar{\lambda}_p > 0.68$.

The cross-section compressive resistance according to the new CSM for plated cross-sections with $\bar{\lambda}_p \leq 0.68$ is given by Equation (3.31) and with $\bar{\lambda}_p > 0.68$ by Equation (3.32).

$$N_{c,Rd} = N_{csm,Rd} = \frac{A f_{csm}}{\gamma_{M0}} \tag{3.31}$$

$$N_{c,Rd} = N_{csm,Rd} = \frac{\varepsilon_{csm}}{\varepsilon_y} \frac{A f_y}{\gamma_{M0}} \tag{3.32}$$

with

$$f_{csm} = f_y + E_{sh} \varepsilon_y \left(\frac{\varepsilon_{csm}}{\varepsilon_y} - 1\right) \tag{3.33}$$

where $N_{c,Rd}$ is the cross-section compressive resistance, A is the gross cross-section area, f_{csm} is the limiting stress determined from the strain hardening model, E_{sh} is the strain hardening slope.

The cross-section bending resistance according to the new CSM for doubly symmetric and mono symmetric cross-sections in bending about an symmetry axis with ε_{csm} / ε_y $\geq$ 1.0 is given by Equation (3.34) and with ε_{csm} / ε_y < 1.0 by Equation (3.35).

$$M_{c,Rd} = M_{csm,Rd} = \frac{W_{pl} f_y}{\gamma_{M0}} \left[1 + \frac{E_{sh}}{E} \frac{W_{el}}{W_{pl}} \left(\frac{\varepsilon_{csm}}{\varepsilon_y} - 1\right) - \frac{\left(1 - \frac{W_{el}}{W_{pl}}\right)}{\left(\frac{\varepsilon_{csm}}{\varepsilon_y}\right)^{\alpha}}\right] \tag{3.34}$$

$$M_{\mathrm{c,Rd}} = M_{\mathrm{csm,Rd}} = \frac{\varepsilon_{\mathrm{csm}}}{\varepsilon_{\mathrm{y}}} \frac{W_{\mathrm{el}} f_{\mathrm{y}}}{\gamma_{\mathrm{M0}}} \tag{3.35}$$

where α is for SHS and RHS equal to 2.0.

The interaction formulae for cross-sections loaded by combination of axial compression and bending is according to the new CSM for the RHS with $\bar{\lambda}_{\mathrm{p}} \leq 0.60$ given by Equations (3.36) to (3.38) for major axis, minor axis and biaxial bending plus axial compressive force, respectively, and with $\bar{\lambda}_{\mathrm{p}} > 0.60$ by Equation (3.39) [5].

$$M_{\mathrm{y,Ed}} \leq M_{\mathrm{R,csm,y,Rd}} = M_{\mathrm{csm,y,Rd}} \frac{(1 - n_{\mathrm{csm}})}{(1 - 0.5 a_{\mathrm{w}})} \leq M_{\mathrm{csm,y,Rd}} \tag{3.36}$$

$$M_{\mathrm{z,Ed}} \leq M_{\mathrm{R,csm,z,Rd}} = M_{\mathrm{csm,z,Rd}} \frac{(1 - n_{\mathrm{csm}})}{(1 - 0.5 a_{\mathrm{f}})} \leq M_{\mathrm{csm,z,Rd}} \tag{3.37}$$

$$\left[\frac{M_{\mathrm{y,Ed}}}{M_{\mathrm{csm,y,Rd}}}\right]^{\alpha_{\mathrm{csm}}} + \left[\frac{M_{\mathrm{z,Ed}}}{M_{\mathrm{csm,z,Rd}}}\right]^{\beta_{\mathrm{csm}}} \leq 1.0 \tag{3.38}$$

$$\frac{N_{\mathrm{Ed}}}{N_{\mathrm{csm,Rd}}} + \frac{M_{\mathrm{y,Ed}}}{M_{\mathrm{csm,y,Rd}}} + \frac{M_{\mathrm{z,Ed}}}{M_{\mathrm{csm,z,Rd}}} \leq 1.0 \tag{3.39}$$

where $M_{\mathrm{R,csm,y,Rd}}$ and $M_{\mathrm{R,csm,z,Rd}}$ are the reduced CSM bending moment resistances, n_{csm} is the ratio of loading compressive force N_{Ed} to CSM cross-section resistance $N_{\mathrm{csm,Rd}}$, a_{w} is the ratio of the web area to the gross cross-section area, a_{f} is the ratio of the flange area to the gross cross-section area and α_{csm} and β_{csm} are the interaction coefficient for biaxial bending calculated according to Equation (3.40).

$$\alpha_{\mathrm{csm}} = \beta_{\mathrm{csm}} = \frac{1.66}{1 - 1.13 n_{\mathrm{csm}}^2} \tag{3.40}$$

Comparison of the design approach for cross-sections loaded by combined loading is described herein only, evaluation of the pure compression and pure bending can be found in mentioned literature. Firstly, the Class 1 and 2 cross-section stub-columns were evaluated in Zhao et al. [50], [51]. Information about the stainless steel investigated cross-sections are summarized in Table 3.9. The comparison of the CSM with Eurocode [1] and American SEI/ASCE 8-02 [52] was made in [51]. Furthermore, the same comparison was made for Class 4 cross-sections in [49], with the extension by Australian/New Zealand standard [53], where the data were gathered from the literature. Furthermore, austenitic, ferritic and duplex stainless steel groups were considered.

Table 3.9 *Stub-column information used in Zhao et al. [50], [51].*

Stainless steel group	Austenitic, duplex
Cross-section	Cold-formed RHS and SHS
Cross-section Class	Class 1, 2
Non-dimensional slenderness range	Stub-columns
End-moment ratio	ψ = 1, 0, -1

The results of EN 1993-1-4 [1] are rather conservative which is probably caused by neglection of strain hardening. Design approach given by American standard SEI/ASCE 8-02 [52] is even more conservative for both stainless steel groups of stocky cross-sections. In the case of Class 4 cross-sections both American [52] and Australian/New Zealand [53] codes provides good results on average, however with larger scatter. In all cases, the CSM provides more accurate results with lower scatter than the current design standards for SHS and RHS stainless steel cross-section load-bearing capacity predictions.

3.9.2 Direct Strength Method

Direct Strength Method (DSM) is a method for cross-section load-bearing capacity calculation considering effect of local buckling by gross cross-section resistance reduction instead of reduction of widths of separate elements. It was developed by Schafer and Peköz [54]. Later, it was implemented into the North American Specification AISI-S100-12 [55] for carbon steel structures. Even though the procedure describes carbon steel local buckling behaviour, Arrayago et al. [56] assessed that it provides good predictions for stainless steel as well. DSM local buckling curve for carbon steel is given by Equation (3.41).

$$\frac{\varepsilon_{\mathrm{csm}}}{\varepsilon_{\mathrm{y}}} = \begin{cases} 1.0 & \text{for } \bar{\lambda}_{\mathrm{p}} \leq 0.776 \\ \dfrac{1}{\bar{\lambda}_{\mathrm{p}}^{0.8}} - \dfrac{0.15}{\bar{\lambda}_{\mathrm{p}}^{1.6}} & \text{for } \bar{\lambda}_{\mathrm{p}} > 0.776 \end{cases} \tag{3.41}$$

3.10 Beam-column

Beam-column is a structural member loaded by combination of compression and bending. As bending may be caused a compressive force eccentricity, end moments or transverse load, it is a

very common member in a construction. A simple analytical background of a beam-column design is given in this chapter.

For simply supported slender beam-column with initial global geometric imperfection e_0 loaded by axial compressive force N_{Ed} and end moments M_{Ed}, causing uniform bending, the internal forces diagrams are given by Figure 3.6. As can be seen, besides the first order internal forces (blue), additional bending due to second order effect occurred. Consequently, the elastic second order verification formula for the critical cross-section is given by Equation (3.42).

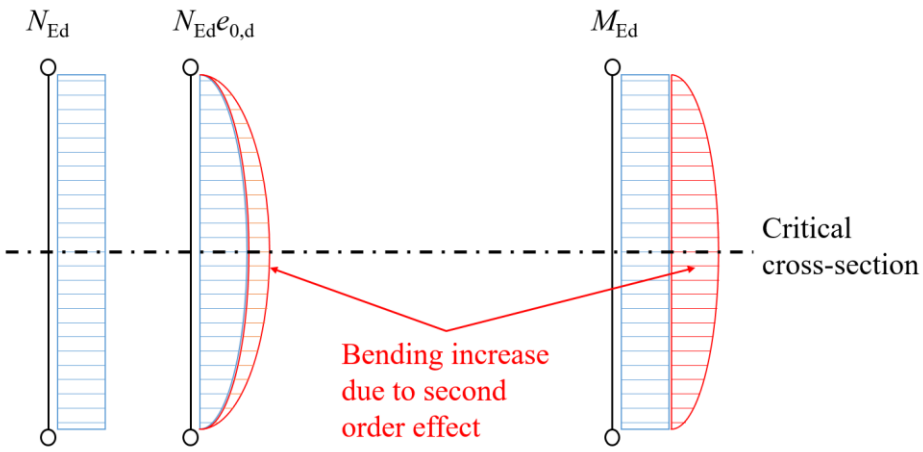

Figure 3.6 *Diagrams of internal forces.*

$$\frac{N_{Ed}}{N_{Rd}} + \frac{1}{1 - \frac{N_{Ed}}{N_{cr}}} \frac{N_{Ed} e_0}{M_{Rd}} + \frac{M_{Ed}^{II}}{M_{Rd}} \leq 1.0 \tag{3.42}$$

where $1 / (1 - N_{Ed} / N_{cr})$ is the amplification term due to second order effect and M_{Ed}^{II} is the second order bending moment.

Presented example has obvious critical cross-section position due to a uniform bending moment along the member length. However, various bending moment diagrams may occur which makes difficult to determine critical cross-section position and the second order effect to that cross-section internal force. Therefore, a coefficient C_m [57] considering the moment distribution along the member length is introduced. The second order effect of compression is taken into account again by the mentioned amplification term. See Equation (3.43).

$$\frac{N_{Ed}}{N_{Rd}} + \frac{1}{1 - \frac{N_{Ed}}{N_{cr}}} \frac{N_{Ed} e_0}{M_{Rd}} + \frac{1}{1 - \frac{N_{Ed}}{N_{cr}}} \frac{C_m M_{Ed}}{M_{Rd}} \leq 1.0 \tag{3.43}$$

Previous considerations are based on the elastic second order theory. However, there is also significant influence of inelastic material behaviour affecting cross-section resistance interaction of Class 1 and 2 cross-sections as well as the member second order effect. If the member is only compressed, the flexural buckling resistance $N_{b,Rd} = \chi N_{pl,Rd}$ can be determined from Equation (3.43). Subsequently, the initial equivalent geometric imperfection e_0 is given by Equation (3.44) and then, Equation (3.43) can be rearranged into Equation (3.45).

$$e_0 = \frac{(1-\chi)\left(1-\frac{\chi N_{\mathrm{pl,Rd}}}{N_{\mathrm{cr}}}\right)}{\chi}\frac{M_{\mathrm{el,Rd}}}{N_{\mathrm{pl,Rd}}} \tag{3.44}$$

$$\frac{N_{\mathrm{Ed}}}{\chi N_{\mathrm{pl,Rd}}} + \mu\frac{C_{\mathrm{m}}M_{\mathrm{Ed}}}{\left(1-\frac{N_{\mathrm{Ed}}}{N_{\mathrm{cr}}}\right)kM_{\mathrm{pl,Rd}}} \leq 1.0 \tag{3.45}$$

with

$$\mu = \frac{1-\frac{N_{\mathrm{Ed}}}{N_{\mathrm{cr}}}}{1-\frac{\chi N_{\mathrm{Ed}}}{N_{\mathrm{cr}}}} \tag{3.46}$$

where k is the coefficient covering in-plane elastic-plastic interaction between bending and compression.

3.11 Current beam-column design procedures

This chapter describes individual procedures for stainless steel beam-column design that are currently available. Firstly, the procedures given by European, American and Australian/New Zealand standards are described, procedures and comprehensive studies developed by researchers, containing both evaluation of the European standard procedures and new improvements of the beam-column design, follows.

3.11.10 Universities of Aveiro and Coimbra – Portugal

3.11.11 TU Graz – Austria

3.11.12 CTU in Prague – Czech Republic

3.11.13 Imperial College London – United Kingdom

3.11.14 University of Politècnica de Catalunya – Spain

3.11.1 EN 1993-1-4

Currently, the design procedure for stainless steel members loaded by compression and bending moment is given in EN 1993-1-4 [1]. The design standard adopts the general format of the interaction formulae used in ENV 1993-1-1 [58] for carbon steel. It is given by condition (3.47) and for members susceptible to lateral torsional buckling by condition (3.48) in addition to the previous one.

$$\frac{N_{\mathrm{Ed}}}{\left(N_{\mathrm{b,Rd}}\right)_{\mathrm{min}}} + k_{\mathrm{y}}\left(\frac{M_{\mathrm{y,Ed}} + N_{\mathrm{Ed}}e_{\mathrm{Ny}}}{\beta_{\mathrm{W,y}}\frac{W_{\mathrm{pl,y}}f_{\mathrm{y}}}{\gamma_{\mathrm{M1}}}}\right) + k_{\mathrm{z}}\left(\frac{M_{\mathrm{z,Ed}} + N_{\mathrm{Ed}}e_{\mathrm{Nz}}}{\beta_{\mathrm{W,z}}\frac{W_{\mathrm{pl,z}}f_{\mathrm{y}}}{\gamma_{\mathrm{M1}}}}\right) \leq 1.0 \qquad (3.47)$$

$$\frac{N_{\mathrm{Ed}}}{\left(N_{\mathrm{b,Rd}}\right)_{\mathrm{min,1}}} + k_{\mathrm{LT}}\left(\frac{M_{\mathrm{y,Ed}} + N_{\mathrm{Ed}}e_{\mathrm{Ny}}}{M_{\mathrm{b,Rd}}}\right) + k_{\mathrm{z}}\left(\frac{M_{\mathrm{z,Ed}} + N_{\mathrm{Ed}}e_{\mathrm{Nz}}}{\beta_{\mathrm{W,z}}\frac{W_{\mathrm{pl,z}}f_{\mathrm{y}}}{\gamma_{\mathrm{M1}}}}\right) \leq 1.0 \qquad (3.48)$$

where e_{Ny} and e_{Nz} are the shifts of the neutral axes of the effective cross-section in compression. $\beta_{\mathrm{w,i}} = 1$ for Class 1 and 2 cross-sections, $\beta_{\mathrm{w,i}} = W_{\mathrm{el,i}} / W_{\mathrm{pl,i}}$ for Class 3 cross-sections and $W_{\mathrm{eff,i}} / W_{\mathrm{pl,i}}$ for Class 4 cross-sections. $(N_{\mathrm{b,Rd}})_{\mathrm{min}}$ is the lowest value of $N_{\mathrm{b,Rd}}$ for the following four buckling modes: flexural buckling about the y axis; flexural buckling about the z axis; torsional buckling and torsional-flexural buckling. $(N_{\mathrm{b,Rd}})_{\mathrm{min,1}}$ is the smallest value of $N_{\mathrm{b,Rd}}$ for the following three buckling modes: flexural buckling about the z axis; torsional buckling and torsional-flexural buckling. $M_{\mathrm{b,Rd}}$ is the lateral torsional buckling resistance and k_{y}, k_{z} and k_{LT} are the interaction factors.

Determination of the interaction factors k_{y}, k_{z} and k_{LT} according to EN 1993-1-4 [1] is given by Equations (3.49), (3.50) and (3.51).

$$k_{\mathrm{y}} = 1.0 + 2\left(\bar{\lambda}_{\mathrm{y}} - 0.5\right)\frac{N_{Ed}}{N_{\mathrm{b,Rd,y}}} \qquad \text{but} \quad 1.2 \leq k_{\mathrm{y}} \leq 1.2 + 2\frac{N_{Ed}}{N_{\mathrm{b,Rd,y}}} \qquad (3.49)$$

$$k_z = 1.0 + 2(\bar{\lambda}_z - 0.5)\frac{N_{Ed}}{(N_{b,Rd,y})_{min,1}} \quad \text{but} \quad 1.2 \le k_y \le 1.2 + 2\frac{N_{Ed}}{(N_{b,Rd,y})_{min,1}} \tag{3.50}$$

$$k_{LT} = 1.0 \tag{3.51}$$

These interaction factor formulae have several simplifications. Firstly, the lower value of boundary conditions (k_y and $k_z \ge 1.2$) makes the design approach conservative for many members with low second order effect. In the case of negligible compressive force and dominant bending moment, the designed member will be used at 80 % of its bending capacity.

Secondly, there is no consideration of the moment distribution along the member length and uniform bending moment distribution is considered only. It is clear that the interaction of compressive force and non-uniform bending moment is more favourable than the interaction of the same compressive force and bending moment with the uniform moment diagram. This results in additional conservativeness of the design procedure in cases of non-uniform moment diagram.

Finally, the design procedure does not consider the strain hardening effect in bending and compression resistance.

3.11.2 ENV 1993-1-1

A proposal for combination of compressive force and bending moment of steel members was given in ENV 1993-1-1 [58] but this standard has been replaced by final Eurocodes. As was already mentioned, the procedure for stainless steel structures is based on this standard, although it was developed for carbon steel beam-columns design. So the verification conditions (3.52) and (3.53) are similar.

$$\frac{N_{Ed}}{\chi_{min} A \frac{f_y}{\gamma_{M1}}} + \frac{k_y(M_{y,Ed} + N_{Ed}e_{Ny})}{W_y \frac{f_y}{\gamma_{M1}}} + \frac{k_z(M_{z,Ed} + N_{Ed}e_{Nz})}{W_z \frac{f_y}{\gamma_{M1}}} \le 1.0 \tag{3.52}$$

$$\frac{N_{Ed}}{\chi_z A \frac{f_y}{\gamma_{M1}}} + \frac{k_{LT}(M_{y,Ed} + N_{Ed}e_{Ny})}{\chi_{LT} W_y \frac{f_y}{\gamma_{M1}}} + \frac{k_z(M_{z,Ed} + N_{Ed}e_{Nz})}{W_z \frac{f_y}{\gamma_{M1}}} \le 1.0 \tag{3.53}$$

In this case, the interaction factors are given by Equations (3.54) to (3.56).

$$k_y = 1 - \frac{\mu_y N_{Ed}}{\chi_y A f_y} \quad \text{but} \quad k_y \le 1.5 \tag{3.54}$$

$$k_z = 1 - \frac{\mu_z N_{Ed}}{\chi_z A f_y} \qquad \text{but} \qquad k_z \leq 1.5 \tag{3.55}$$

$$k_{LT} = 1 - \frac{\mu_{LT} N_{Ed}}{\chi_z A f_y} \qquad \text{but} \qquad k_{LT} \leq 1.5 \tag{3.56}$$

with μ_y, μ_z and μ_{LT} given by Equations (3.57) to (3.59).

$$\mu_y = \bar{\lambda}_y(2\beta_{My} - 4) + \left[\frac{W_{pl,y} - W_{el,y}}{W_{el,y}}\right] \qquad \text{but} \qquad \mu_y \leq 0.9 \tag{3.57}$$

$$\mu_z = \bar{\lambda}_z(2\beta_{Mz} - 4) + \left[\frac{W_{pl,z} - W_{el,z}}{W_{el,z}}\right] \qquad \text{but} \qquad \mu_z \leq 0.9 \tag{3.58}$$

$$\mu_{LT} = 0.15\bar{\lambda}_z\beta_{M,LT} - 0.15 \qquad \text{but} \qquad \mu_{LT} \leq 0.9 \tag{3.59}$$

where β_{My} and β_{Mz} are the equivalent flexural buckling factors for uniform bending moment and $\beta_{M,LT}$ is the equivalent linear moment factor for the lateral torsional buckling. All of these factors are determined by Equation (3.60) in the cases of uniform and linear moment diagram.

$$\beta_{M,i} = 1.8 - 0.7\psi_i \tag{3.60}$$

Determination of the interaction factors is quite different in comparison with the EN 1993-1-4 [1]. In this method, lower bound of the interaction factors is not introduced and moment distribution along the member length is covered, so less conservative results may be expected in terms of bending moment distribution. Suitability of the procedure for stainless steel was not verified, therefore, it may leads to unsafe predictions.

3.11.3 EN 1993-1-1 Method 1

There are two other procedures given by current standard for carbon steel EN 1993-1-1 [2], Method 1 and Method 2 (resp. Annex A and Annex B of EN 1993-1-1). This chapter deals with Method 1. Method 1 was developed by Boissonnade et al. [59] in 2004. The resistance verification according to Method 1 is given by Equations (3.61) and (3.62).

$$\frac{N_{Ed}}{\frac{\chi_y N_{Rk}}{\gamma_{M1}}} + k_{yy}\frac{M_{y,Ed} + \Delta M_{y,Ed}}{\frac{\chi_{LT} M_{y,Rk}}{\gamma_{M1}}} + k_{yz}\frac{M_{z,Ed} + \Delta M_{z,Ed}}{\frac{M_{z,Rk}}{\gamma_{M1}}} \leq 1.0 \tag{3.61}$$

$$\frac{N_{\mathrm{Ed}}}{\frac{\chi_{\mathrm{z}} N_{\mathrm{Rk}}}{\gamma_{\mathrm{M1}}}} + k_{\mathrm{zy}} \frac{M_{\mathrm{y,Ed}} + \Delta M_{\mathrm{y,Ed}}}{\frac{\chi_{\mathrm{LT}} M_{\mathrm{y,Rk}}}{\gamma_{\mathrm{M1}}}} + k_{\mathrm{zz}} \frac{M_{\mathrm{z,Ed}} + \Delta M_{\mathrm{z,Ed}}}{\frac{M_{\mathrm{z,Rk}}}{\gamma_{\mathrm{M1}}}} \leq 1.0 \tag{3.62}$$

where k_{ij} are the interaction factors.

Researchers [59] were focused on a more accurate determination of the interaction factors based mainly on analytical expressions. Because the determination of these factors is quite complex and interaction factor equations are divided into two groups depending on the cross-section Class (Classes 1, 2 and Classes 3, 4), determination for compressive force and uniaxial major axis bending for Classes 1 and 2 is shown in this section only. The interaction factors are given by Equations (3.63) and (3.64).

$$k_{\mathrm{yy}} = C_{\mathrm{my}} C_{\mathrm{mLT}} \frac{\mu_{\mathrm{y}}}{1 - \frac{N_{\mathrm{Ed}}}{N_{\mathrm{cr,y}}}} \frac{1}{C_{\mathrm{yy}}} \tag{3.63}$$

$$k_{\mathrm{zy}} = C_{\mathrm{my}} C_{\mathrm{mLT}} \frac{\mu_{\mathrm{z}}}{1 - \frac{N_{\mathrm{Ed}}}{N_{\mathrm{cr,y}}}} \frac{1}{C_{\mathrm{zy}}} 0.6 \sqrt{\frac{w_{\mathrm{y}}}{w_{\mathrm{z}}}} \tag{3.64}$$

with

$$\mu_{\mathrm{i}} = \frac{1 - \frac{N_{\mathrm{Ed}}}{N_{\mathrm{cr,i}}}}{1 - \chi_{\mathrm{i}} \frac{N_{\mathrm{Ed}}}{N_{\mathrm{cr,i}}}} \tag{3.65}$$

$$C_{\mathrm{my}} = C_{\mathrm{my,0}} + \left(1 - C_{\mathrm{my,0}}\right) \frac{\sqrt{\varepsilon_{\mathrm{y}}} \alpha_{\mathrm{LT}}}{1 + \sqrt{\varepsilon_{\mathrm{y}}} \alpha_{\mathrm{LT}}} \tag{3.66}$$

$$C_{\mathrm{mLT}} = C_{\mathrm{my}}^2 \frac{\alpha_{\mathrm{LT}}}{\sqrt{\left(1 - \frac{N_{\mathrm{Ed}}}{N_{\mathrm{cr,z}}}\right)\left(1 - \frac{N_{\mathrm{Ed}}}{N_{\mathrm{cr,T}}}\right)}} \geq 1.0 \tag{3.67}$$

where

$$w_{\mathrm{i}} = \frac{W_{\mathrm{pl,i}}}{W_{\mathrm{el,i}}} \leq 1.5 \tag{3.68}$$

$$\varepsilon_{\mathrm{y}} = \frac{M_{\mathrm{y,Ed}}}{N_{\mathrm{Ed}}} \frac{A}{W_{\mathrm{el,y}}} \tag{3.69}$$

$$C_{\mathrm{my,0}} = 0.79 + 0.21 \psi_{\mathrm{y}} + 0.36 \left(\psi_{\mathrm{y}} - 0.33\right) \frac{N_{\mathrm{Ed}}}{N_{\mathrm{cr,y}}} \tag{3.70}$$

The other coefficients not described here can be found in Annex A of EN 1993-1-1 [2]. Equation (3.70) for the calculation of $C_{my,0}$ contains N_{Ed} / $N_{cr,y}$ ratio in order to include the second order effect of compressive force influence on bending moment. That makes this procedure rare, because other procedures neglect it.

As could be seen, determination of the interaction factors according to EN 1993-1-1 Method 1 [2] is complex and lengthy. There is also no limitation in respect to the cross-section type. On the other hand, due to many coefficients and factors, the proposal is susceptible to mistakes in calculation.

3.11.4 EN 1993-1-1 Method 2

As mentioned above, there are two procedures for the design of steel members loaded by compressive force and bending moment provided by EN 1993-1-1 [2]. Method 2 was developed by Greiner and Lindner [60] in 2006 and the researchers were focused on more accurate determination of the interaction factors too. Method 2 is given by Annex B of EN 1993-1-1 [2], so the resistance verification conditions are the same as for Method 1.

The interaction factors are divided into several groups and limited to open I cross-sections and rectangular hollow cross-sections. They depends on the cross-section Class (Classes 1, 2 and Classes 3, 4) and whether the members are susceptible to torsion or not. Herein, only the case of compressive force and uniaxial bending moment interaction of Class 1 and 2 cross-section members is described. Interaction factor for members not susceptible to torsional deformations (presence of lateral torsional buckling) k_{yy} is given by equation (3.71) and k_{zy} is equal to $0.6k_{yy}$, for members susceptible to torsional deformations are both interaction factors given by equations (3.71) to (3.73) with equivalent bending moment C_{my} according to [57], see Equation (3.74).

$$k_{yy} = C_{my}\left[1 + \left(\bar{\lambda}_y - 0.2\right)\frac{N_{Ed}}{\frac{\chi_y N_{Rk}}{\gamma_{M1}}}\right] \quad \text{but} \quad k_{yy} \leq C_{my}\left[1 + 0.8\frac{N_{Ed}}{\frac{\chi_y N_{Rk}}{\gamma_{M1}}}\right] \tag{3.71}$$

then for $\bar{\lambda}_z \geq 0.4$:

$$k_{zy} = \left[1 - \frac{0.1\bar{\lambda}_z}{(C_{mLT} - 0.25)}\frac{N_{Ed}}{\frac{\chi_z N_{Rk}}{\gamma_{M1}}}\right] \quad \text{but} \quad k_{zy} \geq C_{my}\left[1 - \frac{0.1}{(C_{mLT} - 0.25)}\frac{N_{Ed}}{\frac{\chi_z N_{Rk}}{\gamma_{M1}}}\right] \tag{3.72}$$

and for $\bar{\lambda}_z < 0.4$:

$$k_{zy} = 0.6 + \bar{\lambda}_z \qquad \text{but} \quad k_{zy} \leq C_{my}\left[1 - \frac{0.1}{(C_{mLT} - 0.25)}\frac{N_{Ed}}{\frac{\chi_z N_{Rk}}{\gamma_{M1}}}\right] \tag{3.73}$$

with

$$C_{my} = 0.6 + 0.4\psi_y \geq 0.4 \tag{3.74}$$

where $\bar{\lambda}_i$ is the non-dimensional slenderness with regard to each axis.

These are all the equations necessary for the design of stainless steel beam-columns. In the comparison with Method 1, this proposal is much more simple. Consideration of the non-uniform bending moment distribution is included in Method 2 too and it is given by coefficient C_{my}. Equation (3.74) shows the case of linearly distributed bending moment along the member length.

3.11.5 EN 1993-1-1 General Method

EN 1993-1-1 [2] provides another, alternative design approach for steel members loaded by combination of compressive force and bending moment, which enables complex solutions of steel structures stability. This method could be also used when the other EN 1993-1-1 procedures, described above, do not apply. It allows also verification of the resistance for members subjected to lateral and lateral torsional buckling for following structural components:

- single members, built-up or not, uniform or not, with complex support conditions or not, or
- plane frames or sub-frames composed of such members,

which are subjected to compression and/or uniaxial bending in the plane, but which do not contain plastic hinges. The General Method is based on GNIA, geometrically non-linear analysis with both sway and bow imperfections (Figure 3.7). It is designed primarily to cover flexural buckling ($P - \delta$) and sway ($P - \Delta$) effect in plane of a structure.

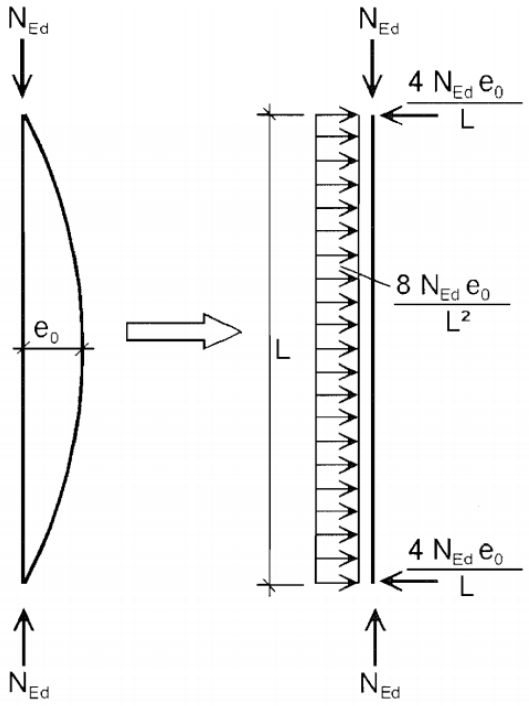

Figure 3.7 *Initial bow imperfection [2].*

The initial bow imperfection e_0 can be generally obtained from Table 3.10 provided by EN 1993-1-1 [2], depending on the buckling curve and type of analysis.

Table 3.10 *Design values of the initial bow imperfection e_0 / L [2].*

Buckling curve	e_0 / L	
	Elastic analysis	Plastic analysis
a_0	1 / 350	1 / 300
a	1 / 300	1 / 250
b	1 / 250	1 / 200
c	1 / 200	1 / 150
d	1 / 150	1 / 100

Nevertheless, the values provided by EN 1993-1-1 [2] could be conservative for some members, so the e_0 value can be calculated for each member separately by Equation (3.75).

$$e_0 = \alpha\left(\bar{\lambda} - \bar{\lambda}_0\right)\frac{M_{\mathrm{Rk}}}{N_{\mathrm{Rk}}}\frac{1 - \frac{\chi\bar{\lambda}^2}{\gamma_{\mathrm{M1}}}}{1 - \chi\bar{\lambda}^2} \tag{3.75}$$

However, new revision of carbon steel design standard prEN 1993-1-1 [61] distinguishes initial bow imperfection for flexural buckling and for lateral torsional buckling. Initial bow imperfection for the case of flexural buckling $e_{0,new}$ should be calculated according to Equation (3.76), whereas for second order analysis taking into account lateral torsional buckling $e_{0,LT,new}$ according to Equation (3.77).

$$e_{0,\mathrm{new}} = \frac{\alpha}{\varepsilon}\beta L \tag{3.76}$$

$$e_{0,\mathrm{LT,new}} = \beta_{\mathrm{LT}}\frac{L}{\varepsilon} \tag{3.77}$$

where β is the reference relative bow imperfection according to Table 3.11 and β_{LT} is the reference relative bow imperfection for lateral torsional buckling according to Table 3.12.

Table 3.11 *Reference relative bow imperfection β [61].*

Buckling about axis	Elastic cross-section verification	Plastic cross-section verification
y - y	1 / 110	1 / 75
z - z	1 / 200	1 / 68

Table 3.12 *Reference relative bow imperfection β_{LT} for lateral torsional buckling [61].*

Cross-section	Condition	Elastic cross-section verification	Plastic cross-section verification
rolled	$h / b \leq 2.0$	1 / 110	1 / 75
	$h / b > 2.0$	1 / 200	1 / 68
welded	$h / b \leq 2.0$	1 / 200	1 / 150
	$h / b > 2.0$	1 / 150	1 / 100

According to General Method, out-of-plane buckling condition for any structural component is given by Equation (3.78).

$$\frac{\chi_{\mathrm{op}}\alpha_{\mathrm{ult,k}}}{\gamma_{\mathrm{M1}}} \geq 1.0 \tag{3.78}$$

where χ_{op} is the reduction factor for the non-dimensional slenderness $\bar{\lambda}_{\mathrm{op}}$, to take account of lateral and lateral torsional buckling, $\alpha_{ult,k}$ is the minimum load amplifier of the design loads to reach the characteristic resistance of the most critical cross-section of the structural component considering its in-plane behaviour without taking lateral or lateral torsional buckling into account, however, accounting for all effects due to in-plane geometrical deformation and imperfections, global and local, where relevant.

The global non-dimensional slenderness $\bar{\lambda}_{\mathrm{op}}$ for the structural component should be determined by Equation (3.79).

$$\bar{\lambda}_{\mathrm{op}} = \sqrt{\frac{\alpha_{\mathrm{ult,k}}}{\alpha_{\mathrm{cr,op}}}} \tag{3.79}$$

where $\alpha_{cr,op}$ is the minimum amplifier for the in-plane design loads to reach the elastic critical resistance of the structural component with regards to lateral or lateral torsional buckling without accounting for in-plane flexural buckling.

The reduction factor χ_{op} can be determined from either of the following methods:

- the minimum value of χ (out of plane flexural buckling χ_z; torsional buckling χ_T and torsional flexural buckling χ_{TF}) or χ_{LT} using the global non-dimensional slenderness $\bar{\lambda}_{\mathrm{op}}$ which leads to Equation (3.80);
- the value interpolated between the values χ or χ_{LT} as determined in the previous method, by using the formula for $\alpha_{ult,k}$ corresponding to the critical cross-section which leads to Equation (3.81).

$$\frac{N_{\mathrm{Ed}}}{\frac{N_{\mathrm{Rk}}}{\gamma_{\mathrm{M1}}}} + \frac{M_{\mathrm{Ed}}^{\mathrm{II}}}{\frac{M_{\mathrm{y,Rk}}}{\gamma_{\mathrm{M1}}}} \leq \chi_{\mathrm{op}} \tag{3.80}$$

$$\frac{N_{\mathrm{Ed}}}{\chi\frac{N_{\mathrm{Rk}}}{\gamma_{\mathrm{M1}}}} + \frac{M_{\mathrm{Ed}}^{\mathrm{II}}}{\chi_{\mathrm{LT}}\frac{M_{\mathrm{y,Rk}}}{\gamma_{\mathrm{M1}}}} \leq 1.0 \tag{3.81}$$

where $M_{\mathrm{Ed}}^{\mathrm{II}}$ is the bending moment calculated by GNIA considering the second-order effect on a structure with imperfections.

Because this method is based on GNIA, which is suitable only for materials with linear stress-strain diagram, some shortcomings could be expected in the case of stainless steel due to its non-linear stress-strain diagram.

3.11.6 EN 1999-1-1

EN 1999-1-1 [62] is the design standard for aluminium alloys but the design approach for the case of compressive force and bending moment combination, described by Höglund and Tindall [63], may be suitable for stainless steel too. Design procedure given by EN 1999-1-1 [62] for aluminium alloys has a very different approach. The verification conditions are shown below, Equation (3.82) for the case of compressive force and uniaxial major axis bending moment and Equation (3.83) for the case of compressive force and minor axis or bi-axial bending moment.

$$\left(\frac{N_{\mathrm{Ed}}}{\omega_{\mathrm{x}} N_{\mathrm{y,b,Rd}}}\right)^{\xi_{\mathrm{yc}}} + \frac{M_{\mathrm{y,Ed}}}{M_{\mathrm{y,Rd}}} \leq 1.0 \tag{3.82}$$

$$\left(\frac{N_{\mathrm{Ed}}}{\omega_{\mathrm{x}} N_{\mathrm{z,b,Rd}}}\right)^{\eta_{\mathrm{c}}} + \left(\frac{M_{\mathrm{y,Ed}}}{\omega_{\mathrm{x,LT}} M_{\mathrm{y,b,Rd}}}\right)^{\gamma_{\mathrm{c}}} + \left(\frac{M_{\mathrm{z,Ed}}}{M_{\mathrm{z,Rd}}}\right)^{\xi_{\mathrm{zc}}} \leq 1.0 \tag{3.83}$$

with $\eta_{\mathrm{c}} = 0.8$ or may alternatively be taken as $\eta_{\mathrm{c}} = \eta_0 \chi_z$ but $\eta_{\mathrm{c}} \geq 0.8$ (3.84)

$\xi_{\mathrm{yc}} = 0.8$ or may alternatively be taken as $\xi_{\mathrm{yc}} = \xi_0 \chi_y$ but $\xi_{\mathrm{yc}} \geq 0.8$ (3.85)

$\xi_{\mathrm{zc}} = 0.8$ or may alternatively be taken as $\xi_{\mathrm{zc}} = \xi_0 \chi_z$ but $\xi_{\mathrm{zc}} \geq 0.8$ (3.86)

being $\eta_0 = 1.0$ or may alternatively be taken as $\eta_0 = \alpha_{\mathrm{z}}^2$ but $1 \leq \eta_0 \leq 2$ (3.87)

$\gamma_0 = 1.0$ or may alternatively be taken as $\gamma_0 = \alpha_{\mathrm{z}}^2$ but $1 \leq \gamma_0 \leq 1.56$ (3.88)

$\xi_0 = 1.0$ or may alternatively be taken as $\xi_0 = \alpha_{\mathrm{y}}^2$ but $1 \leq \xi_0 \leq 1.56$ (3.89)

and
$$\alpha_{\mathrm{i}} = \frac{M_{\mathrm{i,Rd}}}{W_{\mathrm{i,el}} \frac{f_{\mathrm{y}}}{\gamma_{\mathrm{M0}}}} \tag{3.90}$$

Then, there are two more factors that are very important in this proposal, these are ω_{x} and $\omega_{\mathrm{x,LT}}$ in Equations (3.82) and (3.83), respectively. There are no interaction factors as in the procedures before, but factors ω_{x} and $\omega_{\mathrm{x,LT}}$ are used instead. They are calculated by following formulae.

$$\omega_{\mathrm{x}} = \frac{1}{\chi + (1-\chi)\sin\frac{\pi x_{\mathrm{s}}}{l_{\mathrm{cr}}}} \tag{3.91}$$

$$\omega_{\mathrm{x,LT}} = \frac{1}{\chi_{\mathrm{LT}} + (1-\chi_{\mathrm{LT}})\sin\frac{\pi x_{\mathrm{s}}}{l_{\mathrm{cr}}}} \tag{3.92}$$

where l_{cr} is the buckling member length, x_{s} is the distance from the critical cross-section to a pin-ended support or a flexure point of the deflection curve for elastic flexural buckling. The distance is calculated by Equation (3.93) where $M_{\mathrm{Ed,1}}$ and $M_{\mathrm{Ed,2}}$ are end moments.

$$\cos\frac{\pi x_{\mathrm{s}}}{l_{\mathrm{cr}}} = \frac{\left(M_{\mathrm{Ed,1}} - M_{\mathrm{Ed,2}}\right)}{M_{\mathrm{Rd}}} \frac{N_{\mathrm{Rd}}}{N_{\mathrm{Ed}}} \frac{1}{\frac{1}{\chi} - 1} \qquad \text{but} \qquad x_{\mathrm{s}} \geq 0 \tag{3.93}$$

In the proposal it is not considered use of the member by compressive force and bending moment separately but position of the most critical cross-section considering compressive force and bending moment is calculated firstly. Then, the cross-section is verified using coefficients ω_{x} and $\omega_{\mathrm{x,LT}}$.

However, there are also factors η_{c}, ξ_{yc}, ξ_{zc} and γ_{c} in Equations (3.82) and (3.83) and related coefficients η_0, ξ_0 and γ_0. With regards to Eurocode, these factors are given by Equations (3.84) to (3.89) but as could be seen, there are two values for each coefficient, except γ_{c}, that could be consider. One is a more accurate calculation by a formula and the second is a fixed conservative number.

The procedure has an interesting idea with investigating of the critical cross-section where the combination of compressive force and bending moment leads to the highest use of the cross-section. Nevertheless, the procedure contains several coefficients and the way of calculation differs significantly from the rules for steel members. Every moment distribution is covered by ω_{x} factor and exponents in the interaction factor formulae account for the influence of plasticity and local buckling.

There has been no solid background published [63] for the formulae and the development is therefore not clear. However, based on the investigation of Höglund [64] the procedure is in draft for a next revision of EN 1993-1-3 [65] for cold-formed steel.

3.11.7 SEI/ASCE 8-02

Except the European standards, there are other codified procedures for stainless steel beam-column design. One of them is the American specification SEI/ASCE 8-02 [52]. It was derived based on the second order theory of elasticity and the interaction formula is given by Equation (3.94).

$$\frac{N_{\mathrm{Ed}}}{N_{\mathrm{b,n}}} + \frac{C_{\mathrm{m}} M_{\mathrm{Ed}}}{M_{\mathrm{n}} \alpha_{\mathrm{n}}} \leq 1 \tag{3.94}$$

where $N_{\mathrm{b,n}}$ is the column buckling resistance calculated according to Clause 3.4 of SEI/ASCE 8-02 [52], M_{n} is the bending resistance calculated according to Clause 3.3.1.1 of SEI/ASCE [52], C_{m} is the equivalent moment factor and α_{n} is the amplification factor calculated as $(1 - N_{\mathrm{Ed}}/N_{\mathrm{cr}})$.

Non-linear material behaviour of stainless steel is introduced to the $N_{\mathrm{b,n}}$ column buckling resistance by the utilisation of the tangent modulus approach. SEI/ASCE 8-02 [52] neglects plasticity in the cross-section bending capacity M_{n} determination which is given by elastic moment capacity for stocky cross-sections and reduced elastic moment capacity for slender cross-sections.

For more information about the stainless steel beam-column design according to American specification see SEI/ASCE 8-02 [52].

3.11.8 AS/NZS 4673

Another procedure for stainless steel beam-column design is given by Australian/New Zealand standard AS/NZS 4673 [53]. The interaction formula is very similar to the American SEI/ASCE 8-02 [52], see Equation (3.95).

$$\frac{N_{\mathrm{Ed}}}{N_{\mathrm{b,a}}} + \frac{C_{\mathrm{m}} M_{\mathrm{Ed}}}{M_{a} \alpha_{\mathrm{n}}} \leq 1 \tag{3.95}$$

where $N_{\mathrm{b,a}}$ is the column buckling resistance and M_{a} is the bending moment resistance.

However, both column buckling and final resistances are calculated differently. Column buckling resistance $N_{b,a}$ is calculated according to alternative explicit method developed by Rasmussen and Rondal [27], [66] based on the Perry-Robertson buckling formulation considering different imperfection parameters regarding to stainless steel grade. Bending moment resistance calculation considers the same in-elastic reserve capacity but the use of full plastic moment capacity is allowed.

To get more information about the stainless steel beam-column design according to Australian/New Zealand see AS/NZS 4673 [53].

3.11.9 Technical Research Centre of Finland VTT – Finland

The very first research of stainless steel beam-columns was (at least as the Author is aware) made at the Technical Research Centre in Finland VTT in 90s. Researchers Talja and Salmi [67] investigated accuracy of the design procedures of the only existing design procedure ENV 1993-1-1 [58] for carbon steel at that time. Information about the used specimens is shown in Table 3.13.

Table 3.13 *Member information used in Talja and Salmi´s research [67].*

Stainless steel group	Austenitic
Cross-section	Cold-formed RHS
Cross-section Class	1 and 2
End-moment ratio	1

ENV 1993-1-1 [58] showed generally inaccurate and unsafe predictions in comparison with the experiment results. Therefore, Talja and Salmi proposed a small modification of ENV 1993 1-1 [58] using the same interaction formulae (Equations (3.52) and (3.53)) just without the upper bound of the interaction factor. Then the interaction factors adjusted for stainless steel are given by Equations (3.96) and (3.97). Values of μ_i are calculated as described in Chapter 3.11.2.

$$k_y = 1 - \frac{\mu_y N_{Ed}}{\chi_y A f_y} \tag{3.96}$$

$$k_z = 1 - \frac{\mu_z N_{Ed}}{\chi_z A f_y} \tag{3.97}$$

Based on the results of Talja and Salmi´s research [67], this modification should leads to more accurate and safe results, mainly in the case of slender members loaded mostly by compression.

3.11.10 Universities of Aveiro and Coimbra – Portugal

In Portugal, two universities cooperated in the stainless steel beam-columns investigation, namely University of Aveiro and University of Coimbra. Researchers Lopes et al. [68] made a numerical study and developed a new proposal. There are two main parts of the research:

- stainless steel members are laterally and torsionally restrained along their length - lateral torsional buckling cannot occur;
- stainless steel members are not restrained along their length - lateral torsional buckling can occur.

The numerical study considered all three stainless steel groups (austenitic, ferritic and duplex) but in [68] only results for austenitic stainless steel beam-columns are shown. Some information about considered members and loading states are summarised in Table 3.14. The weak part of the numerical research is that the stress-strain diagram was used as defined in EN 1993-1-2 [69] for the case of fire. Despite the temperature of 20 °C was assumed, the stress-strain relationship differs significantly from the more accurate Ramberg-Osgood definition.

Table 3.14 *Member information used in Lopes et al. research [68].*

Stainless steel group	Austenitic, ferritic, duplex
Cross-section	Welded HEA and HEB
Cross-section Class	1 and 2
Non-dimensional slenderness range	From 0.37 to 1.45
End-moment ratio	1, 0, -1

Beam-columns without lateral torsional buckling

For members without lateral torsional buckling, there was considered a case of compressive force with flexural buckling and bending moment around the major axis (the member was restrained to the minor axis) and a case of compressive force with flexural buckling and bending around the minor axis (the element was restrained to the major axis).

As was mentioned before, Lopes et al. [68] developed a new proposal for stainless steel beam-column design. In the proposal, the verification condition is given by Equation (3.47) but the formulae for the interaction factors were modified and they are given by Equations (3.98) and (3.99).

$$k_{\mathrm{y}} = 1 - \frac{\mu_{\mathrm{y}} N_{\mathrm{Ed}}}{\chi_{\mathrm{y}} A \frac{f_{\mathrm{y}}}{\gamma_{\mathrm{M1}}}} \quad \text{with} \quad k_{\mathrm{y}} \leq 1.5 \quad \text{and} \quad k_{\mathrm{y}} \geq \mu_{\mathrm{y}} - 0.7 \tag{3.98}$$

$$k_{\mathrm{z}} = 1 - \frac{\mu_{\mathrm{z}} N_{\mathrm{Ed}}}{\chi_{\mathrm{z}} A \frac{f_{\mathrm{y}}}{\gamma_{\mathrm{M1}}}} \quad \text{with} \quad k_{\mathrm{y}} \leq 1.5 \quad \text{and} \quad k_{\mathrm{z}} \geq \mu_{\mathrm{z}} - 0.7 \tag{3.99}$$

being

$$\mu_{\mathrm{y}} = \left(0.97\beta_{\mathrm{M,y}} - 2.11\right)\bar{\lambda}_{\mathrm{y}} + 0.44\beta_{M,y} + 0.09 \tag{3.100}$$

$$\mu_{\mathrm{z}} = \left(1.09\beta_{\mathrm{M,z}} - 2.32\right)\bar{\lambda}_{\mathrm{z}} + 0.29\beta_{M,z} + 0.48 \tag{3.101}$$

with

$$\mu_{\mathrm{i}} \leq 1.0 \quad \text{if} \quad \bar{\lambda}_{\mathrm{i}} \leq 0.3 \tag{3.102}$$

$$\mu_{\mathrm{i}} \leq 0.9 \quad \text{if} \quad \bar{\lambda}_{\mathrm{i}} > 0.3 \tag{3.103}$$

where $\beta_{\mathrm{M,i}}$ is the equivalent uniform bending moment factor as defined in ENV 1993-1-1 [58], see Equation (3.60).

Beam-columns with lateral torsional buckling

For members where lateral torsional buckling may occur, the formula is the same as in EN 1993-1-4 [1] again, see Equation (3.48). Only the interaction factor k_{LT} is modified and it is given by Equation (3.104).

$$k_{\mathrm{LT}} = 1 - \frac{\mu_{\mathrm{LT}} N_{\mathrm{Ed}}}{\chi_{\mathrm{z}} A \frac{f_{\mathrm{y}}}{\gamma_{\mathrm{M1}}}} \quad \text{with} \quad k_{\mathrm{LT}} \leq 1.5 \quad \text{and} \quad k_{\mathrm{LT}} \geq \mu_{\mathrm{LT}} - 0.7 \tag{3.104}$$

being

$$\mu_{\mathrm{LT}} = \left(-0.07\beta_{\mathrm{M,z}} - 0.07\right)\bar{\lambda}_{\mathrm{z}} + 0.6\beta_{\mathrm{M,LT}} - 0.1 \tag{3.105}$$

with

$$\mu_y \leq 1.0 \quad \text{if} \quad \bar{\lambda}_y \leq 0.3 \tag{3.106}$$

$$\mu_y \leq 0.9 \quad \text{if} \quad \bar{\lambda}_y > 0.3 \tag{3.107}$$

where $\beta_{M,LT}$ is calculated by Equation (3.60).

Summary

Lopes, Real and da Silva made the numerical study and developed the new proposal [68]. The procedure provides better results in comparison with the proposals given by EN 1993-1-1 [2] (Method 1 and Method 2). However, the study and verification was made for Class 1 and 2 I cross-sections only. Therefore the verification for the other cross-section geometries and cross-section Classes is necessary. Also, the used material model derived primarily for steel in fire is not accurate enough for description of stainless steel at the room temperature.

3.11.11 TU Graz – Austria

Other research was carried out at the University in Graz, Austria. Greiner and Kettler [70] made a study of stainless steel beam-columns and tried to improve the interaction factors for stainless steel members. The verification conditions were considered the same as for Method 2 given by EN 1993-1-1 [2] for carbon steel (Equations (3.61) and (3.62)), so only the interaction factors were changed. Stainless steel grades, cross-sections, load conditions and other information about the used members in research are summarized in Table 3.15.

Table 3.15 *Member information used in Greiner and Kettler´s research [70].*

Stainless steel group	Austenitic, duplex
Cross-section	Welded IPE Cold-formed RHS and SHS
Cross-section Class	1 and 2
End-moment ratio	1

Greiner and Kettler [70] derived interaction curves firstly, the axial force was applied for certain value of N_{Ed}, then the additional bending moment was applied and increased up to M_{Ed} value given by Equation (3.109).

$$N_{\mathrm{Ed}} = \bar{n}_{\mathrm{i}} \chi_{\mathrm{i}} A f_{\mathrm{y}} \tag{3.108}$$

$$M_{\mathrm{Ed,i}} = R_{\mathrm{ult,i}} \chi_{\mathrm{LT}} W_{\mathrm{pl,i}} f_{\mathrm{y}} \tag{3.109}$$

where R_{ult} is the load proportionality factor at the ultimate limit point.

$$\bar{n}_{\mathrm{i}} = \frac{N_{Ed}}{\chi N_{\mathrm{pl,Rd,i}}} = \frac{N_{Ed}}{\chi A f_{\mathrm{y}}} \tag{3.110}$$

$$\bar{m}_{\mathrm{i}} = \frac{M_{Ed,i}}{\chi_{\mathrm{LT}} M_{\mathrm{pl,Rd,i}}} = \frac{M_{Ed,i}}{\chi_{\mathrm{LT}} W_{\mathrm{pl,i}} f_{\mathrm{y}}} \tag{3.111}$$

Then, the interaction factor k_{i} was calculated from the Equation (3.112) which is related to $\bar{n}_{\mathrm{i}}$.

$$k_{\mathrm{i}} = \frac{1 - \bar{n}_{\mathrm{i}}}{R_{\mathrm{ult,i}}} \tag{3.112}$$

$$R_{\mathrm{ult,i}} = k_{\mathrm{i}} \bar{m}_{\mathrm{i}} \tag{3.113}$$

Proposed interaction factors formulae are linear or bilinear approximations of the calculated interaction curves. Four types of interaction factors formulae were developed for different mechanical behaviour and cross-sections. The developed equations for determination of interaction factors for flexural and lateral torsional buckling are given by Equations (3.114) to (3.118).

k_{y}	I cross-sections	$k_{\mathrm{y}} = 0.9 + 2.2\bar{n}_{\mathrm{y}}\left(\bar{\lambda}_{\mathrm{y}} - 0.4\right) \leq 0.9 + 2.42\bar{n}_{\mathrm{y}}$	(3.114)
$k_{\mathrm{y}}, k_{\mathrm{z}}$	CHS, welded RHS	$k_{\mathrm{i}} = 0.9 + 2.2\bar{n}_{\mathrm{i}}\left(\bar{\lambda}_{\mathrm{i}} - 0.4\right) \leq 0.9 + 2.42\bar{n}_{\mathrm{i}}$	(3.115)
$k_{\mathrm{y}}, k_{\mathrm{z}}$	Cold-formed RHS	$k_{\mathrm{i}} = 0.9 + 3.5(\bar{n}_{\mathrm{i}})^{1.8}\left(\bar{\lambda}_{\mathrm{i}} - 0.5\right) \leq 0.9 + 1.75(\bar{n}_{\mathrm{i}})^{1.8}$	(3.116)
k_{z}	I cross-sections	$k_{\mathrm{z}} = 1.2 + 1.5\bar{n}_{\mathrm{z}}\left(\bar{\lambda}_{\mathrm{z}} - 0.7\right) \leq 1.2 + 1.95\bar{n}_{\mathrm{z}}$	(3.117)
k_{LT}	I cross-sections	$k_{\mathrm{LT}} = 1 - 0.4(\bar{n}_{\mathrm{z}})^{1.3}$	(3.118)

The numerical study and the new formulae for interaction factors for beam-columns proposed by Greiner and Kettler [70] was described. The study covered wide range of practical cross-section types, but many parameters were not investigated. For example, only cross-sections of Class 1 and Class 2 were considered (beam elements were used in the FE models), so the suitability of

proposed approach for both Class 3 and Class 4 is not verified. Further, the load conditions of biaxial and non-uniform bending moment diagrams were not verified. It can be noted, that the new interaction factors formulae provide good results but only for a small scope of members and cross-sections, so a verification of other cross-sections and loading conditions is necessary.

3.11.12 CTU in Prague – Czech Republic

Jandera and Syamsuddin [71] made a comparison of existing interaction formulae. In addition, a small modification of procedure developed by Lopes, Real and Silva [68] (Chapter 3.11.10) was proposed. Information of considered members is given in Table 3.16.

Table 3.16 *Member information used in Jandera and Syamsuddin´s research [71].*

Stainless steel group	Austenitic, ferritic, duplex
Cross-section	Welded I Cold-formed RHS and SHS
Cross-section Class	1, 2 and 4
Non-dimensional slenderness range	From 0.31 to 1.67
End-moment ratio	1, 0, -1

Herein, the accuracy is evaluated by the ratio k / k_{FEM} where k is the interaction factor calculated according to corresponding design procedure and k_{FEM} is the interaction factor derived from a FEM resistance. The value greater than unity indicates safe result and lower than unity unsafe result. Then the standard deviation is also given. The comparison is summarized in Table 3.17.

Table 3.17 *Comparison of beam-column design methods [71].*

	EC3 1-4 [1]	EC3 1-1 Method 1 [2]	EC3 1-1 Method 2 [2]	ENV 1993-1-1 [58]	Talja and Salmi [67]	Lopes et al. [68]	Greiner and Kettler [70]	EC9 1-1 [62]
k / k_{FEM}	1.235	0.969	0.925	0.997	1.129	0.828	1.053	0.966
St. dev.	1.012	0.472	0.315	0.215	0.282	0.140	0.937	0.524

As could be seen, the design standard EN 1993-1-4 [1] for stainless steel showed reasonably good and mostly conservative results but with large scatter. This scatter is caused mainly by the over-conservativeness of the procedure for non-uniform bending moment diagram cases. Both EN 1993-1-1 methods [2] showed lower scatter but most of the results were on the unsafe side, similar conclusion was found for the ENV 1993-1-1 [58]. Talja and Salmi´s procedure [67] using the same equations as ENV 1993-1-1 [58] but without upper bound of interaction factors was found perhaps as the most suitable one due to the good agreement on average and reasonable standard deviation. Then, there are methods used in EN 1999-1-1 [62] for aluminium alloys and the proposal published by Greiner and Kettler [70]. Both of these methods showed good predictions on average, but results were very scattered for cases of non-uniform bending moment diagram which led to large standard deviation. Finally, the method presented by Lopes et al. [68] has the lowest scatter but results are very unsafe on average.

Jandera and Syamsuddin [71] proposed a small modification of the method developed by Lopes et al. [68]. The interaction factor formulae could be multiplied by 1.2 and the upper and lower bounds omitted, with the other factors left without change. See Equations (3.119) and (3.120).

$$k_{\mathrm{y}} = 1.2 - \frac{1.2\mu_{\mathrm{y}} N_{\mathrm{Ed}}}{\chi_{\mathrm{y}} A \frac{f_{\mathrm{y}}}{\gamma_{\mathrm{M1}}}} \tag{3.119}$$

$$k_{\mathrm{z}} = 1.2 - \frac{1.2\mu_{\mathrm{z}} N_{\mathrm{Ed}}}{\chi_{\mathrm{z}} A \frac{f_{\mathrm{y}}}{\gamma_{\mathrm{M1}}}} \tag{3.120}$$

The modified formulae giving better agreement but still some results may be unsafe. The unsafe results are especially in the cases of non-uniform bending moment diagram of members loaded by small bending and therefore not very important cases. However, the disadvantage of EN 1994-1-4 [1] with possible value of $k_{\mathrm{y}} = 1.2$ for cases with low axial load remains here. The average value and the standard deviation are shown in Table 14.

Table 3.18 *Comparison of modified Lopes et al. procedure [71].*

	Modified Lopes et al.
k / k_{FEM}	1.00
Standard deviation	0.166

The results were very similar for all considered stainless steel groups and it can be noted, that although many procedures were developed, none of them is accurate and suitable enough for stainless steel structures.

3.11.13 Imperial College London – United Kingdom

At the Imperial College London in the United Kingdom a new method for calculation of cross-section compressive and bending resistance has been developed. The new approach is called CSM (Continuous Strength Method) and it was described in Chapter 3.9.

Development of the CSM led also to an improvement of the beam-column design procedure given by EN 1993-1-4 [1]. A new interaction factor formula was derived and the consideration of the bending resistance according to CSM [49] and flexural buckling resistance according to the new buckling curves [41] was suggested.

Investigation was focused on SHS, RHS and CHS stainless steel beam-column behaviour, respectively.

SHS and RHS beam-columns

Zhao et al. [72] made research of stainless steel SHS and RHS members loaded by combination of compressive force and bending moment. The information about the investigated members is given in Table 3.19.

Table 3.19 *Member information used in Zhao et al. [72].*

Stainless steel group	Austenitic, ferritic, duplex
Cross-section	Cold-formed SHS and RHS
Cross-section Class	1, 2, and 3
Non-dimensional slenderness range	From 0.2 to 3.0

It was proposed a new procedure to design stainless steel beam-columns. This procedure considers a similar interaction formula to the one given by EN 1993-1-4 [1], see Equation (3.121). There is a new interaction factor k_{csm} being calculated according to Equation (3.122), where M_{Rd} was replaced by $M_{csm,Rd}$ calculated according to CSM and $N_{b,Rd}$ was calculated considering the buckling curves developed by Afshan et al. [41].

$$\frac{N_{\mathrm{Ed}}}{N_{\mathrm{b,Rd}}} + k_{\mathrm{csm}} \frac{M_{\mathrm{Ed}}}{M_{\mathrm{csm,Rd}}} \leq 1.0 \tag{3.121}$$

$$k_{\mathrm{csm}} = 1 + D_1\left(\bar{\lambda} - D_2\right)\frac{N_{\mathrm{Ed}}}{N_{\mathrm{b,Rd}}} \leq 1 + D_1(D_3 - D_2)\frac{N_{\mathrm{Ed}}}{N_{\mathrm{b,Rd}}} \tag{3.122}$$

where D_1 and D_2 are the coefficients defining the linear relationship between k_{csm} and $\bar{\lambda}$ in the lower non-dimensional slenderness range, while D_3 is a limit value beyond which the interaction factor k_{csm} remains constant. The coefficients values are shown in Table 3.20 depending on stainless steel group.

Table 3.20 *Coefficient D_i values [72].*

Stainless steel group	D_1	D_2	D_3
Austenitic	2.0	0.30	1.3
Ferritic	1.3	0.45	1.6
Duplex	1.5	0.40	1.4

By comparison was found that procedure given by EN 1993-1-4 [1] provides conservative results in all cases again. The SEI/ASCE [52] and AS/NZS [53] proposals lead to more accurate results on average with less scattered results, nonetheless some predictions are still on the unsafe side, especially in cases with significantly non-uniform moment distribution. The proposed method [72] is generally found accurate with safe strength predictions for all considered moment distributions and stainless steel grades.

It should be noted, that the procedure was developed on a limited number of results [73]. Only two cross-sections were considered, namely RHS 200x100x8 mm and RHS 200x100x8 mm. Austenitic, ferritic and duplex stainless steel groups were considered, however, only one grade of each which not cover a wide range of stainless steel material properties. Cross-section slenderness values were in a range from 0.21 to 0.62, consequently, only stocky cross-sections were considered. Analytical approximations of load-bearing capacities predictions were used [41], [48] instead numerical or experimental ones. Furthermore, when the procedure was developed, the last modification of the CSM [49] considering improvement for slender cross-sections did not exist.

CHS beam-columns

Following research conducted at Imperial College in London was focused on circular hollow cross-sections (CHS). Zhao et al. [74] made another research dealing with CHS stainless steel members loaded by compressive force and bending moment combination. Information about specimens and loading cases are summarized in Table 3.21.

Table 3.21 *Member information used in Zhao et al. research [74].*

Stainless steel group	Austenitic
Cross-section	Cold-formed CHS
Cross-section Class	1, 2 and 3
Non-dimensional slenderness range	From 0.43 to 3.03

In this research [74], only the existing approaches for the stainless steel beam-column design are evaluated, namely codified procedures given by EN 1993-1-4 [1], American SEI/ASCE 8-02 [52] and Australian/New Zealand AS/NZS [53] for Classes 1 to 3 of the cross-section and approach developed by Greiner and Kettler [70] for Classes 1 and 2 of the cross-section (it is not suitable for Classes of 3 and 4 of the cross-section as was mentioned above). Furthermore, AS/NZS [53] is evaluated in two modifications regarding the column buckling resistance calculation: tangent modulus approach (named as AS/NZS-T), as used in SEI/ASCE 8-02 [52], and the explicit method (named as AS/NZS-E) developed by Rasmussen and Rondal [27], [66].

Comparison shown [74] that EN 1993-1-4 [1] provides relatively accurate strength prediction for stainless steel beam-columns of Class 1 and 2 of the cross-section, but shows quite conservative for Class 3 cross-sections. Design procedure given by American specification [52] indicates safe results on the average but in the loading cases of dominant compressive force, the results are slightly unsafe. Vice versa, in the cases of dominant bending moment it is over-conservative due to assignment of the elastic moment resistance to all three cross-section classes. Both AS/NZS-T and AS/NZS-E procedures based on the AS/NZS [53] lead to underestimation of the interaction effect between compression and bending, thus the results are in many predictions on the unsafe side, especially for Class 1 and 2 cross-sections. Greiner and Kettler´s [70] procedure is accurate on average, however, it also leads to many unsafe predictions.

Generally, all methods have some limitations. These are usually caused by inaccurate cross-section and member load-bearing capacity predictions and interaction factor predictions of

loading cases, where the loading compressive force or bending moment is dominant. Later, stainless steel CHS beam-column behaviour was investigated by Buchanan et al. [75].

3.11.14 University of Politècnica de Catalunya – Spain

At the University of Politècnica de Catalunya in Barcelona, Spain, comprehensive experimental and numerical studies of stainless steel beam-columns were conducted, mostly focused on the square and rectangular hollow cross-sections and ferritic stainless steel group.

Modification of the proposal developed by Lopes et al. [68] provided by Jandera and Syamsuddin [71] was made. Comparison of this modification for beam-columns of ferritic stainless steel group was conducted by Arrayago et al. [76] and Arrayago et al. [77] for different loading conditions.

Firstly (Arrayago et al. [76]) design approaches provided by EN 1993-1-4 [1] and Jandera and Syamsuddin´s modification [71] were evaluated only. Available information about specimens and loading conditions are summarized in Table 3.22. It is necessary to note, that in this research, compared to other, only minor axis bending was considered in the case of RHS.

Table 3.22 *Member information used in Arrayago et al. [76].*

Stainless steel group	Ferritic
Cross-section	Cold-formed SHS and RHS
Non-dimensional slenderness range	From 0.65 to 1.72
End-moment ratio	1

Corresponding design procedures given by EN 1993-1-4 [1] and Jandera and Syamsuddin´s modification [71] of the proposal developed by Lopes et al. [68] were described in the chapters before. Evaluation shown [76] that both methods provide safe results, however, mostly over-conservative.

The second research conducted by Arrayago et al. [77] covers SHS and RHS but bending was considered around both major and minor axis and as in most cases, members were restrained along their length against the lateral buckling. More information of considered members and loading conditions are shown in Table 3.23.

Table 3.23 *Member information used in Arrayago et al. [77].*

Stainless steel group	Ferritic
Cross-section	Cold-formed SHS and RHS
End-moment ratio	1, 0, -1

Except the procedure provided by EN 1993-1-4 [1] and the one developed by Jandera and Syamsuddin [71], the original proposal developed by Lopes et al. [68] and formulae provided by Greiner and Kettler [70] were also evaluated. Additionally, new formula for the interaction factor determination was proposed and evaluated then. The formula was developed based on the flexural buckling and bending resistances given by experiments and numerical models, then Equations (3.96) and (3.97) were modified. The proposed formula is given by Equation (3.123). Boundary conditions and all coefficients in this formula are the same as in the Lopes et al. [68], only the constant is changed.

$$k_{\mathrm{i}} = 1 - 0.92\frac{\mu_{\mathrm{i}} N_{\mathrm{Ed}}}{N_{\mathrm{b,Rd,i}}} \tag{3.123}$$

Again, EN 1993-1-4 [1] and Greiner and Kettler´s [70] procedures provide quite conservative results but there are some unsafe predictions of the member ultimate capacities. Design approach developed by Lopes et al. [68] for austenitic I cross-sections seems to be the one providing more accurate and less scattered results, but there are several unsafe predictions too. Modification of this proposal developed by Jandera and Syamsuddin [71] eliminates most of the mentioned unsafe predictions but results are more conservative and more scattered. New interaction formula provides the best agreement and the lowest standard deviation, nevertheless, because interaction factor formula was developed based on few experimental results only, further research would be useful.

Other, very similar research was carried out by Arrayago et al. [78] for ferritic cold-formed SHS and RHS beam-columns. There was no new formula developed in the publication, only comparison of existing design approaches was provided. These are procedures of: EN 1993-1-4 [1], Lopes et al. [68], Jandera and Syamsuddin´s modification [71], Arrayago et al. modification [77], Greiner and Kettler [70], American specification SEI/ASCE [52] and Australian/New Zealand standard AS/NZS [53].

Generally, all the design approaches provide safe and quite accurate results for the tested members on average, but all of these methods have some unsafe predictions as explained before.

In 2015, Arrayago and Real [79] published their study of stainless steel stub-columns loaded by combination of compression and bending, where the accuracy of the proposals given by EN 1993-1-4 [1] and CSM [42] - [49] developed at Imperial College in London were evaluated. As mentioned before, experiments were conducted only for hollow cross-sections of ferritic stainless steel group, more information about the tested specimens are in Table 3.24.

Table 3.24 *Member information used in Arrayago and Real´s research [79].*

Stainless steel group	Ferritic
Cross-section	Cold-formed SHS and RHS
Cross-section Class	1 - 4
End-moment ratio	1

EN 1993-1-4 [1] with the current cross-sectional classification provides quite accurate and safe results with some conservativeness in few cases. Nevertheless, in the case of revised cross-sectional classification [36], the average ultimate capacity prediction is slightly better, although the classification of several cross-sections was found too optimistic. Comparison of the CSM indicates very low standard deviation, especially in the case of simplified CSM which provides the most accurate results on average with very low scatter, so it could be noted that the CSM was found to be the most accurate one.

3.12 Concluding remarks

Current stainless steel beam-column design procedures given by the European standards together with proposals developed by many researchers were presented in this chapter. Furthermore, many evaluations of these procedures made in the literature were presented too.

It was shown that all procedures provided by the European standards have some shortcomings, usually because they are adopted from the standard for carbon steel and due to neglection of the strain hardening of stainless steel. Generally, the results provided by the European standard procedures are mostly over-conservative.

Design procedure provided by American specification indicates good results on average, however, if loading by compression or bending is dominant it exhibits some unsafe and over-conservative results.

Australian/New Zealand standard procedure exhibits underestimation of the interaction phenomenon between compressive force and bending moment. That leads to unsafe results in many cases.

Developments of the stainless steel beam-column design carried out by researchers in recent decades were presented together with their evaluations. Most of them considered very similar interaction formula as the one provided by EN 1993-1-4 [1] and were focused on a more accurate interaction factor formulae development.

As was described, most of presented procedures contain some drawbacks. The procedure developed by Zhao et al. [72] provides the best results. Predictions are both accurate and safe. Consequently, it is expected including of the procedure into next edition of stainless steel design standard. However, the procedure is dependent on material properties. It is necessary consider specific constants for the appropriate stainless steel group. Furthermore, it was developed based on limited data. Therefore, there is still possibility of some improvement.

Chapter 4

Experimental study

4.1 Introduction

Experimental study was conducted in laboratory of the Czech Technical University in Prague with the aim of investigating stainless steel slender beam-column behaviour. Six cold-formed hollow cross-sections were tested, namely SHS 40x2, SHS 60x2, SHS 80x3, SHS 80x5, RHS 80x60x2 and RHS 100x40x4. All members were fabric from austenitic stainless steel group, SHS 80x3 and SHS 80x5 from 1.4404 grade whereas the others from 1.4301 grade. In total, 20 members loaded by the combination of compressive force and uniform bending moment were tested. Specimens were numbered from 1 to 20. Experimental test setup and obtained experimental data are described in this chapter including material properties and imperfections.

4.2 Geometry measurement

Width and depth of the cross-sections were measured three times on both sides and thickness of the wall was measured three times on each wall. Member length was measured three times on each side as well. Average values of the measured data are summarized in Table 4.1, where h and b are the cross-section dimensions, t is the thickness of the wall, L_{nom} is the nominal member length and L is the length of the specimen considering additional experimental support equipment (nominal member length extended by 90 mm on both ends). Detail information of supports is given in Chapter 4.5.

Table 4.1 *Measured cross-section and member dimensions.*

Specimen	Cross-section	h	b	t	L_{nom}	L
		[mm]	[mm]	[mm]	[mm]	[mm]
1	SHS 80x3	79.74	79.74	2.8	2430	2610
2	SHS 80x3	79.74	79.74	2.8	2440	2620
3	SHS 80x5	80.00	80.00	4.76	2445	2625
4	SHS 80x5	80.00	80.00	4.76	2395	2575
5	SHS 40x2	39.90	39.90	1.91	1000	1180
6	SHS 40x2	39.90	39.90	1.91	1000	1180
7	SHS 40x2	39.90	39.90	1.91	1500	1680
8	SHS 40x2	39.90	39.90	1.91	1495	1675
9	SHS 60x2	60.02	60.02	1.87	1000	1180
10	SHS 60x2	60.02	60.02	1.87	1000	1180
11	SHS 60x2	60.02	60.02	1.87	2000	2180
12	SHS 60x2	60.02	60.02	1.87	1990	2170
13	RHS 80x60x2	80.12	59.96	1.95	1005	1185
14	RHS 80x60x2	80.12	59.96	1.95	1005	1185
15	RHS 80x60x2	80.12	59.96	1.95	2005	2185
16	RHS 80x60x2	80.12	59.96	1.95	1990	2170
17	RHS 100x40x4	100.32	40.54	4.04	990	1170
18	RHS 100x40x4	100.32	40.54	4.04	990	1170
19	RHS 100x40x4	100.32	40.54	4.04	2005	2185
20	RHS 100x40x4	100.32	40.54	4.04	2000	2185

4.3 Material testing

Four coupons were cut from each cross-section in longitudinal direction of the member. Location of the coupons is both for SHS and RHS given by Figure 4.1. Dimensions of the flat coupons were in accordance with the EN ISO 6892-1 [80]. Corner coupons length were the same as for the flat ones with a constant width along the whole length. Tensile test coupons geometry is shown in Figure 4.2.

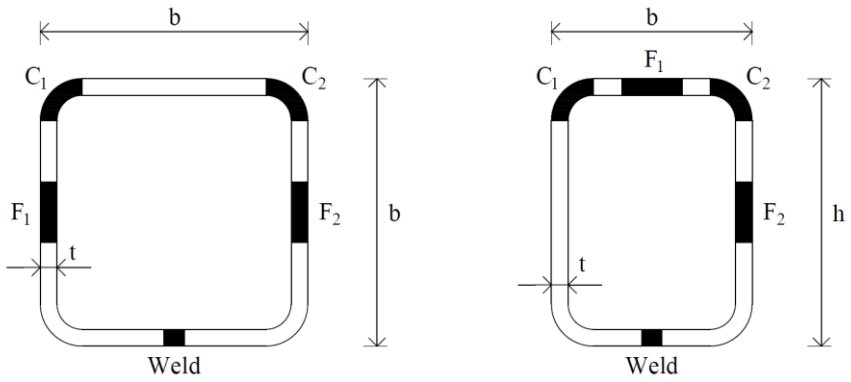

Figure 4.1 *Tensile test coupons location of the SHS (left) and RHS (right) cross-sections.*

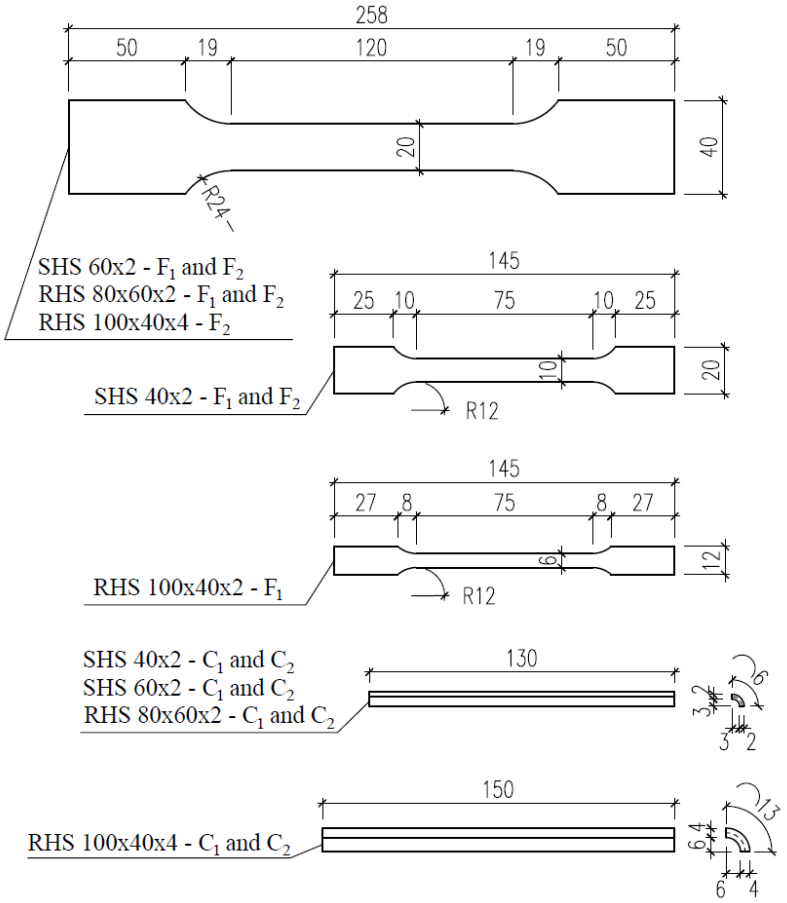

Figure 4.2 *Tensile test coupons geometry.*

Material tests of 1.4404 grade cross-sections were conducted by Mařík [14] recently. Therefore, only 1.4301 grade cross-sections material testing is presented herein. Tensile tests were carried out using Shimadzu 300 kN and MTS Qtest 100 kN electromechanical testing machines for flat

and corner coupons, respectively. The rate of displacement was established based on the coupon length. Distance between the jaws edges multiplied by the strain displacement $\dot{\varepsilon} = 7\text{x}10^{-5}$ mm/s and $2.5\text{x}10^{-3}$ mm/s was used for stroke value up to 5 mm and beyond 5 mm, respectively. The lower strain rate (up to 5 mm stroke) always covered $\sigma_{0.2}$ proof stress used for the stress-strain diagram description safely. For the measurement, flat coupons were attached by strain gauges at the mid-length on both sides, see Figure 4.3. Furthermore, additional optical extensometer was used, as shown in Figure 4.4. Corner coupons were equipped by mechanical extensometer only, see Figure 4.5.

For the material properties description, the two-stage models developed by Gardner and Nethercot [22] were used. Model considering 1.0 % proof stress, see Equation (3.11), was used for all flat coupons and most of corner coupons. However, in two cases of corner coupons the 1.0 % proof stress was not reached, therefore, material model considering σ_u instead of $\sigma_{1.0}$ was used, see Equation (3.10). Average values of the flat and corner coupon material properties of the appropriate cross-section are summarized in Table 4.2 and Table 4.3, respectively. It should be noted, that the initial Young's modulus of corner coupons was measured by additional mechanical extensometer that is not as accurate as the strain gauges. This caused that the Young's modulus of SHS 40x2 is higher than expected, whereas of RHS 100x40x4 is slightly lower.

Figure 4.6 shows stress-strain diagram of SHS 80x3 which represents typical material response. As could be seen, flat part of the cross-section exhibits great ductility but lower stress level, when compared to a corner part, significantly influenced by cold-working.

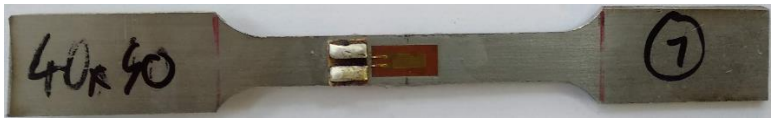

Figure 4.3 *Tensile coupon with strain gauges.*

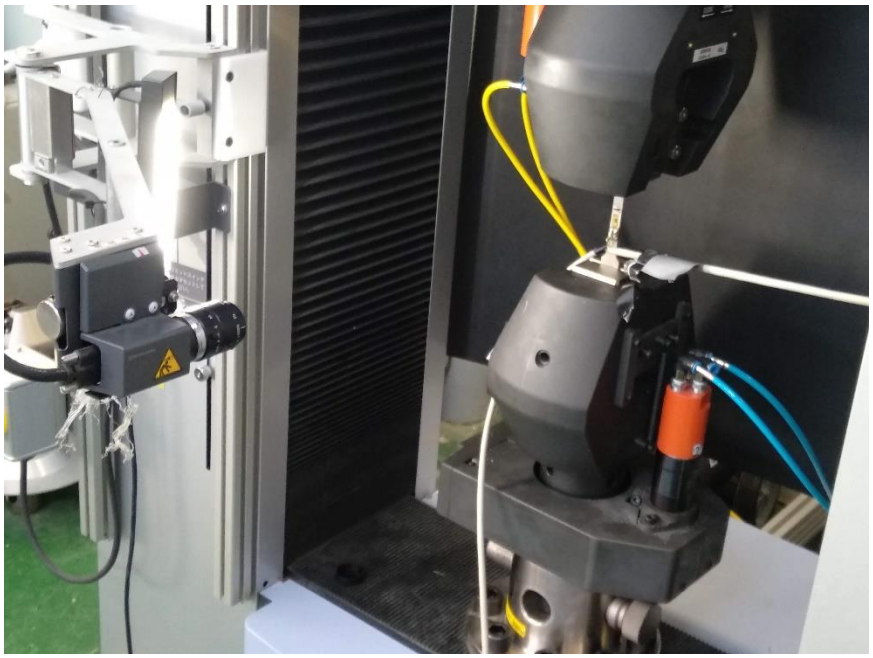

Figure 4.4 *Flat coupons material testing setup.*

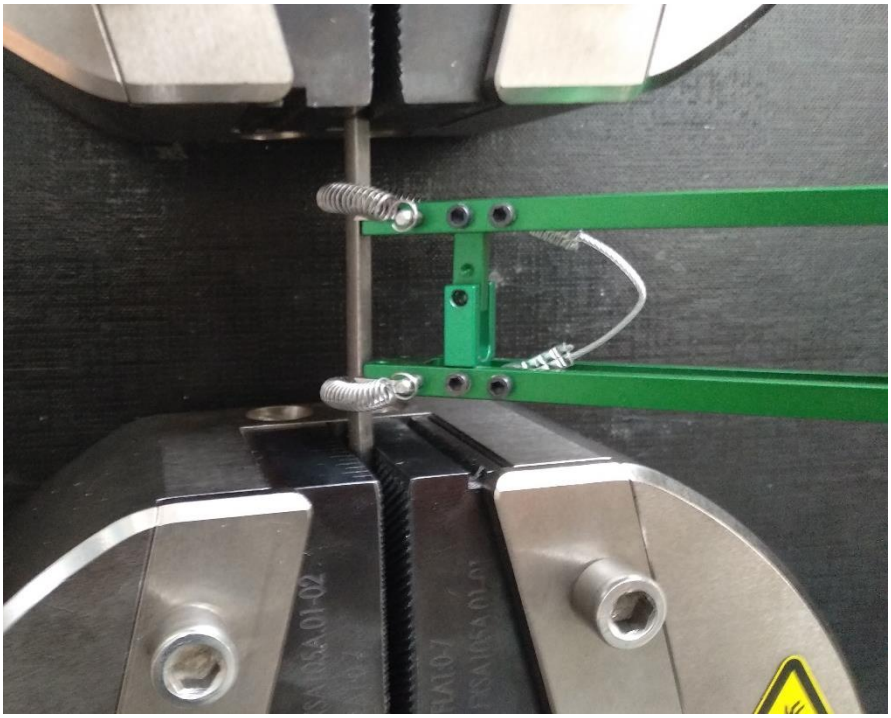

Figure 4.5 *Corner coupons material testing setup.*

Table 4.2 *Average values of measured flat material properties.*

Cross-section	E_0	$E_{0.2}$	$\sigma_{0.2}$	$\sigma_{1.0}$	σ_u	n	$n_{0.2,1.0}$	ε_u
	[GPa]	[GPa]	[MPa]	[MPa]	[MPa]	[-]	[-]	[-]
SHS 80x3	183.3	29.9	397.1	465.3	627.6	3.1	4.3	0.47
SHS 80x5	190.5	29.3	448.1	516.2	627.4	3.4	4.5	0.54
SHS 40x2	185.4	17.0	469.7	498.5	641.9	5.3	2.3	0.38
SHS 60x2	188.4	15.4	436.2	465.1	706.5	5.2	1.9	0.44
RHS 80x60x2	183.7	17.6	409.5	449.2	598.2	5.4	2.6	0.32
RHS 100x40x4	190.4	21.8	574.1	592.9	696.0	4.6	2.0	0.29

Table 4.3 *Average values of measured corner material properties.*

Cross-section	E_0	$E_{0.2}$	$\sigma_{0.2}$	$\sigma_{1.0}$	σ_u	n	$n_{0.2,1.0}$	ε_u
	[GPa]	[GPa]	[MPa]	[MPa]	[MPa]	[-]	[-]	[-]
SHS 80x3	210.8	16.8	681.6	714.1	741.9	14.4	4.2	0.11
SHS 80x5	215.3	17.5	726.3	764.5	771.8	15.4	6.2	0.07
SHS 40x2	287.5	62.5	763.7	941.5	959.6	3.8	3.2	0.015
SHS 60x2	192.6	40.0	650.7	-	732.9	6.0	4.5*	0.01
SHS 80x60x2	202.4	58.8	662.8	819.1	842.0	3.8	5.2	0.08
RHS 100x40x4	164.2	37.0	782.8	-	837.4	5.5	5.0*	0.013

* Material did not reach 1.0 % proof stress, therefore the value represents $n_{0.2,u}$ instead of $n_{0.2,1.0}$.

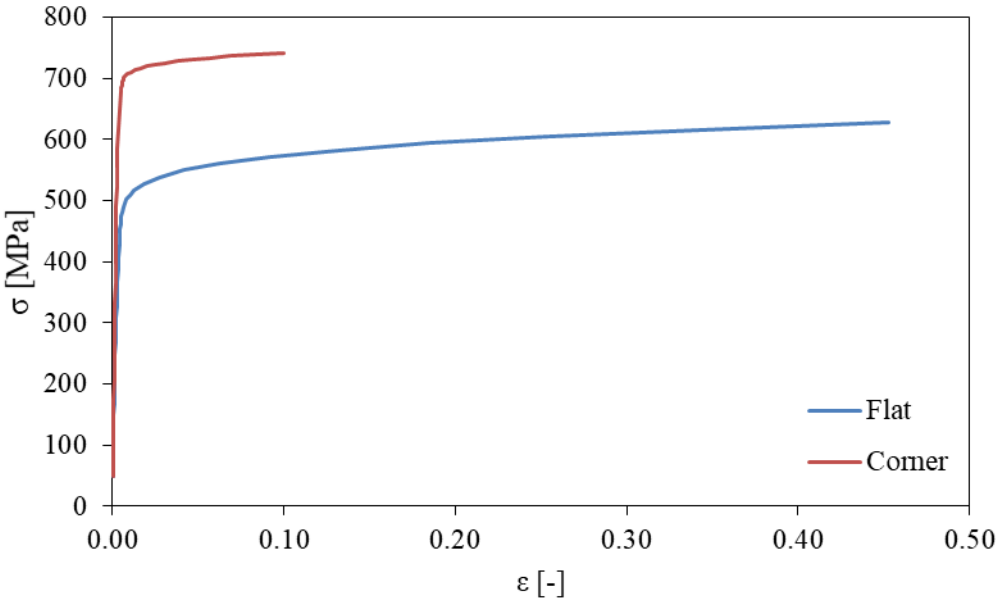

Figure 4.6 *Stress-strain diagram of flat and corner part of SHS 80x3.*

Based on the material characteristics given by Table 4.2 and Table 4.3, the cross-sections were classified according to Gardner and Theofanous [36] cross-section limits. Firstly, the weighted average of the flat and corner coupons 0.2 % proof stress and Young's modulus regarding flat and corner area of the cross-section was calculated. As mentioned before, according to [10] - [13] the corner area should be extended by two times the wall thickness due to enhanced material properties caused by cold-forming, whereas according to [14], [15] consideration of no extensions is more accurate. Therefore, the weighted average of material characteristics and cross-section classification were calculated for both cases, see Table 4.4, where 0*t* represents enhanced material properties in the corner area only and 2*t* represents the area extended by two times of the wall thickness into flat parts of the cross-section.

Table 4.4 *Weighted average of material characteristics (initial Young's modulus of elasticity and 0.2 % proof stress) and the cross-section classification.*

Cross-section	0t			2t		
	E_0	$\sigma_{0.2}$	Class	E_0	$\sigma_{0.2}$	Class
	[GPa]	[MPa]	[-]	[GPa]	[MPa]	[-]
SHS 80x3	186.5	430.7	3	190.7	473.4	4
SHS 80x5	195.7	506.6	1	202.4	581.0	1
SHS 40x2	202.3	518.2	1	223.7	580.0	1
SHS 60x2	188.8	458.5	4	189.4	486.9	4
RHS 80x60x2	185.4	432.9	4	187.6	462.6	4
RHS 100x40x4	185.1	616.2	4	178.4	669.8	4

As could be expected, $\sigma_{0.2}$ is higher if higher corner area is considered. Despite the difference in material characteristics, the cross-section Class is the same for all cross-sections, with exception of SHS 80x3 which due to enhancement of the 0.2 % proof stress value felt into Class 4 of the cross-section.

Based on the measured cross-section and member dimensions, given by Table 4.1, and weighted average of the material properties obtained from the tensile tests given by Table 4.4, the non-dimensional slenderness $\bar{\lambda}$ values are given by Table 4.5. Both considerations of the enhanced material properties areas were used, again.

Table 4.5 *Non-dimensional slenderness values of the tested members.*

Specimen	Cross-section	0*t*		2*t*	
		$\bar{\lambda}_y$	$\bar{\lambda}_z$	$\bar{\lambda}_y$	$\bar{\lambda}_z$
		[-]	[-]	[-]	[-]
1	SHS 80x3	1.28	1.28	1.32	1.32
2	SHS 80x3	1.29	1.29	1.32	1.32
3	SHS 80x5	1.41	1.41	1.48	1.48
4	SHS 80x5	1.38	1.38	1.45	1.45
5	SHS 40x2	1.24	1.24	1.25	1.25
6	SHS 40x2	1.24	1.24	1.25	1.25
7	SHS 40x2	1.77	1.77	1.78	1.78
8	SHS 40x2	1.76	1.76	1.77	1.77
9	SHS 60x2	0.74	0.74	0.75	0.75
10	SHS 60x2	0.74	0.74	0.75	0.75
11	SHS 60x2	1.37	1.37	1.39	1.39
12	SHS 60x2	1.36	1.36	1.39	1.39
13	RHS 80x60x2	0.54	0.67	0.55	0.68
14	RHS 80x60x2	0.54	0.67	0.55	0.68
15	RHS 80x60x2	0.99	1.24	1.01	1.26
16	RHS 80x60x2	0.99	1.23	1.00	1.25
17	RHS 100x40x4	0.64	1.31	0.66	1.36
18	RHS 100x40x4	0.64	1.31	0.66	1.36
19	RHS 100x40x4	1.19	2.44	1.24	2.55
20	RHS 100x40x4	1.19	2.44	1.24	2.55

4.4 Geometric imperfection measurement

For the global imperfection measurement a tensioned string next to the member wall was used. Distance between the string and the member surface was measured at the mid-span by depth gauge of caliper, see Figure 4.7. Three points along the cross-section width were measured. The accuracy is not great (± 0.5 mm), but it is sufficient.

For the local imperfection amplitude it was necessary to measure longitudinal profile of the member surface in the middle of the web. Which was measured by centesimal dial at appropriate points, see Figure 4.8 and Figure 4.9. Points of measurement were established based on the cross-section dimensions so that distance between the points was equal to 25 % of the measured web width.

Average values of both global and local initial geometric imperfection amplitudes are given in Table 4.6, where $\omega_{GI,0}$ is the global imperfection amplitude and $\omega_{LI,0}$ is the local imperfection amplitude.

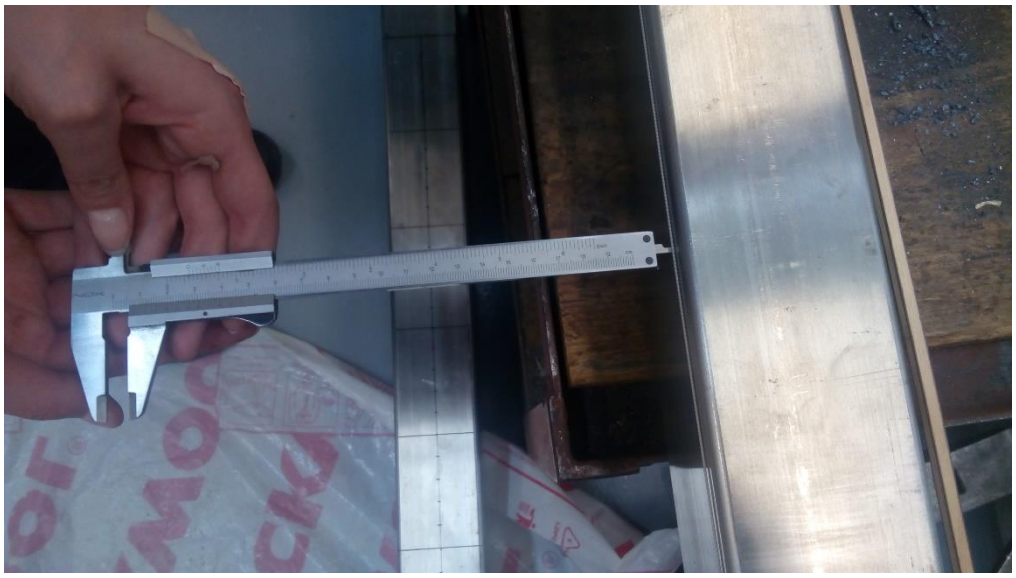

Figure 4.7 *Global imperfection measurement.*

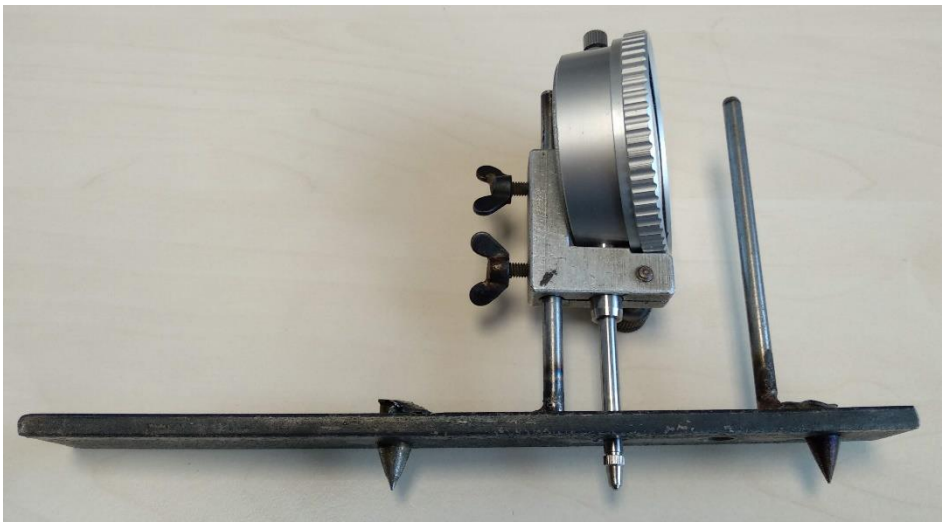

Figure 4.8 *Device for local imperfection measurement.*

Figure 4.9 *Local imperfection measurement.*

Table 4.6 *Global and local initial imperfection amplitude values.*

Specimen	Cross-section	$\omega_{GI,0}$		$\omega_{LI,0}$	
		[mm]	[-]	[mm]	[-]
1	SHS 80x3	0.833	L_{nom} / 2916	0.01	b / 7974
2	SHS 80x3	0.767	L_{nom} / 3183	0.0125	b / 6379
3	SHS 80x5	1.3	L_{nom} / 1881	0.0125	b / 6400
4	SHS 80x5	1.233	L_{nom} / 1942	0.01	b / 8000
5	SHS 40x2	0.5	L_{nom} / 2000	0.0075	b / 5320
6	SHS 40x2	0.5	L_{nom} / 2000	0.01	b / 3990
7	SHS 40x2	0.667	L_{nom} / 2250	0.01	b / 3990
8	SHS 40x2	0.567	L_{nom} / 2242	0.01	b / 3990
9	SHS 60x2	0.5	L_{nom} / 2000	0.01	b / 6020
10	SHS 60x2	0.5	L_{nom} / 2000	0.01	b / 6020
11	SHS 60x2	0.667	L_{nom} / 2999	0.01	b / 6020
12	SHS 60x2	0.567	L_{nom} / 3510	0.0075	b / 8027
13	RHS 80x60x2	0.5	L_{nom} / 2010	0.01	h / 8012
14	RHS 80x60x2	0.5	L_{nom} / 2010	0.01	h / 8012
15	RHS 80x60x2	0.667	L_{nom} / 3006	0.0075	h / 10683
16	RHS 80x60x2	0.667	L_{nom} / 2984	0.01	h / 8012
17	RHS 100x40x4	0.617	L_{nom} / 1605	0.02	h / 5016
18	RHS 100x40x4	0.5	L_{nom} / 1980	0.02	h / 5016
19	RHS 100x40x4	1.3	L_{nom} / 1542	0.015	h / 6688
20	RHS 100x40x4	1.07	L_{nom} / 1869	0.015	h / 6688

4.5 Beam-column tests

Together, 20 tests under compression and uniaxial bending were conducted in order to obtain SHS and RHS stainless steel slender beam-column behaviour. In the cases of RHS specimens, only the major axis bending was performed. Nominal eccentricity value *e* was given by cross-section dimensions. The axis of the acting loading force was situated at the cross-section wall, with exception of specimens 1, 3, 19 and 20 where the eccentricity was equal to 20 mm. The eccentricities for all specimens are given in Table 4.7.

Both top and bottom supports were considered as pin-ended to major axis and fixed to minor axis of the specimen cross-section. Both supports were formed by a wedge plate with two oval holes for appropriate eccentricity setup, and a plate containing a V-shaped groove. The top plate was bolted to hydraulic jack, whereas the bottom plate was situated on the floor with horizontal displacement restricted. Every specimen was equipped with a 10 mm thick end-plate on each end which were bolted to the wedge plates. End-plate bolt holes were of oval shape as well, to allow specimen rectification in both directions. Geometry of pin-ended supports is shown in Figure 4.10. Figure 4.11 and Figure 4.12 show a bottom and a top pin-ended supports, respectively, set with a specimen.

During the beam-column tests, specimens were loaded by compression induced by a hydraulic loading jack. Both loading force and axial shortening of the specimen were measured. Four displacement potentiometers were situated at the specimen mid-span, located at the cross-section corners where local buckling influence is not present. The recording was for two specimen walls perpendicular to each other in order to measure the mid-span displacement in both directions, see Figure 4.13.

The tests were controlled by displacement. In order to obtain appropriate displacement rate, preliminary numerical model (see Chapter 5) considering measured material properties and both cross-section and member geometry was made. Based on the specimen shortening at the ultimate load, the displacement rate was calculated so the minimal test duration was 15 min. Such rate is safely below the strain rate used for material tests and allows full development of all instabilities.

The whole test setup scheme and picture of a tested member are shown in Figure 4.14 and Figure 4.15, respectively.

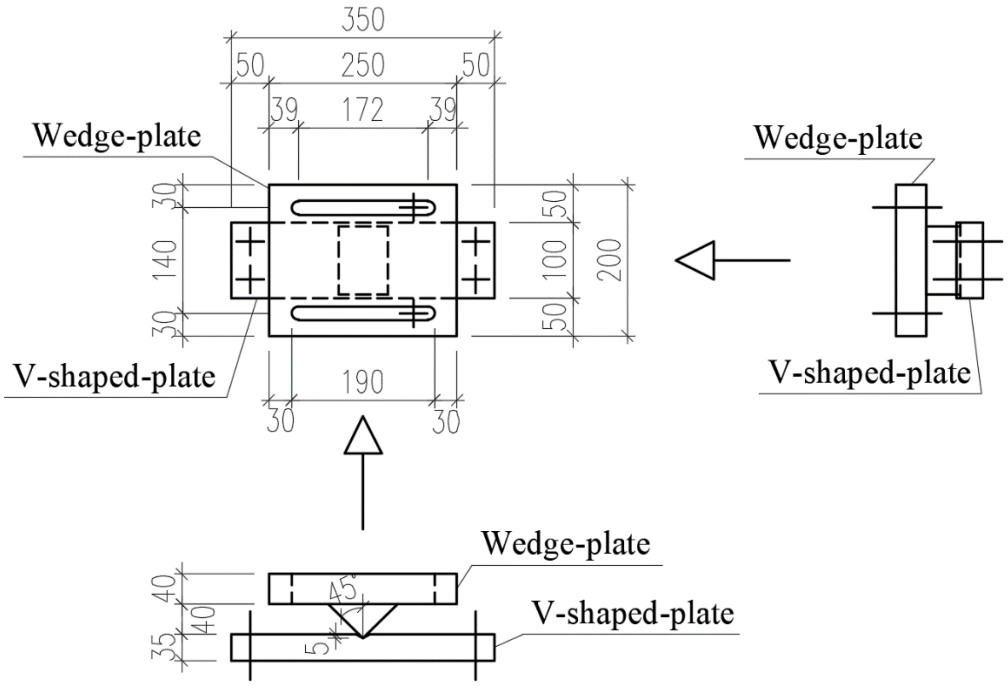

Figure 4.10 *Geometry of pin-ended supports.*

Figure 4.11 *Bottom pin-ended support.*

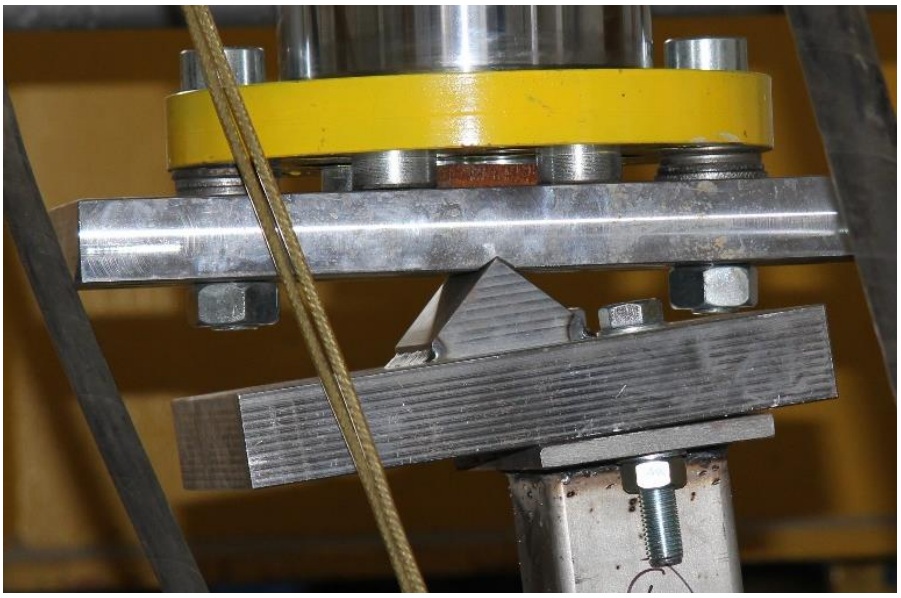

Figure 4.12 *Top pin-ended support.*

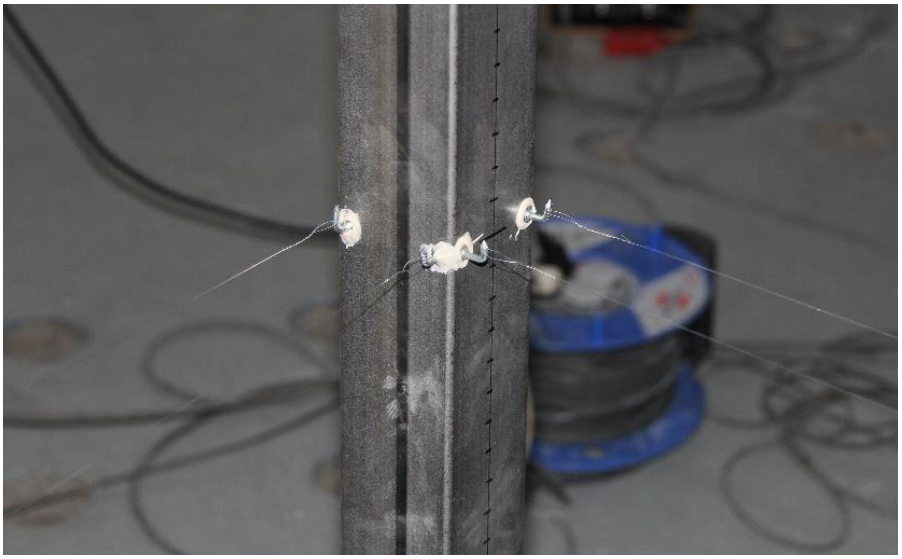

Figure 4.13 *Displacement potentiometers location.*

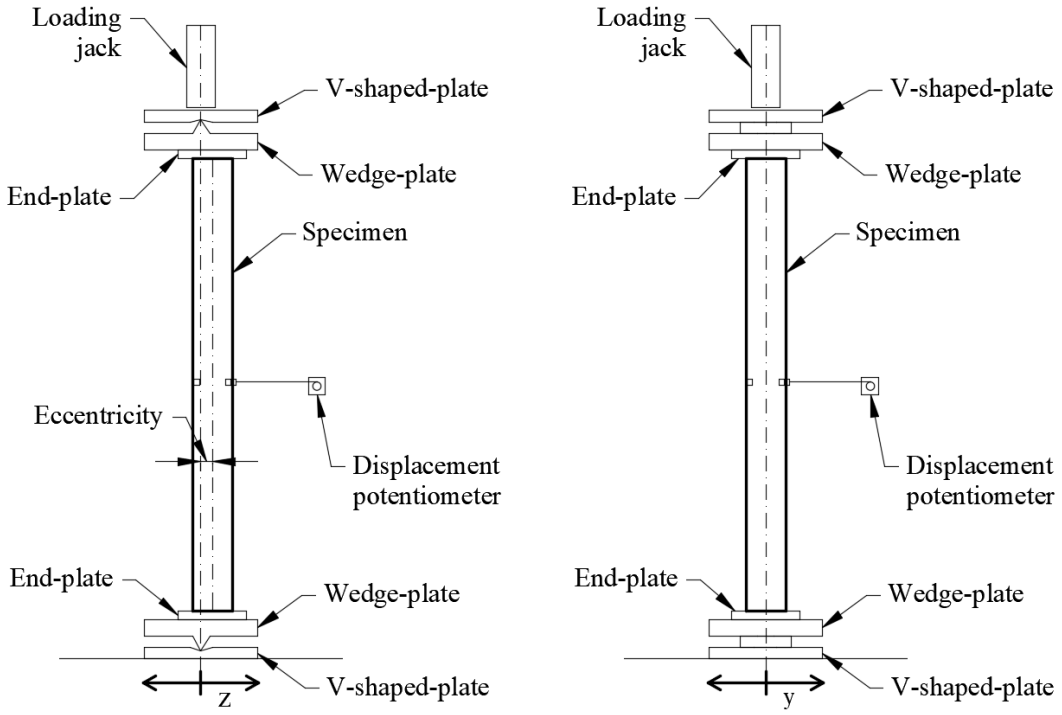

a) Pin-ended - Pin-ended

b) Fixed - Fixed

Figure 4.14 *Test setup scheme.*

Figure 4.15 *Specimen photo.*

As expected, two main failure modes occurred: local buckling failure (occurred in the cases of slender cross-sections and low non-dimensional slenderness values) and flexural buckling failure (occurred in the cases of stocky cross-sections and slender members). Figure 4.16 and Figure 4.17 show typical local buckling and flexural buckling failure, respectively.

Figure 4.16 *Local buckling failure.*

Figure 4.17 *Flexural buckling failure.*

Experimental test results are summarised in Table 4.7, where e is the initial load eccentricity, $N_{u,exp}$ is the ultimate load, δ_{Mj} is the major axis mid-span deflection at the ultimate load, δ_{Mi} is the minor axis mid-span deflection at the ultimate load, FB – Mj is the major axis flexural buckling, FB – Mi is the minor axis flexural buckling and LB – Mj is the major axis local buckling. Measured mid-span deflection curves are given in Figure 4.18 to Figure 4.27.

As mentioned before, all members were loaded by eccentric compressive force leading to major axis bending with $L_{cr,z} \approx 0.5\ L_{cr,y}$. Therefore, dominant mid-span deflection was to major cross-section axis in most cases (δ_{Mj}). However, there are some members of rectangular cross-section (17, 19 and 20) with significant minor axis mid-span deflection (δ_{Mi}). That is attributed to inaccuracies of test setup, such as imperfectly welded end-plates. Furthermore, the supports were not absolutely restrained in minor axis direction, some rotation could occurred. Due to the tolerances and inaccuracies of the support, small minor axis deflections were measured in other samples as well. These are given in Table 4.7 as well as in the Figure 4.18 to Figure 4.27.

Table 4.7 *Member test results.*

Specimen	Cross-section	e	$N_{u,exp}$	δ_{Mj}	δ_{Mi}	Failure mode
		[mm]	[kN]	[mm]	[mm]	
1	SHS 80x3	20	97.79	52.32	11.61	FB - Mj
2	SHS 80x3	40	84.14	60.33	1.56	FB - Mj
3	SHS 80x5	20	182.54	63.59	-2.27	FB - Mj
4	SHS 80x5	40	143.62	67.97	9.07	FB - Mj
5	SHS 40x2	20	35.66	31.22	3.37	FB - Mj
6	SHS 40x2	20	32.28	33.10	7.48	FB - Mj
7	SHS 40x2	20	23.11	50.87	5.68	FB - Mj
8	SHS 40x2	20	22.79	51.78	3.10	FB - Mj
9	SHS 60x2	30	71.04	25.09	7.20	LB - Mj
10	SHS 60x2	30	72.01	22.17	7.76	LB - Mj
11	SHS 60x2	30	42.91	56.49	8.83	FB - Mj
12	SHS 60x2	30	43.78	56.62	6.79	FB - Mj
13	RHS 80x60x2	40	87.70	22.55	2.14	LB – Mj
14	RHS 80x60x2	40	84.39	17.70	8.35	LB - Mj
15	RHS 80x60x2	40	59.09	46.58	9.69	LB - Mj
16	RHS 80x60x2	40	59.05	48.06	6.95	LB - Mj
17	RHS 100x40x4	50	240.40	29.74	18.12	FB - Mi
18	RHS 100x40x4	50	226.44	23.57	7.65	FB - Mj
19	RHS 100x40x4	20	176.52	22.29	27.80	FB - Mi
20	RHS 100x40x4	20	191.31	24.66	19.73	FB - Mi

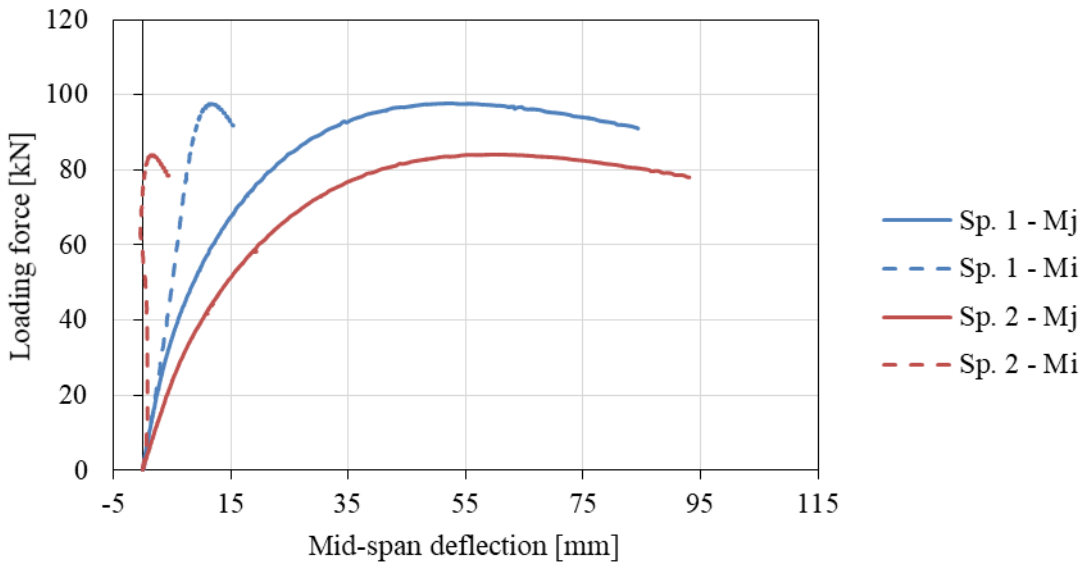

Figure 4.18 *Test results of specimens 1 and 2.*

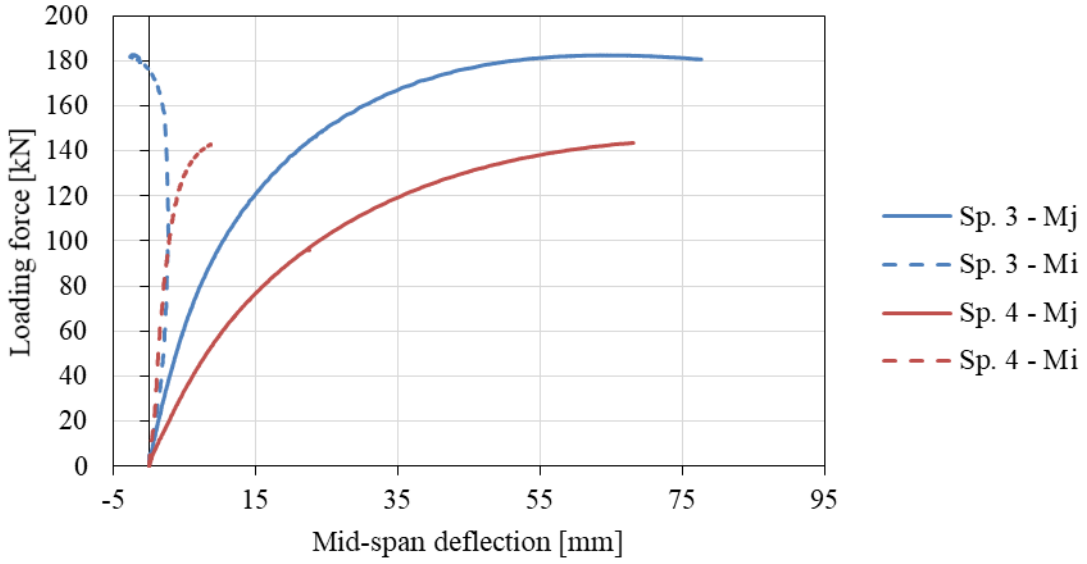

Figure 4.19 *Test results of specimens 3 and 4.*

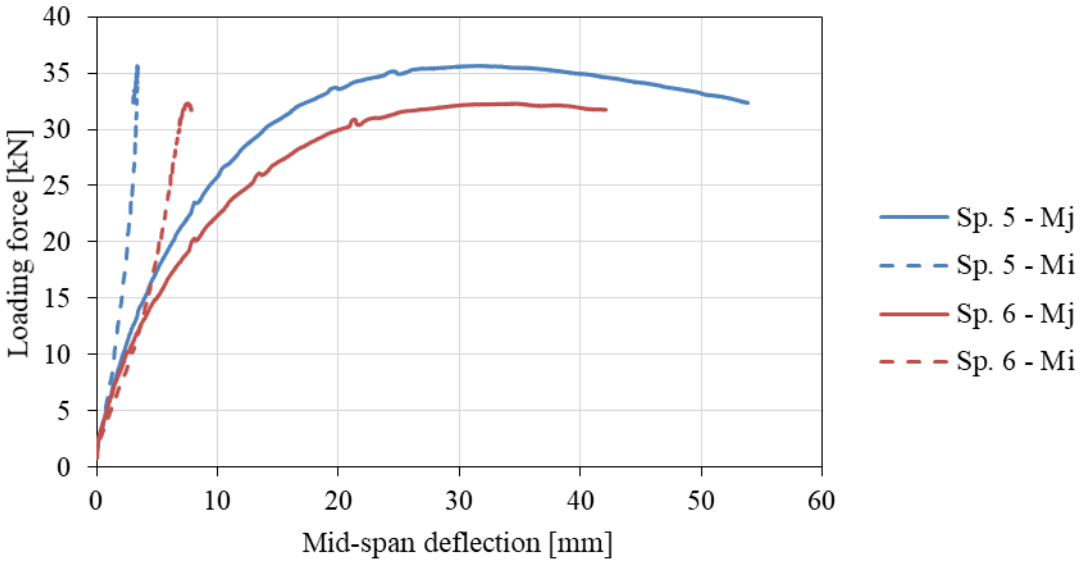

Figure 4.20 *Test results of specimens 5 and 6.*

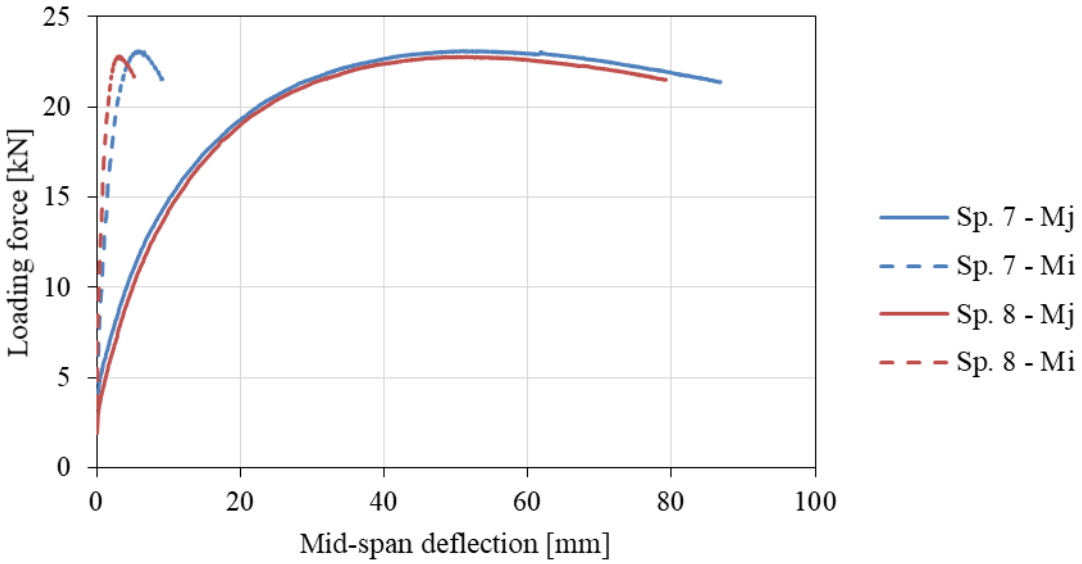

Figure 4.21 *Test results of specimens 7 and 8.*

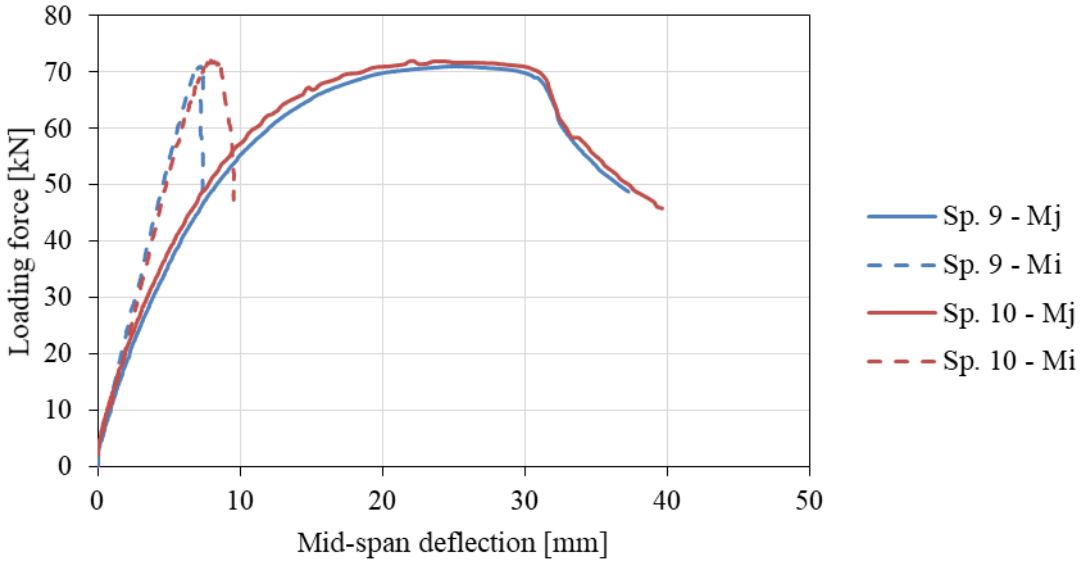

Figure 4.22 *Test results of specimens 9 and 10.*

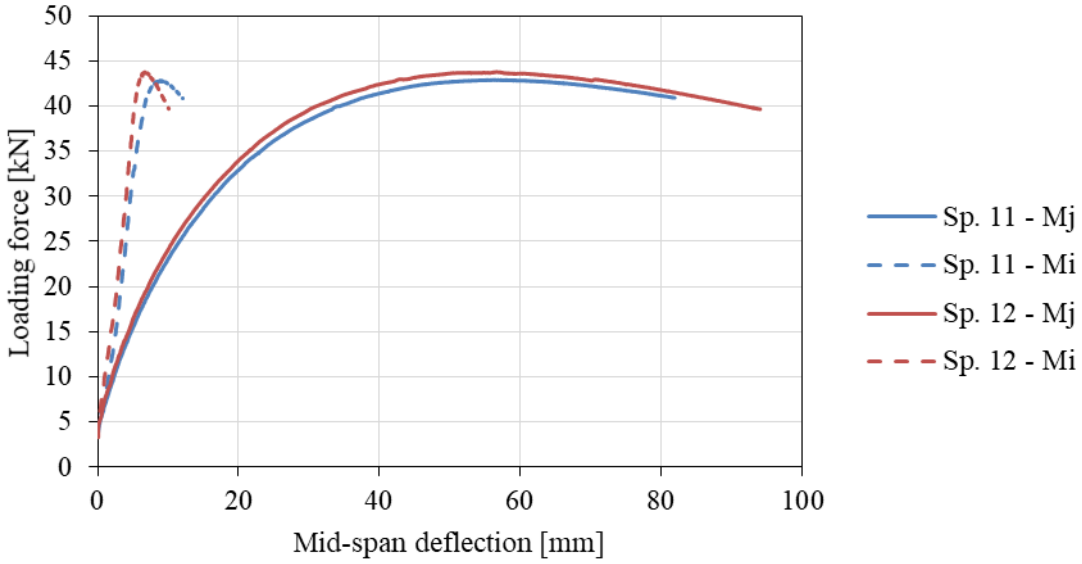

Figure 4.23 *Test results of specimens 11 and 12.*

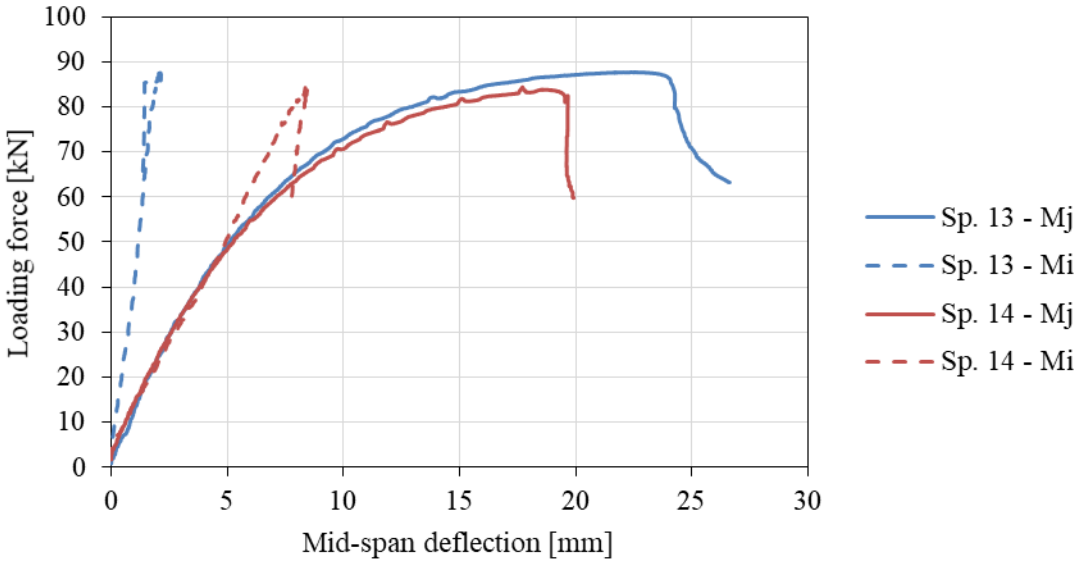

Figure 4.24 *Test results of specimens 13 and 14.*

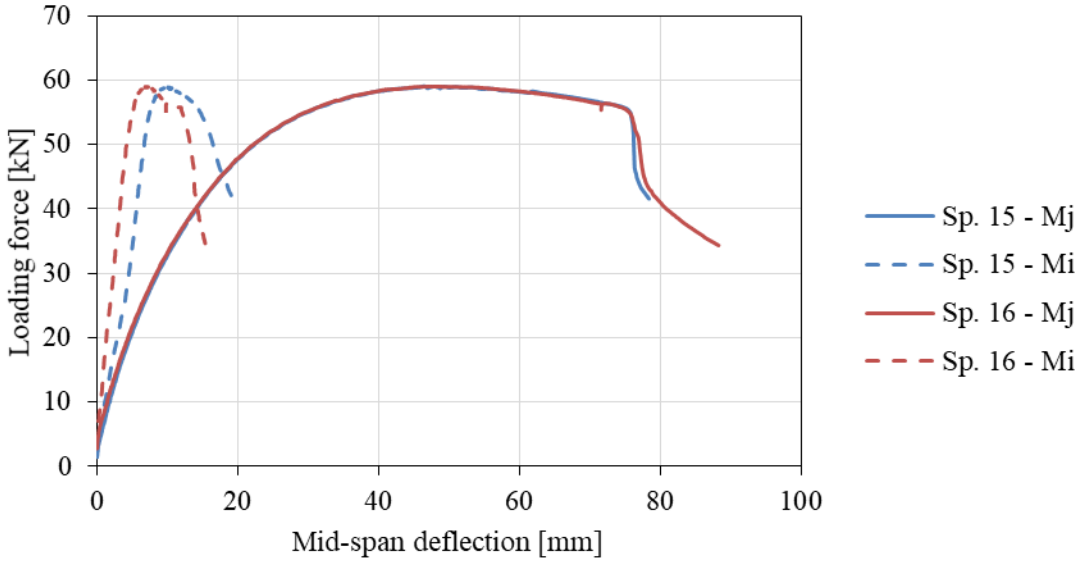

Figure 4.25 *Test results of specimens 15 and 16.*

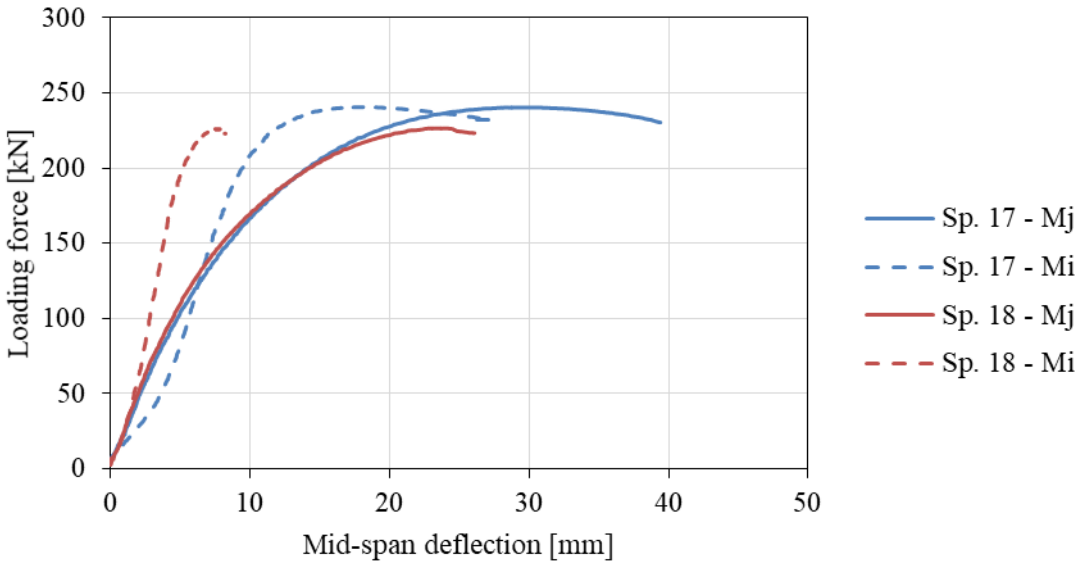

Figure 4.26 *Test results of specimens 17 and 18.*

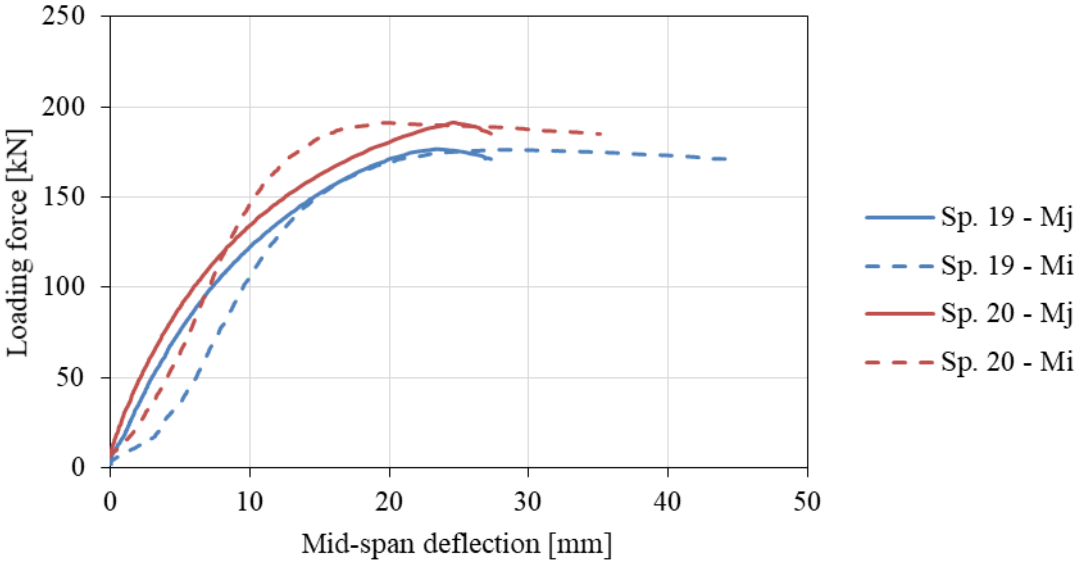

Figure 4.27 *Test results of specimens 19 and 20.*

Chapter 5

Numerical study

5.1 Introduction

Experimental programme consisting of 20 tests was described in the previous chapter. However, it was necessary to obtain comprehensive amount of data covering variables such as material properties, both member and cross-section slenderness and loading state. Therefore, numerical study was conducted. Numerical model was created in software Abaqus using finite element method. The numerical model, its validation and comprehensive numerical parametric study is described in this chapter.

5.2 Numerical modelling

As was mentioned before, the numerical model was made in software Abaqus using finite element method. As an element type a four-node doubly curved general shell element with reduced integration and finite membrane strain, S4R, which is commonly used for SHS and RHS stainless steel members modelling, was used. See Figure 5.1.

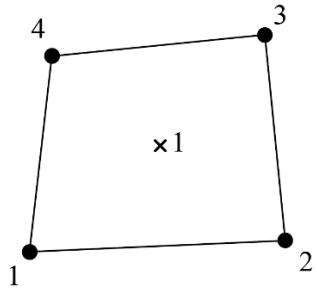

Figure 5.1 *4-node reduced integration element (S4R).*

In order to represent the real behaviour of stainless steel beam-columns geometrically and materially non-linear analysis with imperfections (GMNIA) was used for the calculation with RIKS (arc-length) method which is able to describe the post-ultimate behaviour.

Material was considered as multi linear elastic-plastic defined by the initial Young's modulus of elasticity E_0, Poisson's ratio v, which is for stainless steel equal to 0.3.

Boundary conditions were introduced through reference points situated at the cross-section centroid on both member ends which were rigidly coupled with the member edges (Figure 5.2 left). Pin-ended boundary conditions were considered. One reference point was set by support restraining all degrees of freedom with exception of major axis bending rotation, whereas the other reference point allowed displacement in the direction of the member axis in addition (Figure 5.2 middle). Both compressive force and bending moment were introduced through reference points as well (Figure 5.2 right).

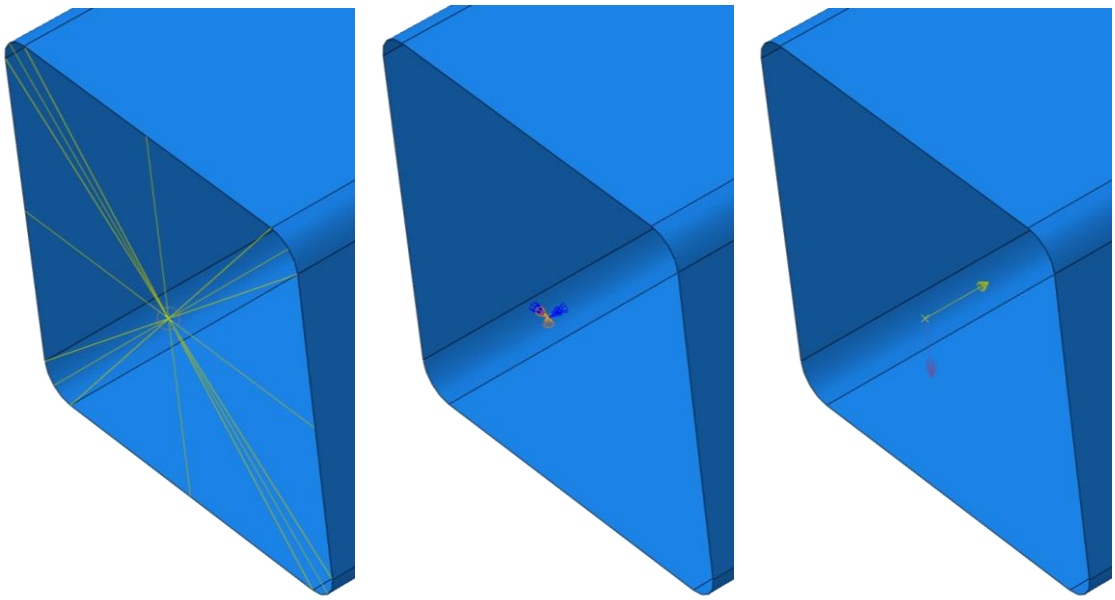

Figure 5.2 *Reference point coupling (left); Boundary conditions (middle); Load (right).*

The cross-section contains residual stresses due to cold-forming, however, both membrane and bending residual stresses were neglected, as was explained in Chapter 3.4.

All structural members contain initial geometric imperfections that have a significant influence on both cross-section and member load-bearing capacity, especially in the cases of thin-walled members. There are two main initial geometric imperfections, namely global and local geometric imperfections. Global geometric imperfection has influence on member stability (flexural buckling). Local imperfection has influence on cross-section stability (local buckling) and it is significant mainly for slender cross-sections. For the introduction of global and local initial geometric imperfections into the numerical model, elastic buckling eigen-modes obtained from linear elastic analysis were used. The imperfection shape was assigned by the corresponding eigen-mode, see Figure 5.3. The considered amplitudes for both initial geometric imperfections are specified later.

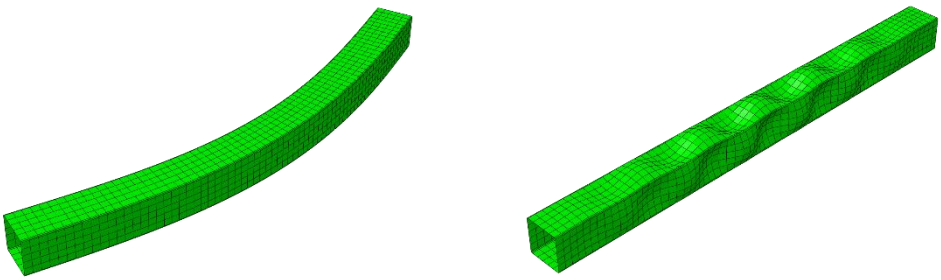

Figure 5.3 *Eigen-mode for global (left) and local (right) initial geometric imperfections.*

5.2.2 Element size

Element size (mesh) was established based on the mesh sensitivity study. On one hand a fine mesh leads to accurate results, on the other hand the finer mesh the more time consuming calculation. Therefore, element size study was made in order to find the element size providing accurate results in reasonable time.

For the element size study the ferritic SHS 80x3 member with non-dimensional slenderness $\bar{\lambda}$ = 1.05 was used. Three types of loading were considered, namely pure compression (flexural buckling), pure bending and combination of compression and bending. The element size was considered regarding the number of nodes situated on the cross-section flat part from 3 to 30 nodes. As a reference value for the accuracy comparison, mesh of 5 nodes across the flat part was used, see Figure 5.4. Results of the sensitivity study are given in Table 5.1.

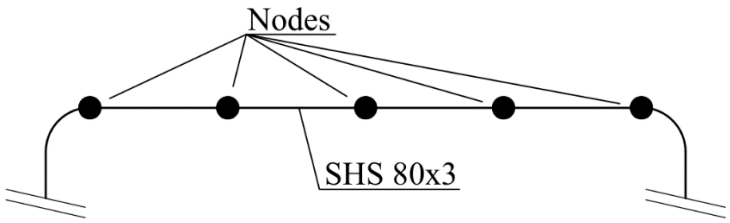

Figure 5.4 *Nodes consideration.*

Table 5.1 *Element size sensitivity study results.*

Number of nodes	Accuracy			Time		
	N [%]	M [%]	N+M [%]	N [min]	M [min]	N+M [min]
3	-3.38	1.19	1.56	1.3	0.22	0.12
4	0.82	0.27	0.40	1.38	0.47	0.2
5	-	-	-	1.95	0.65	0.37
6	0.66	-0.19	-0.35	3.4	0.93	0.45
8	0.31	-0.33	-0.66	7.17	1.4	0.88
10	0.83	-0.45	-0.41	9.75	2.72	1.5
15	0.65	-0.39	-0.52	25.67	6.57	6.08
30	0.35	-0.76	-0.96	198.08	36.53	56.53

With exception of the case with 3 nodes across the web, there is almost no difference (lower than 1.0 %) between the results of the investigated mesh. However, the calculation time differs significantly. Considering the fact that the number of nodes greater than 4 provides almost the same results, the main parameter for the mesh selection was the calculation time.

Finally, 5 nodes on the cross-section flat part were chosen for numerical modelling. It was proved that 5 nodes provide accurate results in reasonable time. In the case of RHS cross-section, 5 nodes are considered across the narrow web of the cross-section. Wide web of the cross-section respect the mesh of the narrow web, see Figure 5.5.

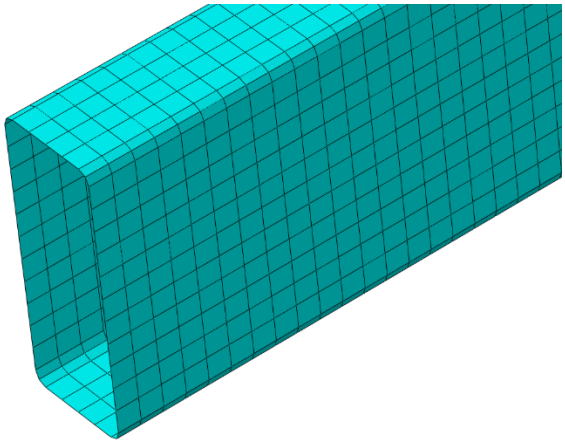

Figure 5.5 *Mesh of RHS 100x40x2.*

5.2.3 Numerical model validation

For the numerical model validation, it was necessary to model the very same members as tested. Therefore, both cross-section and member geometry were adopted from measured values as well as the global and local initial imperfection amplitude values, see Table 4.1 and Table 4.6.

Material properties were adopted from the material tensile tests for both flat and corner part of the cross-section, see Table 4.2 and Table 4.3. However, only engineering stress and strain values were given, therefore it was necessary to calculate true stress and strain values using Equations (5.1) and (5.2).

$$\sigma_{\mathrm{True}} = \sigma_{\mathrm{Nom}}(1 + \varepsilon_{\mathrm{Nom}}) \tag{5.1}$$

$$\varepsilon_{\mathrm{True}} = \ln(1 + \varepsilon_{\mathrm{Nom}}) \tag{5.2}$$

where σ_{Nom} and $\varepsilon_{\mathrm{Nom}}$ are the nominal (engineering) stress and strain values and σ_{True} and $\varepsilon_{\mathrm{True}}$ are the true stress and strain values.

Investigated members were fabricated by cold-rolling, therefore, there is a significant strength enhancement in corner regions of the cross-sections due to induced plastic deformation. As discussed, according to [10] - [13] the area of the enhanced material properties exceeds the corner area which should be extended into the flat parts of the cross-section. The extension was defined as two times of the cross-section wall thickness. However, according to [14], [15] consideration of the enhanced material properties in the corner area only is more accurate. Therefore, during the numerical model validation, the area of enhanced material properties was considered again both with and without the extension.

Numerical model validation was made by the comparison of relationship between loading force and mid-span deflection obtained from experiments and numerical simulations. Typical validation results are given by Figure 5.6, Figure 5.7 and Figure 5.8 representing members with major axis flexural buckling failure, local buckling failure and minor axis flexural buckling failure, respectively, where *FEM – 0t* means numerical results with enhanced material properties considered in the corner area and *FEM – 2t* means consideration with corner extensions into flat parts of the cross-section.

Validation results for all members are given by Chapter 8.

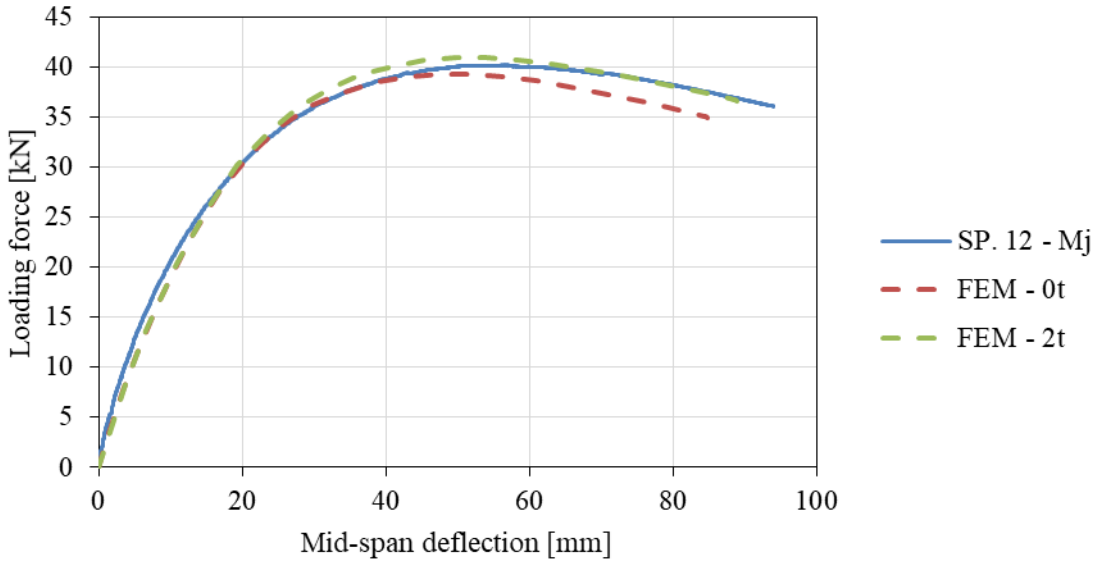

Figure 5.6 *Numerical model validation on specimen 12 (major axis flexural buckling failure).*

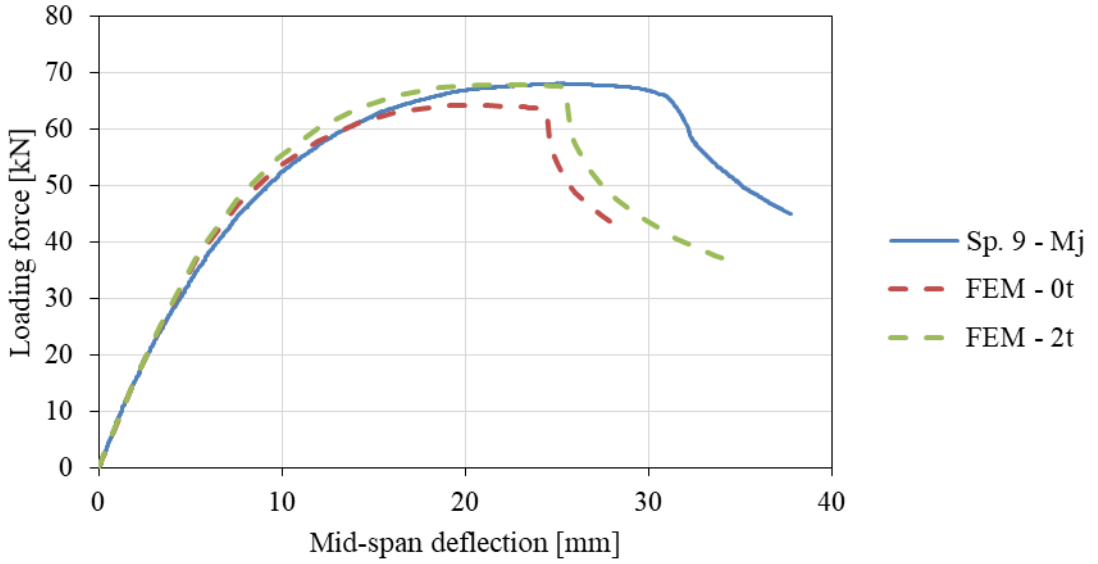

Figure 5.7 *Numerical model validation on specimen 9 (local buckling failure).*

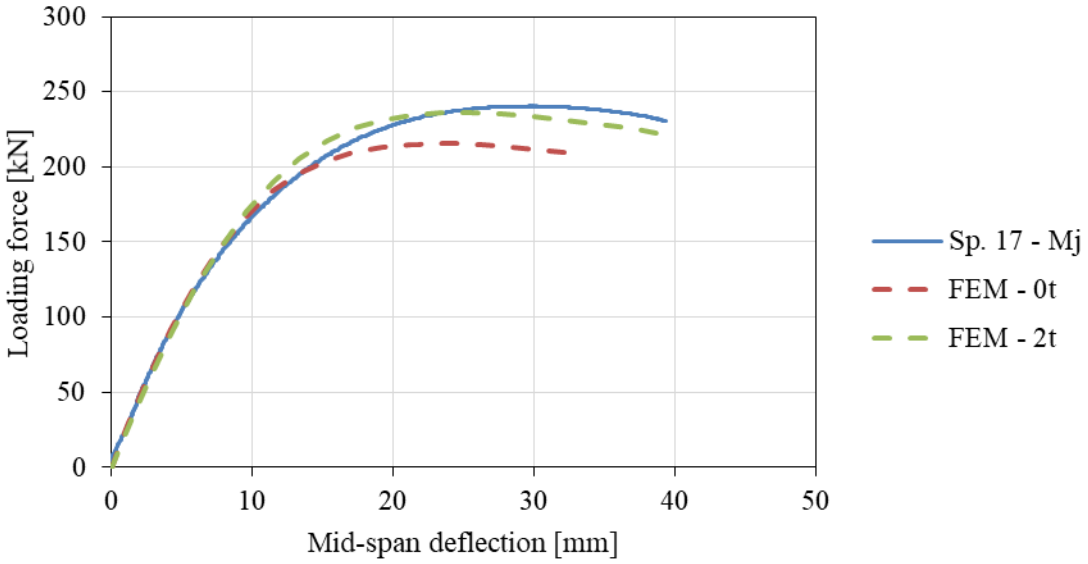

a) Major axis deflection

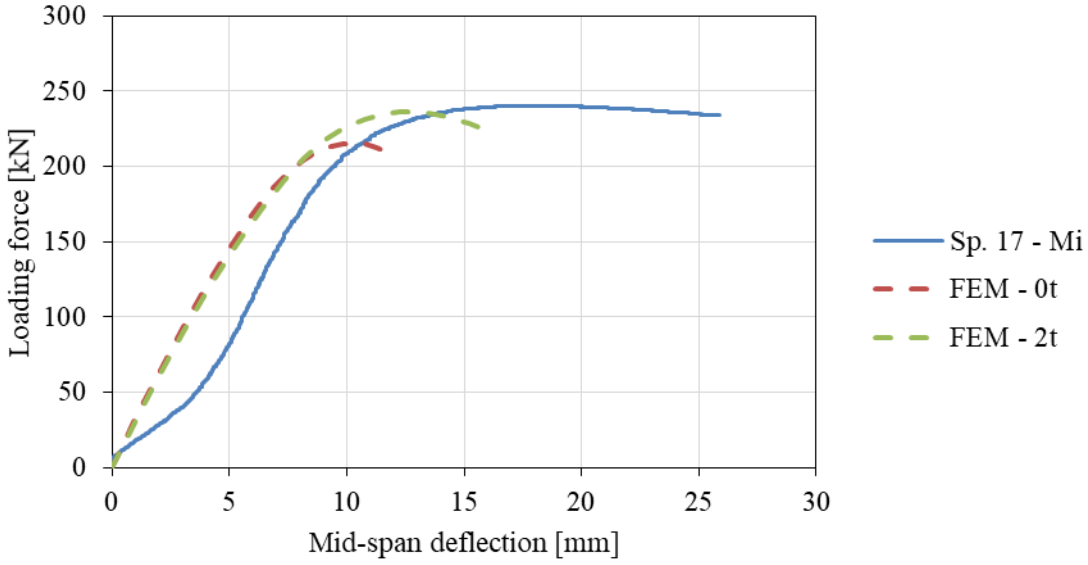

b) Minor axis deflection

Figure 5.8 *Numerical model validation on specimen 17 regarding major axis deflection (a) and minor axis deflection (b) (minor axis flexural buckling failure).*

As could be seen in Figure 5.6, there is a very good agreement between the experimental and numerical results. Experimental resistance is slightly higher than the numerical one without the corner area extension and slightly lower than the one with the extension consideration. In the case of local buckling failure, see Figure 5.7, there is a good agreement as well, however, with little difference in mid-span deflection at failure. That is most probably caused by the fact, that the

local imperfections were introduced to the numerical model by the most unfavourable eigen-mode that could be slightly different compared to the tested member wall profile. Figure 5.8 shows minor axis flexural buckling failure. As was mentioned in Chapter 4.5, the initial minor axis deflection was probably caused by some inaccuracies in test setup, therefore, a very small minor axis rotation equal to 1.5° was allowed at boundary conditions of the numerical model which initiated the minor axis deflection. As could be seen, major axis deflection is in good agreement again, whereas minor axis deflection exhibits little difference in the initial deflection (up to 40 MPa of the stress).

The ultimate loads obtained from the tests were compared to the numerical predictions, considering enhanced material properties only in the corner region and with the extensions as well. The comparison is given in Table 5.2, where $F_{u,test}$, $F_{u,FEM,0t}$ and $F_{u,FEM,2t}$ are the ultimate compressive forces obtained from tests and numerical simulations without and with the corner region extension, respectively.

Table 5.2 *Comparison of test results with numerical predictions.*

Specimen	$F_{u,test}$	$F_{u,FEM,0t}$	$F_{u,FEM,2t}$	$F_{u,test}$ / $F_{u,FEM,0t}$	$F_{u,test}$ / $F_{u,FEM,2t}$
	[kN]	[kN]	[kN]	[-]	[-]
1	97.8	95.4	106.0	1.025	0.923
2	84.1	79.8	88.8	1.054	0.948
3	182.5	171.8	196.3	1.062	0.930
4	143.6	140.9	161.9	1.019	0.887
5	35.7	34.1	38.2	1.045	0.933
6	32.3	34.1	38.2	0.946	0.845
7	23.1	23.3	25.9	0.993	0.892
8	22.8	23.3	26.0	0.978	0.878
9	71.0	64.2	68.0	1.107	1.045
10	72.0	64.2	68.0	1.122	1.060
11	42.9	39.1	40.7	1.098	1.055
12	43.8	39.2	40.9	1.116	1.070
13	87.7	85.6	92.7	1.025	0.946
14	84.4	85.6	92.7	0.986	0.910
15	59.1	57.9	61.1	1.020	0.967
16	59.0	58.3	61.7	1.013	0.957
17	240.4	215.5	236.1	1.116	1.018
18	226.4	218.5	240.6	1.036	0.941
19	176.5	194.5	204.0	0.907	0.865
20	191.3	198.4	206.2	0.964	0.928
Average value				1.032	0.950
Standard deviation				0.059	0.065

Based on the Figure 5.6 to Figure 5.8 could be said that consideration of the corner area extensions provides more accurate predictions, however, data given by Table 5.2 show that in some cases consideration of the pure corner area gives better agreement with the test results. In general, both considerations provide accurate predictions on average with low standard deviation. However, results of the numerical model with no extensions of the corner area exhibit slightly safer and more consistent predictions.

Furthermore, the comparison of local buckling, major and minor axis flexural buckling failure modes of experimental and numerical results are given by Figure 5.9, Figure 5.10 and Figure 5.11, respectively. It should be noted that due to very similar results, numerical results are shown only for model considering the corner area extensions.

The numerical predictions are in very good agreement with data obtained from the conducted tests, therefore, numerical model is accurate and suitable for the following numerical parametric study.

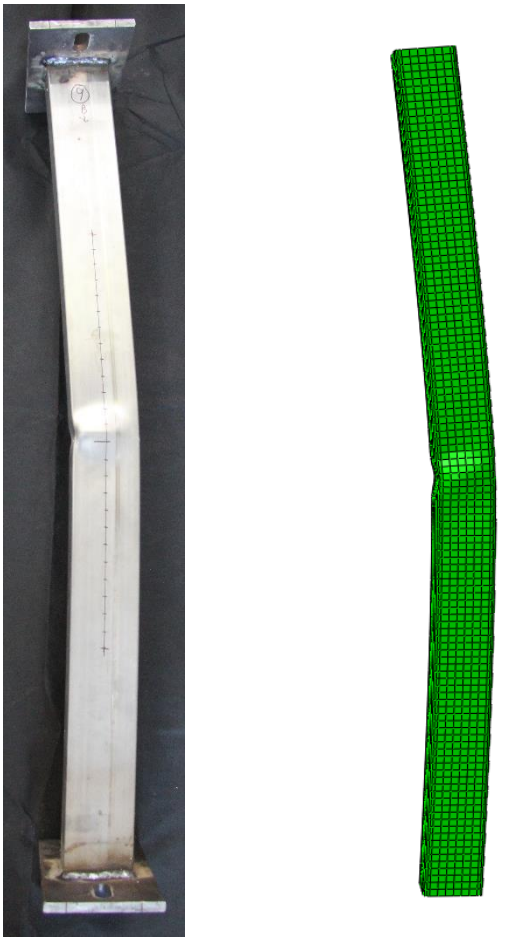

Figure 5.9 *Test and numerical local buckling failure of specimen 13.*

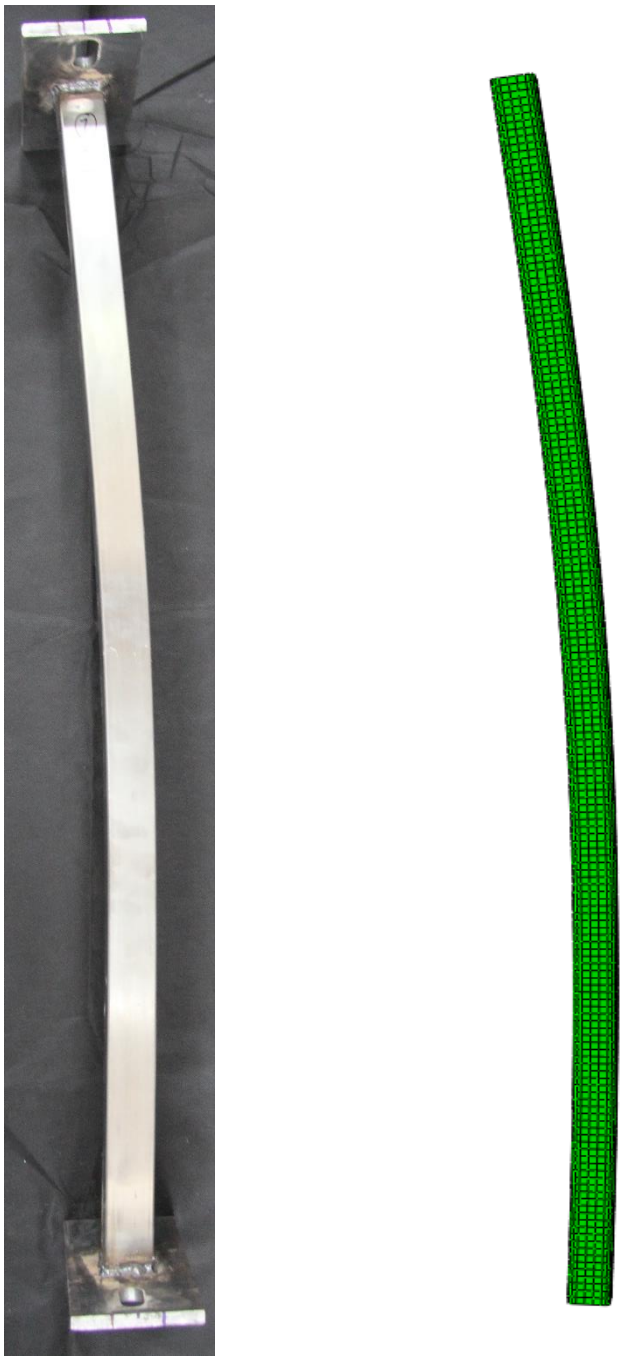

Figure 5.10 *Test and numerical major axis flexural buckling failure of specimen 5.*

Figure 5.11 *Test and numerical minor axis flexural buckling failure of specimen 17.*

5.2.4 Numerical parametric study

The numerical parametric study was made based on the validated numerical model in order to extend the amount of results for stainless steel SHS and RHS beam-column resistance. It considers various cross-section dimensions, cross-section and non-dimensional slendernesses, material properties and loading states (n_b). In total, 738 simulations of beam-column and 324 of flexural buckling and bending were carried out.

Material properties considering three main stainless steel groups, namely austenitic, ferritic and duplex, were used. One grade of each stainless steel group was investigated, however, with consideration of two values of strain hardening exponent *n*, representing upper and lower bound for material non-linearity. The chosen stainless steel grades represent materials with low yield strength f_y and low ultimate strength f_u (ferritic grade), high f_y and high f_u (duplex grade) and the greatest ratio between f_u and f_y (austenitic grade). Young's modulus E_0 = 200 GPa, as given by [5], was considered for all investigated materials. In the numerical parametric study, material properties were considered the same among the whole cross-section, as is used in practice, and they are summarized in Table 5.3. Furthermore, Figure 5.12 shows initial part of stress-strain diagrams.

As a stress-strain diagram, two-stage Ramberg-Osgood model described by Equation (3.3) for the first stage and Equation (3.10) for the second stage was used. Tangent modulus $E_{0.2}$ and strain hardening exponent $n_{0.2,u}$ were calculated according to Equation (3.8) and Equation (3.9), respectively. Ultimate strain ε_u was calculated according to [1] as $1 - (f_y / f_u)$.

Both SHS and RHS members were investigated. Cross-section dimensions were considered as 80 mm for SHS and 100x40 mm for RHS, representing typical SHS and RHS with highest *h* / *b* ratio commonly used. Cross-section centreline was modelled with corner radii equal to two times of the wall thickness. Wall thickness *t* was set as a variable parameter and calculated regarding the appropriate material to cover the cross-section Classes 1 and 4 for SHS and Classes 1, 3 and 4 for RHS. The cross-section classification limits developed by Gardner and Theofanous [36] were used. Wall thickness was considered in a range from 1.5 mm to 8 mm. Consequently, cross-section slenderness $\bar{\lambda}_p$ was given by the most slender cross-section element. It was calculated according to DMSSS Annex D [5] and was in a range from 0.06 to 1.30.

Non-dimensional slenderness $\bar{\lambda}$ values were considered in a range from 0.2 to 3.0 in order to cover both stocky and slender members. Investigated non-dimensional slenderness $\bar{\lambda}$ values are given by Table 5.4, where $\bar{\lambda} = \sqrt{A_{\mathrm{eff}} \sigma_{0.2} / N_{\mathrm{cr}}}$ is the non-dimensional slenderness according to [5], with N_{cr} considered as the Euler buckling load.

Ratio between compressive force and bending moment was investigated based on parameter n_b, which represents ratio between compressive force N_{Ed} and flexural buckling resistance $N_{b,Rd}$. Investigated n_b ratios are given by Table 5.4.

Local and global initial geometric imperfections were considered in the numerical parametric study as well. The global imperfection amplitude was considered as *L / 1000*, where *L* is the member length, whereas local imperfection amplitude was calculated according to Dawson and Walker formula [23], see Equation (3.14), with modification for stainless steel [12].

Data obtained from the comprehensive numerical parametric study were used as a background for the beam-column design procedures evaluation and derivation of new interaction factor formulae.

Table 5.3 *Material properties considered in the numerical parametric study.*

Stainless steel group	E_0	f_y	f_u	n	$n_{0.2,u}$	ε_u
	[GPa]	[MPa]	[MPa]	[-]	[-]	[-]
Austenitic	200	220	520	4.5	2.5	0.58
Austenitic	200	220	520	14	2.5	0.58
Ferritic	200	210	380	4.5	2.9	0.44
Ferritic	200	210	380	14	2.9	0.44
Duplex	200	480	660	4.5	3.5	0.27
Duplex	200	480	660	14	3.5	0.27

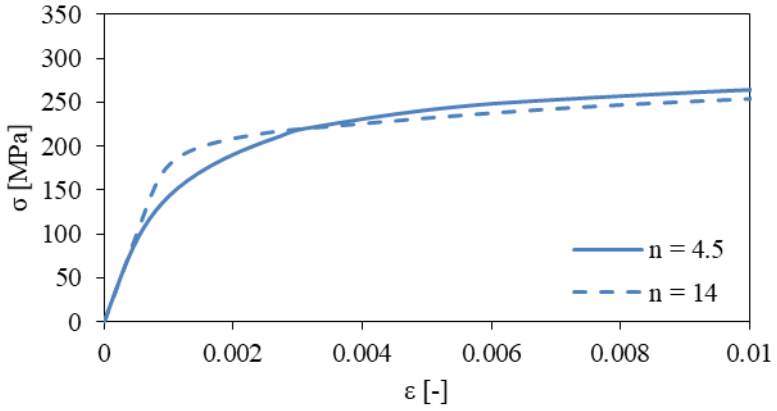

a) Austenitic stainless steel

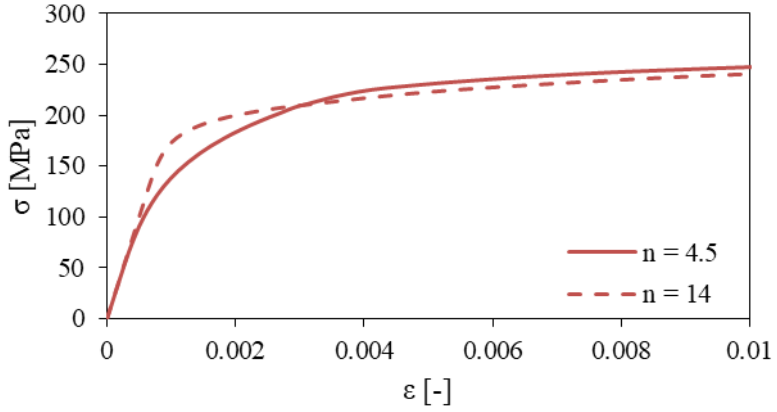

b) Ferritic stainless steel

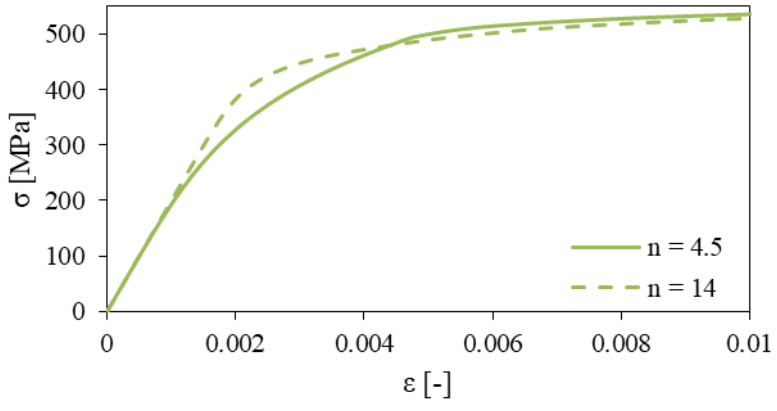

c) Duplex stainless steel

Figure 5.12 *Material stress-strain diagrams considered in the numerical parametric study from 0 to 0.01 of strain (ε).*

Table 5.4 *Non-dimensional slenderness $\bar{\lambda}$ and loading state n_b values considered in the numerical parametric study.*

SHS members		RHS members	
$\bar{\lambda}$	n_b	$\bar{\lambda}$	n_b
0.2	0.05	0.5	0.05
0.3	0.3	0.8	0.1
1.0	0.5	1.0	0.2
1.5	0.7	1.5	0.5
2.0	0.8	2.0	0.8
3.0			

Chapter 6

Proposal for stainless steel beam-column design

Currently, there is a design procedure for stainless steel members loaded by compression and bending given in EN 1993-1-4 [1]. Many improvements of the design approach or developments of absolutely new procedures were made in order to derive both accurate and safe design procedure (see Chapter 3.11). The most recent procedure was developed by Zhao et al. [72], which is also considered for the next edition of EN 1993-1-4, and it is compared below. Finally, a new design formula for SHS and RHS stainless steel beam-columns is proposed in this section.

Design procedure comparison was commonly made based on the comparison of the interaction factor k. Recently, comparison of the ultimate loading force N_u acting on eccentricity against the cross-section centroid causing bending, was used. In this work, comparison of the whole interaction formula result governing the beam-column design is used.

Consequently, the interaction factor may not be absolutely accurate in dominant compression cases due to its low influence. In comparison, a compressive N_{FEM} and bending moment M_{FEM} load values obtained from the numerical model were considered. Flexural buckling resistance $N_{b,Rd,i}$ and bending resistance $M_{Rd,i}$ were calculated according to the appropriate analytical procedure, see chapters below. Comparison was made according to Equation (6.1). Results greater than unity indicate safe results, whereas results lower than unity indicate unsafe results. Results were compared as variable on two criteria, namely n_b ratio and non-dimensional slenderness $\bar{\lambda}$. The reliability conditions are given by Figure 6.1. Procedure given by EN 1993-1-4 [1] is not compared herein, because it is not accurate, as was presented above, and will not be involved in following standard editions.

$$\frac{N_{FEM}}{N_{b,Rd,i}} + k\frac{M_{FEM}}{M_{Rd,i}} \leq 1.0 \tag{6.1}$$

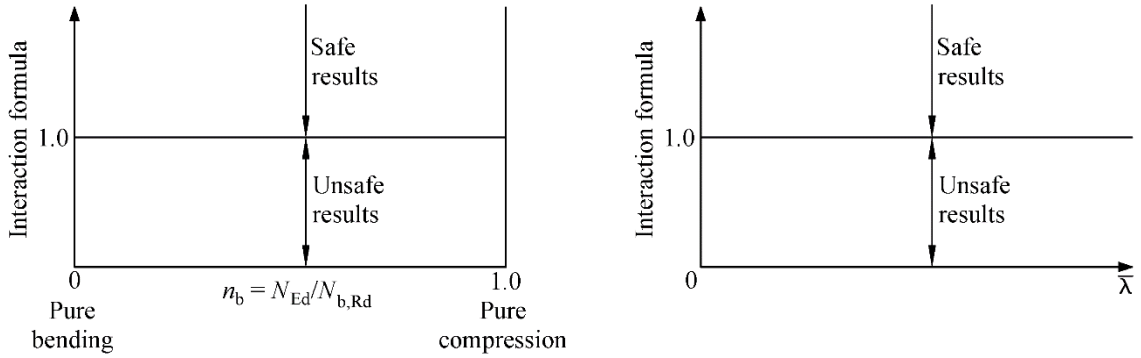

Figure 6.1 *Definition of the design procedure comparison as dependent on n_b ratio (left) and non-dimensional slenderness $\bar{\lambda}$ (right).*

6.2 Comparison of proposal of Zhao et al. [72]

Design procedure developed by Zhao et al. [72] is a most developed procedure for stainless steel SHS and RHS beam-column design. As mentioned before, the procedure is suitable for the main three stainless steel groups, namely austenitic, ferritic and duplex and provides separate constants for each.

For the procedure evaluation, the numerical parametric study results were used. Flexural buckling resistance was calculated according to EN 1993-1-4 [1] considering revised buckling curves [41]. The cross-section bending resistance was calculated according to CSM, as was considered during its development. However, with modification for slender cross-sections [49].

Comparison of the procedure is given by Figure 6.2 and Figure 6.3 as dependent on non-dimensional slenderness $\bar{\lambda}$ and n_b ratio, respectively.

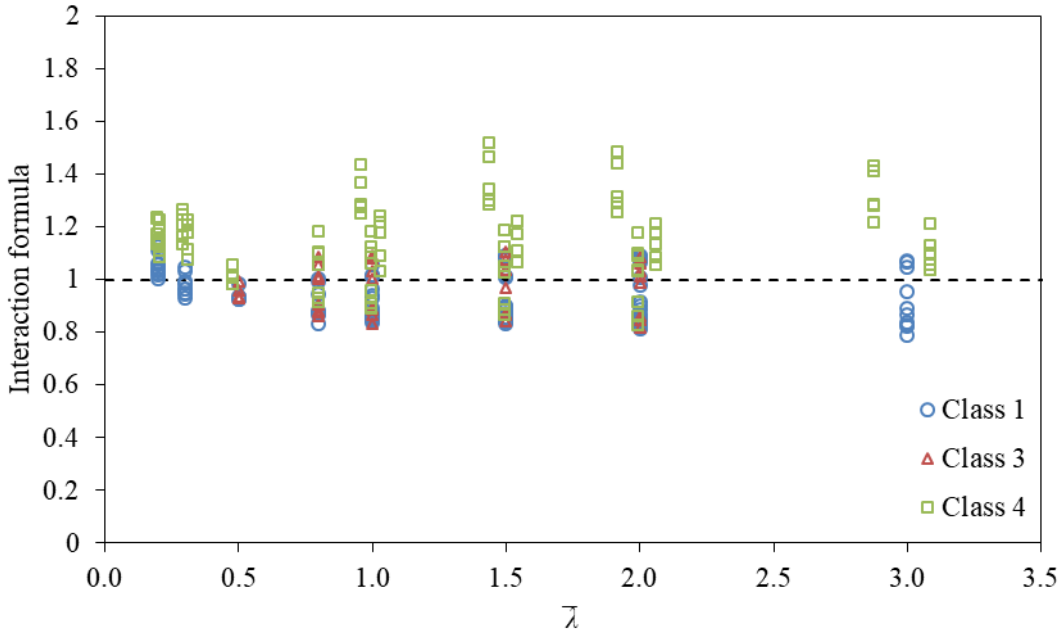

a) Austenitic stainless steel

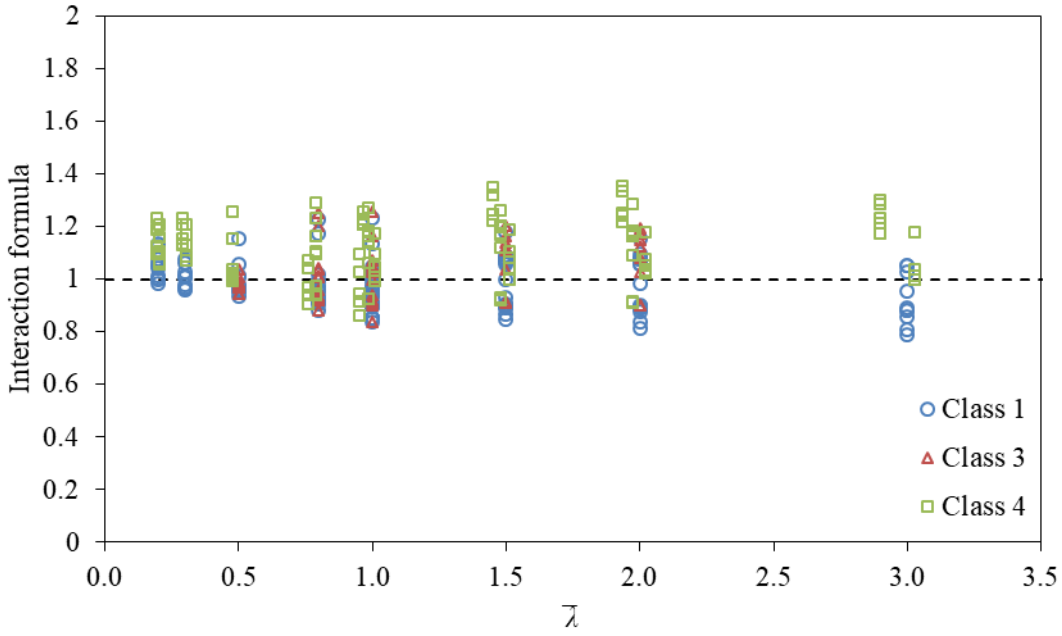

b) Ferritic stainless steel

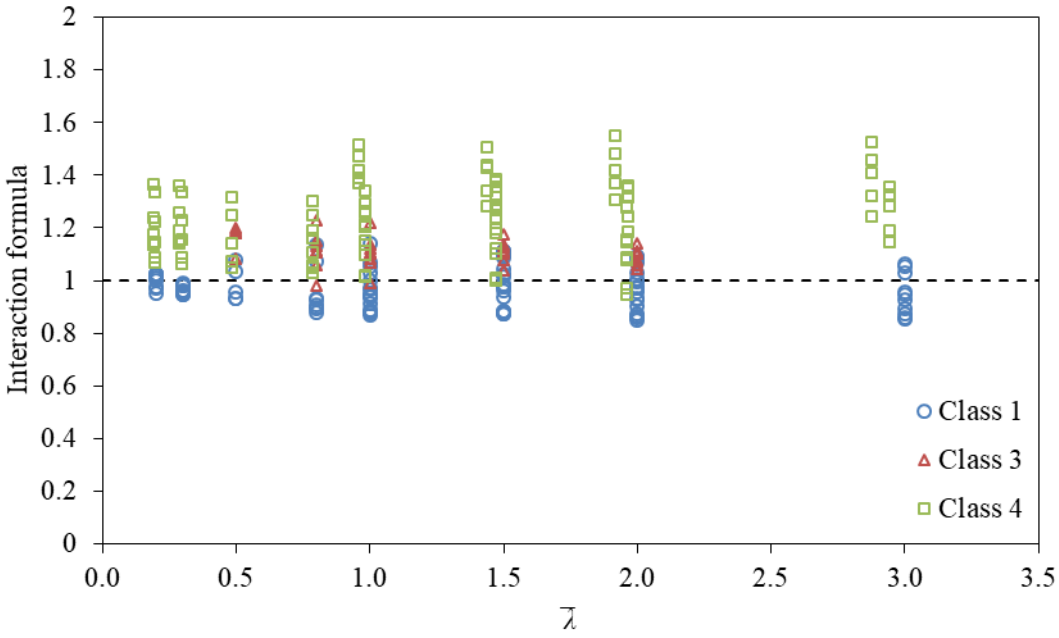

c) Duplex stainless steel

Figure 6.2 *Comparison of the Zhao et al. procedure [72] as dependent on non-dimensional slenderness $\bar{\lambda}$.*

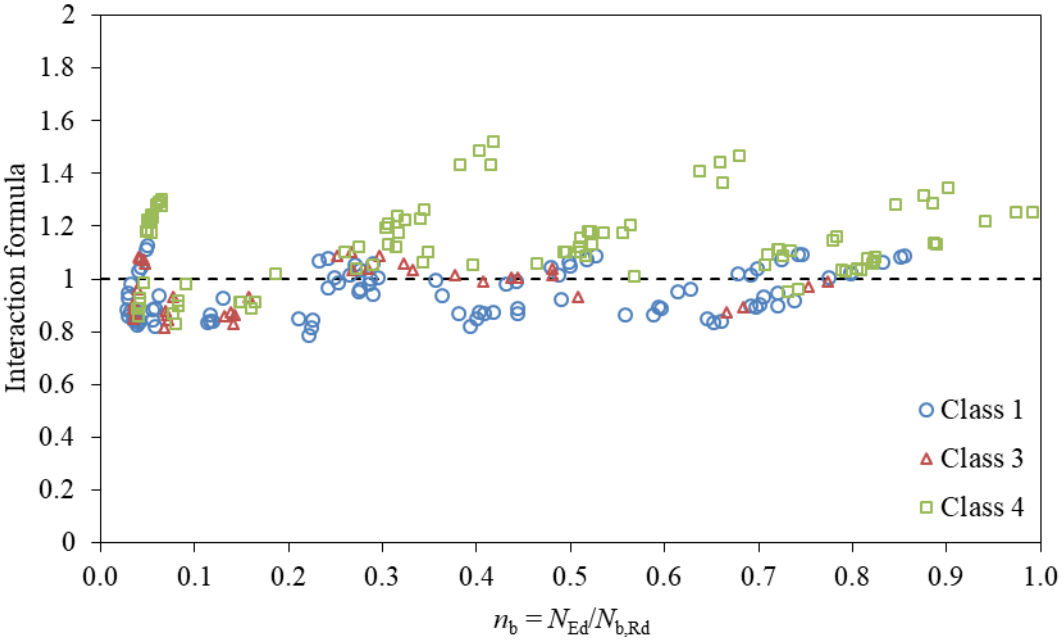

a) Austenitic stainless steel

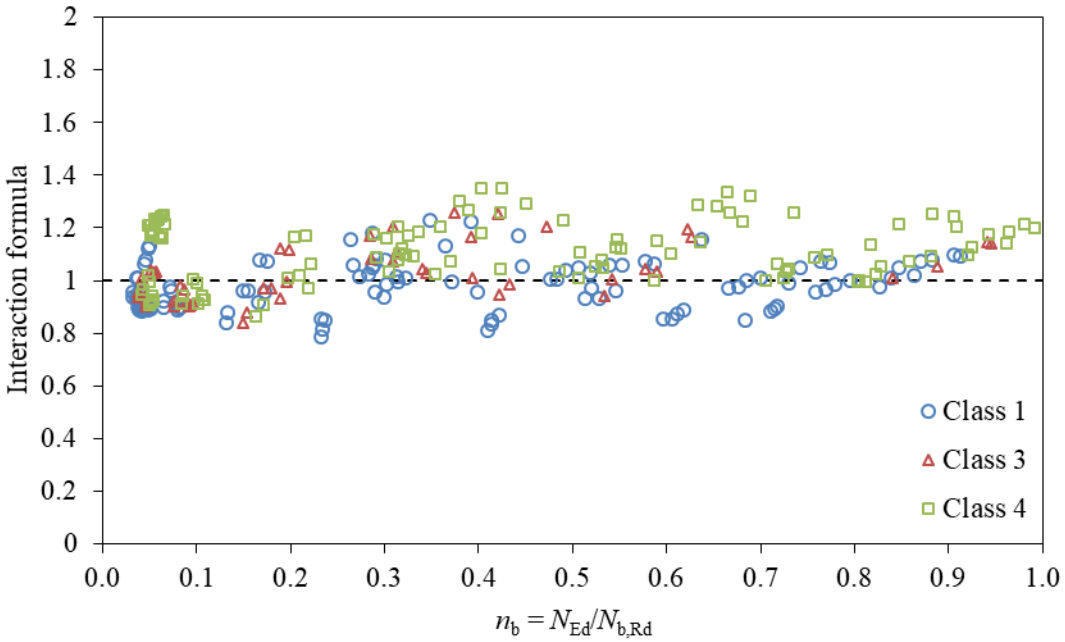

b) Ferritic stainless steel

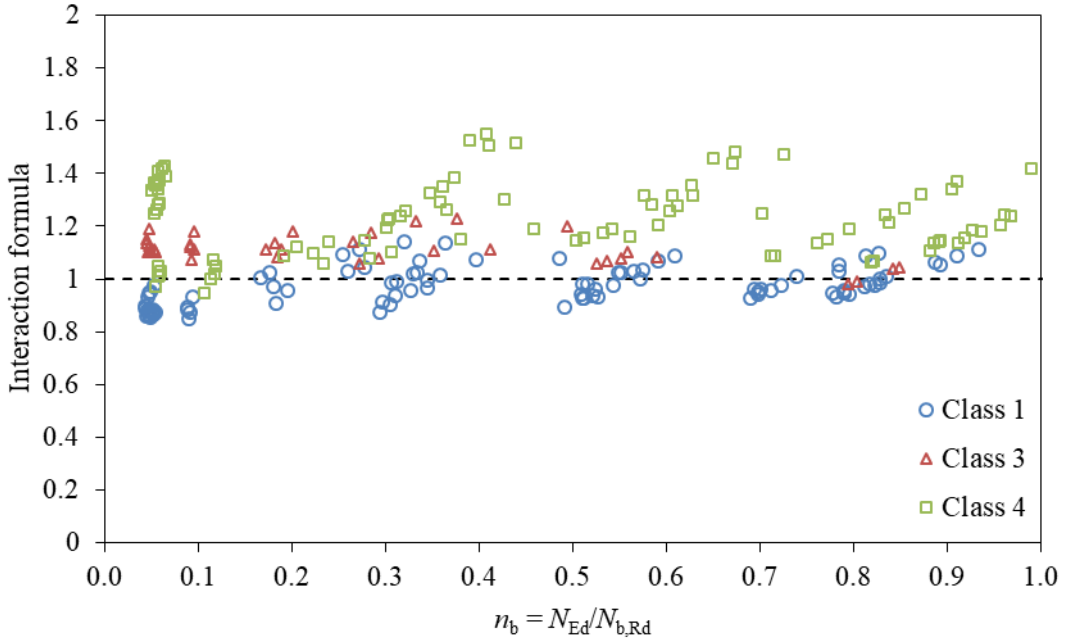

c) Duplex stainless steel

Figure 6.3 *Comparison of the Zhao et al. procedure [72] as dependent on n_b ratio.*

Due to the fact that the analytically calculated resistances (flexural buckling and bending) were combined with the ultimate loads obtained from the numerical model, some conservativeness was expected. As could be seen, results provided by design approach developed by Zhao et al. [72] provides good predictions in general. However, results for Class 4 cross-sections are slightly scattered and conservative in some cases of all stainless steel groups. That could be caused by the fact that during the procedure development the improvement of CSM for slender cross-sections [49] did not exist. On the other hand, for all three stainless steel groups some results for Class 1 cross-sections are slightly unsafe with increasing non-dimensional slenderness. Class 3 cross-section results are very good in the case of duplex stainless steel group, however, for austenitic and ferritic steels exhibit slightly unsafe predictions in dominant bending moment cases.

6.3 New proposal for the design of SHS and RHS beam-columns under uniform bending moment

The procedure developed by Zhao et al. [72] was found accurate on average, however, with some conservative and unsafe predictions in a few specific cases as it was developed on a limited number of results. Therefore, a new proposal for the design of stainless steel SHS and RHS members loaded by compressive force and bending moment combination is presented in this chapter. The procedure was developed based on the data obtained from the numerical parametric study. For the new proposal development, the ultimate compressive force N_{FEM} and bending moment M_{FEM} were obtained from the numerical model, as well as column resistance $N_{\mathrm{b,Rd,FEM}}$ and cross-section bending resistance $M_{\mathrm{Rd,FEM}}$.

6.3.1 New proposal development

The same interaction formulae as given by EN 1993-1-4 [1] was considered, see Equations (3.47) and (3.48). Their simplifications for the combination of compressive force and uniaxial major or minor axis bending moment are given by Equations (6.2) to (6.4). Cross-section load-bearing capacity conditions were considered as well, see Equations (6.5) and (6.6). However, they were never governing.

$$\frac{N_{\mathrm{Ed}}}{N_{\mathrm{b,Rd,y}}} + k_{\mathrm{yy}} \frac{M_{\mathrm{Ed,y}}}{M_{\mathrm{Rd,y}}} \leq 1.0 \tag{6.2}$$

$$\frac{N_{\mathrm{Ed}}}{N_{\mathrm{b,Rd,z}}} + k_{\mathrm{zy}} \frac{M_{\mathrm{Ed,y}}}{M_{\mathrm{Rd,y}}} \leq 1.0 \tag{6.3}$$

$$\frac{N_{\mathrm{Ed}}}{N_{\mathrm{b,Rd,z}}} + k_{\mathrm{zz}} \frac{M_{\mathrm{Ed,z}}}{M_{\mathrm{Rd,z}}} \leq 1.0 \tag{6.4}$$

$$\frac{N_{\mathrm{Ed}}}{N_{\mathrm{Rd}}} + \frac{M_{\mathrm{Ed,y}}}{M_{\mathrm{Rd,y}}} \leq 1.0 \tag{6.5}$$

$$\frac{N_{\mathrm{Ed}}}{N_{\mathrm{Rd}}} + \frac{M_{\mathrm{Ed,z}}}{M_{\mathrm{Rd,z}}} \leq 1.0 \tag{6.6}$$

For the new proposal development both ultimate applied loads and load-bearing capacities were obtained from the numerical model. Therefore, Equations (6.2) to (6.6) can be modified and written as Equations (6.7) to (6.11).

$$\frac{N_{\mathrm{FEM}}}{N_{\mathrm{b,Rd,FEM,y}}} + k_{\mathrm{new,yy}} \frac{M_{\mathrm{FEM,y}}}{M_{\mathrm{Rd,FEM,y}}} \leq 1.0 \tag{6.7}$$

$$\frac{N_{\mathrm{FEM}}}{N_{\mathrm{b,Rd,FEM,z}}} + k_{\mathrm{new,zy}} \frac{M_{\mathrm{FEM,y}}}{M_{\mathrm{Rd,FEM,y}}} \leq 1.0 \tag{6.8}$$

$$\frac{N_{\mathrm{FEM}}}{N_{\mathrm{b,Rd,FEM,z}}} + k_{\mathrm{new,zz}} \frac{M_{\mathrm{FEM,z}}}{M_{\mathrm{Rd,FEM,z}}} \leq 1.0 \tag{6.9}$$

$$\frac{N_{\mathrm{FEM}}}{N_{\mathrm{Rd,FEM}}} + \frac{M_{\mathrm{FEM,y}}}{M_{\mathrm{Rd,FEM,y}}} \leq 1.0 \tag{6.10}$$

$$\frac{N_{\mathrm{FEM}}}{N_{\mathrm{Rd,FEM}}} + \frac{M_{\mathrm{FEM,z}}}{M_{\mathrm{Rd,FEM,z}}} \leq 1.0 \tag{6.11}$$

where $k_{\mathrm{new,y}}$ and $k_{\mathrm{new,z}}$ are the new interaction factors regarding appropriate axis.

Equations (6.7) to (6.9) were used for the new interaction factor $k_{\mathrm{new,yy}}$, $k_{\mathrm{new,zy}}$ and $k_{\mathrm{new,zz}}$ formulae development. There was the aim to develop a safe and accurate stainless steel SHS and RHS beam-column design procedure general enough, to be used for any material properties, loading state and both member and cross-section slenderness. Therefore, data obtained from the numerical parametric study were used.

A new interaction factor is proposed by Equations (6.12) and (6.13) for combination of compression and major axis bending with Equation (6.14) for uniaxial and biaxial symmetric

cross-sections and by Equations (6.15) and (6.16) for compression and minor axis bending combination.

$$k_{\mathrm{new,yy}} = 1 + 1.5\bar{\lambda}_{\mathrm{y}} n_{\mathrm{b,y}}^{\beta_{\mathrm{y}}} \quad \text{for} \quad \bar{\lambda}_{\mathrm{y}} \leq 1.0 \tag{6.12}$$

$$k_{\mathrm{new,yy}} = 1 + 1.5\bar{\lambda}_{\mathrm{y}} n_{\mathrm{b,y}}^{\beta_{\mathrm{y}}} \frac{0.8}{\sqrt{\bar{\lambda}_{\mathrm{y}} - 0.36}} \quad \text{for} \quad \bar{\lambda}_{\mathrm{y}} > 1.0 \tag{6.13}$$

$$k_{\mathrm{new,zy}} = 0.5 k_{\mathrm{yy}} \tag{6.14}$$

$$k_{\mathrm{new,zz}} = 1 + 1.5\bar{\lambda}_{\mathrm{z}} n_{\mathrm{b,z}}^{\beta_{\mathrm{z}}} \quad \text{for} \quad \bar{\lambda}_{\mathrm{z}} \leq 1.0 \tag{6.15}$$

$$k_{\mathrm{new,zz}} = 1 + 1.5\bar{\lambda}_{\mathrm{z}} n_{\mathrm{b,z}}^{\beta_{\mathrm{z}}} \frac{0.8}{\sqrt{\bar{\lambda}_{\mathrm{z}} - 0.36}} \quad \text{for} \quad \bar{\lambda}_{\mathrm{z}} > 1.0 \tag{6.16}$$

with

$$n_{\mathrm{b,y}} = \frac{N_{\mathrm{Ed}}}{N_{\mathrm{b,Rd,y}}} \tag{6.17}$$

$$n_{\mathrm{b,z}} = \frac{N_{\mathrm{Ed}}}{N_{\mathrm{b,Rd,z}}} \tag{6.18}$$

$$\beta_{\mathrm{y}} = \left(\frac{M_{\mathrm{el,y}}}{M_{\mathrm{Rd,y}}}\right)^2 \tag{6.19}$$

$$\beta_{\mathrm{z}} = \left(\frac{M_{\mathrm{el,z}}}{M_{\mathrm{Rd,z}}}\right)^2 \tag{6.20}$$

where $M_{\mathrm{el,y}}$ and $M_{\mathrm{el,z}}$ are the elastic bending moment capacity for the appropriate axis calculated as the appropriate elastic cross-section modulus $W_{\mathrm{el,i}}$ times 0.2 % proof stress $\sigma_{0.2}$.

In the proposal, non-dimensional slenderness $\bar{\lambda}$ as well as loading state (n_{b}) are considered. For the consideration of cross-section slenderness (Class) factor β_{i} was introduced. Usually, interaction factor is defined by a bi-linear curve with a plateau beyond specific non-dimensional slenderness value. However, it was found there is still increasing trend of the interaction factor value with increasing slenderness. Therefore, the second stage of the interaction factor ($\bar{\lambda} > 1.0$) is increasing with non-dimensional slenderness, but the slope is reduced by introduction of an additional factor. Numerator constant was derived based on numerical study data, whereas denominator considers non-dimensional slenderness influence. Square root constant ensures interaction factor curve continuity, because if $\bar{\lambda} = 1.0$ the whole fraction is equal to unity as well.

Figure 6.4 shows interaction factor k in relation with non-dimensional slenderness $\bar{\lambda}$ for two n_b ratio values and β factor equal to unity. There is a steep increase up to $\bar{\lambda} = 1.0$ beyond which the increase is lower. The more compression the steeper slope. Figure 6.5 provides very similar curves, however, for two values of factor β with $n_b = 0.5$.

Figure 6.6 and Figure 6.7 provide a comparison of the interaction factor k_{new} curve calculated according to the new proposal with the interaction factor values k_{FEM} obtained from the numerical model. Comparison is made for $n_b = 0.2$ and 0.7 with $\beta \geq 0.195$ and ≥ 0.318, respectively. As can be seen, k_{new} is mostly safe and cover the trend of k_{FEM} accurately.

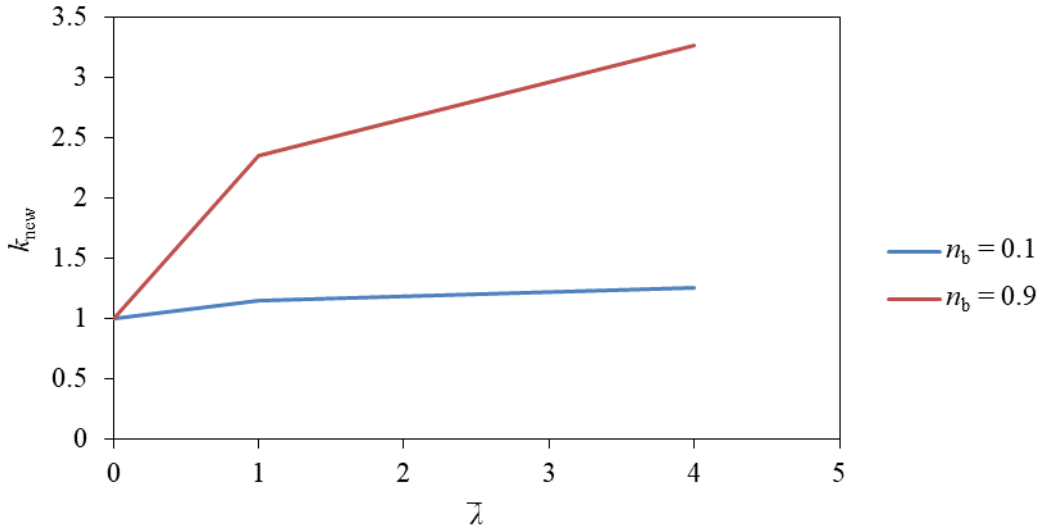

Figure 6.4 *New interaction factor curve with β = 1.0 as dependent on non-dimensional slenderness $\bar{\lambda}$.*

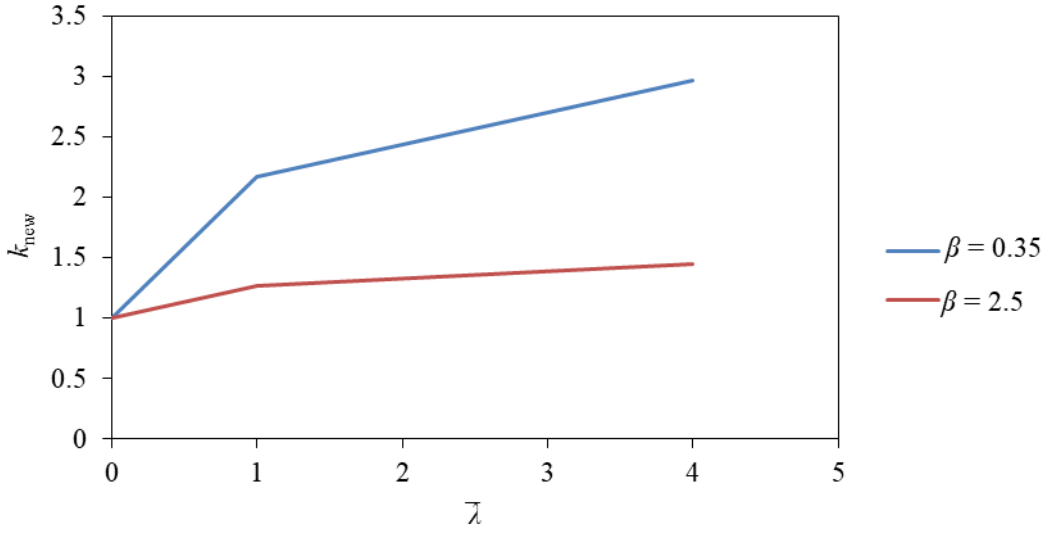

Figure 6.5 *New interaction factor curve with n_b = 0.5 as dependent on non-dimensional slenderness $\bar{\lambda}$.*

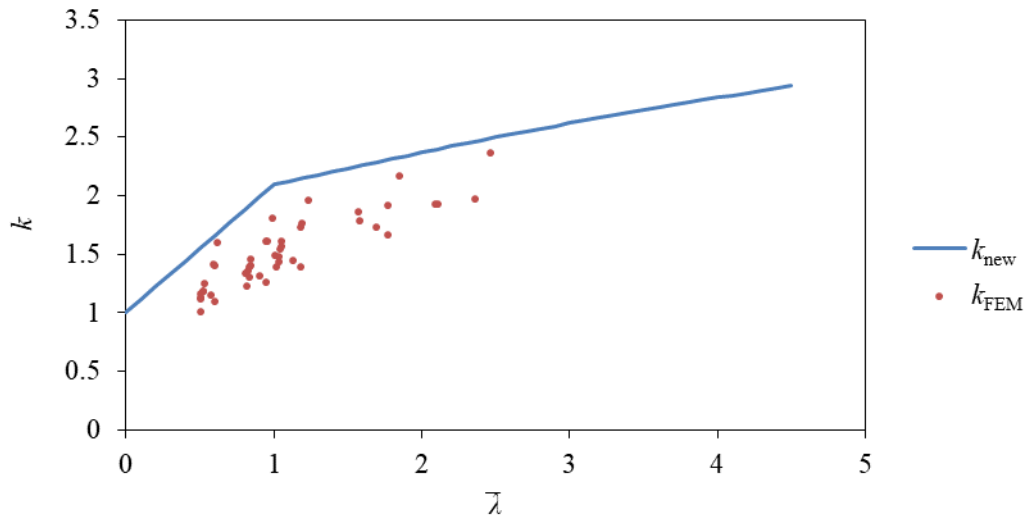

Figure 6.6 *Comparison of the interaction factors k_{new} and k_{FEM} for n_b = 0.2 with $\beta \geq 0.195$ as dependent on non-dimensional slenderness $\bar{\lambda}$.*

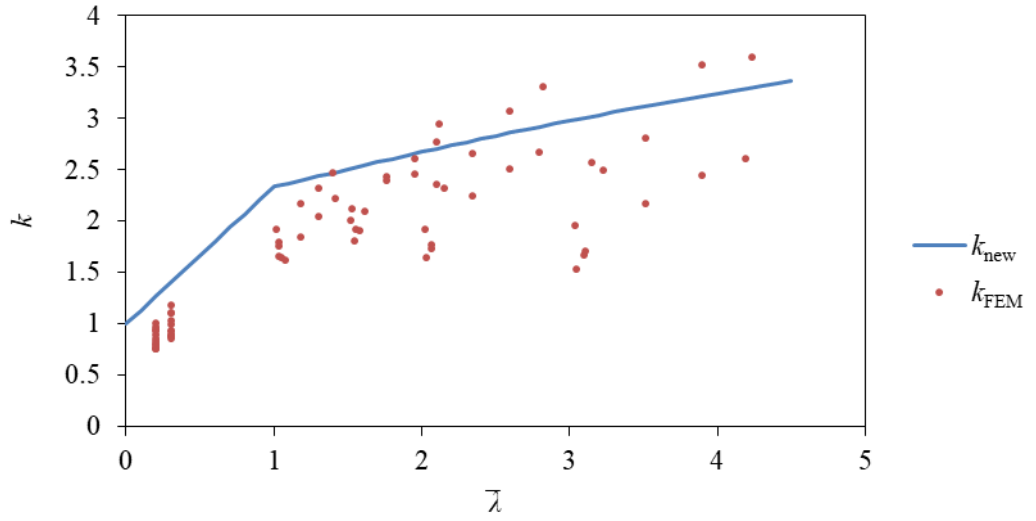

Figure 6.7 *Comparison of the interaction factors k_{new} and k_{FEM} for n_b = 0.7 with $\beta \geq 0.318$ as dependent on non-dimensional slenderness $\bar{\lambda}$.*

6.3.2 New proposal comparison

The procedure was developed based on the numerically calculated load-bearing capacities. Comparison considering load-bearing capacities and both compressive and bending load from the numerical study with the new interaction factor was made. Figure 6.8 provides comparison results as dependent on non-dimensional slenderness $\bar{\lambda}$, whereas Figure 6.9 as dependent on n_b ratio.

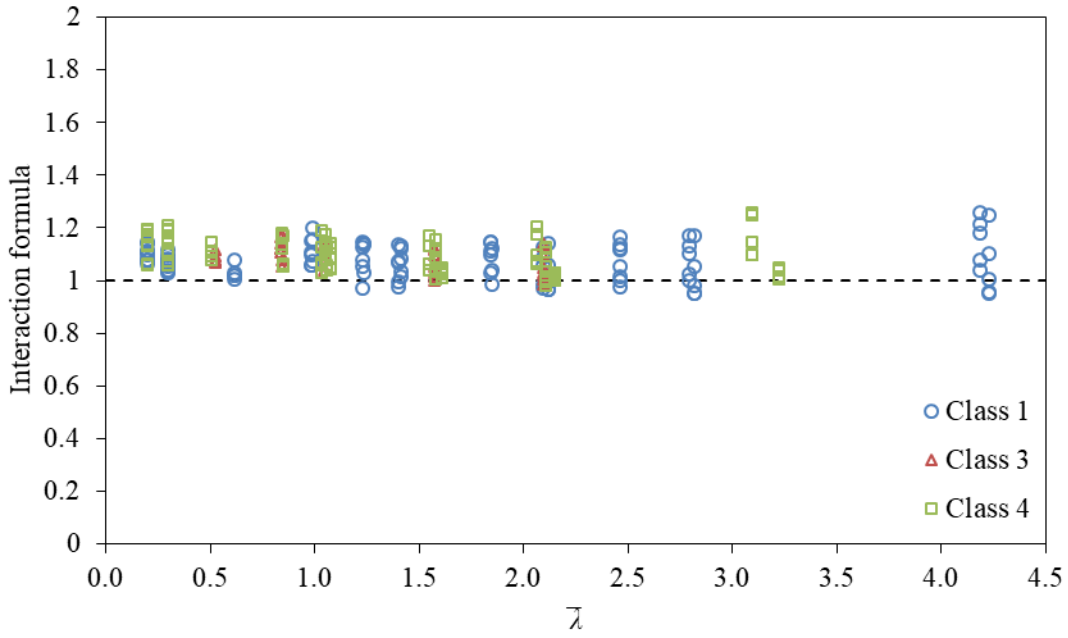

a) Austenitic stainless steel

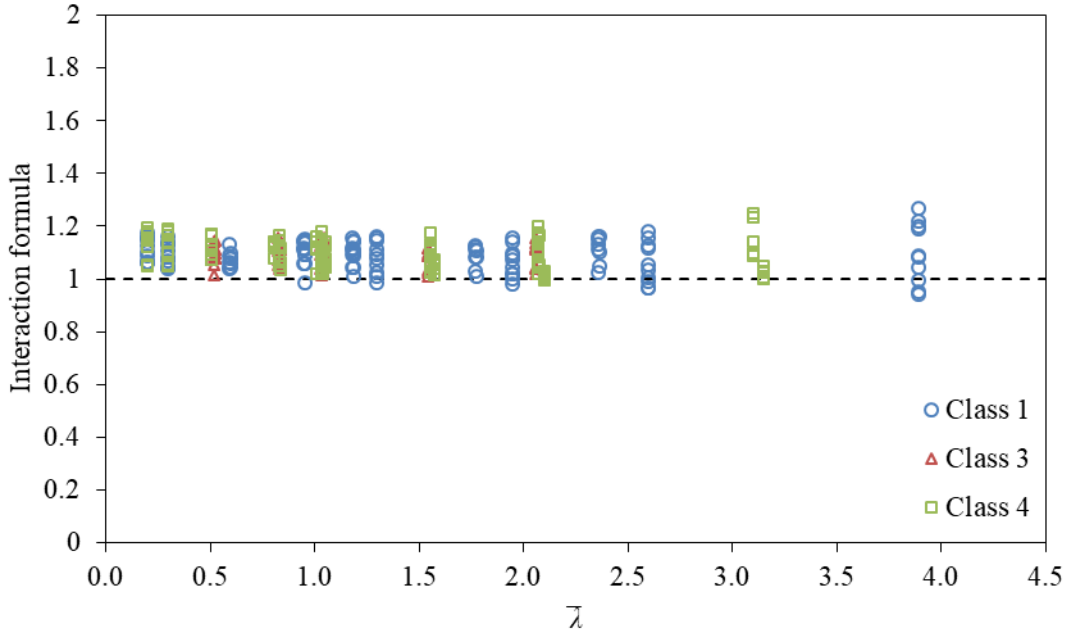

b) Ferritic stainless steel

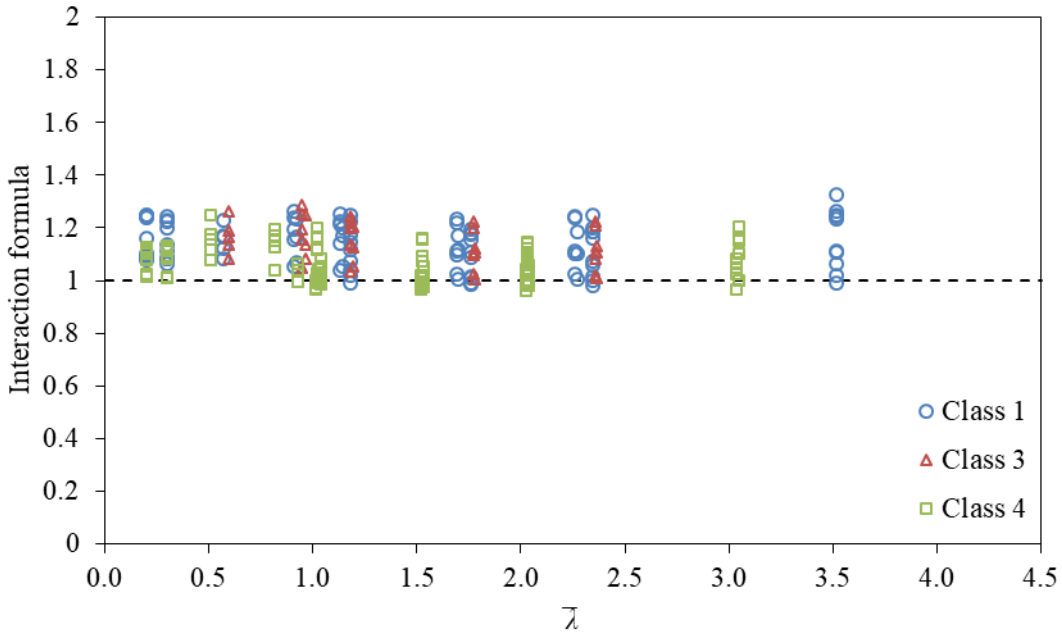

c) Duplex stainless steel

Figure 6.8 *Comparison of the new proposal as dependent on non-dimensional slenderness $\bar{\lambda}$, considering numerical load-bearing capacities ($N_{b,Rd,FEM}$ and $M_{Rd,FEM}$).*

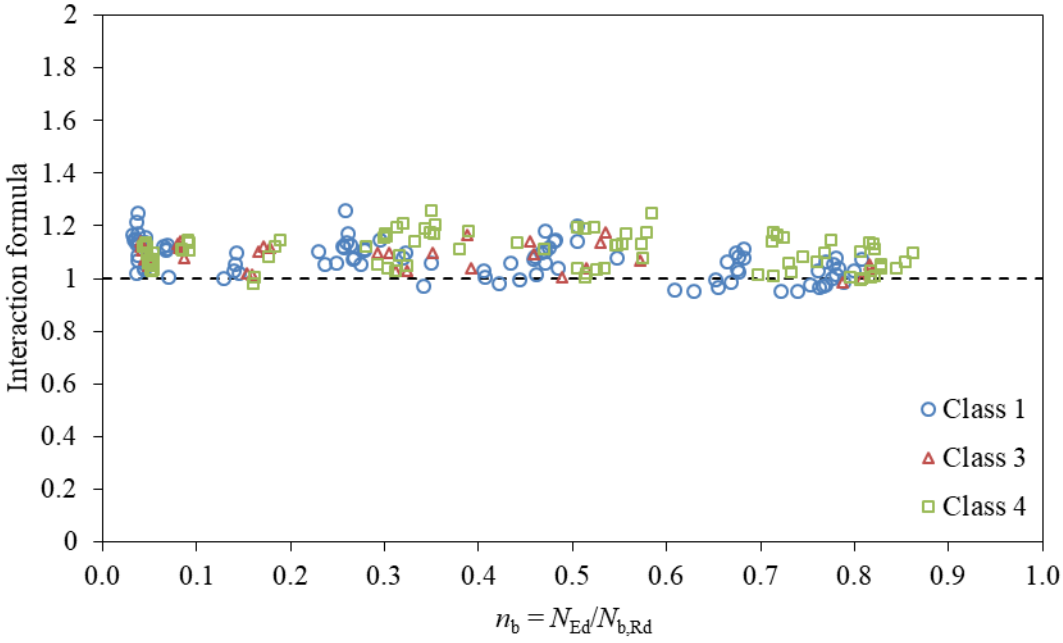

a) Austenitic stainless steel

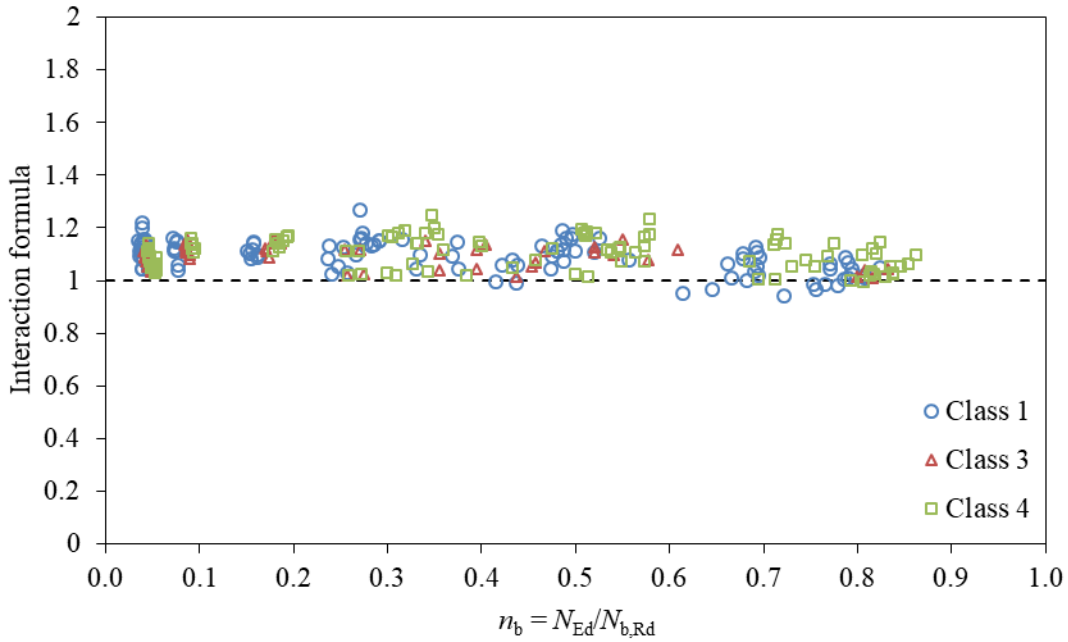

b) Ferritic stainless steel

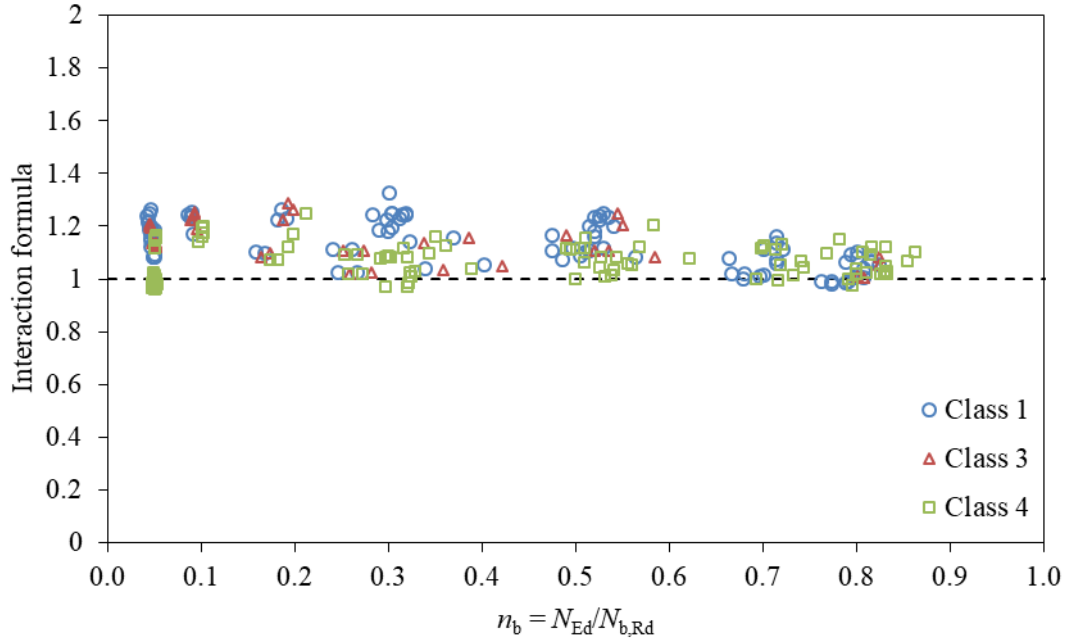

c) Duplex stainless steel

Figure 6.9 *Comparison of the new proposal as dependent on n_b ratio, considering numerical load-bearing capacities ($N_{b,Rd,FEM}$ and $M_{Rd,FEM}$).*

As could be seen in Figure 6.8 and Figure 6.9, the new proposal provides both safe, accurate and consistent predictions for SHS and RHS stainless steel beam-columns. It is a general proposal for stainless steel SHS and RHS beam-column design.

It was assessed that the new proposal is in very good agreement with the real behaviour of SHS and RHS stainless steel beam-columns but only with the consideration of the real load-bearing capacities. Due to the fact that analytically calculated approximations of the real flexural buckling and bending resistances are being used in design practice, comparison with these is necessary.

6.3.3 Load-bearing capacities according to EN 1993-1-4 with revised flexural buckling curves.

Evaluation of the new proposal was also done considering flexural buckling resistance according to EN 1993-1-4 [1] with revised stainless steel flexural buckling curves developed by Afshan et al. [41] and cross-section bending resistance according to EN 1993-1-4 [1]. As only simple approximations of the real column and cross-section resistances are considered, more scattered results could be expected. Figure 6.10 shows evaluation of the new proposal as dependent on the non-dimensional slenderness $\bar{\lambda}$, while Figure 6.11 as dependent on n_b ratio. Furthermore, evaluation of the new proposal based on the experimental data is given by Figure 6.12, where 0t and 2t mean consideration of the cross-section without and with the corner region extension, respectively.

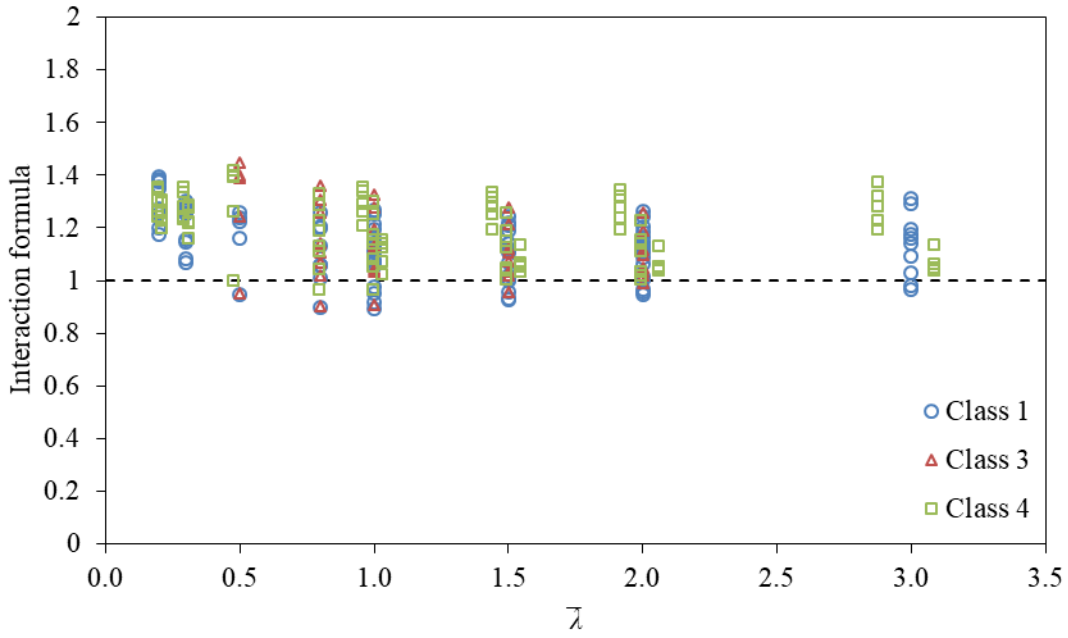

a) Austenitic stainless steel

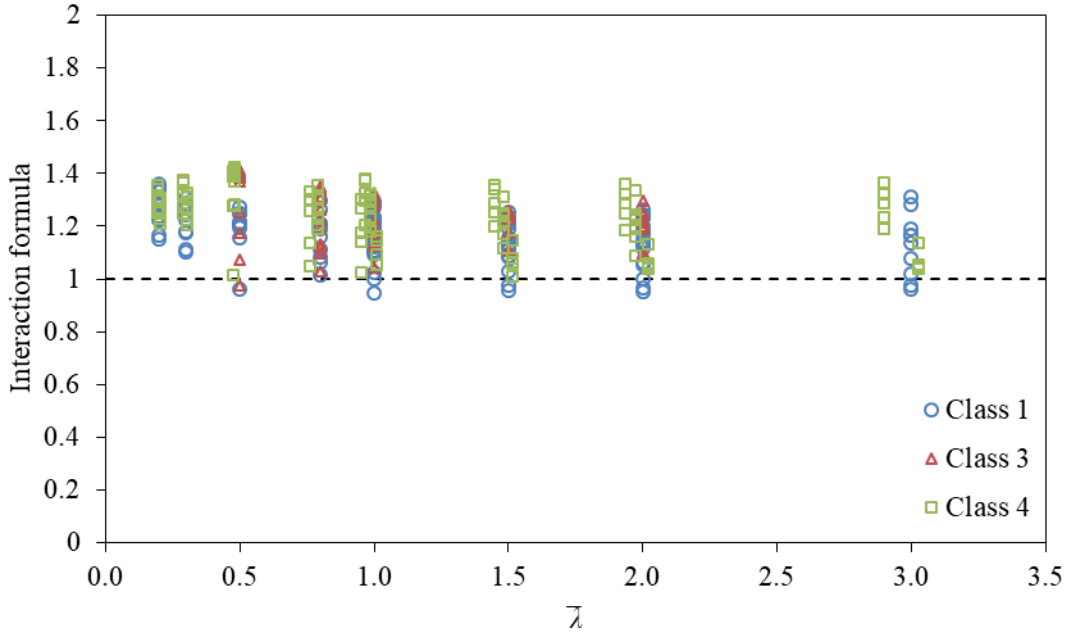

b) Ferritic stainless steel

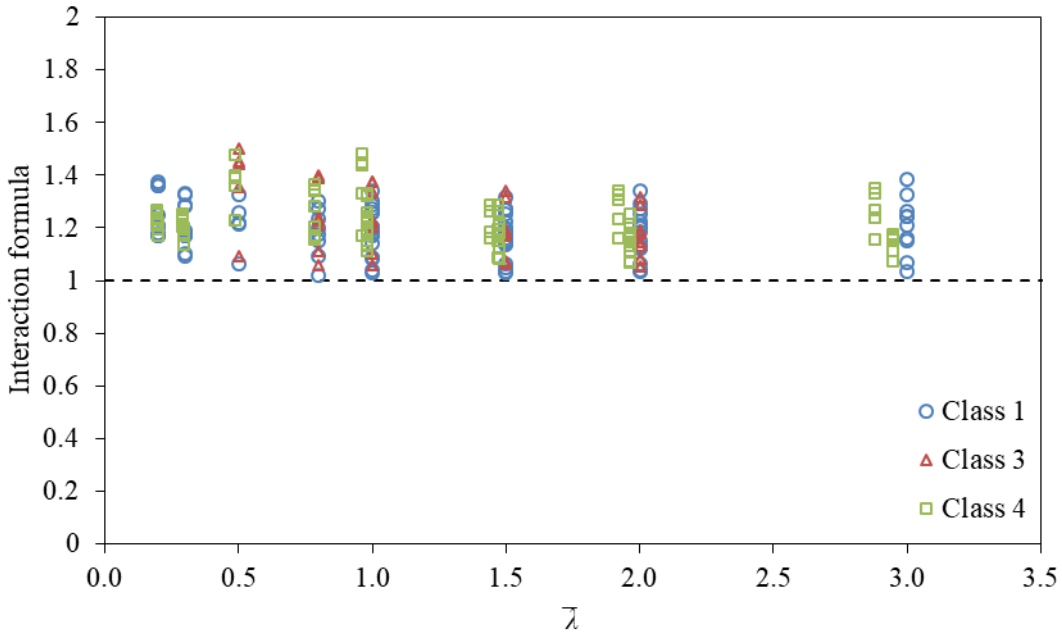

c) Duplex stainless steel

Figure 6.10 *Comparison of the new proposal as dependent on non-dimensional slenderness $\bar{\lambda}$, considering flexural buckling and bending resistance according to Afshan et al. and EN 1993-1-4, respectively.*

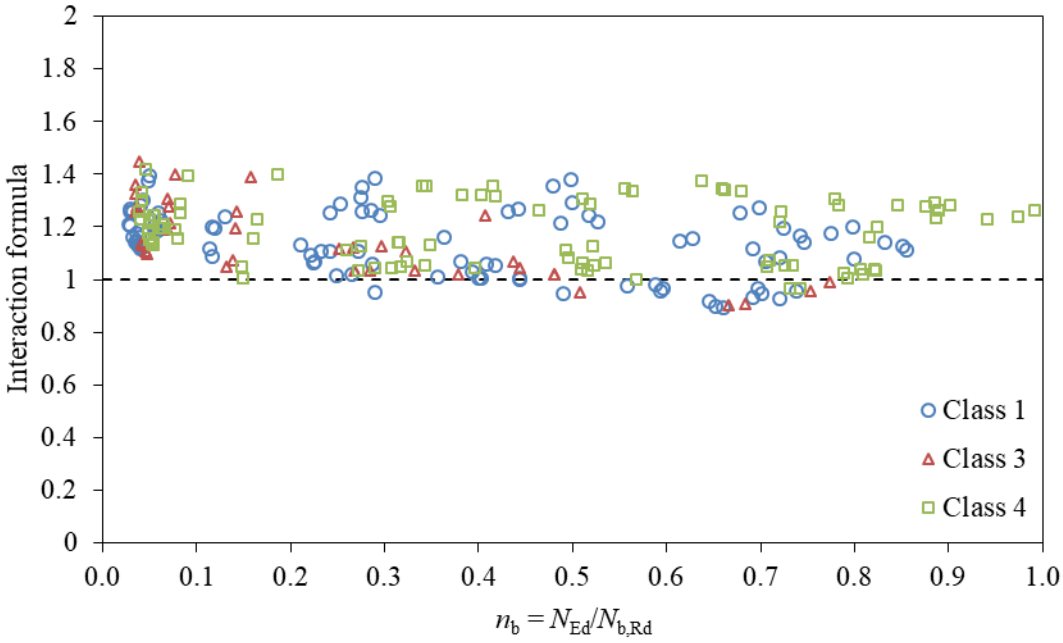

a) Austenitic stainless steel

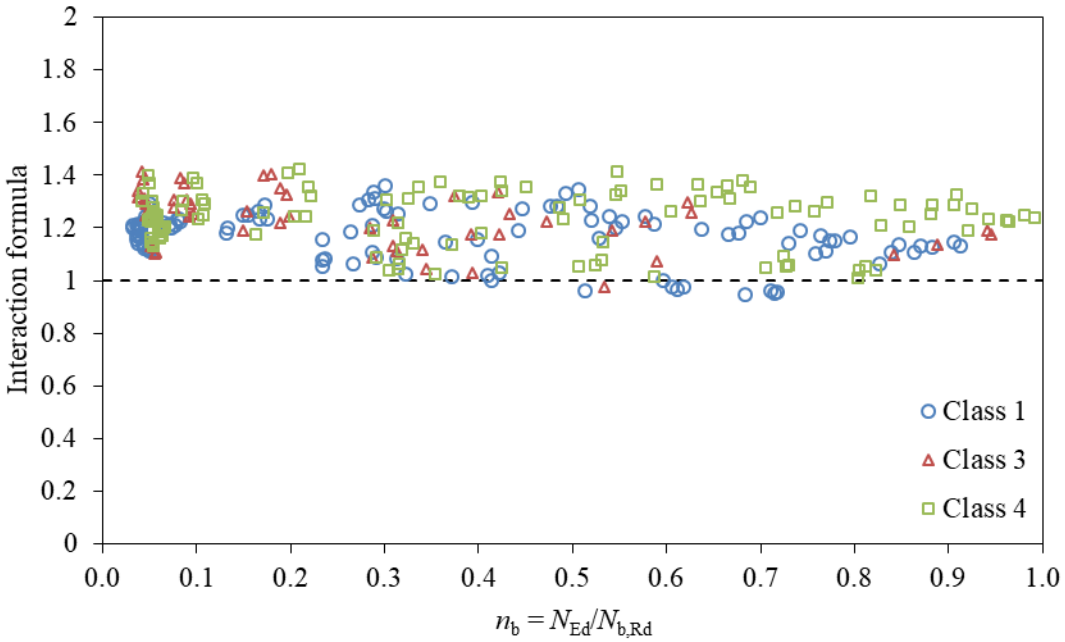

b) Ferritic stainless steel

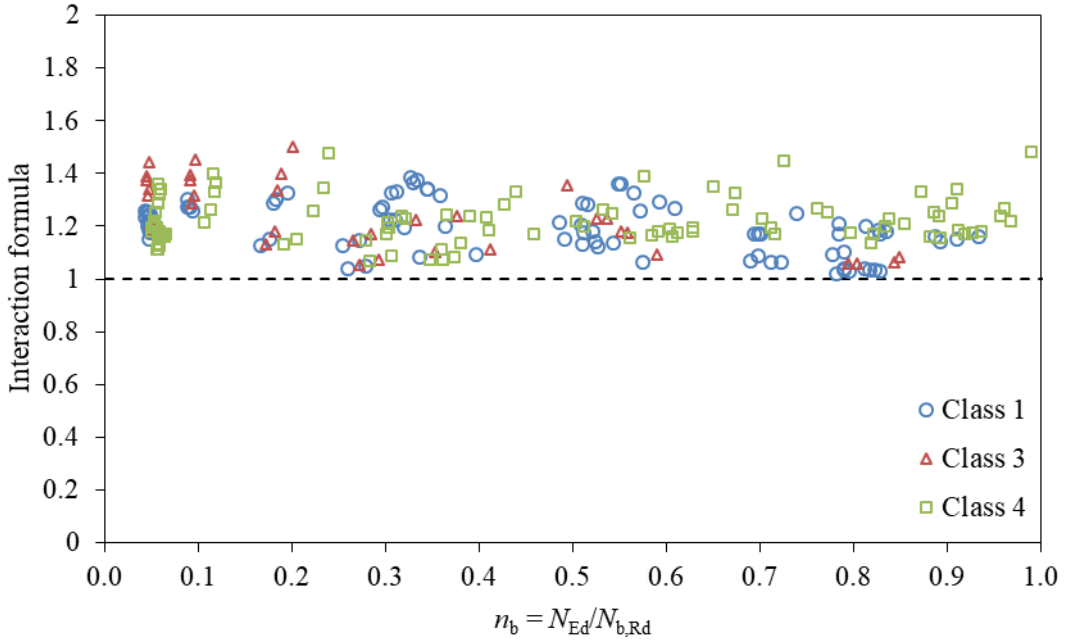

c) Duplex stainless steel

Figure 6.11 *Comparison of the new proposal as dependent on n_b ratio, considering flexural buckling and bending resistance according to Afshan et al. and EN 1993-1-4, respectively.*

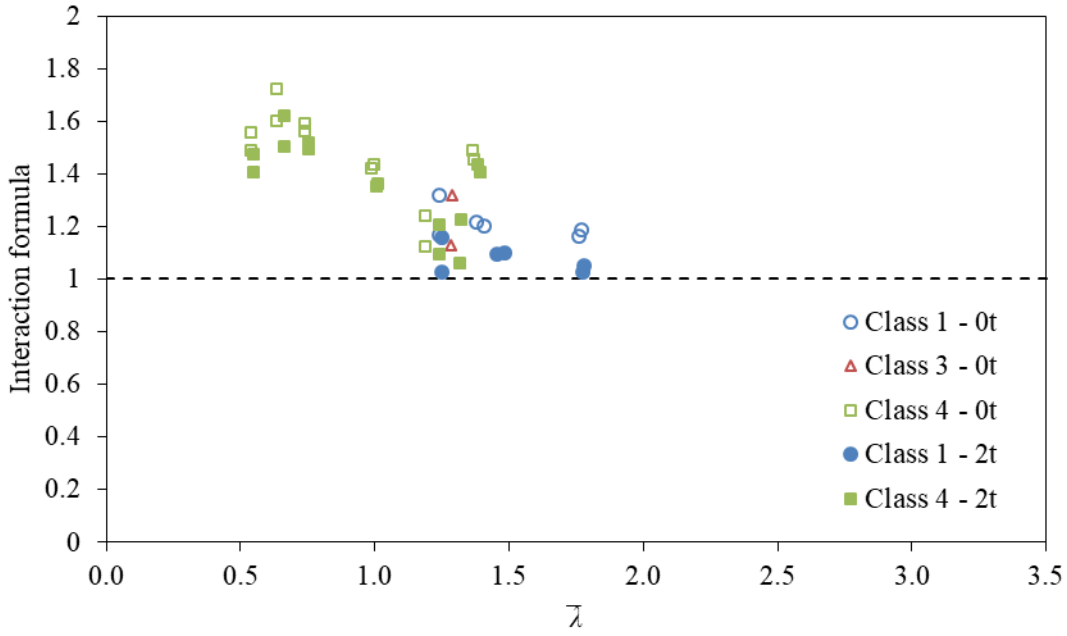

a) Non-dimensional slenderness $\bar{\lambda}$

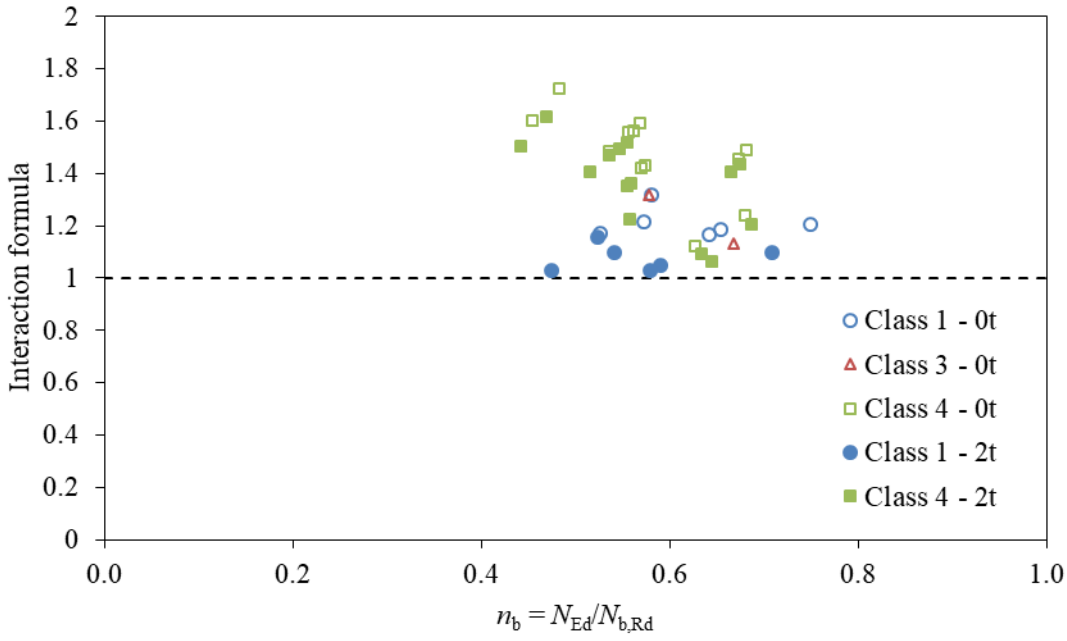

b) n_b ratio

Figure 6.12 *Comparison of the new proposal considering experimental data with flexural buckling and bending resistance according to Afshan et al. and EN 1993-1-4, respectively.*

Figure 6.10 and Figure 6.11 show the results are slightly more scattered than in comparison where column and bending resistance were obtained from the numerical study. However, the results are more conservative in general. There are only few slightly unsafe results of austenitic and ferritic stocky cross-section members with non-dimensional slenderness value around unity and predominant loading by compressive force caused by significant plasticity. The new proposal provides safe and consistent predictions for duplex stainless steel members in all cases.

Comparison of the new proposal considering experimental data provides very good results for both stocky (Class 1) and slender (Class 4) cross-sections. However, for lower non-dimensional slenderness it becomes slightly over-conservative. That is caused by increasing influence of the cross-section resistance which was calculated approximately and conservatively. Results with the consideration of the corner extensions for the material strength enhancement are slightly lower than with the pure corner area, as the cross-section load-bearing capacities are higher.

In general, the new proposal predictions of stainless steel beam-columns resistance considering flexural buckling resistance according to EN 1993-1-4 [1] with modification made by Afshan et al. [41] and bending resistance according to EN 1993-1-4 [1] are low scattered, safe and consistent. Reliability analysis of the new proposal considering mentioned load-bearing capacities is given by Chapter 6.3.6.

6.3.4 Load-bearing capacities according to EN 1993-1-4 with revised flexural buckling curves and CSM.

Comparison of the new proposal considering flexural buckling resistance calculated according to EN 1993-1-4 [1] with modification developed by Afshan et al. [41] and bending resistance according to CSM [49] is shown in this chapter. The comparison is shown below, where Figure 6.13 shows results as dependent on non-dimensional slenderness $\bar{\lambda}$, whereas Figure 6.14 provides comparison as dependent on n_b ratio. Comparison based on the experimental data is given by Figure 6.15.

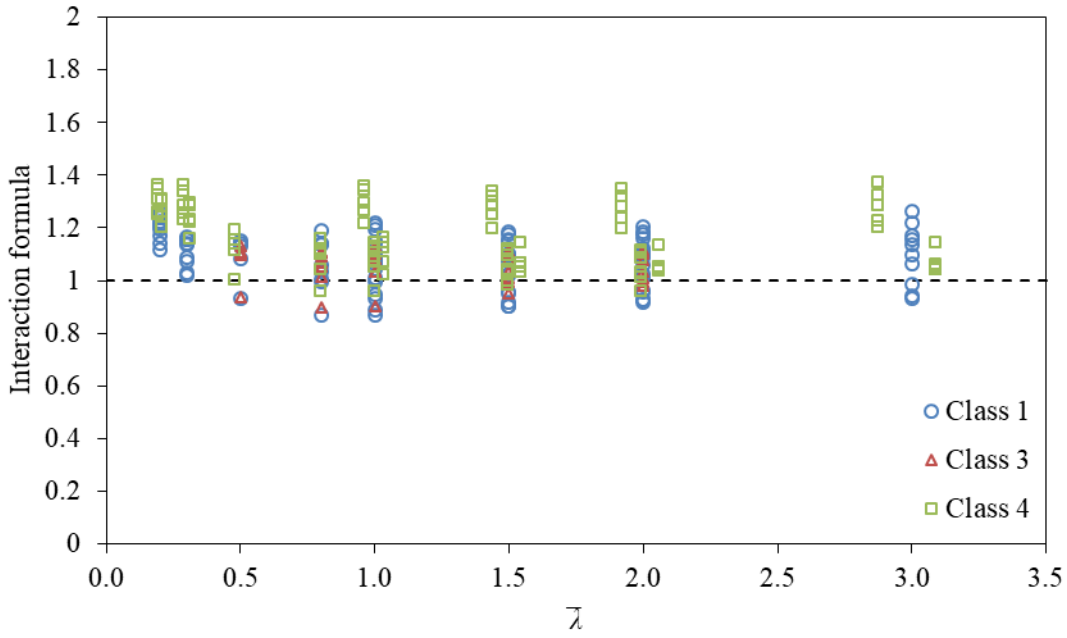

a) Austenitic stainless steel

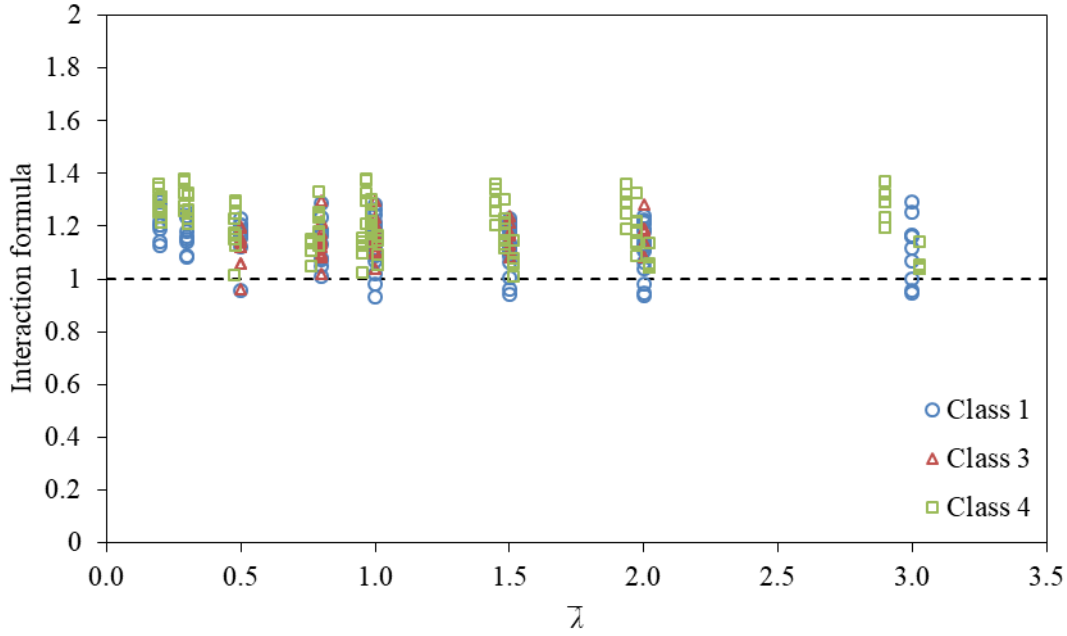

b) Ferritic stainless steel

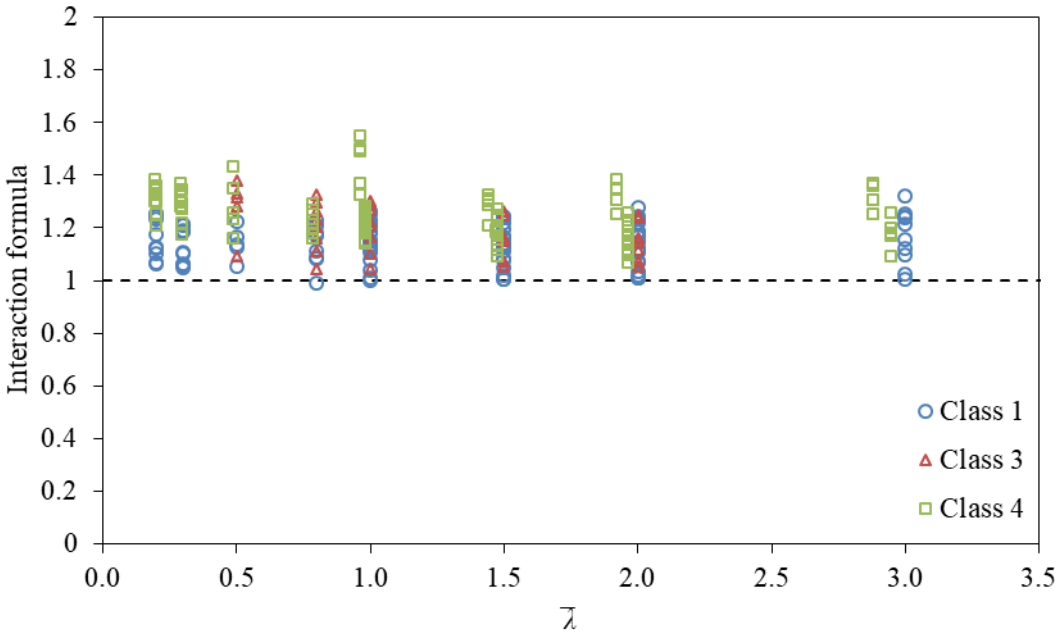

c) Duplex stainless steel

Figure 6.13 *Comparison of the new proposal as dependent on non-dimensional slenderness $\bar{\lambda}$, considering flexural buckling and bending resistance according to Afshan et al. and CSM, respectively.*

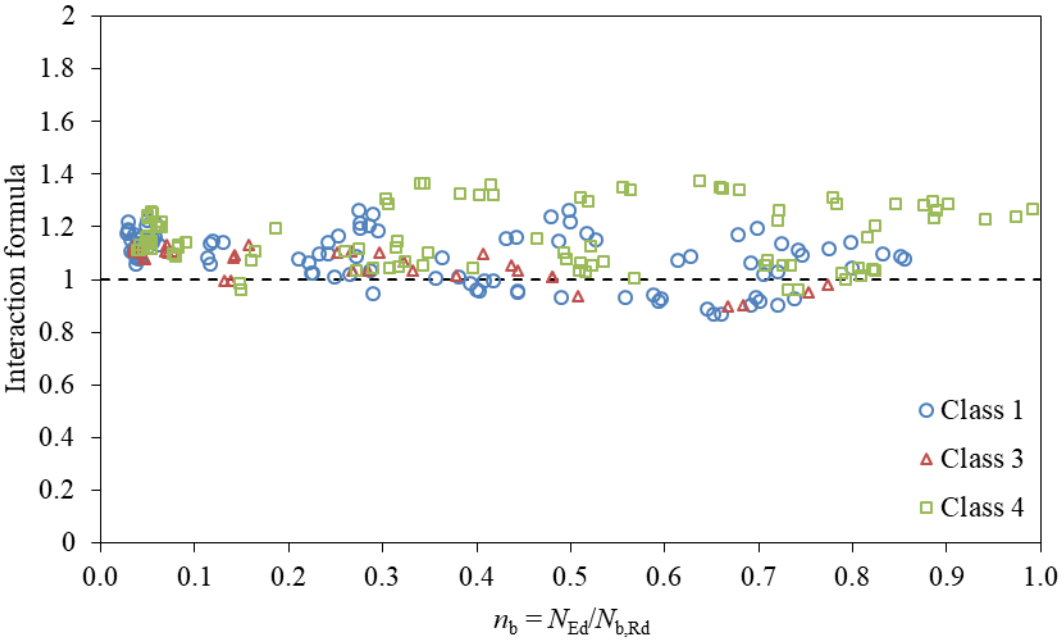

a) Austenitic stainless steel

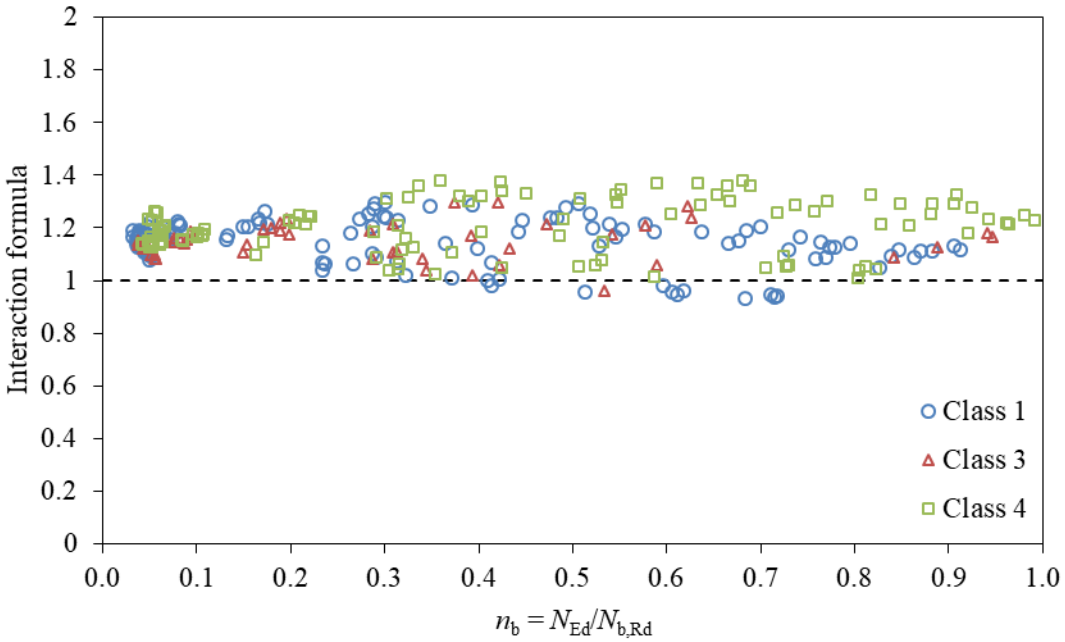

b) Ferritic stainless steel

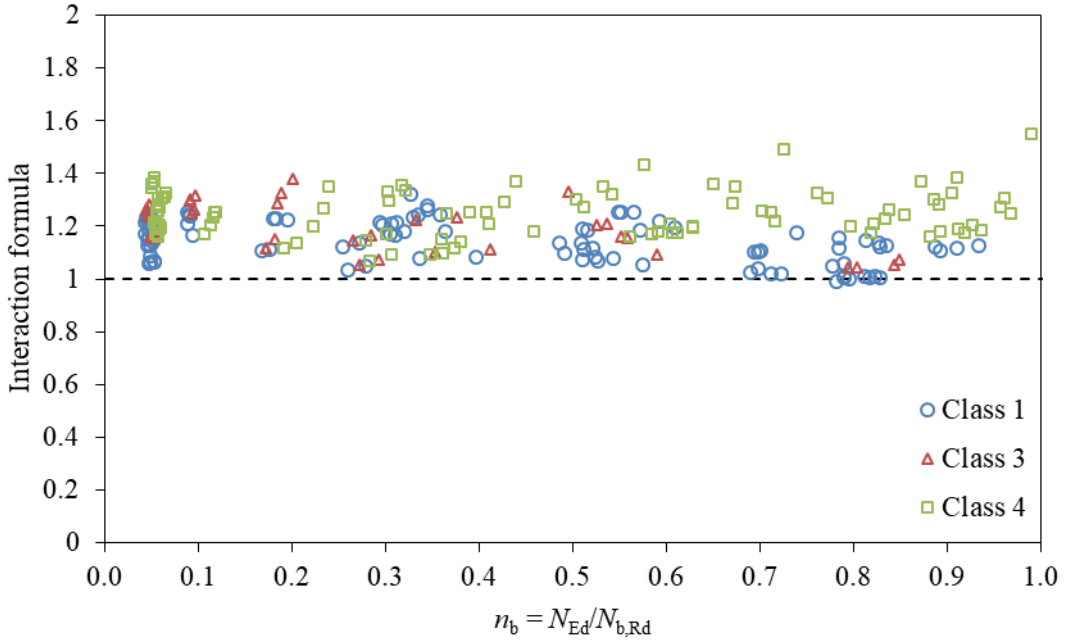

c) Duplex stainless steel

Figure 6.14 *Comparison of the new proposal as dependent on n_b ratio, considering flexural buckling and bending resistance according to Afshan et al. and CSM, respectively.*

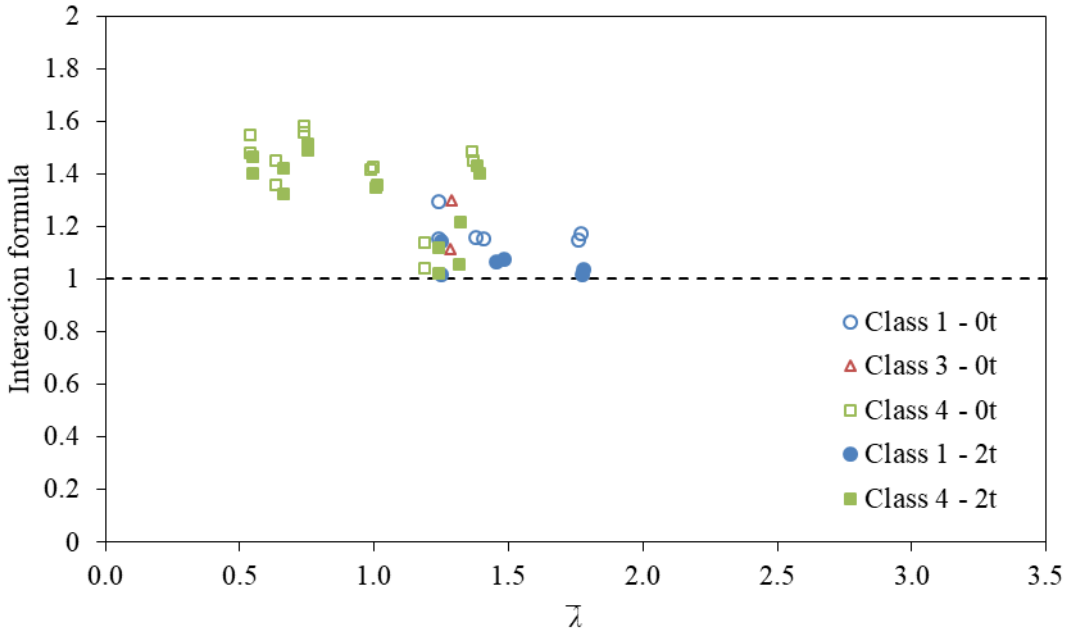

a) Non-dimensional slenderness $\bar{\lambda}$

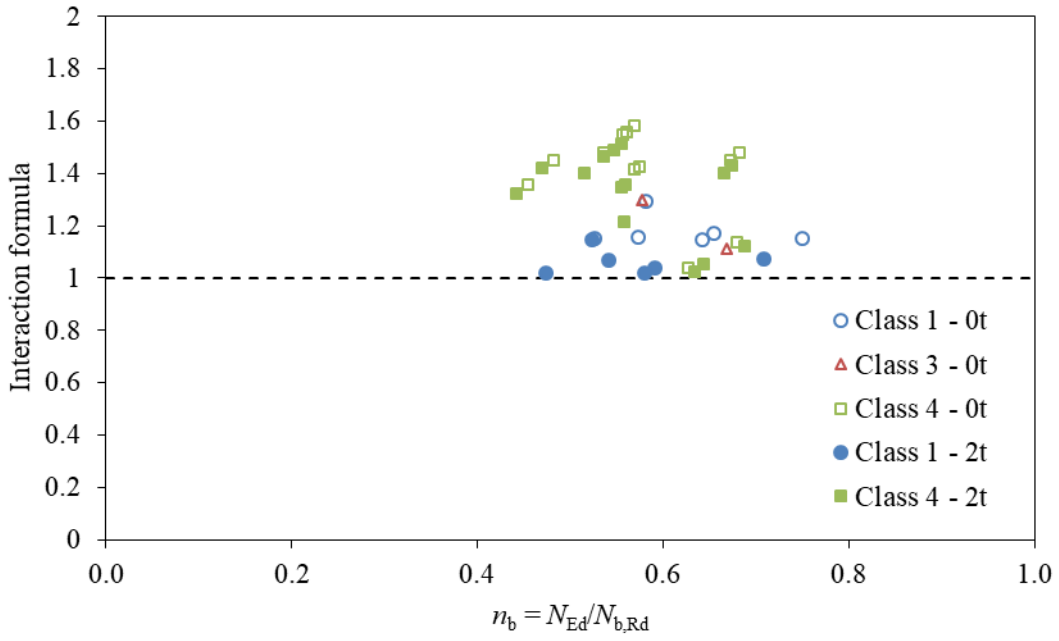

b) n_b ratio

Figure 6.15 *Comparison of the new proposal considering experimental data with flexural buckling and bending resistance according to Afshan et al. and CSM, respectively.*

The comparison shows that the predictions of the new proposal are similar to those with bending moment capacity calculated according to EN 1993-1-4 [1]. However, there is some improvement in cases of dominant bending moment where results exhibit lower scatter for all stainless steel groups and cross-section classes. On the other hand, there are few unsafe predictions for stocky cross-sections (Class 1) of non-dimensional slenderness $\bar{\lambda} \approx 1.0$ and predominant compressive force influence. In these cases, the lower value of strain hardening exponent $n = 4.5$ was considered in material model. On the other hand, for $n = 14$ the results are conservative.

The comparison of the new proposal with the experimental data consideration provides very similar results to the ones in the previous chapter, with a little improvement in the slender (Class 4) cross-section cases.

Assuming bending moment resistance according to CSM [49] leads to improvement of predictions for all three stainless steel groups and all investigated cross-sections when bending moment is dominant ($n_b \leq 0.3$). However, with increasing influence of compressive force, results became slightly more scattered. Chapter 6.3.6 provides reliability analysis of the procedure.

6.3.5 Load-bearing capacities according to EN 1993-1-4 with revised flexural buckling curves and DSM.

As was mentioned, Arrayago et al. [56] investigated that DSM provides good predictions for stainless steel. Therefore, comparison considering flexural buckling resistance according to EN 1993-1-4 [1] with revised flexural buckling curves [41] and bending resistance calculated according to CSM [49] with DSM local buckling curve for carbon steel [56] was made. The CSM local buckling curve [49] given by Equation (3.30) was replaced by the DSM carbon steel local buckling curve [56] given by Equation (3.41). Subsequent cross-section bending moment capacity calculation remained the same as for CSM.

The evaluation is shown below, where Figure 6.16 provides predictions as dependent on non-dimensional slenderness $\bar{\lambda}$ and Figure 6.17 as dependent on n_b ratio. Comparison considering data obtained from the conducted experiments is given by Figure 6.18.

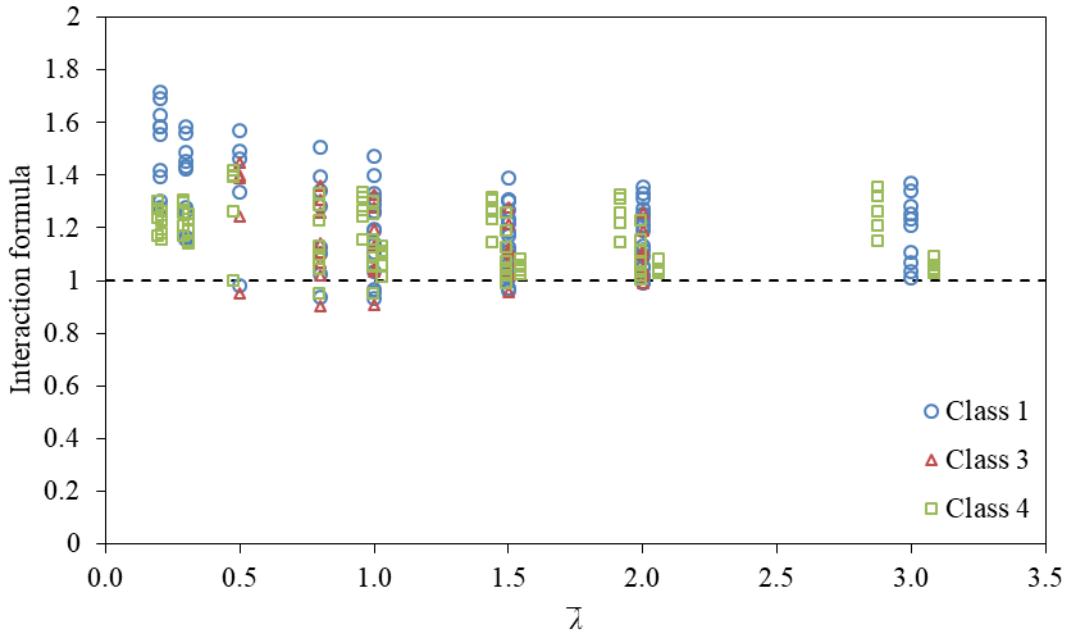

a) Austenitic stainless steel

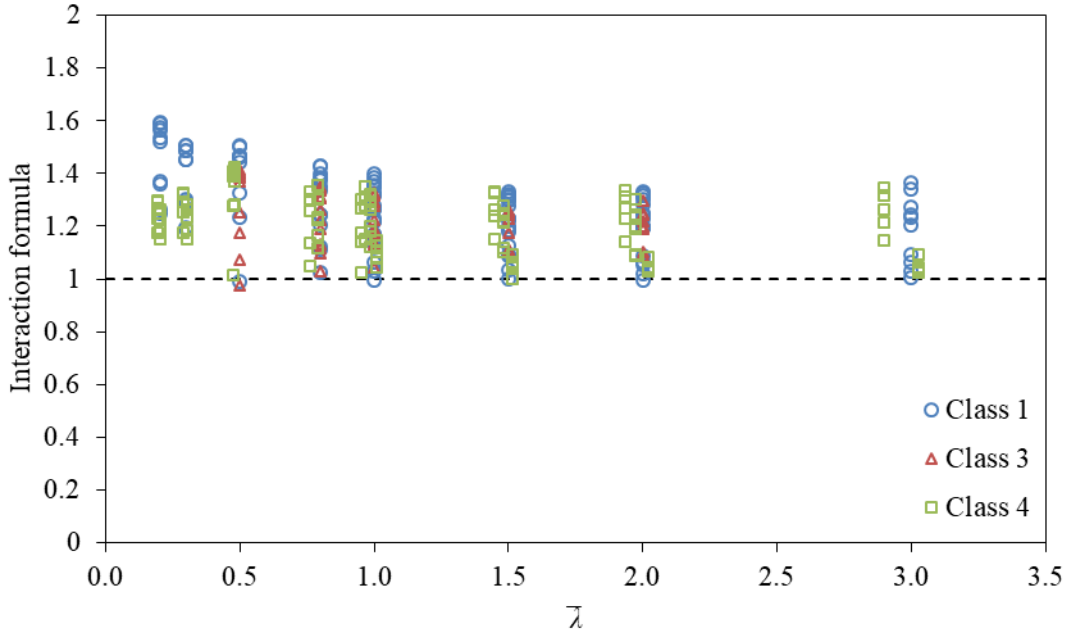

b) Ferritic stainless steel

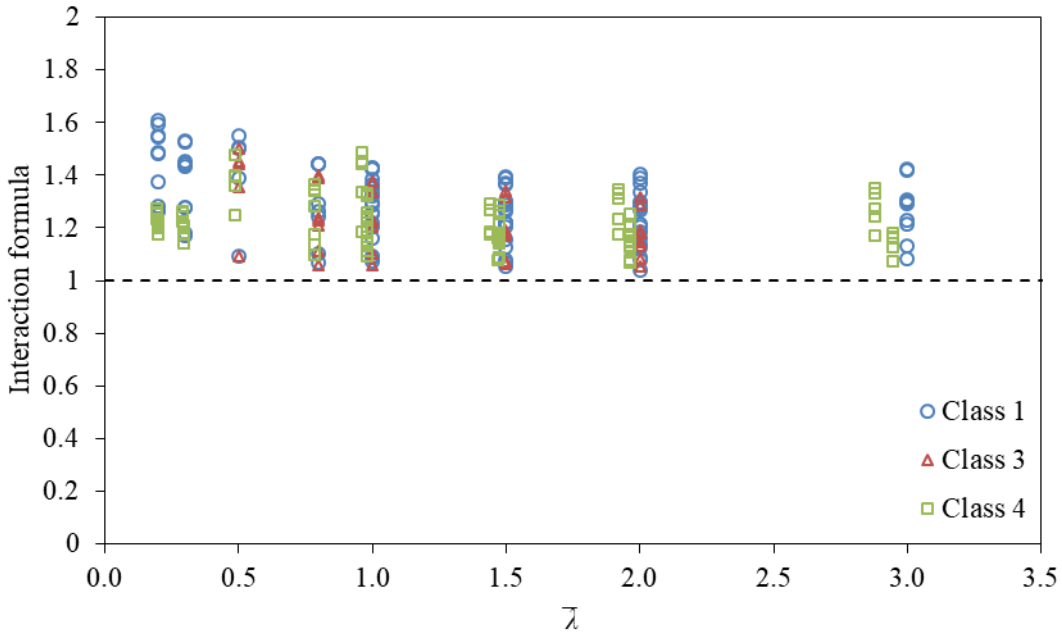

c) Duplex stainless steel

Figure 6.16 *Comparison of the new proposal as dependent on non-dimensional slenderness $\bar{\lambda}$, considering flexural buckling and bending resistance according to Afshan et al. and DSM, respectively.*

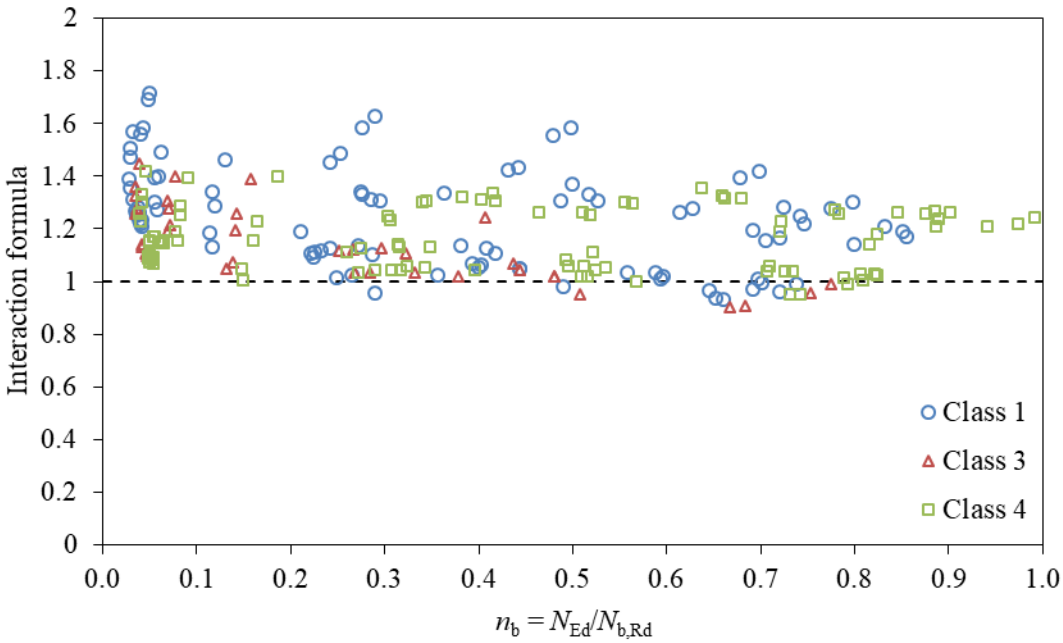

a) Austenitic stainless steel

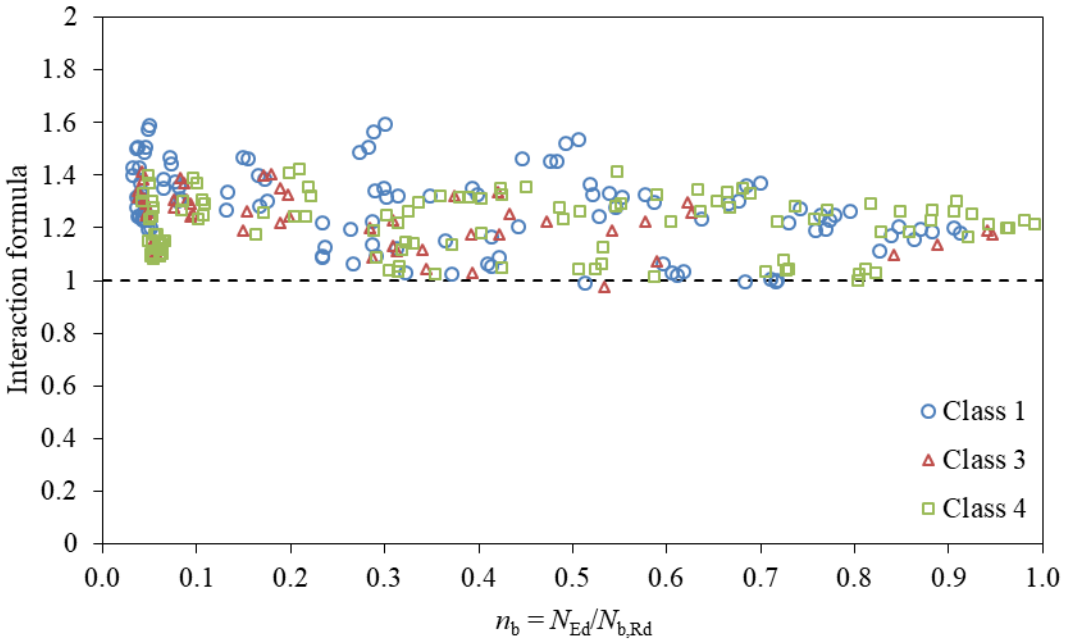

b) Ferritic stainless steel

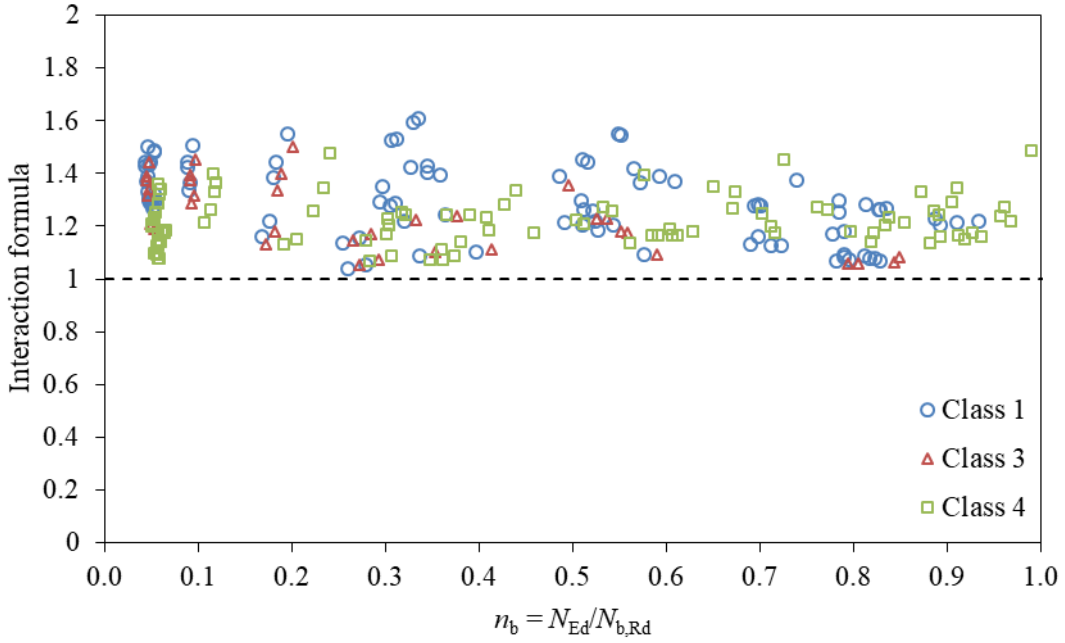

c) Duplex stainless steel

Figure 6.17 *Comparison of the new proposal as dependent on n_b ratio, considering flexural buckling and bending resistance according to Afshan et al. and DSM, respectively.*

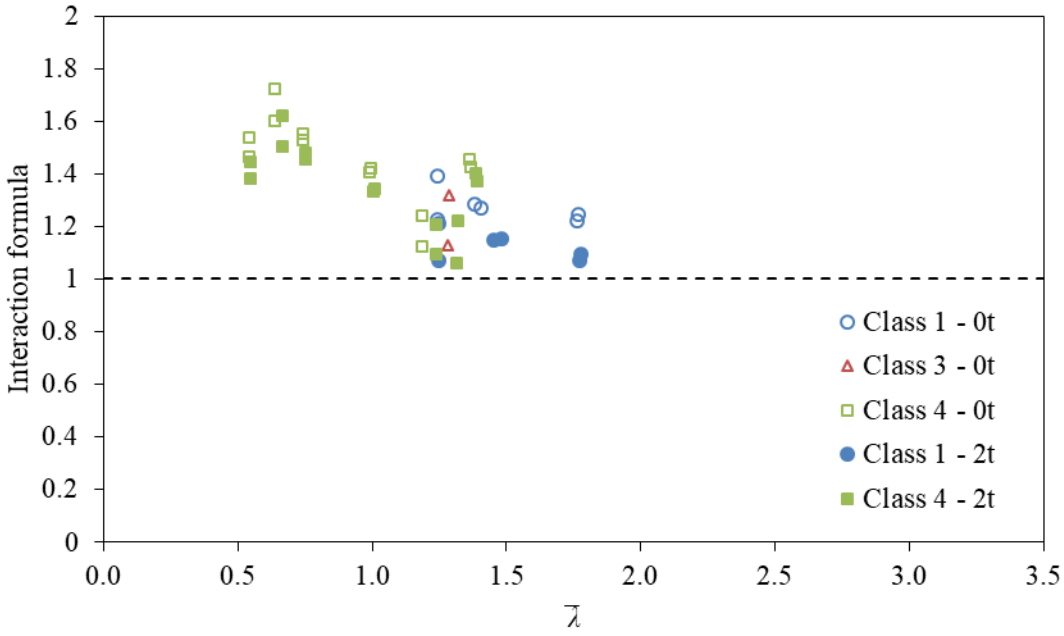

a) Non-dimensional slenderness $\bar{\lambda}$

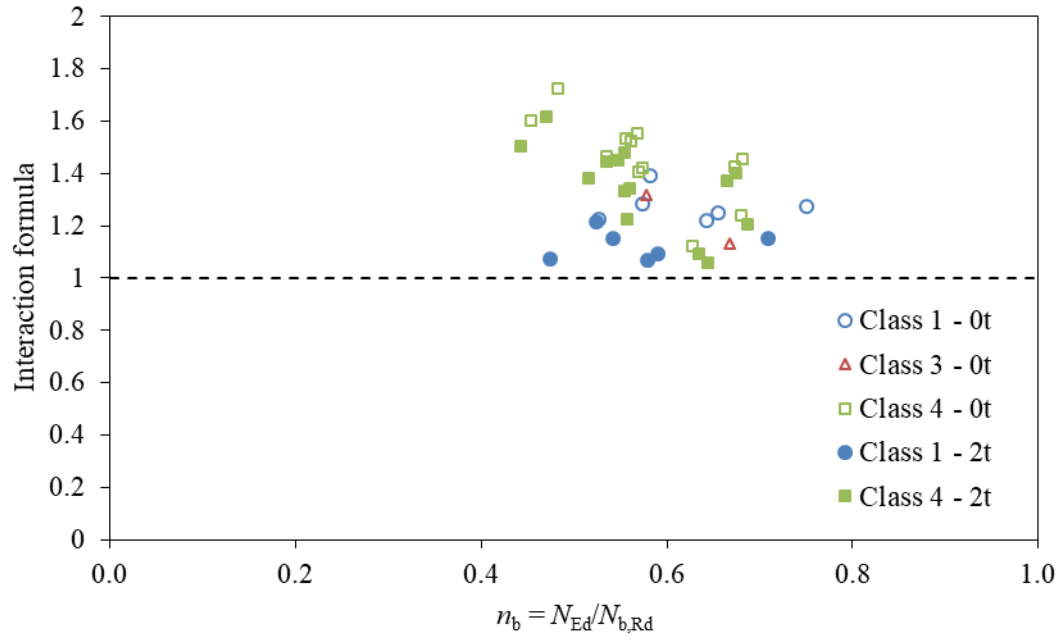

b) n_b ratio

Figure 6.18 *Comparison of the new proposal considering experimental data with flexural buckling and bending resistance according to Afshan et al. and DSM, respectively.*

As could be seen in Figure 6.16 and Figure 6.17 results for stocky (Class 1) cross-sections, as well as Class 3 cross-section predictions, became conservative. The DSM [56] unlike CSM [49] does not consider strain hardening phenomenon. As DSM local buckling curve [56] is lower than CSM local buckling curve [49], the results are slightly safer for slender (Class 4) cross-section predictions.

Very similar change of results could be seen in Figure 6.18 for the experimental data. Neglection of strain hardening and lower local buckling curve results in more conservative predictions.

As CSM [49] provides accurate cross-section predictions for stocky cross-sections, DSM local buckling curve [56] made the procedure very conservative in general. However, with some improvement for slender (Class 4) cross-sections. Reliability analysis of the procedure is given in Chapter 6.3.6.

6.3.6 Reliability analysis

Stainless steel SHS and RHS beam-column design procedures were presented in previous chapters with their comparisons. The reliability analysis of the procedures are made in this chapter according to EN 1990 [81] provisions, namely Annex D. The target partial safety factor is γ_{M1} = 1.1, as recommended by EN 1993-1-4 [1]. Determination of the γ_M^* partial safety factor for the proposed procedure is shown below.

The main idea of the reliability is that resistance must be greater than effect of actions, see Equation (6.21).

$$R > E \tag{6.21}$$

where R is the resistance and E is the effect of actions.

The interaction formula represents utilization of the member which is compared to unity, representing 100 % utilization. Therefore, unity was considered as the effect of actions E and inverse value of the member utilization as the resistance R. Subsequently, the mean value of the correction factor b was calculated as:

$$b = \sum_{i=1}^{n} r_{e,i} r_{t,i} \Big/ \sum_{i=1}^{n} r_{t,i}^2 \tag{6.22}$$

where $r_{t,i}$ is a theoretical resistance function calculated considering nominal values of variables, set as cross-section area A and 0.2 % proof stress $\sigma_{0.2}$ for each specimen (inverse values

of the left side of the interaction formula) and $r_{e,i}$ is the partial experimental resistance for each specimen, considered as unity for all cases (right side of the interaction formula).

As the next step, the coefficient of variation V_δ of the error terms δ_i of the resistance function was calculated according to Equations (6.23) to (6.26).

$$V_\delta = \sqrt{\exp^{s_\Delta^2} - 1} \tag{6.23}$$

with

$$s_\Delta^2 = \frac{1}{n-1}\sum_{i=1}^{n}(\Delta_i - \bar{\Delta})^2 \tag{6.24}$$

being

$$\bar{\Delta} = \frac{1}{n}\sum_{i=1}^{n}\Delta_i \tag{6.25}$$

$$\Delta_i = \ln\left(\frac{r_{e,i}}{b r_{t,i}}\right) = \ln(\delta_i) \tag{6.26}$$

where Δ_i is the logarithm of the error term δ_i, $\bar{\Delta}$ is the estimated value for $E_{(\Delta,i)}$ (mean value of Δ_i), n is the number of samples and s_Δ^2 is the estimated value for σ_Δ^2 (variance of the term Δ_i).

Influence of the basic inputs variations on the resistance function is accounted by the error propagation term $V_{rt,i}$ for each sample. The calculation procedure of the error propagation term $V_{rt,i}$ is quite complex, however, simplification used in Tankova et al. [82] was used herein, see Equation (6.27). It should be noted that the simplification often leads to conservative results. As was mentioned above, the input variables were set as cross-section area A and 0.2 % proof stress $\sigma_{0.2}$. For the reliability analysis the coefficient of variation of the inputs is necessary. They were adopted as suggested by Afshan et al. [83], see Table 6.1, where V_{mat} and V_{geom} represent material and geometrical coefficients of variation, respectively and $V_{rt,i}$ is the calculated value of the error propagation term. Then, the log-normal variation coefficients were calculated by Equations (6.28) to (6.31).

$$V_{rt,i} \approx \sqrt{\left[\max\left(V_{mat,i}\right)\right]^2 + \left[\max\left(V_{geom,i}\right)\right]^2} \tag{6.27}$$

Table 6.1 *Material and geometrical coefficient of variation values according to Afshan et al. [83] and calculated error propagation term $V_{rt,i}$.*

Stainless steel group	$V_{mat,i}$	$V_{geom,i}$	$V_{rt,i}$
Austenitic	0.060	0.05	0.078
Ferritic	0.045	0.05	0.067
Duplex	0.030	0.05	0.058

$$Q_{\mathrm{rt,i}} = \sqrt{\ln\left(V_{\mathrm{rt,i}}^2 + 1\right)} \tag{6.28}$$

$$Q_{\delta} = \sqrt{\ln\left(V_{\delta}^2 + 1\right)} \tag{6.29}$$

$$\mathrm{Q_i} = \sqrt{\ln\left(V_{\mathrm{r,i}}^2 + 1\right)} \tag{6.30}$$

with

$$V_{\mathrm{r,i}} = \sqrt{V_{\mathrm{rt,i}}^2 + V_{\delta}^2} \tag{6.31}$$

where $Q_{rt,i}$, Q_{δ} and Q_i are the log-normal variation coefficients and the $V_{r,i}$ is the coefficient of variation considering error propagation term and deviation.

Design value of the resistance r_d was calculated, subsequently. There are two equations for the resistance calculation depending on the number of samples. If the number of samples does not exceed 100, Equation (6.32) should be used, otherwise Equation (6.33) should be used.

$$r_{\mathrm{d,i}} = b g_{\mathrm{rt,i}}\left(\underline{X}_{\mathrm{m}}\right)\exp\left(-k_{\mathrm{d},\infty}\frac{Q_{\mathrm{rt,i}}^2}{Q_{\mathrm{i}}} - k_{\mathrm{d,n}}\frac{Q_{\delta}^2}{Q_{\mathrm{i}}} - 0.5Q_{\mathrm{i}}^2\right) \tag{6.32}$$

$$r_{\mathrm{d,i}} = b g_{\mathrm{rt,i}}\left(\underline{X}_{\mathrm{m}}\right)\exp\left(-k_{\mathrm{d},\infty}\frac{Q_{\mathrm{rt,i}}^2}{Q_{\mathrm{i}}} - 0.5Q_{\mathrm{i}}^2\right) \tag{6.33}$$

where $g_{\mathrm{rt,i}}\left(\underline{X}_{\mathrm{m}}\right)$ is the value of a design function (the new design proposal in this case) calculated using the mean values (given below), $k_{d,n}$ is the design fractile factor given by table D2 of the EN 1990 [81] and $k_{d,\infty}$ is the value of $k_{d,n}$ for the volume of samples n tending to infinity and is equal to 3.04.

Design function calculated with consideration of the mean values of basic variables is, in other words, inverse value of the interaction formula where the nominal values of the basic variables are replaced by the mean values. As basic variables, the geometry represented by the cross-section area A and material properties represented by the 0.2 % proof stress $\sigma_{0.2}$ were considered. There is no difference in the nominal and mean value of the geometry, therefore, the cross-section area remains the same. In the case of material properties some difference in the 0.2 % proof stress $\sigma_{0.2}$ of nominal and mean values exists. Afshan et al. [83] defined criteria for the relationships between nominal and mean values of the 0.2 % proof stress description. The mean 0.2 % proof stress $\sigma_{0.2,mean}$ to nominal 0.2 % proof stress $\sigma_{0.2,nom}$ ratio is equal to 1.3, 1.2 and 1.1 for austenitic, ferritic and duplex stainless steel group, respectively. In other words, the nominal 0.2 % proof stress $\sigma_{0.2,nom}$ multiplied by the appropriate constant results in the mean 0.2 % proof stress $\sigma_{0.2,mean}$.

Eventually, the required partial safety factor γ_M^* applicable for the new beam-column design proposal based on the nominal input data was calculated by Equation (6.34).

$$\gamma_M^* = \frac{1}{n}\sum_{i=1}^{n}\frac{r_{t,nom,i}}{r_{d,i}} \tag{6.34}$$

where $r_{t,nom,i}$ is the design function for each individual sample based on the nominal values.

The reliability analysis was made by the comparison of the partial safety factor γ_M^* obtained from the Equation (6.34) and partial safety factor recommended by EN 1993-1-4 [1] for beam-column design γ_{M1} which is equal to 1.1. For the safe prediction the γ_M^* value should be lower than γ_{M1} value. However, if the γ_M^* value exceed γ_{M1} very slightly, then acceptance limits can be used [84]. The acceptance limits representing some tolerances derived based on the past practice were developed by Taras et al. [84]. Slightly modified condition of the acceptance criterion is given by Equation (6.35). The recommended values of the acceptance limits f_a are given by Table 6.2 regarding V_r value.

$$\gamma_M^* \leq f_a \gamma_{M1} \tag{6.35}$$

where f_a is the acceptance limit.

Table 6.2 *Recommended values of f_a according to [84].*

Range of V_r	f_a
$0.00 < V_r < 0.04$	1.03
$0.00 \leq V_r < 0.20$	$1.03 + 0.75\ (V_r - 0.04)$
$V_r > 0.20$	1.15

Statistical evaluations of the stainless steel beam-column design procedures for SHS and RHS members described in Chapter 6.3 are shown herein. For the reliability analysis, the approach presented above was used. Table 6.3, Table 6.4 and Table 6.5 provide reliability analysis of the new proposal considering analytical flexural buckling capacity according to EN 1993-1-4 [1] considering the revised flexural buckling curves [41] with bending moment resistance according to EN 1993-1-4 [1], CSM [49] and CSM with DSM local buckling curve [56], respectively. n is the sample volume, b is the correction factor, $k_{d,n}$ is the design fractile factor, V_δ is the variation coefficient of the error term, V_r is the variation coefficient considering error propagation term and deviation, γ_M^* is the partial safety factor obtained from the reliability analysis and $f_a\gamma_{M1}$ is the limit for the γ_M^* value considering tolerances. For the total results, $f_a\gamma_{M1}$ was calculated as a weighted average of $f_a\gamma_{M1}$ values of the three stainless steel groups. It should be noted, that the results obtained from the comprehensive numerical parametric study were considered.

Table 6.3 *Reliability analysis of the new proposal considering analytical load-bearing capacities according to EN 1993-1-4 with revised flexural buckling curves.*

Group	n	b	$k_{d,n}$	V_δ	V_r	γ_M^*	$f_a\gamma_{M1}$
Austenitic	231	1.132	3.133	0.110	0.124	1.122	1.202
Ferritic	276	1.187	3.126	0.091	0.118	1.053	1.197
Duplex	231	1.198	3.133	0.081	0.113	1.060	1.193
Total	738	1.172	3.103	0.096	-	1.086	1.197

Table 6.4 *Reliability analysis of the new proposal considering analytical flexural buckling resistance according to EN 1993-1-4 with revised flexural buckling curves and bending resistance according to CSM.*

Group	n	b	$k_{d,n}$	V_δ	V_r	γ_M^*	$f_a\gamma_{M1}$
Austenitic	231	1.092	3.133	0.099	0.121	1.146	1.200
Ferritic	276	1.153	3.126	0.081	0.114	1.064	1.194
Duplex	231	1.179	3.133	0.084	0.109	1.101	1.190
Total	738	1.140	3.103	0.092	-	1.117	1.194

Table 6.5 *Reliability analysis of the new proposal considering analytical flexural buckling resistance according to EN 1993-1-4 with revised flexural buckling curves and bending resistance according to DSM.*

Group	n	b	$k_{d,n}$	V_δ	V_r	γ_M^*	$f_a\gamma_{M1}$
Austenitic	231	1.155	3.133	0.130	0.152	1.162	1.225
Ferritic	276	1.214	3.126	0.105	0.125	1.067	1.203
Duplex	231	1.232	3.133	0.098	0.114	1.081	1.194
Total	738	1.120	3.103	0.114	-	1.111	1.207

Generally, the procedures are different only in the cross-section bending resistance calculation method. If the current codified procedure for the cross-section bending resistance calculation was used [1], the results are safe for the ferritic and duplex stainless steel groups. In the case of austenitic stainless steel group, results are slightly unsafe, however, within the tolerance. Furthermore, results are safe in total. Consideration of the CSM [49] for the bending moment resistance calculation leads to safe results for the ferritic and duplex stainless steel groups and slightly unsafe predictions for the austenitic group, as well. However, within tolerances safely. In total, results are slightly unsafe, nevertheless, very close to $\gamma_{M1} = 1.1$ limit. If the CSM [49] with DSM carbon steel local buckling curve [56] is considered, calculated values of γ_M^* are little bit more unsafe for austenitic stainless steel group, however, more accurate for duplex group. In the case of ferritic group and results in total, there is only negligible change compared to CSM [49].

In the summary, predictions of the ferritic and duplex stainless steel groups are safe in all three design approaches. On the other hand, austenitic stainless steel group exhibits little unsafeness which is maybe caused by consideration of very different strain hardening exponent n values

having more significant influence on stress-strain diagram compared to ferritic and duplex groups (austenitic grade considered has a great ratio of ultimate strength to yield strength). Results in total are safe if EN 1993-1-4 [1] is used, however, in the other two cases are very close to γ_{M1} = 1.1 as well. Even with some slight unsafeness all results are safely within tolerances. Furthermore, as was mentioned above, the simplification used during the reliability analysis according to Tankova et al. [82] often leads to conservative results.

6.4 Beam-columns under bending moment gradient

The new proposal was developed for stainless steel beam-columns loaded by uniform bending moment. However, uniform bending moment along the member length occurs in practice rarely, therefore, a brief comparison for compressive force and non-uniform bending moment is shown herein.

The same design procedure with the new interaction factor formulae as developed for the uniform bending moment was used, see Chapter 6.3.1. However, with the equivalent bending moment factor developed by Austin [57] included. Its general form is given by Equation (6.37). The general interaction formula considering linear bending moment gradient is given by Equation (6.36).

$$\frac{N_{\mathrm{Ed}}}{N_{\mathrm{b,Rd}}} + C_{\mathrm{m}} k_{\mathrm{new}} \frac{M_{Ed}}{M_{Rd}} \leq 1.0 \tag{6.36}$$

$$C_{\mathrm{m}} = 0.6 + 0.4\psi \geq 0.4 \tag{6.37}$$

where ψ is the ratio of end moments.

It was necessary to extend the numerical parametric study by members loaded by compressive force and bending moment with gradient along the member length. The models for the most unsafe comparison results made in Chapter 6.3 were chosen for the investigation. Finally, two cross-sections of austenitic stainless steel group were considered. The material properties are given in Table 6.6 and other variables (cross-section, non-dimensional slenderness $\bar{\lambda}$, ratio of compressive force to flexural buckling resistance n_{b} and end-moment ratio ψ) in Table 6.7. It should be noted that the RHS cross-section members were loaded by minor axis bending.

Table 6.6 *Material properties considered for bending moment gradient investigation.*

Stainless steel group	E_0	f_y	f_u	n
	[GPa]	[MPa]	[MPa]	[-]
Austenitic	200	220	520	4.5

Table 6.7 *Investigated variables for combination of compressive force and non-uniform bending.*

Cross-section	SHS 80x8; RHS 100x40x6
Cross-section class	1
Non-dimensional slenderness	0.2, 1.0, 1.5, 2.0
$n_b = N_{Ed}/N_{b,Rd}$	0.05, 0.5, 0.8
End-moment ratio	0, -1

Comparison was made in the same way as for uniform bending moment. Firstly, the procedure was compared with the consideration of both flexural buckling and bending resistance obtained from the numerical model that represents the real member behaviour or its closest prediction (Figure 6.19 and Figure 6.20). Then, analytically calculated load-bearing capacities, that are commonly used in design practice, were considered, namely flexural buckling resistance according to EN 1993-1-4 [1] procedure considering revised buckling curves [41] and bending moment resistance according to EN 1993-1-4 [1] (Figure 6.21 and Figure 6.22), CSM [49] (Figure 6.23 and Figure 6.24) and CSM [49] with the consideration of DSM carbon steel local buckling curve [56] (Figure 6.25 and Figure 6.26).

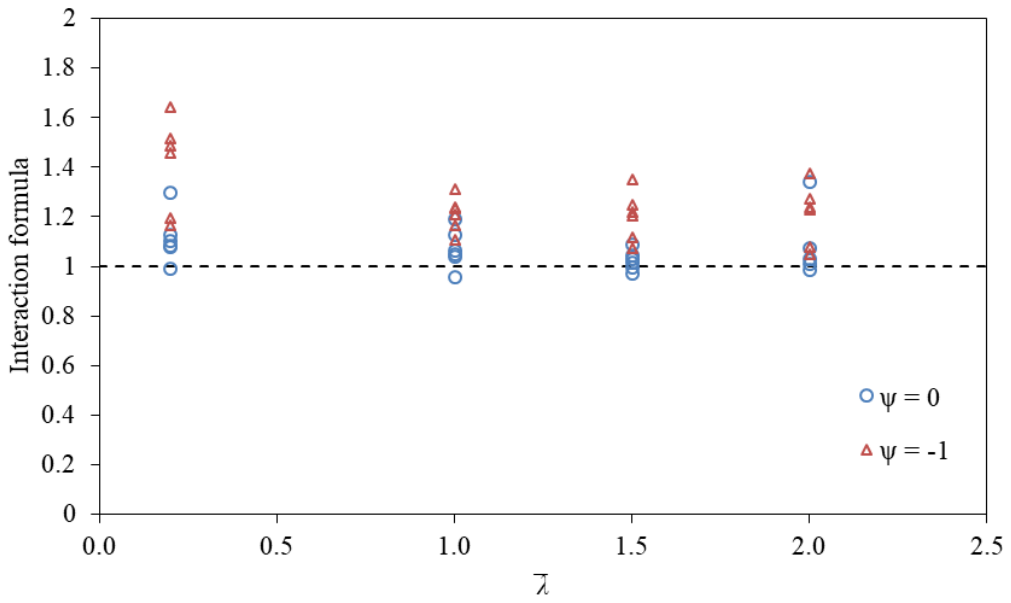

Figure 6.19 *Comparison of the new proposal as dependent on non-dimensional slenderness $\bar{\lambda}$, considering numerical load-bearing capacities ($N_{b,Rd,FEM}$ and $M_{Rd,FEM}$) for non-uniform bending moment.*

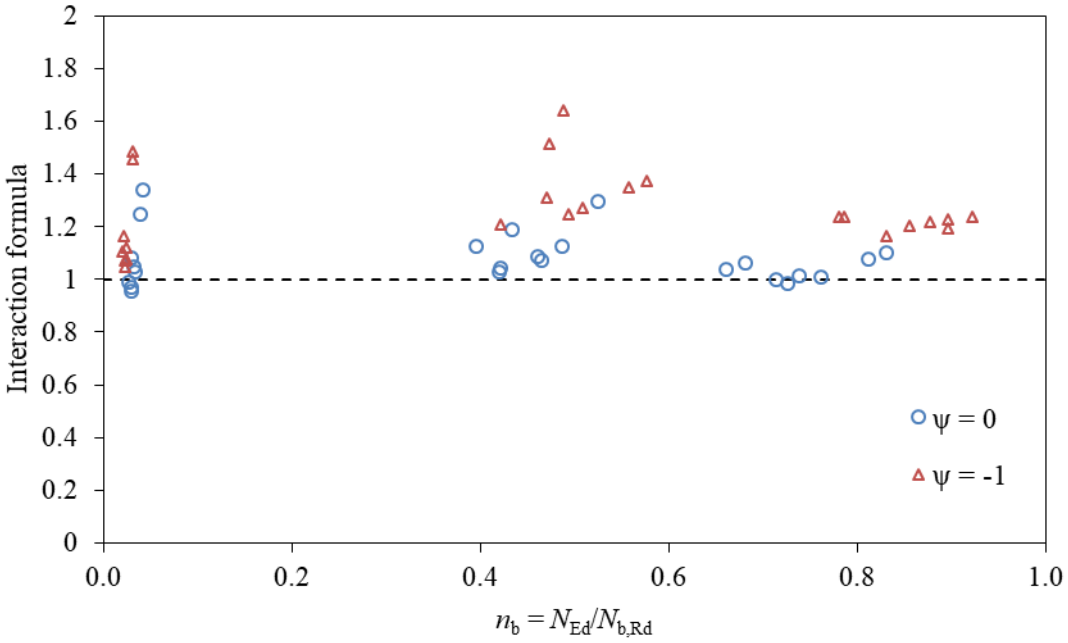

Figure 6.20 *Comparison of the new proposal as dependent on n_b ratio, considering numerical load-bearing capacities ($N_{b,Rd,FEM}$ and $M_{Rd,FEM}$) for non-uniform bending moment.*

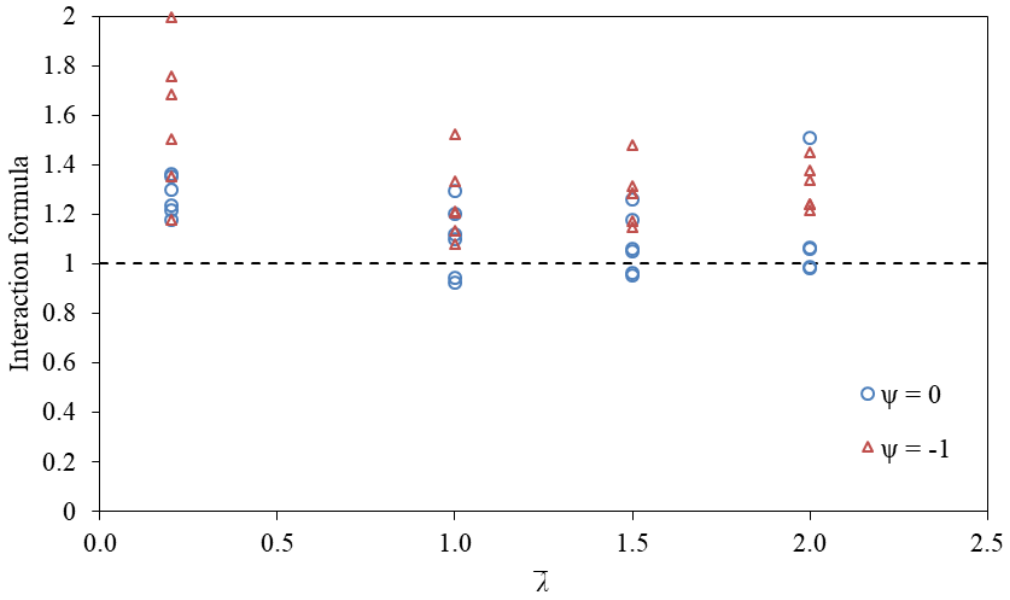

Figure 6.21 *Comparison of the new proposal as dependent on non-dimensional slenderness $\bar{\lambda}$, considering flexural buckling and bending resistance according to Afshan et al. and EN 1993-1-4, respectively, for non-uniform bending moment.*

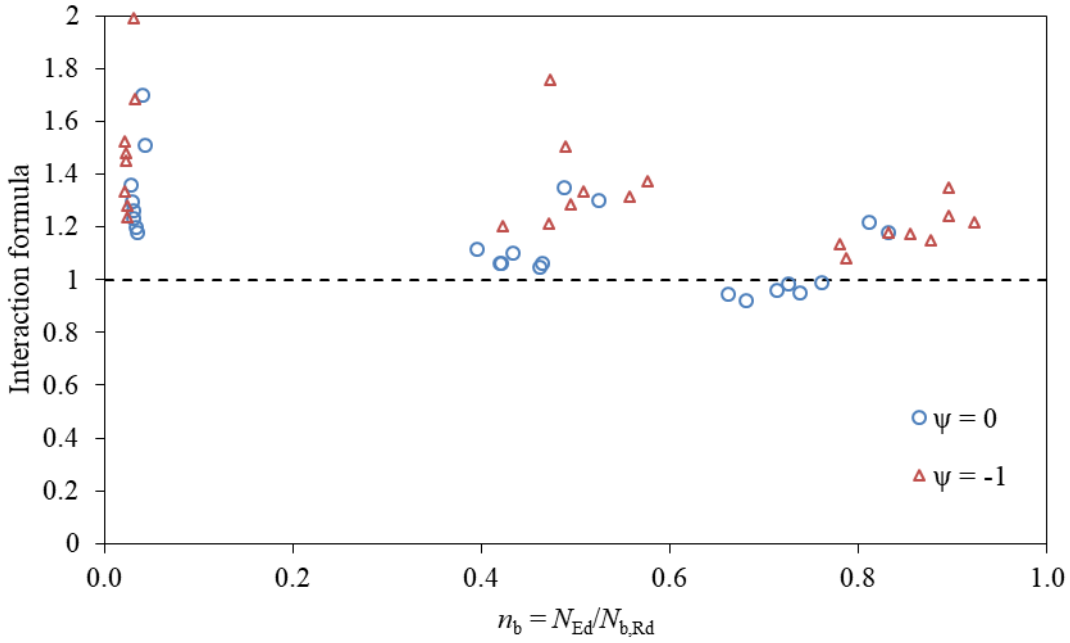

Figure 6.22 *Comparison of the new proposal as dependent on n_b ratio, considering flexural buckling and bending resistance according to Afshan et al. and EN 1993-1-4, respectively, for non-uniform bending moment.*

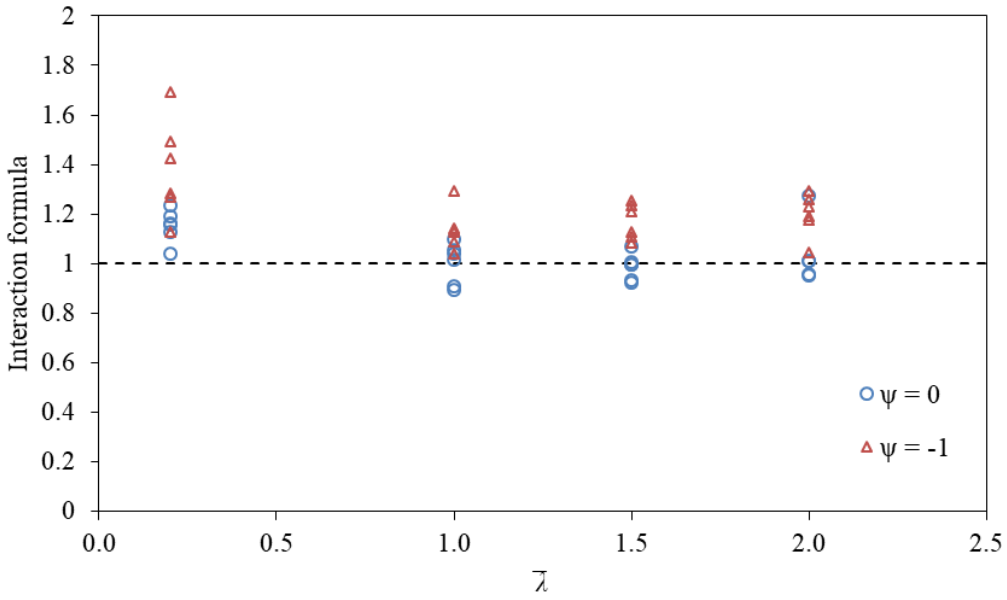

Figure 6.23 *Comparison of the new proposal as dependent on non-dimensional slenderness $\bar{\lambda}$, considering flexural buckling and bending resistance according to Afshan et al. and CSM, respectively, for non-uniform bending moment.*

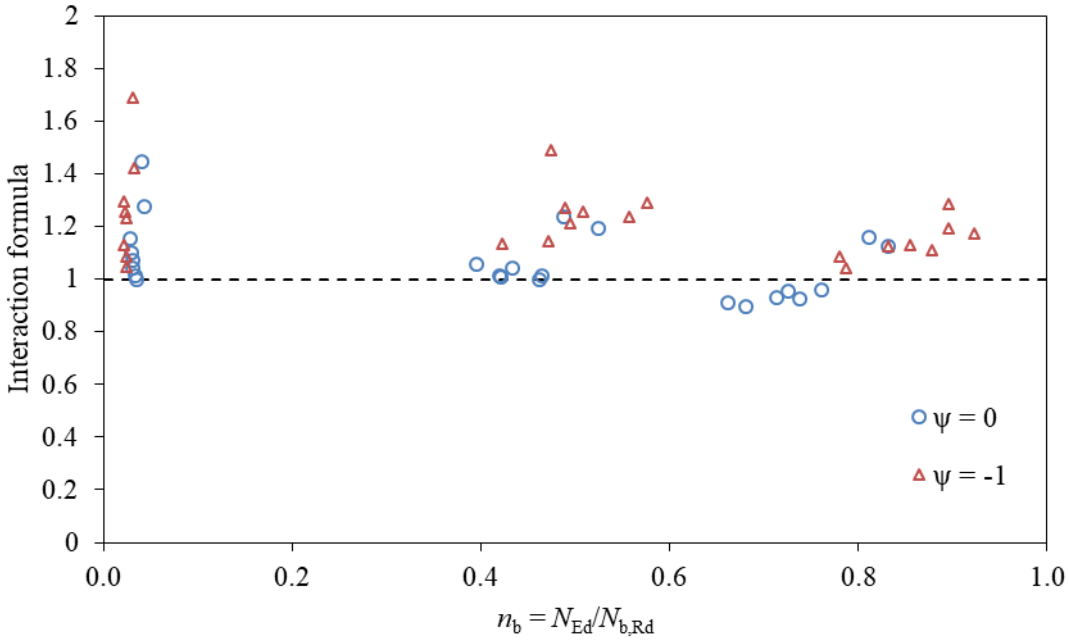

Figure 6.24 *Comparison of the new proposal as dependent on n_b ratio, considering flexural buckling and bending resistance according to Afshan et al. and CSM, respectively, for non-uniform bending moment.*

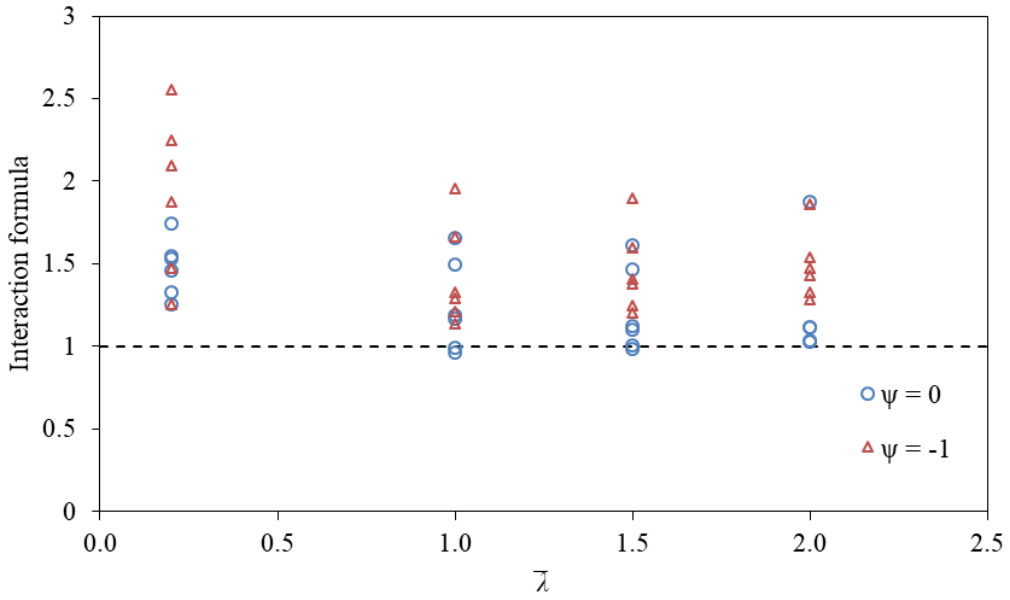

Figure 6.25 *Comparison of the new proposal as dependent on non-dimensional slenderness $\bar{\lambda}$, considering flexural buckling and bending resistance according to Afshan et al. and DSM, respectively, for non-uniform bending moment.*

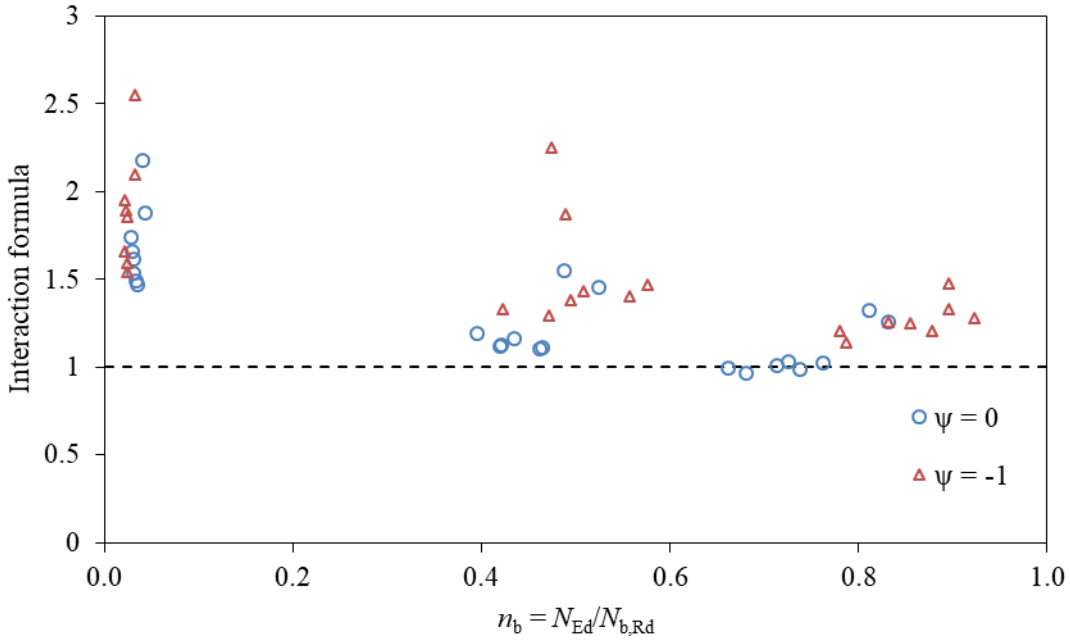

Figure 6.26 *Comparison of the new proposal as dependent on n_b ratio, considering flexural buckling and bending resistance according to Afshan et al. and DSM, respectively, for non-uniform bending moment.*

As could be seen in Figure 6.19 and Figure 6.20, consideration of the numerical load-bearing capacities, representing the real behaviour, provides safe results in all cases. Mostly over-conservative, especially for the end-moment ratio ψ = -1. Therefore, the new interaction factor formulae is safe for members loaded by compressive force and non-uniform bending moment combination, however, with some conservativeness which is attributed to the simplification of the non-uniform bending moment distribution effect given by C_m Equation (6.37).

Figure 6.21 to Figure 6.26 provides evaluation for the consideration of analytically calculated flexural buckling resistance according to EN 1993-1-4 [1] with revised buckling curves [41] and bending resistance according to appropriate procedure. Consideration of the bending moment resistance according to EN 1993-1-4 [1] provides, in general, slightly more scattered results with greater conservativeness due to the fact that the analytical calculations of the load-bearing capacities are only conservative approximations of the real ones. The CSM [49] includes strain hardening of stocky cross-sections which should improve the bending resistance accuracy. As could be seen in Figure 6.23 and Figure 6.24 there is noticeable improvement of results that are less scattered and more accurate compared to the consideration of bending resistance according to EN 1993-1-4 [1]. The use of DSM [56] carbon steel local buckling curve for CSM [49] leads, as was expected, to significantly over-conservative results due to the neglection of the strain hardening phenomenon of the stocky (Class 1) cross-sections, see Figure 6.25 and Figure 6.26.

6.5 General Method of EN 1993-1-1

The General Method is an alternative design approach provided by EN 1993-1-1 [2]. It was described in Chapter 3.11.5 in detail. In this section, a very brief investigation of the General Method suitability for stainless steel beam-column design is given.

The numerical model described in Chapter 5.2 was used to obtain Euler's buckling load $N_{cr,FEM}$, cross-section compressive and bending capacities $N_{Rd,FEM}$ and $M_{Rd,FEM}$, flexural buckling resistance $N_{b,Rd,FEM}$ and ultimate compressive and bending load, $N_{Ed,FEM}$ and $M_{Ed,FEM}$. Based on the numerical results, the non-dimensional slenderness $\bar{\lambda}_{FEM}$ and flexural buckling coefficient χ_{FEM} were calculated. Then, the initial bow imperfection e_0 was established according to Equation (3.75), where $\eta = \alpha(\bar{\lambda} - \bar{\lambda}_0)$ was obtained from Equation (3.21) with ϕ_{FEM} calculated from Equation (3.20) considering mentioned values given by numerical model ($\bar{\lambda}_{FEM}$ and χ_{FEM}).

Only two cross-sections were considered, namely SHS 80x3 and 80x5. Material properties were considered the same in the whole cross-section (1.4404 austenitic grade) and they were adopted from the flat coupon tensile tests, see Table 4.2. Together 12 member lengths (1000 mm to

7000 mm) and four loading states ($n_b = N_{Ed} / N_{b,Rd}$) for both cross-sections were used, see Table 6.8.

Table 6.8 *Investigated non-dimensional slenderness $\bar{\lambda}_{FEM}$ and n_b ratio values.*

SHS 80x3		SHS 80x5	
$\bar{\lambda}_{FEM}$	n_b	$\bar{\lambda}_{FEM}$	n_b
0.64	0.3	0.58	0.3
0.76	0.5	0.87	0.5
1.01	0.7	1.15	0.7
1.16	0.8	1.32	0.8
1.26		1.44	
1.51		1.73	
1.77		2.01	
2.02		2.30	
2.27		2.58	
2.52		2.87	
3.02		3.44	
3.53		4.02	

Due to the fact, that the General Method uses elastic material model with GNIA analysis (geometrically non-linear analysis with imperfections), a simplified 2D numerical model using 2-node in a plane linear beam element B21 was created in software Abaqus. A uniform mesh of size 10 mm was considered. Numerical model structural scheme is given in Figure 6.27. A cross-section shape was simplified into a box cross-section with modified wall thickness in order to keeping the same value of the second moment of area. Consequently, very little difference in the cross-section area occurred, however, the influence was negligible, therefore it was not considered. The member lengths were the same as for the 3D complex models. Material properties were represented only by the Young's modulus E_0 and Poisson's ratio ν. The initial imperfection e_0 was introduced by the first elastic buckling eigen-mode. The value of e_0 was calculated according to Equation (3.75) using the cross-section resistances calculated by 3D model.

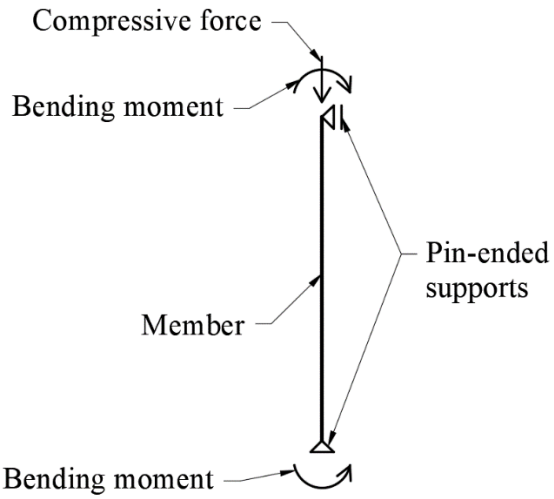

Figure 6.27 *Numerical model structural scheme for the General Method.*

The comparison was made based on the ratio of the ultimate loading compressive force obtained from the 3D complex model $N_{Ed,FEM}$ to simplified 2D model ultimate loading compressive force $N_{Ed,FEM,GM}$ representing the General Method. In other words, results above unity indicate safe predictions, whereas below unity unsafe predictions. Evaluation is given by Figure 6.28 both for SHS 80x3 and 80x5 due to very similar results.

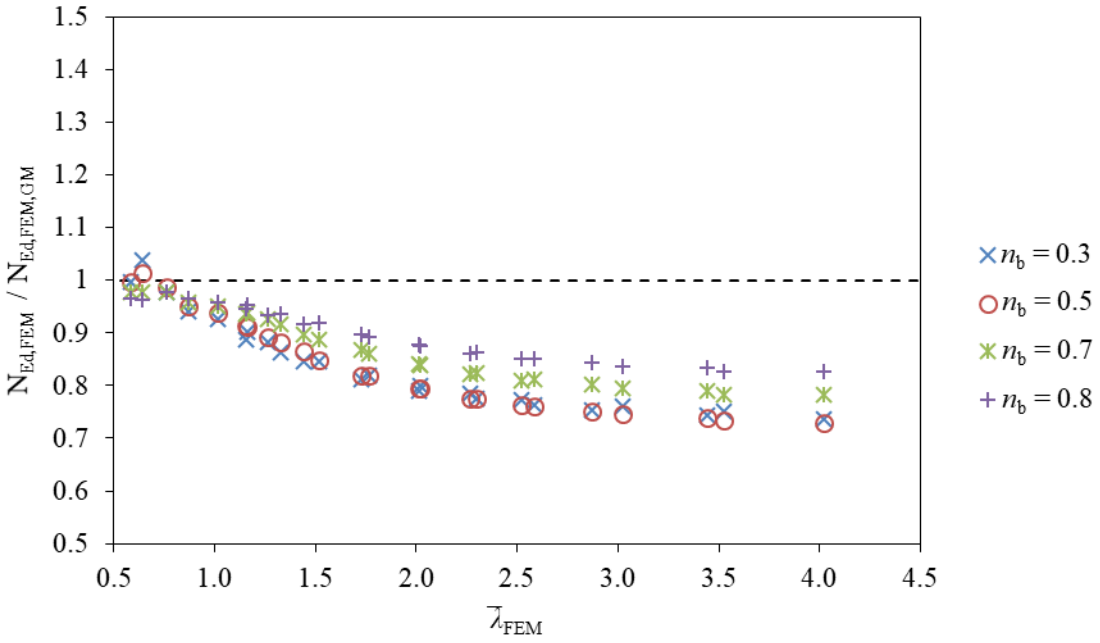

Figure 6.28 *Comparison of the General Method.*

As could be seen, the results are accurate in the cases of low non-dimensional slenderness values, however, with increasing non-dimensional slenderness became unsafe. That is attributed to

member stiffness overestimation. According to loading state, the lower the influence of the compressive force the more unsafe prediction but the trend is the same for all investigated loading states. In general, it could be said that the General Method, as given by EN 1993-1-1 [2], is not suitable for stainless steel beam-column design.

Improvement of the General Method is proposed in this paragraph. Based on results given by Figure 6.28 was mentioned that the procedure overestimate member stiffness, represented mainly by Young's modulus of elasticity E_0. Therefore, the Young's modulus of elasticity E_0 was replaced by the secant elasticity modulus $E_{s,0.2}$ for the stress level equal to the 0.2 % proof stress $\sigma_{0.2}$. The value of the secant elasticity modulus $E_{s,0.2}$ was calculated according to Equation (6.38). Evaluation of the General Method considering proposed modification is given by Figure 6.29.

$$E_{s,0.2} = \frac{\sigma_{0.2}}{\frac{\sigma_{0.2}}{E_0} + 0.002} \tag{6.38}$$

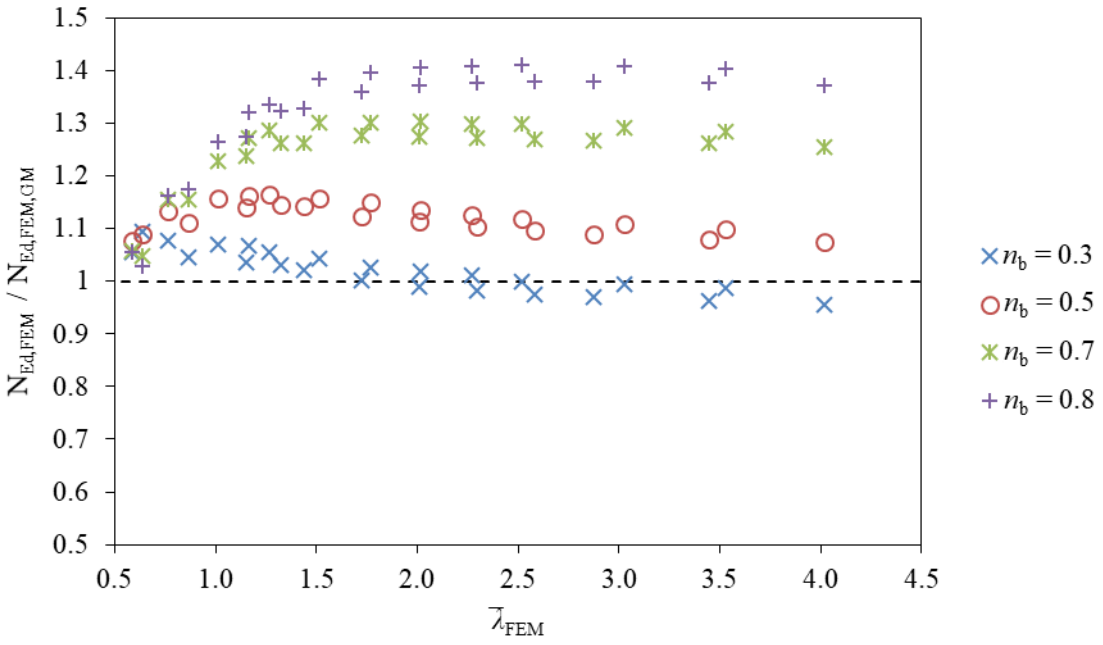

Figure 6.29 *Comparison of the modified General Method.*

Results of the modified General Method indicate very different results regarding the loading state, especially in higher values of the non-dimensional slenderness $\bar{\lambda}_{\mathrm{FEM}}$. In the case of dominant compressive force the results are over-conservative, whereas if bending moment is dominant become much lower. The over-conservatism of the primarily compressed members is caused by the fact that the flexural buckling resistance is significantly influenced by the modified elastic

modulus, whereas in the cases of dominant bending, the cross-section bending resistance has the main influence on the results.

In general could be said that the current state of the General Method provided by EN 1993-1-4 [2] is not suitable for the stainless steel beam-columns design, mainly due to neglection of the material non-linearity and over-estimating of the member stiffness. The modification given by consideration of the secant Elasticity modulus $E_{s,0.2}$ for the stress level equal to the 0.2 % proof stress $\sigma_{0.2}$ leads to over-conservative results in general. Therefore, further investigation of the General Method use for non-linear materials is needed.

Chapter 7

Conclusions

7.1 Research summary

The presented thesis can be divided into four main parts. The first part describes the use of stainless steel in civil engineering, material properties of stainless steel, stainless steel groups and provides the introduction of stainless steel in general. Then, resistance in both flexural buckling and bending is described. Comprehensive state of the art of the stainless steel SHS and RHS members loaded by compression and bending combination is given.

In the second part, the experimental programme conducted at the Czech Technical University in Prague is presented. In total, 20 cold-formed SHS and RHS members loaded by compressive force and uniform major axis bending moment were tested. Both slender and stocky cross-sections were used. Pin-ended boundary conditions were considered.

The material selected was austenitic stainless steel, grades 1.4301 and 1.4404. Material properties were obtained from tensile coupon tests for both flat and corner part of cross-section.

The third part is aimed on the numerical study of stainless steel SHS and RHS members loaded by combination of compressive force and bending moment. A 3D numerical model created in software Abaqus was described in detail and validated on experimental data. Subsequently, it was used to create a comprehensive numerical parametric study covering wide range of investigated variables, namely cross-section slenderness (cross-section Class), non-dimensional slenderness, material properties and loading state (n_b ratio).

The fourth part of the thesis is focused on a design procedure development and its comparison with the numerical results. Based on the results, the most recent procedure for stainless steel SHS and RHS beam-columns developed by Zhao et al. [72] was also compared. It was found that the procedure provides good results in general, however with some conservativeness in the case of slender (Class 4) cross-sections and little unsafe predictions in the cases of stocky (Class 1) cross-sections with increasing non-dimensional slenderness and bending moment influence. It should be noted that the procedure was developed based on the analytically established load-bearing capacities (flexural buckling according to EN 1993-1-4 [1] with revised flexural buckling curves [41] and bending resistance according to CSM [48]).

The new interaction factor formulae were proposed and evaluated. It was shown that the new proposal provides very good results if the numerically estimated load-bearing capacities, representing the real stainless steel beam-column behaviour, are considered. As the analytically established resistances are used in practice, comparison was made for three more cases. The flexural buckling was considered according to EN 1993-1-4 [1] with revised flexural buckling curves [41] in all cases combined with bending moment resistance calculated according to EN 1993-1-4 [1], CSM [49] and CSM with consideration of the DSM carbon steel local buckling curve [56]. In the first combination, the results are slightly scattered but mostly conservative, especially in the cases of slender (Class 4) cross-sections with dominant bending. If the CSM [49] is considered, the results are similar, however, with improvement in dominant bending moment cases, mainly for stocky (Class 1) cross-section predictions. That is caused by the consideration of strain hardening in the CSM [49]. The use of DSM carbon steel local buckling curve [56] indicates slightly more accurate results for slender (Class 4) cross-sections, due to lower buckling curve. However, stocky (Class 1) cross-section predictions are over-conservative due to strain hardening neglection. Furthermore, there are few slightly unsafe results of austenitic stocky (Class 1) cross-section predictions in cases of dominant compressive force for all bending moment resistance calculations. That is attributed to the great strain hardening effect of the

austenitic stainless steel group. It should be noted that the interaction factor has a very low influence on the beam-column design in the cases of dominant compression.

A reliability analysis of the new proposal considering the three mentioned combinations of the load-bearing capacities (described in the previous paragraph) was made. Based on the reliability analysis, it was found that the results are safe (within tolerance) in all cases.

Subsequently, a brief study of stainless steel SHS and RHS members loaded by combination of compressive force and non-uniform bending moment was described. Design approach containing the new interaction factor formulae was compared and showed safe and mostly conservative results due to rough (and over-conservative) consideration of the bending moment gradient factor C_m.

Main benefit of the new proposal is that there is only one procedure for all stainless steel SHS and RHS beam-columns. The procedure is the same for all stainless steel groups, cross-section slendernesses (Classes), non-dimensional slendernesses and loading states (compressive force to flexural buckling resistance ratio). It makes the procedure very general.

Furthermore, a brief study of the General Method given by EN 1993-1-1 [2] was made. It was found that the General Method is not suitable for the stainless steel beam-column design in its current state, because it overestimates member stiffness. Therefore, modification by replacing the initial Young's modulus of elasticity by elastic secant modulus for the stress level equal to the 0.2 % proof stress was used. However, the results are mostly over-conservative, especially for mostly compressed members due to great influence of the lower modulus of elasticity value on flexural buckling resistance.

7.2 Future research

There are some suggestions for the future research resulting from the presented work.

The new proposal was evaluated for stainless steel SHS and RHS beam-columns. However, there are many other cross-sections, whether with respect to cross-sectional shape (hollow and open) or fabrication process (welded, cold- and hot-rolled). Assessment of the new proposal suitability for mentioned cross-sections should be made with the aim to have a general procedure for all cross-sections. Furthermore, open cross-section members may be susceptible to lateral torsional buckling. Therefore, there is still need for investigation of stainless steel open-section beam-columns.

Based on the results of the analytical part of the study, some differences between numerically and analytically established load-bearing capacities were found, that mostly stems from the great strain hardening of significantly non-linear material. Even though the CSM [49] considers strain hardening phenomenon there is some conservativeness of slender (Class 4) cross-sections. The DSM carbon steel local buckling curve [56] provides slightly more accurate results for slender (Class 4) cross-sections, however, strain hardening phenomenon is not taken into account which leads to over-conservative predictions of stocky (Class 1) cross-sections. It could be said, that the combination of the two mentioned methods should provide very accurate bending moment resistance predictions.

The General Method is an alternative beam-column design approach given by the Eurocode. A brief investigation found that it is not suitable for stainless steel structures in its current state. The General Method is quite unexplored field regarding non-linear material members design. Therefore, further research would be worthy.

List of figures

List of tables

References

[1] EN 1993-1-4, *Eurocode 3: Design of steel structures – Part 1-4: General rules – Supplementary rules for stainless steels*, European Committee for Standardization (CEN), Brussels, 2006.

[2] EN 1993-1-1, *Eurocode 3: Design of steel structures – Part 1-1: General rules and rules for buildings*, European Committee for Standardization (CEN), Brussels, 2005

[3] *Design manual for Structural Stainless Steel – Commentary,* Euro Inox and The Steel Construction Institute, 2003.

[4] Cruise, R. B. *The Influence of Production Routes on the Behaviour of Stainless Steel Structural Members,* Ph.D. Thesis, Imperial College London, 2007.

[5] *Design Manual for Structural Stainless Steel – Fourth Edition,* The Steel Construction Institute, 2017.

[6] EN 10027-2, *Designation systems for steels – Part 2: Numerical system,* European Committee for Standardization (CEN), Brussels, 2015.

[7] EN 10088-1, *Stainless steels – Part 1: List of stainless steels*, European Committee for Standardization (CEN), Brussels, 2005.

[8] EN 10088-4, *Stainless steels – Part 4: Technical delivery conditions for sheet/plate and strip of corrosion resisting steels for construction purposes*, European Committee for Standardization (CEN), Brussels, 2005.

[9] EN 10088-5, *Stainless steels – Part 5: Technical delivery conditions for bars, rods, wire, sections and bright products of corrosion resisting steels for construction purposes*, European Committee for Standardization (CEN), Brussels, 2005.

[10] Cruise, R. B. and Gardner, L. *Strength enhancements induced during cold forming of stainless steel sections*, Journal of Constructional Steel Research, 64, 2008, pp. 1310-1316.

[11] Afshan, S., Rossi, B. and Gardner, L. *Strength enhancements in cold-formed structural sections – Part I: Material testing*, Journal of Constructional Steel Research, 83, 2013, pp. 177-188.

[12] Gardner, L. and Nethercot, D. A. *Numerical Modelling of Stainless Steel Structural Components – A Consistent Approach*, Journal of Structural Engineering, 130, 2004, pp. 1586-1601.

[13] Ashraf, M., Gardner, L. and Nethercot, D. A. *Finite element modelling of structural stainless steel cross-sections*, Thin-Walled Structures, 44, 2006, pp. 1048-1062.

[14] Mařík, J. *Mechanical properties of cold-formed stainless steel*, Ph.D. Thesis, CTU in Prague, Czech Republic, 2015.

[15] Mařík, J. and Jandera, M. *Mechanical properties of cold-formed stainless steel*, EUROSTEEL 2017, Copenhagen, Denmark, 2017.

[16] *Design Manual for Structural Stainless Steel - Third Edition*, Euro Inox and The Steel Construction Institute, 2003.

[17] Ramberg, W. and Osgood, W.R. *Description of stress-strain curves by three parameters*, National Advisory Committee for Aeronautics, Technical Note No. 902, Washington, United States of America, 1943.

[18] Hill, H. N. *Determination of stress-strain relations from the offset yield strength values*, National Advisory Committee for Aeronautics, Technical Note No. 927, Washington, United States of America, 1944.

[19] Rasmussen, K. J. R. and Hancock, G. J. *Design of cold-formed stainless steel tubular members II*, Journal of Structural Engineering, 119, 1993, pp. 2368-2386.

[20] Arrayago, I., Real, E. and Gardner, L., *Description of stress-strain curves for stainless steel alloys*, Materials and Design, 87, 2018, pp. 540-552.

[21] Mirambel, E. and Real, E. *On the calculation of deflections in structural stainless steel beams*, Journal of Constructional Steel Research, 54, 2000, pp. 109-133.

[22] Gardner, L. and Nethercot, D. A. *Experiments on stainless steel hollow section – Part 1: Material and cross-sectional behaviour*, Journal of Constructional Steel research, 60, 2004, pp. 191-1318.

[23] Dawson, R. G. and Walker, A. C. *Post-buckling of geometrically imperfect plates*, Journal of the Structural Division ASCE, 98, 1972, pp. 75-94.

[24] Schafer, B.W. and Peköz, T. *Computational Modelling of Cold-Formed Steel: Characterizing Geometric Imperfections and Residual Stresses*, Journal of Constructional Steel Research, 47, 1998, pp. 193-210.

[25] Zhao, O., Rossi, B., Gardner, L. and Young, B. *Behaviour of structural stainless steel cross-sections under combined loading – Part 1: Experimental study*, Engineering Structures, 89, 2015, pp. 236-246.

[26] Zhao, O., Rossi, B., Gardner, L. and Young, B. *Behaviour of structural stainless steel cross-sections under combined loading – Part 2: Numerical modelling and design approach*, Engineering Structures, 89, 2015, pp. 247-259.

[27] Rasmussen, K. J. R. and Rondal, J. *Strength Curves for Metal Columns*, Journal of Structural Engineering, 123, 1997, pp. 721-728.

[28] Rasmussen, K. J. R. and Hancock, G. J. *Design of Cold-Formed Stainless Steel Tubular Members I: Columns*, Journal of Structural Engineering, 119, 1993, pp. 2349-2367.

[29] Young, B. *Test of Cold-Formed Stainless Steel Tubular Columns*, International Experts Seminar "Stainless Steel in Structures", Steel Construction Institute, UK, Ascot, 2003, pp. 49-55.

[30] Elleboy, E. and Young, B. *Structural performance of Cold-Formed High Strength Stainless Steel Columns*, Journal of Constructional Steel Research, 61, 2005, pp. 1631-1649.

[31] EN 1993-1-5, *Eurocode 3 – Design of steel structures – Part 1-5: Plated structural elements*, European Committee for Standardization (CEN), Brussels, 2006.

[32] EN 1090-2, *Technical requirements for the execution of steel structures*, European Committee for Standardization (CEN), Brussels, 2008.

[33] Cruise, R. B. and Gardner, L. *Residual stress analysis of structural stainless steel sections*, Journal of Constructional Steel Research, 64, 2008, pp. 352-366.

[34] Jandera, M., Gardner, L. and Machacek, J. *Residual stress in cold-rolled stainless steel hollow sections*, Journal of Constructional Steel Research, 64, 2008, pp. 1255-1263.

[35] Johnson, A.L. and Winter, G. *The Structural performance of austenitic stainless steel members*, Report No. 327, Department of Structural Engineering, Cornel University, United Stated of America, 1966.

[36] Gardner, L. and Theofanous, M. *Descrete and continuous treatment of local buckling in stainless steel elements*, Journal of Constructional Steel Research, 64, 2008, pp. 1207-1216.

[37] Gardner, L., Law, K. H. and Buchanan, C. *Unfined slenderness limits for structural steel circular hollow sections*, Romanian Journal of Technical Sciences, Applied Mechanics, 59, 2014, pp. 153-163.

[38] Bock, M. and Real, E. *Effective width equations accounting for element interaction for cold-formed stainless steel square and rectangular hollow sections*, Structures, 2, 2015, pp. 81-90.

[39] Euler, L. *Methodus inveniendi lineas curvas maximi minimive proprietate gaudents, sive Solutio problematis isoperimetrici latissimo sensu accepti*, Apud Marcum-Michaelem Bousquet & socios, Lausanne and Geneva, 1744.

[40] Ayrton, W. E. and Perry, J. *On Struts*, The Engineering, 62, 1886, pp. 464-513.

[41] Afshan, S., Zhao, O. and Gardner, L. *Buckling curves for stainless steel tubular columns*, Eurosteel 2017, Copenhagen, Denmark, 2017.

[42] Gardner, L. *A new approach to structural stainless steel design*, Ph.D. Thesis, Imperial College London, 2002.

[43] Gardner, L. and Nethercot, D. A. *Experiments on stainless steel hollow sections – Part 1: Material and cross-sectional behaviour*, Journal of Constructional Steel Research, 60, 2004, pp. 1291-1318.

[44] Gardner, L. and Ashraf, M. *Structural design for non-linear metallic materials*, Engineering Structures, 28, 2006, pp. 926-934.

[45] Ashraf, M., Gardner, L. and Nethercot, D. A. *Compression strength of stainless steel cross-section*, Journal of Constructional Steel research, 62, 2006, pp. 105-115.

[46] Ashraf, M., Gardner, L. and Nethercot, D. A. *Structural stainless steel design: Resistance based on deformation capacity*, Journal of Structural Engineering, (ASCE), 134, 2008, pp. 402-411.

[47] Gardner, L. *The continuous strength method*, Proceeding of the Institution of Civil Engineers-Structures and Buildings, 161, 2008, pp. 127-133.

[48] Afshan, S. and Gardner, L. *The continuous strength method for structural stainless steel design*, Thin-Walled Structures, 68, 2013, pp. 42-49.

[49] Zhao, O., Afshan, S. and Gardner, L. *Structural response and continuous strength method design of slender stainless steel cross-section*, Engineering Structures, 140, 2017, pp. 14-25.

[50] Zhao, O., Rossi, B., Gardner, L. and Young, B. *Behaviour of structural stainless steel cross-sections under combined loading – Part 1: Experimental study*, Engineering Structures, 89, 2015, pp. 236-246.

[51] Zhao, O., Rossi, B., Gardner, L. and Young, B. *Behaviour of structural stainless steel cross-sections under combined loading – Part 2: Numerical modelling and design approach*, Engineering Structures, 89, 2015, pp. 247-259.

[52] SEI/ASCE 8-02, *Specification for the Design of Cold-formed Stainless Steel Structural Members*, ASCE, Reston, VA, 2002.

[53] AS/NZS 4673, *Cold-formed stainless steel structures*, Committee BD-086, Sydney, 2001.

[54] Schafer, B.W. and Peköz, T. *Direct Strength Prediction of Cold-formed Steel members Using Numerical Elastic Buckling Solutions*, Thin-Walled Structures – Research and Development, Elsevier, 1998, pp. 137-144.

[55] AISI-S100-12, *North American Specification for the Design of Cold-formed Steel Structural Members*, American Iron and Steel Institute (AISI), Washington D.C., 2012.

[56] Arrayago, I., Rasmussen, K.J.R. and Real, E. *Full slenderness range DSM approach for stainless steel hollow cross-sections*, Journal of Constructional Steel Research, 133, 2017, pp. 156-166.

[57] Austin, W. J. *Strength and design of metal beam-columns*, Journal of the Structural Division, ASCE, 87, 1961, pp. 1-32.

[58] ENV 1993-1-1, *Eurocode 3: Design of steel structures Part 1.1: General rules and rules for buildings*, European Committee for Standardization (CEN), Brussels, 1992.

[59] Boissonnade, N., Jaspart, J. P., Muzeau, J. P. and Villett, M. *New interaction formula for beam-columns in Eurocode 3: The French-Belgian approach*, Journal of Constructional Steel Research, 60, 2004, pp. 421-431.

[60] Greiner, R. and Lindner, J. *Interaction formulae for members subjected to bending and axial compression in EUROCODE 3-the Method 2 approach*, Journal of Constructional Steel Research, 62, 2006, pp. 757-770.

[61] prEN 1993-1-1 *Eurocode 3: Design of steel structures – Part 1-1: General rules and rules for buildings*, European Committee for Standardization (CEN), Brussels, 202X.

[62] EN 1999-1-1, *Eurocode 9: Design of aluminium structures, Part 1-1: General structural rules*, European Committee for Standardization (CEN), Brussels, 2007.

[63] Höglund, T., Tindall, P. *Designers´ Guide to Eurocode 9: Design of Aluminium Structures*, ICE Publishing, London, 2012.

[64] Höglund, T. *A unified method for the design of steel beam-columns*, Steel Construction, 7, 2014, pp. 230-245.

[65] EN 1993-1-3 *Eurocode 3: Design of steel structures – Part 1-3: General rules – Supplementary rules for cold-formed members and sheeting*, European Committee for Standardization (CEN), Brussels, 2006.

[66] Rasmussen, K.J.R. and Rondal, J. *Column curves for stainless steel alloys*, Journal of Constructional Steel research, 54, 2000, pp. 89-107.

[67] Talja, A. and Salmi, P. *Design of stainless steel RHS beams, columns and beam-columns*, Research Note 1619, VVT Building Technology, Finland, 1995.

[68] Lopes, N., Real, P. V. and Silva, L. S. *Stainless steel beam-columns interaction curves with and without lateral torsional buckling*, 7th EUROMECH Solid Mechanics Conference, Lisbon, Portugal, 2009.

[69] EN 1993-1-2, *Eurocode 3: Design of steel structures – Part 1-2: General rules – Structural fire design*, European Committee for Standardization (CEN), Brussels, 2005.

[70] Greiner, R. and Kettler, M. *Interaction of bending and axial compression of stainless steel members*, Journal of Constructional Steel Research, 64, 2008, pp. 1217-1224.

[71] Jandera, M. and Syamsuddin, D. *Interaction formula for stainless steel structures beam-columns*, EUROSTEEL 2014, Naples, Italy, 2014.

[72] Zhao, O., Gardner, L. and Young, B. *Behaviour and design of stainless steel SHS and RHS beam-columns*, Thin-Walled Structures, 106, 2016, pp. 330-345.

[73] Zhao, O. *Structural Behaviour of Stainless Steel Elements Subjected to Combined Loading*, Ph.D. Thesis, Imperial College London, United Kingdom, 2015.

[74] Zhao, O., Gardner, L. and Young, B. *Testing and numerical modelling of austenitic stainless steel CHS beam-columns*, Engineering Structures, 111, 2016, pp. 263-274.

[75] Buchanan, C., Gardner, L., Zhao, O. and Real, E. *Design of stainless steel CHS beam-columns*, Tubular Structures XVI, Melbourne, Australia, 2017.

[76] Arrayago, I., Real, E. and Mirambell, E. *TESTS ON FERRITIC STAINLESS STEEL RHS AND SHS BEAM-COLUMNS*, Advances in Steel Structures, Lisbon, Portugal, 2015.

[77] Arrayago, I., Picci, F., Real, E. and Mirambell, E. *Interaction of bending and axial load for ferritic stainless steel RHS columns*, Thin-Walled Structures, 91, 2015, pp. 96-107.

[78] Arrayago, I., Real, E. and Mirambell, E. *Experimental study on ferritic stainless steel RHS and SHS beam-columns*, Thin-Walled Structures, 100, 2016, pp. 93-104.

[79] Arrayago, E. and Real, E. *Experimental Study on Ferritic Stainless Steel RHS and SHS Cross-sectional Resistance Under Combined Loading*, Structures, 4, 2015, pp. 69-79.

[80] EN ISO 6892-1, *Metallic materials – Tensile testing – part 1: Method of test at room temperature*, European Committee for Standardization (CEN), Brussels, 2009.

[81] EN 1990, *Eurocode – Basis of structural design*, European Committee for Standardization (CEN), Brussels, 2002.

[82] Tankova, T., Simones da Silva, L., Marques, L., Rebelo, C. and Taras, A. *Towards a standardized procedure for the safety assessment of stability design rules*, Journal of Constructional Steel Research, 102, 2014, pp. 290-302.

[83] Afshan, S., Francis, P., Baddoo, N.R. and Gardner, L. *Reliability analysis of structural stainless steel design provisions*, Journal of Constructional Steel Research, 114, 2015, pp. 293-304.

[84] Taras, A., Dehan, V., Simones da Silva, L., Marques, L. and Tankova, T. *SAFEBRICTILE: Standardization of Safety Assessment Procedures across Brittle to Ductile Failure Modes – Guideline for the Safety Assessment of Design Rules for Steel Structures in Line with EN 1990*, Research Programme of the Research Fund for Coal and Steel (RFCS), 2016.

Chapter 8

Annexes

8.1 Numerical model validation

Validation of the numerical model based on the experimental data regarding the relationship between compressive force and mid-span deflection is given in this Annex for all tested members. Furthermore, figures for both major and minor axis mid-span deflection of RHS 100x40x4 cross-section members are shown (for the other members is the minor-axis deflection negligible). See Figure 8.1 to Figure 8.20, where *Mj* and *Mi* are the major axis and minor axis mid-span deflection and *FEM – 0t* and *FEM – 2t* are the numerical model results considering enhanced material properties in the corner area and extended corner area, respectively.

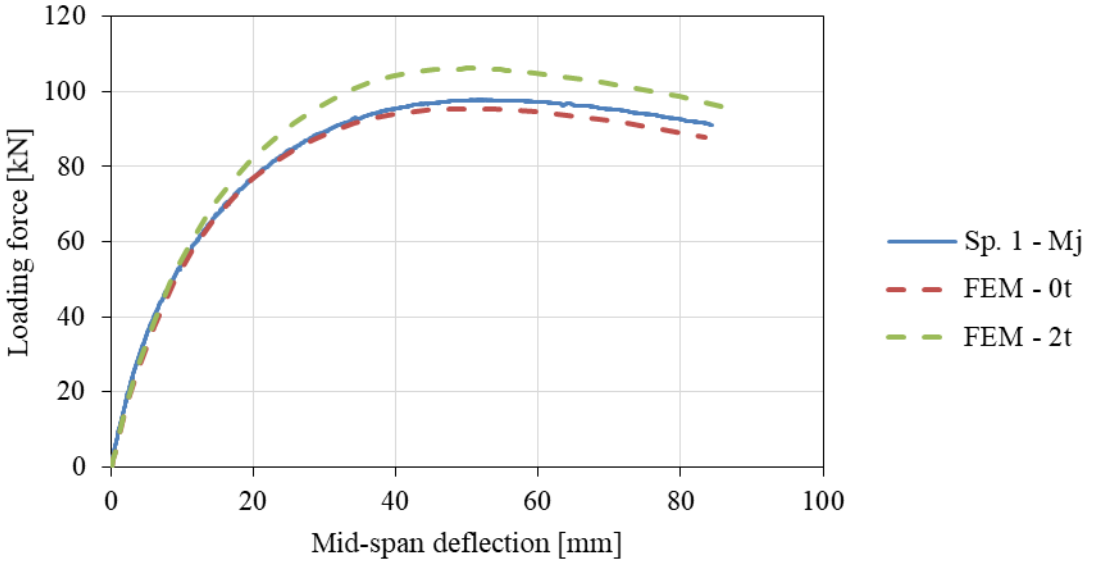

Figure 8.1 *Numerical model validation on test 1.*

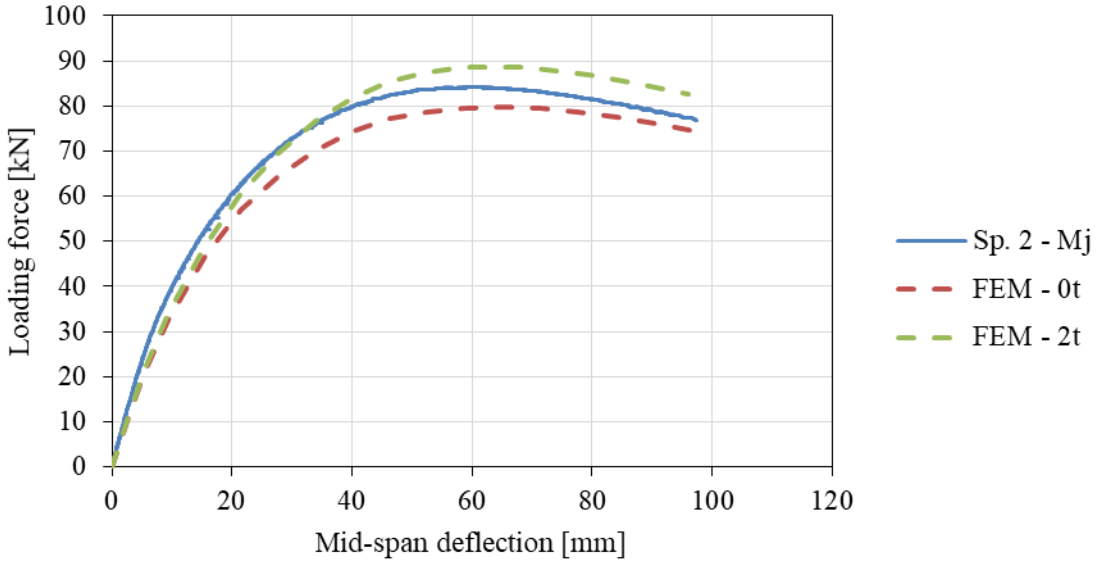

Figure 8.2 *Numerical model validation on test 2.*

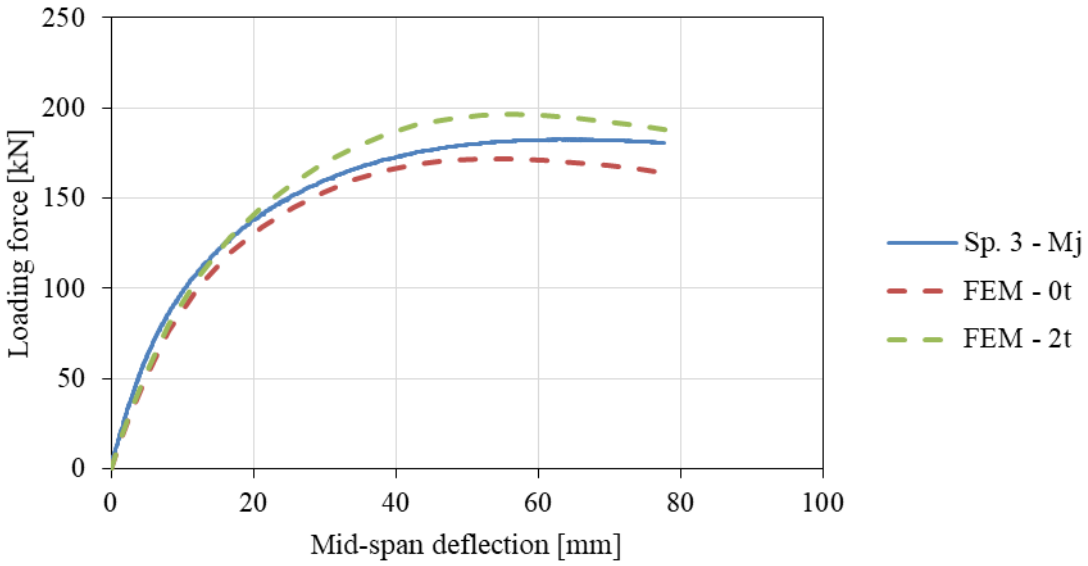

Figure 8.3 *Numerical model validation on test 3.*

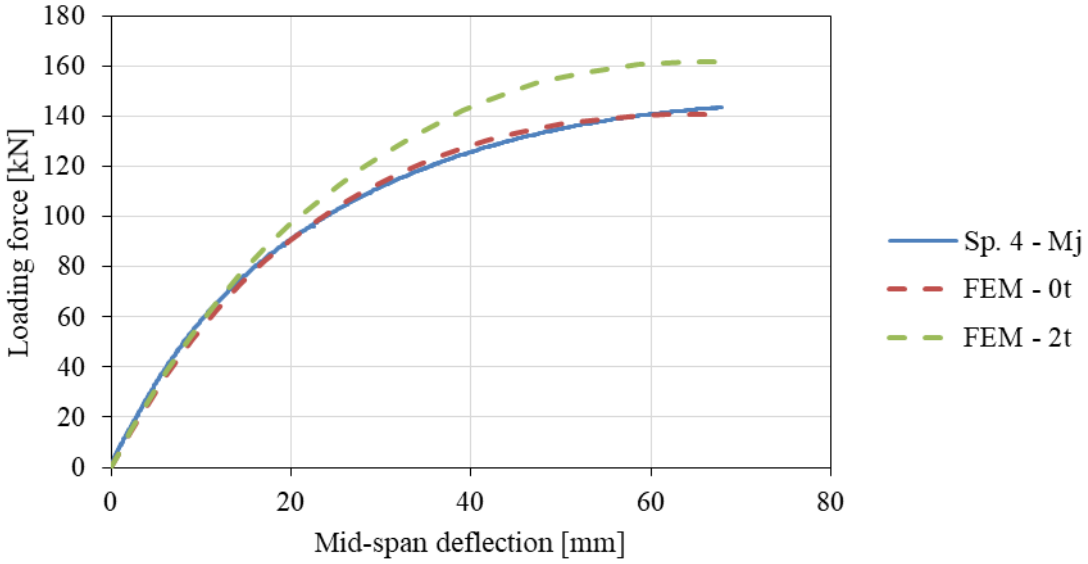

Figure 8.4 *Numerical model validation on test 4.*

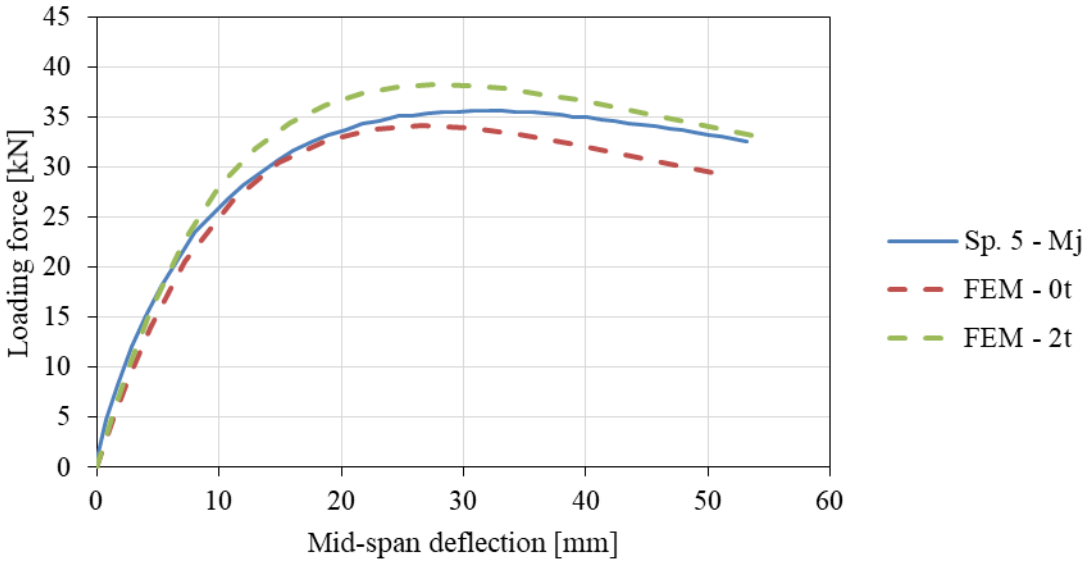

Figure 8.5 *Numerical model validation on test 5.*

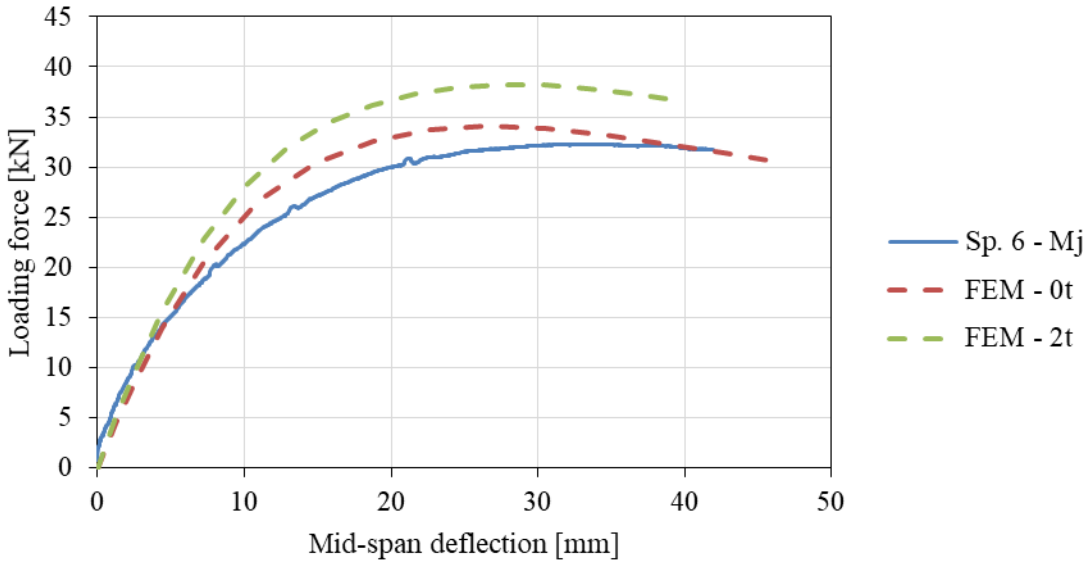

Figure 8.6 *Numerical model validation on test 6.*

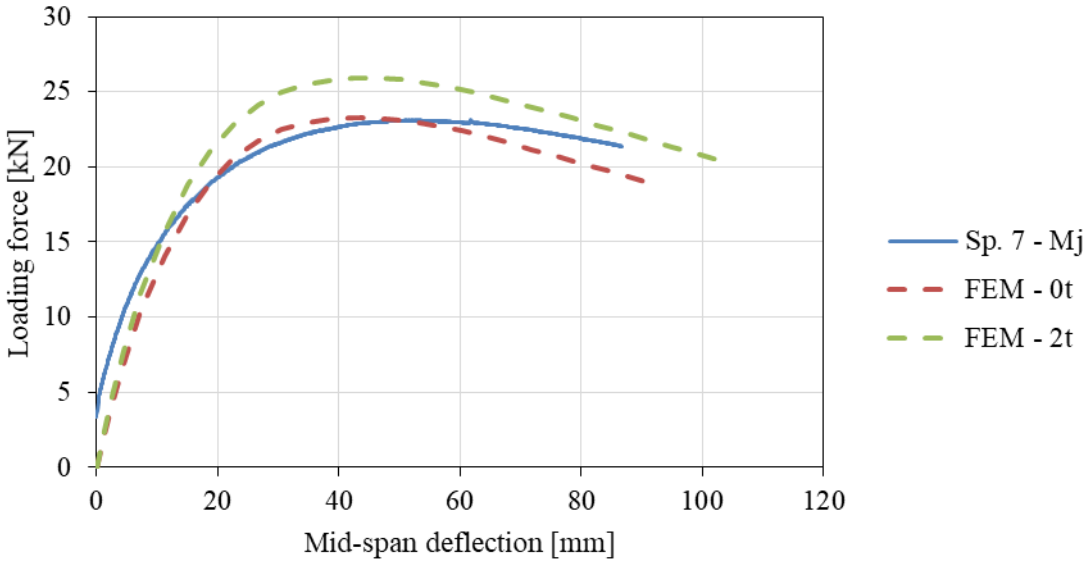

Figure 8.7 *Numerical model validation on test 7.*

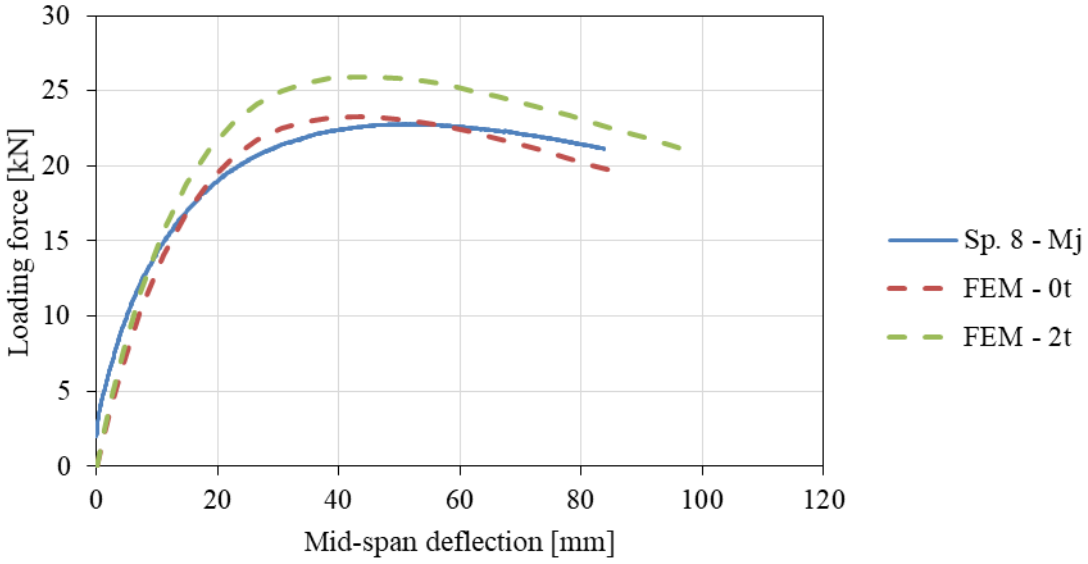

Figure 8.8 *Numerical model validation on test 8.*

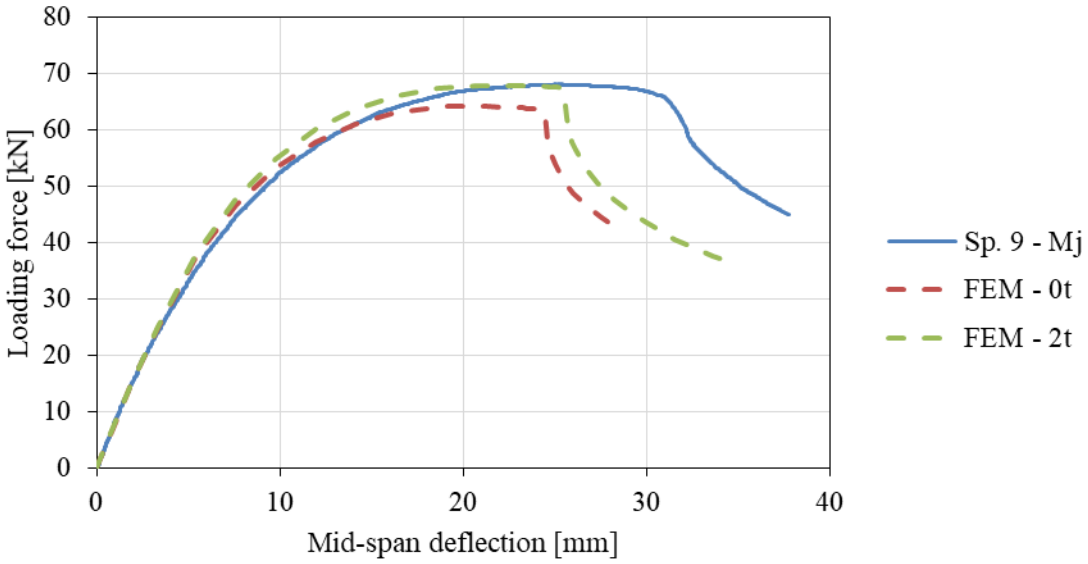

Figure 8.9 *Numerical model validation on test 9.*

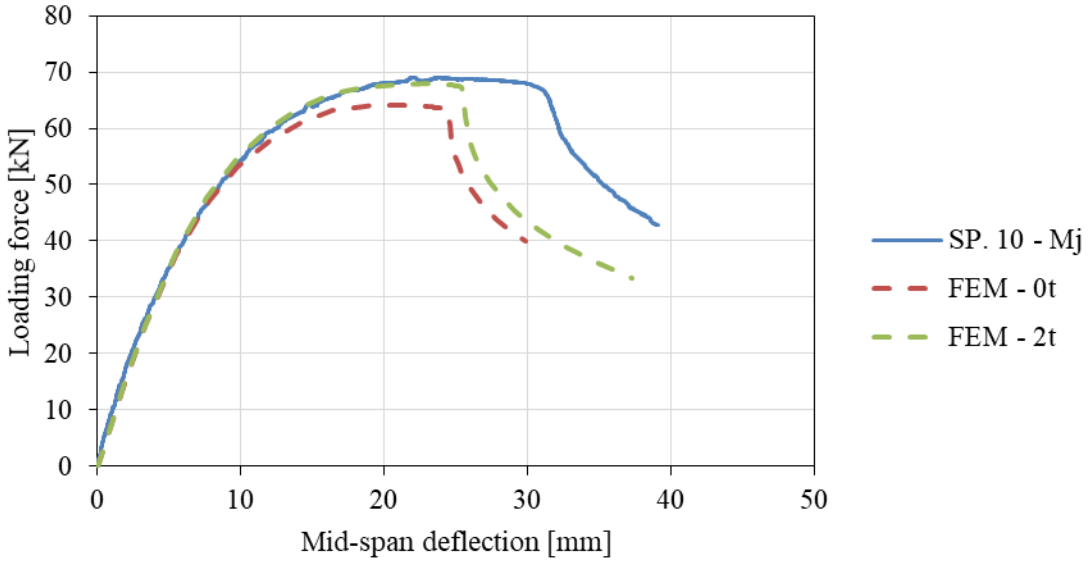

Figure 8.10 *Numerical model validation on test 10.*

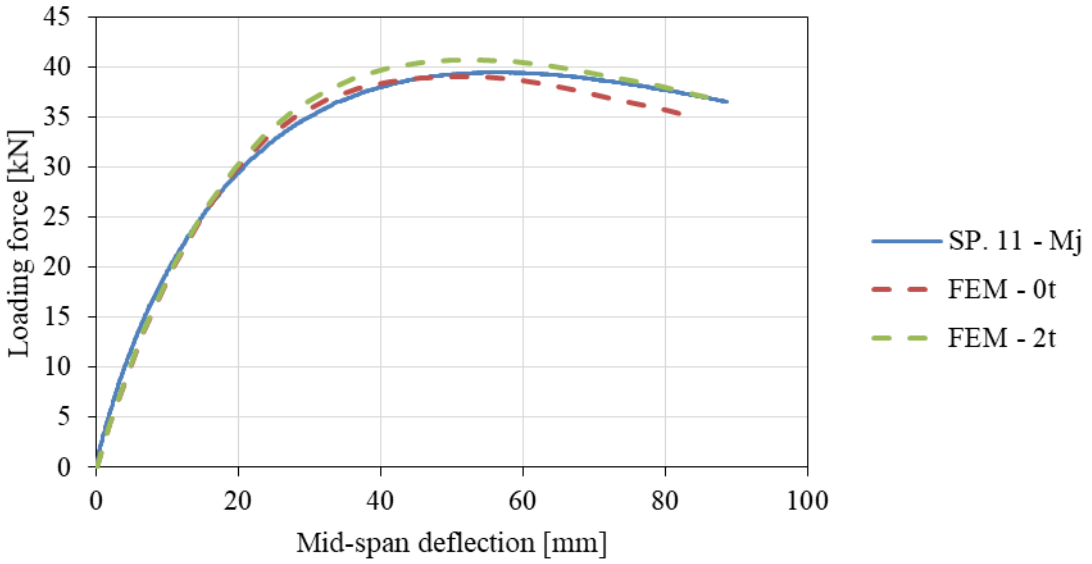

Figure 8.11 *Numerical model validation on test 11.*

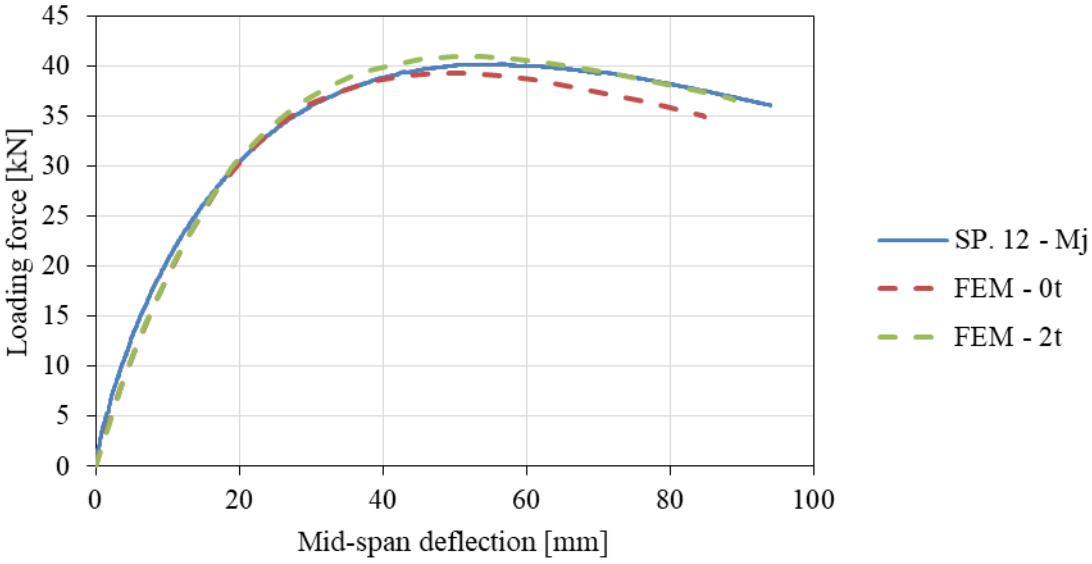

Figure 8.12 *Numerical model validation on test 12.*

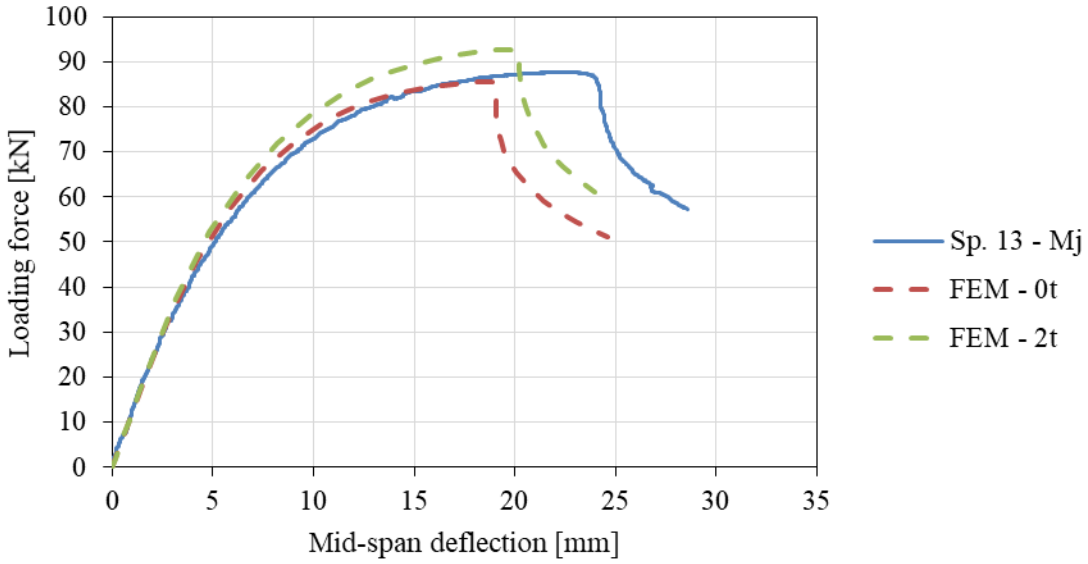

Figure 8.13 *Numerical model validation on test 13.*

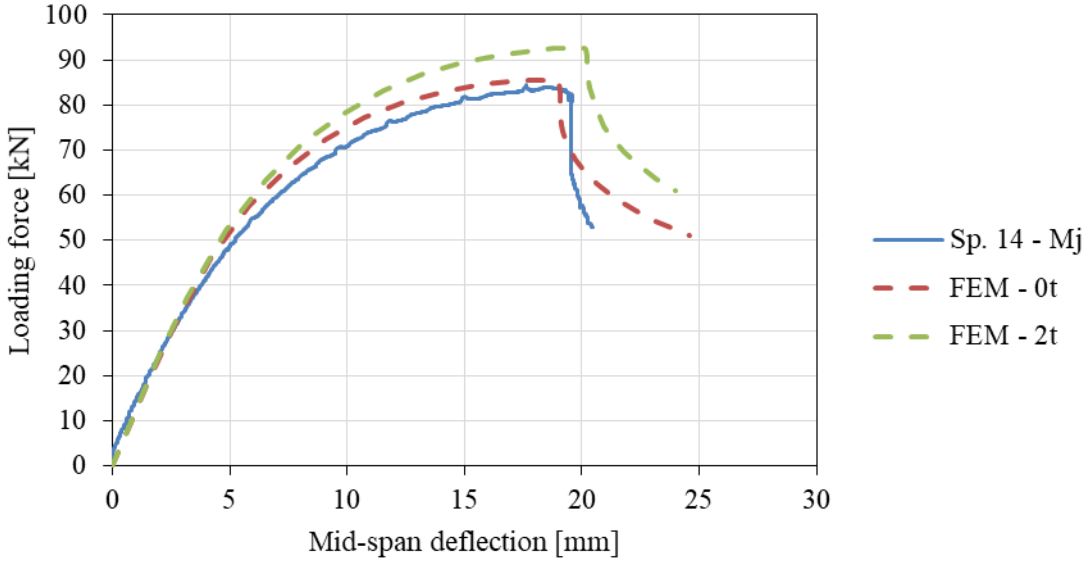

Figure 8.14 *Numerical model validation on test 14.*

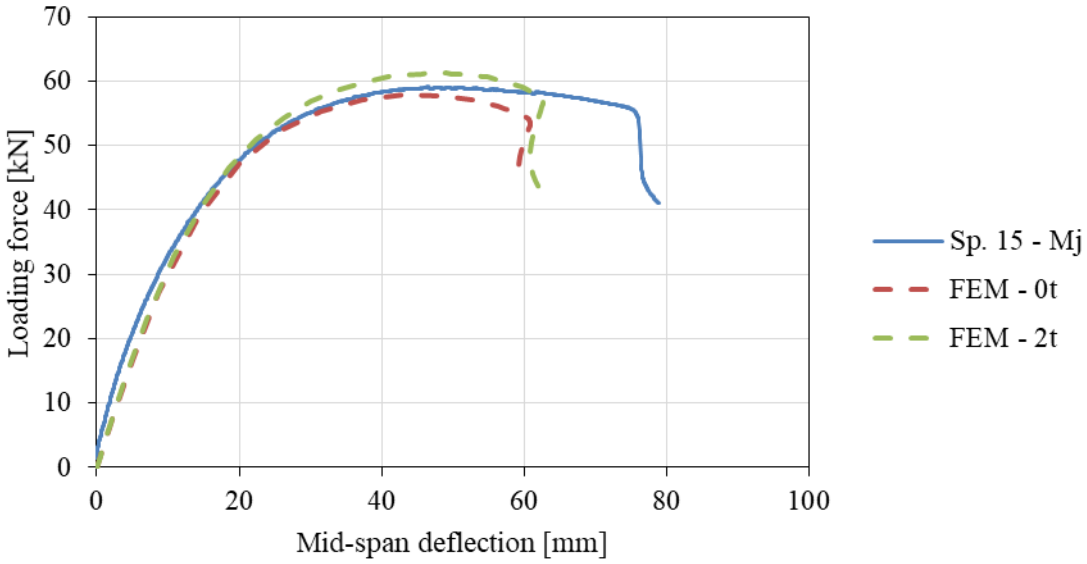

Figure 8.15 *Numerical model validation on test 15.*

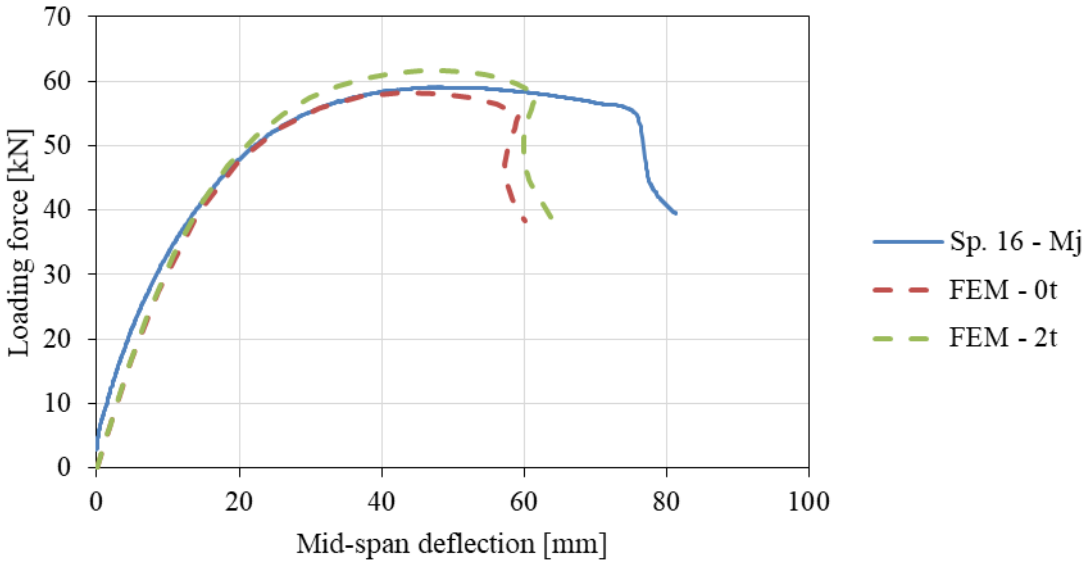

Figure 8.16 *Numerical model validation on test 16.*

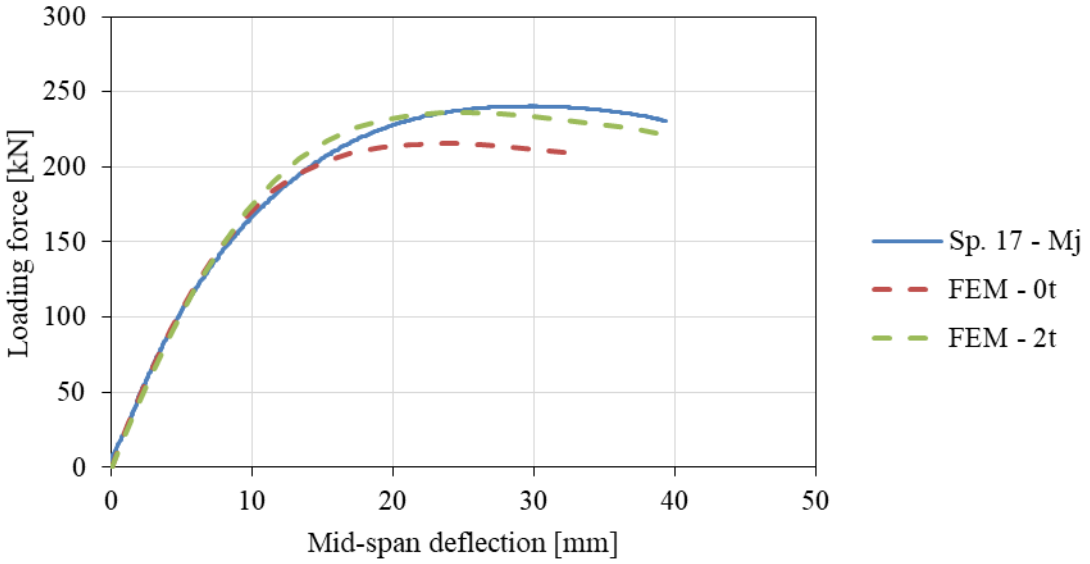

a) Major axis deflection

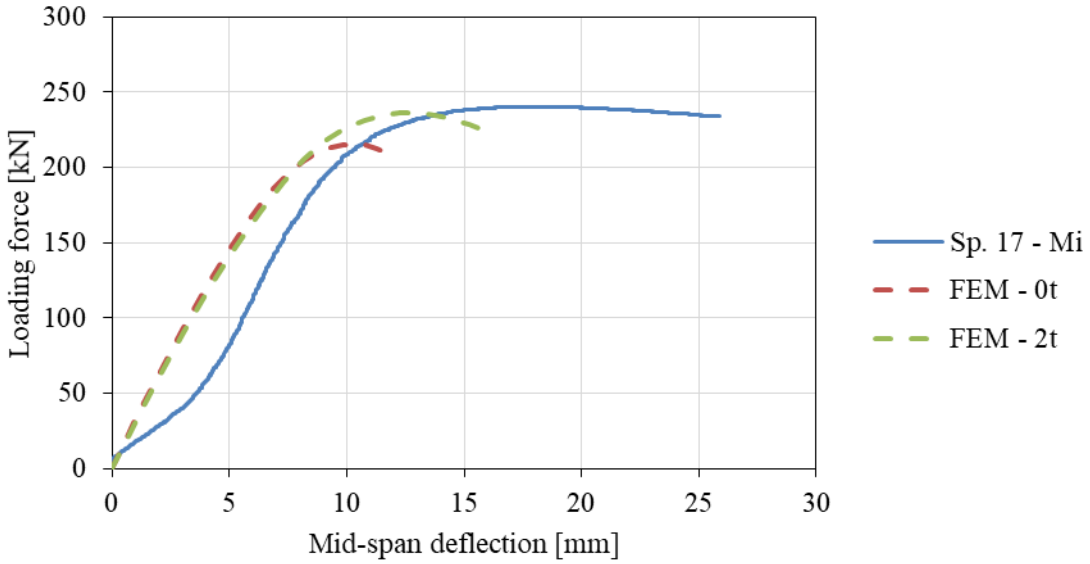

b) Minor axis deflection

Figure 8.17 *Numerical model validation on test 17 regarding major axis (a) and minor axis (b) mid-span deflection.*

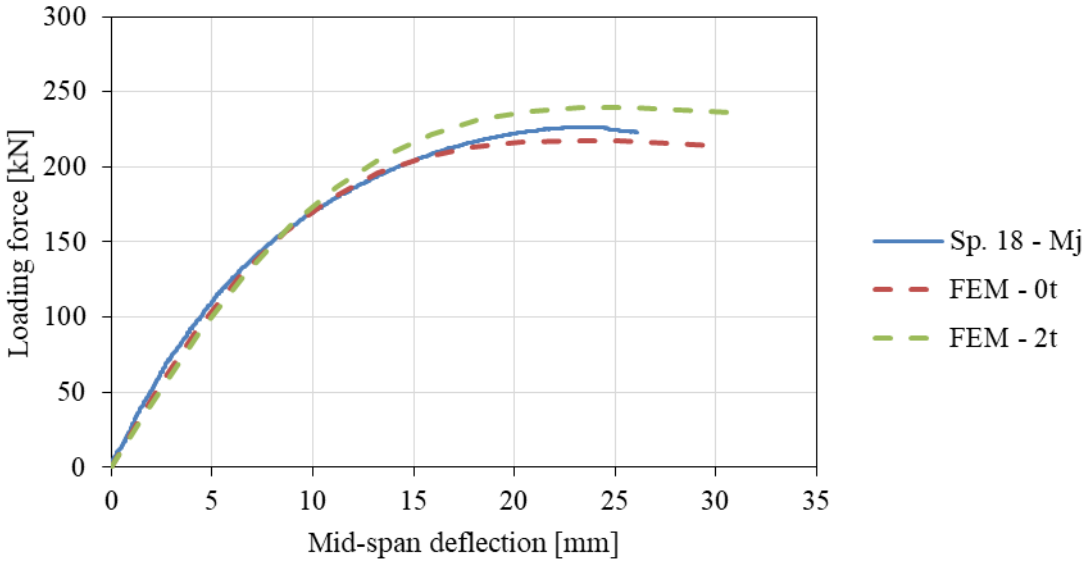

a) Major axis deflection

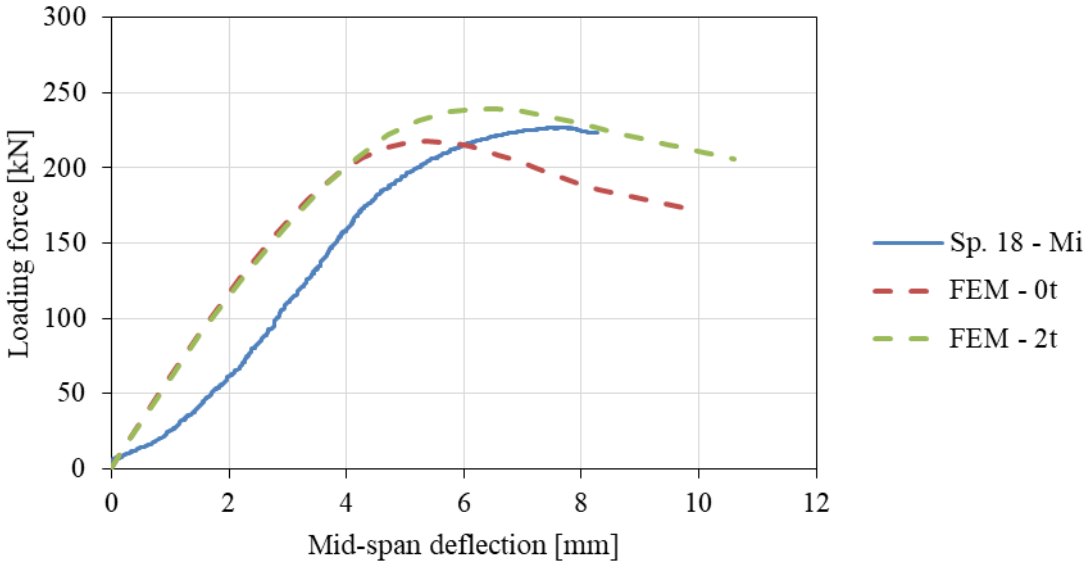

b) Minor axis deflection

Figure 8.18 *Numerical model validation on test 18 regarding major axis (a) and minor axis (b) mid-span deflection.*

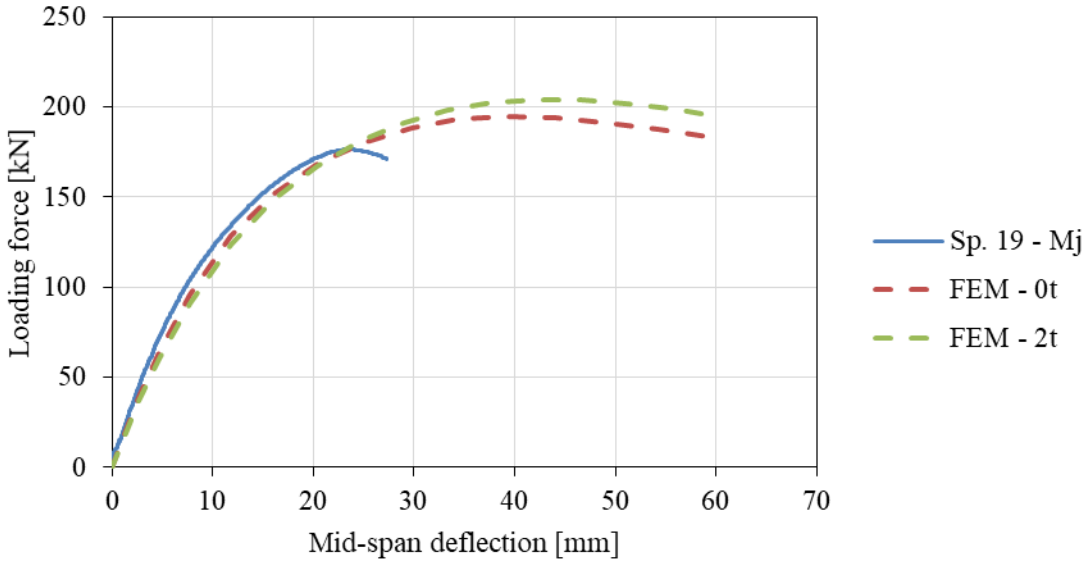

a) Major axis deflection

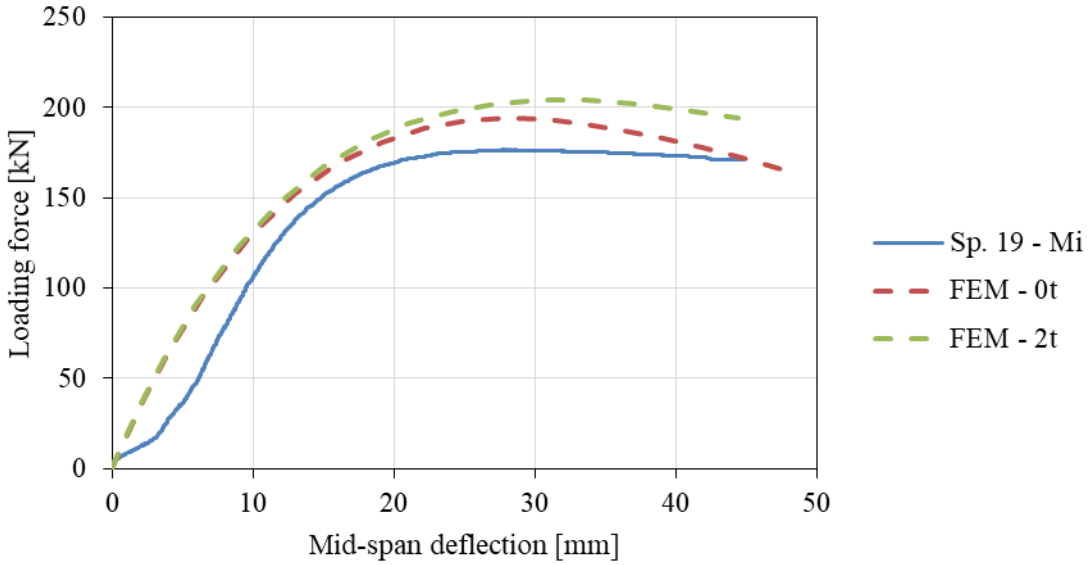

b) Minor axis deflection

Figure 8.19 *Numerical model validation on test 19 regarding major axis (a) and minor axis (b) mid-span deflection.*

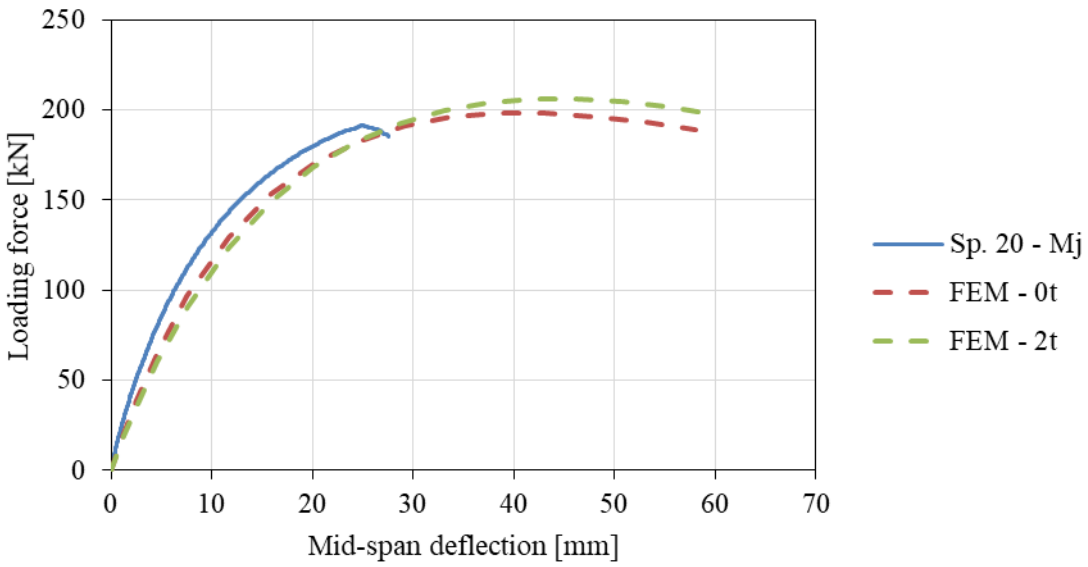

a) Major axis deflection

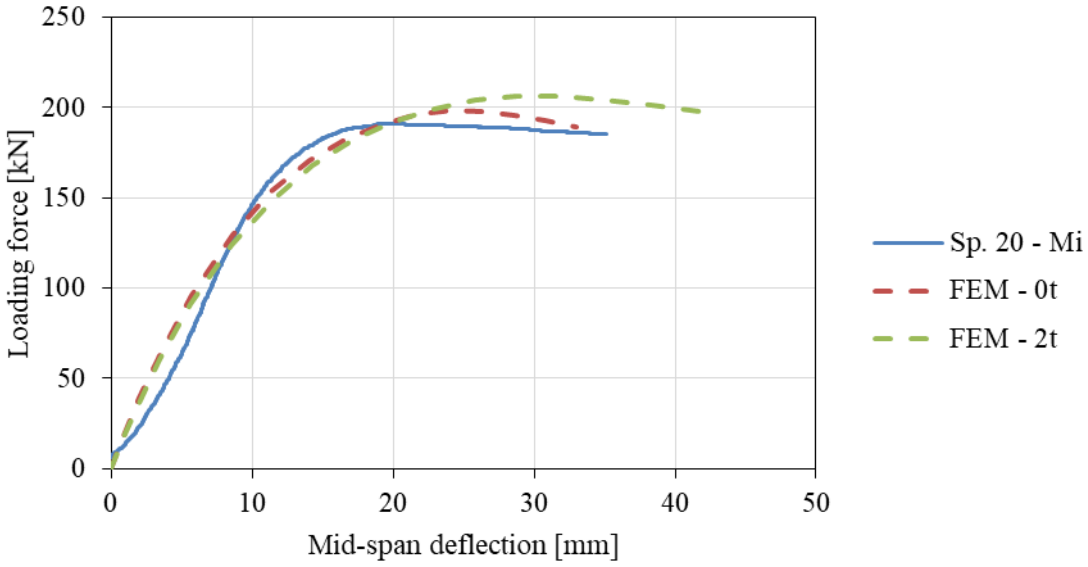

b) Minor axis deflection

Figure 8.20 *Numerical model validation on test 20 regarding major axis (a) and minor axis (b) mid-span deflection.*